Year : 2020

Regulation of Actin Assembly for the Formation of the Fusion Focus in Fission Yeast

Billault-Chaumartin Ingrid

UNIL | Université de Lausanne
Faculté de biologie
et de médecine

Département de Microbiologie Fondamentale

Regulation of Actin Assembly for the Formation of the Fusion Focus in Fission Yeast

Thèse de doctorat ès sciences de la vie (PhD)

présentée à la

Faculté de Biologie et de Médecine
de l'Université de Lausanne

par

Ingrid BILLAULT-CHAUMARTIN

Master de l'Université Pierre et Marie-Curie, Paris, France

Jury

Prof. Andreas Mayer, Président
Prof. Sophie Martin, Directrice de thèse
Prof. David Kovar, Expert
Prof. Marko Kaksonen, Expert
Prof. Serge Pelet, Expert

Lausanne
2022

UNIL | Université de Lausanne
Faculté de biologie
et de médecine

Ecole Doctorale
Doctorat ès sciences de la vie

Imprimatur

Vu le rapport présenté par le jury d'examen, composé de

Président·e	Monsieur	Prof.	Andreas	**Mayer**
Directeur·trice de thèse	Madame	Prof.	Sophie	**Martin**
Expert·e·s	Monsieur	Prof.	David	**Kovar**
	Monsieur	Prof.	Marko	**Kaksonen**
	Monsieur	Dr	Serge	**Pelet**

le Conseil de Faculté autorise l'impression de la thèse de

Ingrid Christiane Bernadette Billault-Chaumartin

Master, Université Paris VI, France

intitulée

Regulation of actin assembly for the formation of the fusion focus in fission yeast

Lausanne, le 4 mars 2022

pour le Doyen
de la Faculté de biologie et de médecine

Prof. Andreas Mayer

Acknowledgements

I like to think that acknowledgments are the first part of PhD manuscripts because we realize that Science is never done alone. Instead, it is the result of a network of incredibly complicated inter-relationships that all cooperate and self-organize in a nebulous and remarkable manner. I'd like to recognize some of these here.

First and perhaps a tad obvious, I'd like to thank Sophie Martin for giving me the opportunity to do my PhD in her lab. My gratefulness goes beyond the typical obligation to thank one's supervisor, because I truly believe, you were the right one for me, and I am truly amazed that random interaction allowed for us to find each other. You raised me as a scientist in a rare mix of both complete trust and availability, never looking over my shoulder, but always excited to discuss the ever so complex details of Science. In the whole, I think you found the perfect way to manage someone like me. I know this isn't easy. All the people that crossed and will cross your way are so vastly different and you have to adapt to all of us in so unique a manner. You have done so for me in a way that I can only look back and be thankful, to have learned and grown from such an amazing female scientist model.

Second, I'd like to thank everybody in Sophie's Lab, for tolerating and sometimes even being fond of the grumpy gremlin that I am in the morning.

Omaya, first, you were the greatest supervisor one could hope for. You deserve a long and successful career in Science and I hope you get it, so many people can be blessed with your wonderful supervision. You gave me everything I needed to grow into the scientist that I have become. I owe you every result in that manuscript.

Laura, my lab neighbour, you were, and, frankly, I guess to everyone else that ever crossed your path in this lab, my pillar in the storm. I cannot even begin to list all the reasons that make you so. That would take the whole manuscript with still forgetting stuff. I think there isn't a person in the lab that was so pure towards science than you. Collaborating with you, being trained by you, I never felt threatened, I always felt encouraged, and you did that with so much honesty. For that, and for making my day to day grumpy life in the lab so much happier with your great sense of humour and conversation skills, I truly thank you. You're a truly wonderful human being, a wonderful scientist, and I would be blessed to grow into someone that resemble you.

Cassandre, you were a reassuring and always available presence in Sophie's lab, for which I am so grateful. This isn't a widespread quality and most people, probably me included, don't make you feel welcomed when you ask a question. You made my starting into this lab a cheerful experience I don't think many people can be blessed with. You taught me cloning and if you know the cloning machine I have become, please measure how good you must have been. You are like that in Science, but most importantly, you are like that as a human being. You are so insightful, so clever in such a humane way, and so caring for the people that surround you. I hope your doing so for me didn't take too much from you, because so much of my work is yours to thank for. So much of me is yours to thank for.

Veneta, you were my mom in this lab. You helped me through the most difficult moments of my PhD, but also of my personal life. You're a bright supernova and you resonate in me. You're rare. To be so

amazingly fast and strong, but yet so graceful, so caring and respectful of others is an antithesis that you make true. To evolve surrounded by you made me thrive to offer my best. I have no idea how you do it all, I don't think you sleep, and I am so grateful to have been one of your colleagues, but most importantly, one of your friends.

Laetitia and Vincent, you're the heart of this lab. Always care, even if sometimes it darkens your day. Because you made me feel like it matters what I am doing with you here. I don't wanna dispose of the technical help you provided, because to be honest it probably saved both of my wrists, but your contribution is so much more than that. You were the day to day light in my PhD and that is so much more important than some big technical contribution, because you made sane foundations for me to build upon. The rest could stand because of it. Your chatter made me happy to come to work to laugh with you every day. Please stay as you are.

Aleks, you are an annoying prick. But you are my annoying prick. Thank you for believing in me.

And to all the remaining people that were or are a part of Sophie's Lab, thank you. You made this experience a truly amazing moment.

Third, I'd like to thank everybody in this department that was ever a part of my journey. You made it smooth. A special thanks goes to Nazife and Jeannette because of all the work you do, which saved me tremendous time. I feel you are often forgotten and I'd like to recognize the hidden part you played in this PhD. Thank you.

Last, I'd like to thank my friends and family from France. Each and every single one of you helped made me into the person I am today.

Mathilde, You're my sun. When everything else is dark, when I ate after midnight and I become a very angry gremlin, when I feel so antisocial that I wouldn't talk to anyone, when I feel like I don't have any remaining energy but to sit and cry, I still welcome your voice. I believe you are the most intelligent person I know and I am so grateful you have elected me in a room full of people in that gray and cold September morning to be part of your life. You made me feel chosen. I love everything about you. I truly and completely rely on you. You know me completely. You fill such a unique place in my life. I believe not many people have someone in their life that compares to you. I sometimes tell to other people 'oh, poor you, you don't have a Mathilde'. But I have a Mathilde. And I am so, very, truly, blessed.

Aurélien, thank you for tolerating and making home to a person doing a PhD. I know it's difficult. I am thankful for all the times you took my PhD-jeopardized mental state into account when I was being annoying. I am grateful for the love, the help and the understanding that you provided me. You had by far the worst of me. I like to think you also get the best. You're my new home.

Bita, even though I met you as part of Sophie's Lab, you have become my closest friend here in Switzerland, and will forever be a part of my life. You are a stuborn and beautiful human being. I respect so much about you. I always said, I don't like people who don't have the strength of their opinions. You are not one of them. I found in you a partner in crime in the city of Lausanne. You are my forever +1. I owe what's left of my sanity to you, and I hope you can rely on me as much as I rely on you.

Mom, Dad, thank you for the love, freedom, trust, and guidance you gave me. You made my childhood a dream. I sometimes reflect on how much a parent can mess up its children and wonder at the fact that I

have honestly nothing to hold against you. I am so blessed to have you guys as my parents and be able to say that. Thank you for making Science a place where my ability to make it was never relevant to the matter. Thank you for never doubting me. Thank you for the understanding you gave me during this PhD. Literally Thank you for everything. I hope this work makes you proud to have made me.

Anaïs, you're roughly 50% of my genotype. We grew up together, and there will never be a person in my life with whom I share so much. We may have grown apart along the years, but I hope you know you will always be a part of me. You're my biggest supporter. You never doubted I could make it. I can never thank you enough for that.

To the other Anais in my life, I am blessed to have you as a friend. I love that you care for me in such a way that you are interested in what I do, even though we do widely different things. It makes me feel home. I always feel home when I'm with you.

And to all the other persons in my life, you made so many little contributions in making me who I am. You contributed in your own unique way in that incredibly complicated network that brings me here today. Thank you.

Scientific summary

Regulation of Actin Assembly for the Formation of the Fusion Focus in Fission Yeast

Ingrid Billault-Chaumartin, Department of Fundamental Microbiology

The actin cytoskeleton is a complex and dynamic array of actin filament networks that provide strength to the cell for a vast range of cellular processes, such as division, migration and polarization. These actin networks emerge and self-organize from a common pool of monomeric actin to form structures of surprisingly specific architecture, allowing them to drive distinct cellular properties. How cells succeed is a very fundamental question which the actin field has been trying to tackle.

Schizosaccharomyces pombe (S. pombe), a yeast distantly related to the baking yeast *Saccharomyces cerevisiae*, is a great model to tackle this question as its actin cytoskeleton is organized in only 4 well-segregated actin networks. These are the actin patches, which are branched, heavily cross-linked actin networks which support intake from the extracellular environment; the actin cables, long parallel bundles which serve as tracks for intracellular transport; the cytokinetic ring, an antiparallel contractile network which supports cell division; and the fusion focus, an aster which supports cell-cell fusion by allowing the concentration of hydrolase-containing vesicle delivery at the region of contact between the two cells, which leads to cell-wall digestion. The last three networks all depend on a particular class of proteins for their nucleation, the formins For3, Cdc12 and Fus1, respectively. While the first two formins are relatively well studied, Fus1 has received comparatively little attention.

The work presented here sheds some light on some of the principles that govern actin network self-segregation. First, I showed that competition between proteins binding different actin networks is instrumental in maintaining the respective structural identity of each network. Capping protein is a heterodimer blocking actin filament dynamics at the barbed ends which associates with actin patches. Its deletion leads to an increase of actin incorporation within its cognate actin network, the patches, but also to weak actin cables, cytokinesis defects and fusion delay, thereby also affecting the other three actin networks. Focusing first on the organisation of *S. pombe* fusion focus as model, I showed that this is due to ectopic relocalization of all three formins at the now free actin filament barbed ends in actin patches. This leads to ectopic recruitment of actin binding proteins specific to linear actin structures to the branched actin patches, giving them a dual identity. Thus, insulation of actin structures from each other, for which capping protein is a key factor, is an important mechanism ensuring their unique identity.

While capping protein protects branched structures from the action of formins, how do different formins assemble distinct actin networks? For Fus1, part of the answer lies in its specific actin assembly properties, such as its elongation rate or nucleation efficiency, but also in additional specific properties, which are tailored to the formin's function in organizing its specific actin network. Indeed, I used chimeras between *S. pombe*'s formins to control for expression levels, expression time and regulation. However, the other formins' specific properties couldn't replace the cognate fusion focus formin Fus1. Building up on existing literature, I showed that this was dependent on at least three parameters: the nucleation efficiency, which has to be kept high, the elongation rate, which has to be kept low, and an additional formin property

which, though I was not able to firmly identify, I was able to pinpoint to a specific amino acid within the FH2 domain of the formin.

Third, I was able to show a new and exciting property of the N-terminal regulatory region of Fus1, which might be involved in its regulation. Indeed, I showed that the N-terminal regulatory region of Fus1 is forming clusters when artificially expressed in interphase. The responsible region is a low complexity region which is essential for fusion, and the phenotype resulting from its absence could be entirely rescued by replacing that region by self-assembling domains. Because the function of the fusion focus is to concentrate vesicular release at the zone of contact between the two cells, Fus1 self-aggregation could be instrumental in focalizing this release. I also showed that this self-assembling property was likely to be regulated in the native Fus1 for proper fusion. As a formin's regulation at the proper time and place in the cell is instrumental in assembling and segregating a specific actin network, these findings are an exciting direction for future research.

Résumé scientifique

Régulation de l'Actine dans le Focus de Fusion chez la Levure Fissipare

Ingrid Billault-Chaumartin, Département de Microbiologie Fondamentale

Le cytosquelette d'actine est un ensemble complexe et dynamique de réseaux de filaments d'actine qui fournissent la force nécessaire à de nombreux processus cellulaires, tels que la division, la migration ou la polarisation. Ces réseaux d'actine s'auto-organisent à partir d'une source cytosolique d'actine monomérique commune et forment des réseaux d'architecture spécifique qui leur permettent de supporter des propriétés cellulaires distinctes. Comment les cellules réussissent cette prouesse est une question fondamentale à laquelle la recherche dans le domaine de l'actine tente de répondre.

Schizosaccharomyces pombe (S. pombe), une levure lointainement apparentée à la levure de boulanger *Saccharomyces cerevisiae*, est un très bon modèle pour adresser cette question puisque son cytosquelette d'actine n'est constitué que de 4 réseaux, qui sont bien ségrégés dans la cellule. Ce sont les patches d'actine, qui sont des réseaux d'actine dont les filaments sont ramifiés et hautement interconnectés, et qui contrôlent l'internalisation de nutriments à partir du milieu extracellulaire ; les câbles d'actine, longs faisceau de filaments parallèles qui servent de rails pour le transport intracellulaire ; l'anneau cytokinetique, un réseau contractile de filaments antiparallèles qui sous-tend la division cellulaire ; et le focus de fusion, un aster de filaments d'actine qui contrôle la fusion cellulaire en permettant la concentration à la région de contact entre les deux cellules de vésicules contenant des hydrolases, ce qui mène à la digestion du mur cellulaire. Les trois derniers réseaux d'actine dépendent tous d'une classe spécifique de protéines pour leur nucléation, les formines For3, Cdc12 et Fus1, respectivement. Alors que ces deux premières formines sont relativement bien étudiées, Fus1 a reçu comparativement peu d'attention.

Le travail présenté dans ce manuscrit permet d'apporter quelques éléments de réponse sur les principes qui gouvernent l'auto-organisation des réseaux d'actines. En premier lieu, j'ai pu montrer que la compétition entre des protéines se liant à différents réseaux d'actine était déterminante pour maintenir l'identité propre de chaque réseau. La protéine de coiffe est un hétéro-dimère qui bloque la polymérisation et la dépolymérisation de l'extrémité barbelée des filaments d'actine dans les patches d'actine. Sa suppression conduit à une augmentation de la quantité d'actine incorporée dans son propre réseau, les patches, mais également à une déstabilisation des cables d'actine, à des défauts de cytokinèse et à un délai de fusion. Ainsi, sa suppression affecte tous les réseaux d'actine, pas seulement celui dans lequel la protéine de coiffe est impliquée. En prenant d'abord l'organisation du focus de fusion chez *S. pombe* comme modèle d'étude, j'ai montré que cela était dû à une relocalisation ectopique des trois formines de *S. pombe* aux extrémités barbelées des patches d'actine, libérées par l'absence des protéines de coiffe. En conséquence, des protéines accessoires spécifiques des réseaux d'actine linéaires sont relocalisées dans le réseau dendritique des patches d'actine, ce qui leur confère une identité double. Ainsi, l'isolation entre les différents réseaux d'actine, pour laquelle la protéine de coiffe est clé, est un important mécanisme qui assure que chaque réseau conserve son identité propre.

Tandis que les protéines de coiffe protègent les réseaux dendritiques de l'action des formines, comment différentes formines assemblent-elles des réseaux d'identité distincte ? Pour Fus1, une partie de la réponse repose sur ses propriétés spécifiques d'assemblage de filaments d'actine, telles que sa vitesse d'élongation ou son efficacité de nucléation, mais aussi sur une propriété spécifique à Fus1, l'ensemble étant adapté à construire le réseau d'actine spécifique qui sous-tend sa fonction. En effet, j'ai utilisé des chimères entre les différentes formines de *S. pombe* pour controler le niveau d'expression de la chimère impliquée dans la formation du focus de fusion, le moment auquel elle était exprimée ainsi que sa régulation, variant seulement les autres propriétés de ces chimères. Cependant, aucune des autres formines n'était capable de remplacer Fus1 dans son rôle d'organisatrice du focus de fusion. En me basant sur la littérature existante, j'ai montré que cela dépendait d'au moins 3 paramètres : l'efficacité de nucléation, qui doit être maintenue haute, la vitesse d'élongation, qui doit rester basse, et une propriété additionnelle qui, bien qu'elle n'ait pas pu être formellement identifiée, a pu être restreinte à un acide aminé spécifique dans le domaine FH2 de la formine Fus1.

Troisièmement, j'ai découvert une nouvelle et passionnante propriété de la région N-terminale de Fus1, qui pourrait être impliquée dans sa régulation. En effet, j'ai montré que la région N-terminale de Fus1, lorsqu'exprimée artificiellement en interphase, dictait la formation de clusters. La région responsable est une région de faible complexité qui est essentielle pour la fusion cellulaire. Les effets de son absence peuvent être complètement annihilés par le remplacement de cette région par des séquences dictant des propriétés d'auto-association. Puisque la fonction du focus de fusion est de concentrer le transport vésiculaire à la région de contact entre les deux cellules, les propriétés d'auto-association de Fus1 pourraient être cruciales pour focaliser ce transport. J'ai également montré que cette propriété d'auto-assemblage était probablement régulée dans la protéine native. Puisque la régulation d'une formine au bon endroit et au bon moment dans la cellule est déterminante pour ségréger dans le temps et l'espace une structure spécifique d'actine, ces résultats fournissent une direction fascinante pour la recherche future.

Public summary

Regulation of Actin Assembly for the Formation of the Fusion Focus in Fission Yeast

Ingrid Billault-Chaumartin, Department of Fundamental Microbiology

How does a cell succeed in assembling multiple actin networks whose architecture, mechanical properties, localization and function are distinct from a common cytosolic pool? This is a fundamental question to which this work provides some answers, by using the fission yeast, a distant cousin from the baker's yeast, and its actin cytoskeleton during cell-cell fusion as a study model.

The actin cytoskeleton is a set of actin filament networks which provide its strength to the cell for numerous cellular mechanisms such as division or migration. In the fission yeast, this cytoskeleton consists of only 4 structures, or actin networks, while mammalian cells organize many more networks. This makes the fission yeast a great model to answer this question. In particular, this organism assemble actin patches for external resources internalization, actin cables for intracellular transport, an actin ring for cellular division, and an actin focus for cell-cell fusion. Each structure has its own specific nucleator, a protein which serves to allow actin polymerization without delay. For the fusion focus, this nucleator is the formin Fus1, and the actin cables and the actin ring are nucleated by proteins of the same family. Each network is decorated by a specific set of accessory proteins, which characterizes the network.

In this work, we were able to contribute in answering the previous question in three ways. First, we showed that competition between proteins belonging to distinct actin networks is essential in maintaining isolation between those different networks. In particular, we showed that each of the fission yeast formins is protected from an ectopic actin patch localization by a patch resident protein called capping protein. Second, we showed that the unique properties of the formin Fus1 were crucial for the realization of the fusion focus function. In particular, the nucleator's actin assembly properties, such as the efficiency with which it initiates actin filaments, or the speed with which it elongates them, are determinant for the fusion focus formation. To change them results into a network of distinct architecture, unable to support cell-cell fusion. In addition, the N-terminal region of a formin is important for its functional regulation. We showed that this region contains self-assembly properties in Fus1, which are essential for the fusion focus function.

Résumé grand public

Régulation de l'Actine dans le Focus de Fusion chez la Levure Fissipare

Ingrid Billault-Chaumartin, Département de Microbiologie Fondamentale

Comment une cellule réussit-elle à assembler plusieurs réseaux d'actine dont l'architecture, les propriétés mécaniques, la localisation et la fonction sont distinctes, à partir d'un réservoir cytosolique commun? C'est la question fondamentale à laquelle nous avons apporté quelques éléments de réponse dans ce travail, en prenant pour modèle d'étude le cytosquelette d'actine pendant la fusion cellulaire chez la levure fissipare, une cousine éloignée de la levure de boulangerie.

Le cytosquelette d'actine est un ensemble de réseaux de filaments d'actine qui confère aux cellules leur force dans de nombreux mécanismes cellulaires, tels que la division, ou la migration. Chez la levure fissipare, ce cytosquelette s'organise en seulement 4 structures, ou réseaux d'actine, contre beaucoup plus pour une cellule humaine. Cela en fait un très bon modèle pour répondre à cette question. En particulier, elle assemble des patches d'actine pour l'internalisation de ressources externes, des câbles d'actine pour le transport intracellulaire, un anneau d'actine pour la division cellulaire, et un focus d'actine pour la fusion cellulaire. Chaque structure possède son nucléateur spécifique, une protéine qui permet à la polymérisation de commencer sans délai. Pour le focus de fusion, il s'agit de la formine Fus1. Les câbles et l'anneau sont également nucléés par des formines. Chaque structure possède également son lot de protéines accessoires, qui la caractérisent.

Dans ce travail, nous avons pu apporter trois éléments de réponse à la question précédente. En premier lieu, nous avons pu montrer que la compétition entre des protéines de réseaux d'actine différents était cruciale pour maintenir l'isolation entre ces différents réseaux. En particulier, nous avons montré que chacune des formines était protégée d'une localisation ectopique aux patches d'actine par une protéine résidente des patches appelée protéine de coiffe. Nous avons ensuite montré que les propriétés uniques de la formine Fus1 étaient déterminantes pour la réalisation de la fonction de son réseau. En particulier, les propriétés d'assemblage de ce nucléateur, telles que l'efficacité avec laquelle il initie des filaments ou la vitesse à laquelle il les allonge, sont cruciales dans la formation du focus de fusion. Les modifier conduit à un réseau de structure distincte, incapable de supporter la fusion cellulaire. De plus, la partie N-terminale d'une formine est cruciale pour une régulation fonctionnelle. Nous avons pu montrer que cette région contient des propriétés uniques d'auto-assemblage chez Fus1, qui sont essentielles à la fonctionnalité du focus de fusion.

Table of contents

1. Introduction

1.1 Fission yeast cell-cell fusion

Cell-cell fusion is an essential process which occurs in all eukaryotes for sexual reproduction and in many organisms during development, as for myoblast fusion for muscle formation. In general, three major steps are needed for efficient cell-cell fusion. First, communication occurs between future partner cells. Second, partners polarize towards each other for pairing. Third, a fusion machinery is assembled at the cell contact site to enable membrane merging. In walled cells, such as fungi, local cell wall digestion is further required to enable plasma membrane apposition. In this section, I will first develop why I chose *Schizosaccharomyces pombe* (*S. pombe*) as a model organism to study the fundamental mechanisms underlying cell-cell fusion. I will then overview the current knowledge on cell-cell fusion's three aforementioned steps in *S. pombe*.

1.1.1 Fission yeast as a model system

Yeasts belong to the Fungi kingdom, which can be roughly separated in two main groups, the *Ascomycetes* and the *Basidiomycetes* (Figure 1.1) (Lecointre et al., 2017), and are distinguished from other fungi by their unicellular, rather than mycelial cell-cycle (Naranjo-Ortiz & Gabaldón, 2019). *Ascomycetes* are distinguished by their sexual spores being formed within a specialized structure called ascus, the latin word for bag, while *Basidiomycetes* reproduce sexually via the formation of specialized club-shaped end cells called basidia that normally bear external meiospores (Naranjo-Ortiz & Gabaldón, 2019). Many fungi used as laboratory organisms, such as *Saccharomyces cerevisiae* (*S. cerevisiae*), or budding yeast, the world-wide known bread making and brewing yeast, *S. pombe*, or fission yeast, our interest here, or *Aspergillus* and *Neurospora* are *Ascomycetes*. In contrast, most fungi encountered in the macroscopic world are instead belonging to the *Basidiomycetes* group (Hoffman et al., 2015).

S. pombe is a unicellular rod-shaped organism about 3.5 µm wide, whose length vary from 7 to 14 µm during exponential growth, which grows by tip elongation and divides by medial fission, hence its nickname (Vyas et al., 2021). It can be grown between 18° and 36°C on minimal and/or rich media with a generation time ranging from 2 to 4 hours (Hayles & Nurse, 2018). It was initially observed and isolated by Saare and colleagues from contaminated millet beer (Hayles & Nurse, 2018). It can be found in various natural sources such as fruit, syrup or kombucha and is also used to make distilled spirits or to reduce acidity in wines (Vyas et al., 2021). It is a member of a small clade currently consisting of four species, *S. pombe*, *S. japonicus*, *S. cryophilus* and *S. octosporus* (Ács-Szabó et al., 2018; Helston et al., 2010; Sipiczki, 2000) (Figure 1.1), which have all been sequenced. In fact, *S. pombe* is the sixth eukaryote model organism to have its genome sequence and annotation published in 2002, and its 3-chromosomes 14-Mb genome has more than 5000 protein coding genes annotated, 67% of which are conserved in humans (Wood et al., 2002). It is a haplophasic organism meaning it spends most of his life, contrary to mammals or *S. cerevisiae*, in its haploid phase (one copy of each chromosome) rather than its diploid phase (two copies of each chromosomes), which is limited to the very short zygotic phase (Hayles & Nurse, 2018). In the lab, though, diploids can be obtained and propagated under specific circumstances (Hayles & Nurse, 2018). Its life cycle

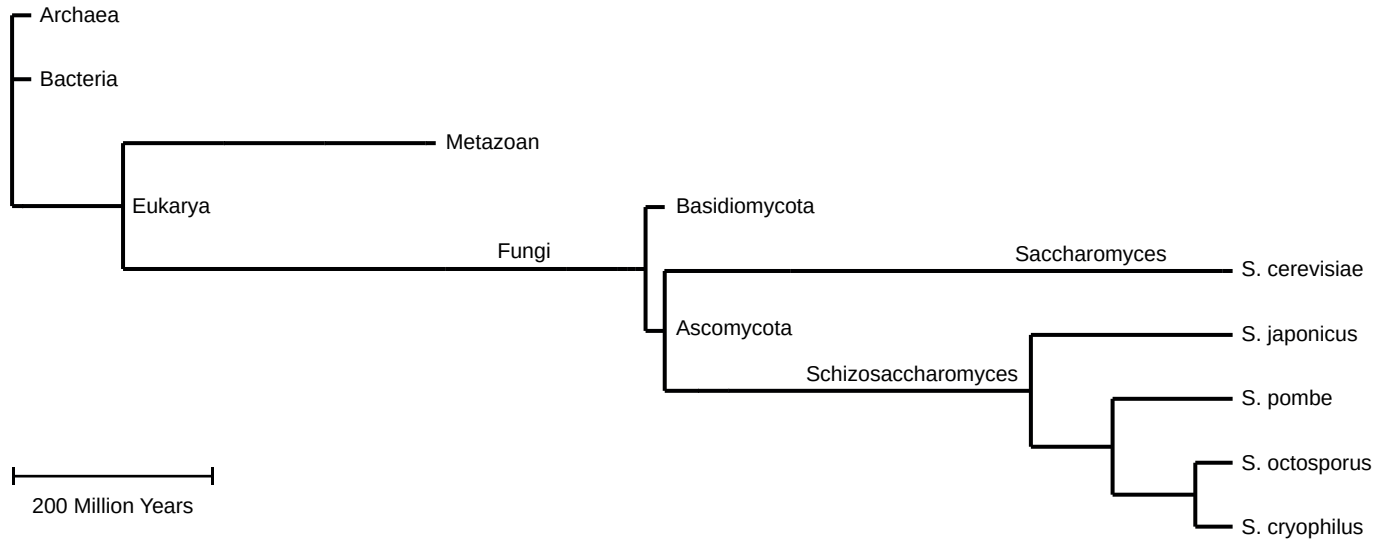

Figure 1.1 Simplified phylogenetic tree of *Saccharomyces cerevisiae* and *Schizosaccharomyces pombe* (adapted from Lecointre et al., 2017)

Consensus phylogenetic tree tracing the divergence distance between *S. pombe*, *S. cerevisiae* and Metazoans, rendered using Biopython (Phylo package) library. The age of Fungi and Metazoans last common ancestor (Opisthokonta) is estimated to be about 1100 Millions years (My) (Dohrmann & Wörheide, 2017) whereas the one of *S. pombe* and *S. cerevisiae* (Ascomycota) is estimated to be 531 My (Shen et al., 2020). Among Schizosaccharomyces, *S. cryophilus* and *S. octosporus* last common ancestor is younger (divergence time estimated about 32 MY (Ács-Szabó et al., 2018)) than the one shared with *S. pombe* (119 MY (Ács-Szabó et al., 2018)) or with *S. japonicus* (Sipiczki, 2000).

consists of an asexual, or vegetative (mitotic) phase and a sexual (meiotic) phase (Hoffman et al., 2015) (Figure 1.2).

The mitotic cell cycle consists of consecutive G1 (each chromosome has one chromatid), S (replication), G2 (each chromosome has two chromatids), and M (mitosis) phases (Vyas et al., 2021) (Figure 1.2). As replication takes place very soon after mitosis, such that the G1 phase is very short and essentially takes place between mitosis and cell separation, with two unreplicated nuclei present in the cell until the septum is cleaved, virtually every newborn daughter is already in G2, containing fully replicated chromosomes (Hoffman et al., 2015). After cytokinesis, cells remain in G2 for about $3/4^{th}$ of the cell cycle, leading up to the next mitosis. New born cells grow from their average 7 µm length to their average 14 µm before division by tip elongation without width change, in a regulated manner during the cell cycle (Hayles & Nurse, 2018). Upon entry into mitosis, cell growth stops as actin is delocalized from the growing ends to relocate to the cell center and an actomyosin band forms over the nucleus, defining the future site of cytokinesis. In newly divided daughters, actin then becomes relocated to the old end, the end that was already present in the mother cell. Later in the cell cycle, actin, and then growth, also becomes localized to the newly formed end. This is known as the New End Take Off (NETO). The size at which cells enter mitosis is modulated by environmental cues such as nutrient levels and stress. In poor nutrient conditions, cells divide at a smaller size (Hayles & Nurse, 2018).

Two mating types exist in *S. pombe*, *h+* and *h-*. As *S. pombe* is an isogamous species, those two mating types produce gametes of similar morphology which respond to each other by differential pheromone and associated receptor expression. In the wild, though, most strains are homothallic, or *h90*, meaning that they are able to switch mating types along mitotic divisions, creating a population mixture of the two mating

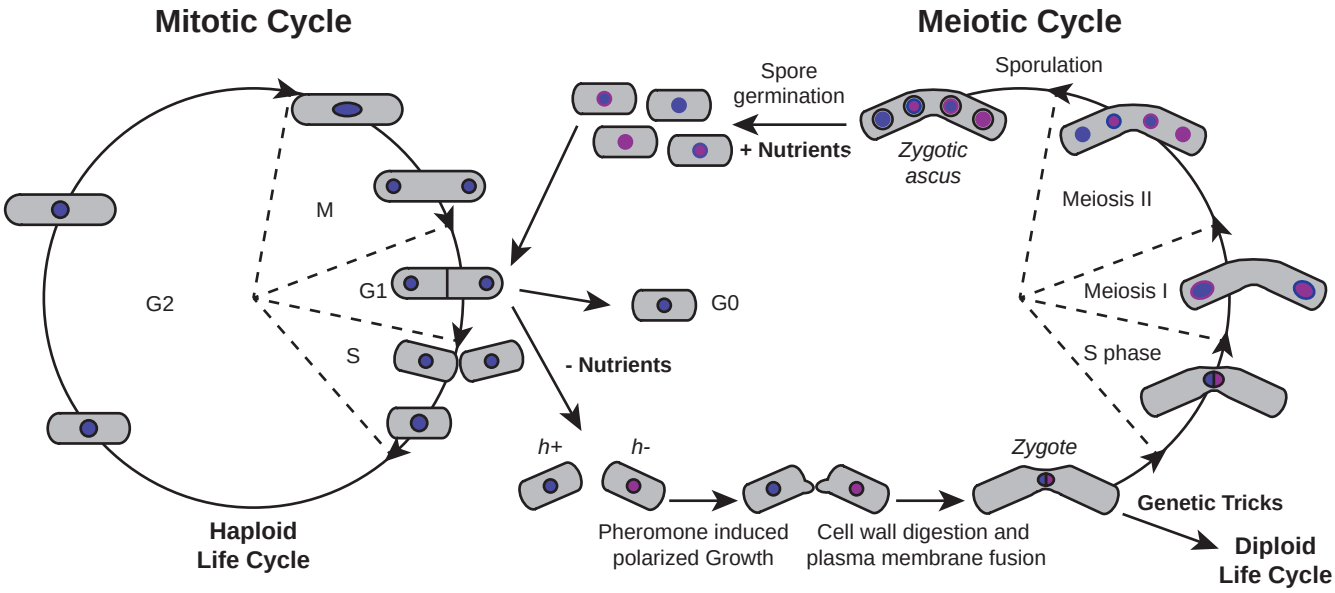

Figure 1.2 Summary of the life cycle of *S. pombe* in haploid states, through the vegetative and sexual reproduction stages (adapted from Vyas et al., 2021)
Fission yeast cells are usually in the haploid life cycle and can shuttle between the vegetative (mitotic) and sexual reproductive (meiotic) cycles. Mating can be triggered between cells of opposite mating types (*h+* and *h-*) through stress such as nutrient deprivation, resulting in the brief generation of a zygote that can undergo the meiotic cycle to produce four zygotic spores which will germinate once nutrient availability improves. However, by use of genetic tricks, it can enter and sustain itself as a diploid cell.

types. This happens because *pombe* cells possess three copies of the mating locus, a silent one containing the *h+* sexual information, another silent one containing the *h-* sexual information, and the last, the only one expressed, one or the other, as these cells can transfer genetic information from either silent locus to the expressed locus (Hoffman et al., 2015). The sexual life cycle is entered in nitrogen-limiting conditions (Figure 1.2). Cells become arrested in G1 and cells of opposite mating type grow in a polarized manner in the direction of their partner and undergo cellular fusion and nuclear fusion, or karyogamy, to form a diploid zygote, known as a zygotic ascus (Merlini et al., 2013). Soon after, the nucleus then enters the meiotic pathway, following which four haploid nuclei are generated and enclosed in a cell wall, thereby forming four spores included within the zygote shell, during the process of sporulation. These zygotic asci typically have a bent shape that reflects the angle between the two cells that fused to generate the zygote (Hoffman et al., 2015). Upon return to rich conditions, the ascus cell wall lyses, the spores germinate and develop into vegetative cells that return to the mitotic life cycle (Figure 1.2).

S. pombe diverged from *S. cerevisiae* approximately 500 million years ago (Shen et al., 2020), while fungi diverged from metazoans about 1 billion years ago (Dohrmann & Wörheide, 2017). The evolutionary distance between *S. pombe* and *S. cerevisiae* is then only half of their respective distance from mammals such as humans (Figure 1.1). In addition, *S. pombe* has retained more ancestral traits than *S. cerevisiae* since their divergence from their common ancestor (Hoffman et al., 2015). Indeed, the proteomic content of *S. pombe* is closer to the common ancestor with *S. cerevisiae* losing more than 300 genes and several biological processes that are conserved between *S.* pombe and complex eukaryotes.

Establishment of fission yeast as an experimental laboratory organism traces back to Urs Leupold. In the 1940s, he developed *S.pombe* for genetic analysis as part of his PhD project (Hayles & Nurse, 2018).

The strains he derived originated from rancid wine and are both homothallic *h90* and heterothallic *h+* and *h-* strains, from which almost all currently used modern strains have been derived. Leupold founded *S. pombe* as a model organism but also established the basis for the nearly isogenic background of all the strains used in research, thereby ensuring the consistency of data from different labs worldwide. These early steps in the development of *S. pombe* as a model organism were followed by Murdoch Mitchison, and for the following two decades the *S. pombe* field was dominated by Leupold and Mitchison and later by their scientific progeny, among which Paul Nurse (Hoffman et al., 2015). During the following decades, *S. pombe* research expanded worldwide, which led to the first international Fission Yeast meeting in 1999, still running today. Since then, *S. pombe* attractiveness as a model organism has only grew, as shown by the increase in fission yeast publications over the years.

S. pombe displays an important number of properties that makes it particularly well suited as a model organism. *S. pombe* relative closeness to higher eukaryotes is one of the important traits that make *S. pombe* a good model organism, as it can be used to study fundamental processes conserved from yeast to humans (Hoffman et al., 2015). However, as *S. pombe* is a unicellular organism, those processes can be studied at the scale of the complete organism with its rich physiology rather than the arguably less physiologically relevant mammalian immortalized cell cultures. The fact that *pombe*'s whole organism is one cell means one can work with extremely large numbers of individuals. One can alter the composition of the growth medium and vary the growth conditions to allow for the discovery of genes involved in a wide variety of processes. Importantly, and much more than mammalian cell lines, *pombe* possesses a vast range of genetic tools to do so. In particular, *pombe* has a highly active homologous recombination mechanism (Hoffman et al., 2015), as 1cM in genetic distance (a measure of meiotic recombination) is approximatively 1 million bp in human but only 6250 bp in *pombe*, which allows the direct introduction of foreign or modified pieces of DNA in targeted places in the genome. This allows one to construct gene deletions, translational fusions or even specific mutants. In addition, the fact that *pombe* is both primarily haploid, but can also be readily amenable to a diploid state is a tremendous advantage in genetics studies (Hoffman et al., 2015). Indeed, any recessive trait which would be hidden by the dominant wild-type allele is readily displayed in a haploid organism. On the other hand, any dominant allele, especially in essential genes, can be studied using the diploid strain.

S. pombe's typical eukaryotic cell cycle, highly polarized growth pattern (which allows the position in the cell-cycle of a single cell to be fairly accurately determined by cell length measurement) and defined shape makes *pombe* a particularly useful model to study mitotic or meiotic cell cycles, cell shape, cellular growth and morphology. In particular, fission yeast is an excellent model for meiosis (Hayles & Nurse, 2018), as it is so easily amenable by switching growth media, and the transition from mitotic to meiotic cycles is a straightforward example of cellular differentiation in a highly malleable model system. In addition, as switching from vegetative to sexual cycles requires cell-cell fusion in all eukaryotes, *S. pombe*'s characteristics make it a great model to study cell-cell fusion. *S. pombe*'s most famous studies are in the area of cell cycle control. In particular, Paul Nurse received the Nobel prize for its discovery of cell cycle regulatory molecules in *S. pombe* in 2001. He showed that the highly conserved Cyclin Dependent Kinases (CDK) were required at control points between cell cycle phase transitions to regulate the timing and size at which cells undergo those transitions (Nurse & Thuriaux, 1980).

S. pombe's conservation of chromosomal features, such as telomeres, centromeres, origins of replication and heterochromatin, which can be formed by both RNAi-dependent and RNAi-independent pathways (Cam & Whitehall, 2016), makes fission yeast a valuable model for the study of eukaryotic chromatin remodeling and centromere function and a key model for the study of biological mechanisms in the area of chromosome dynamics. Indeed, chromosome replication, recombination, and segregation are areas in which *S. pombe* research has played a central role. *S. pombe* also retains degenerate splice site sequences and exonic splicing enhancers, contrary to *S. cerevisiae*, and possesses a relatively simple spliceosome, which makes it a good model organism for research in that area (Fair & Pleiss, 2017). The diversity of silencing mechanisms at the mating locus, telomeric and centromeric regions, also make *pombe* a good model organism to decipher epigenetic gene silencing mechanisms (Hoffman et al., 2015). In particular, *S. pombe* centromeres have helped to establish a "histone code" that associates specific posttranslational modifications of histones with the transcriptional state of the associated chromatin (Jenuwein & Allis, 2001).

1.1.2 Activation of the mating pathway

S. pombe sexual differentiation is triggered by nitrogen starvation. This environmental cue triggers a vast array of cellular responses (Otsubo & Yamamoto, 2012). First, it triggers the arrest of the cells in G1 phase, which is the only pheromone signaling permissive phase. Second, it activates Ste11, the master transcription factor activator of pheromone signaling. Third, it represses the TORC1 and cAMP pathways, which normally repress the transcription factor Ste11 during vegetative growth. Ste11 binds the specific DNA binding motif TTCTTTGTTY, thereby triggering the activation of numerous targets (Mata & Bähler, 2006; Xue-Franzén et al., 2006). In particular, it induces the expression of mating type specific pheromones P-factor and M-factor. P-factor, expressed by the *h+* cell, is soluble and is delivered to the extracellular environment through the secretory pathway, while M-factor, expressed by the *h-* cell, is lipidated and is then secreted through its cognate receptor Mam1, whose expression is also triggered by Ste11. Ste11 also induces the expression of pheromone receptors Map3 and Mam2, and of itself. Receptor Map3, expressed by the *h+* cell, recognizes the M-factor produced by the *h-* cell and receptor Mam2, expressed by the *h-* cell, recognizes the P-factor produced by the *h+* cell. Pheromone binding leads in both mating types to the activation of the receptor.

Both receptors are D-class G protein coupled receptors (GPCRs). GPCRs are a large class of seven pass transmembrane receptors which transduce external signals into intracellular responses and are bound to coupled G proteins, composed of a heterotrimeric Gαβɣ complex (Weis & Kobilka, 2018). When a ligand binds to those receptors, it triggers a conformational change which allows it to act as a guanine nucleotide exchange factor (GEF, activator of GTPases) by promoting the exchange in the coupled G protein of GDP for GTP, thereby activating the protein. The activation results in the GTP bound Gα splitting from the Gβɣ, both of which mediate intracellular responses. In *S. pombe* however, only the Gα, Gpa1, is clearly identified and acts as the main signal transducer. The Gɣ is unknown and the Gβ is only suspected to be Gnr1, which doesn't seem to be involved in activating the downstream pheromone pathway but instead may act as a repressor.

At the core of the pheromone signaling pathway lies the Mitogen-Activated Protein Kinase (MAPK) pathway (Merlini et al., 2013). This pathway consists in a succession of activating phosphorylation events from the MAPKKK Byr2, through the MAPKK Byr1 to the MAPK Spk1 (Figure 1.3A). Its activation requires multiple inputs (Tu et al., 1997). First, the activated Gα Gpa1 indirectly activates Byr2, presumably through mating-specific MAPK cascade adaptor Ste4, which interacts with Byr2 (Barr et al., 1996; Ramachander et al., 2002). Indeed, *Kluyveromyces lactis* Ste4 homologue also binds the Gα in addition of the MAPKKK (Sánchez-Paredes et al., 2011), suggesting that in *S. pombe* Ste4 might directly translate Gpa1 activation to Byr2. Second, Ste11 activates the transcription of *ste6*, encoding a mating-specific GEF for Ras1 GTPase. Ras1 will both directly activate Byr2 and activate Scd1, the GEF for Cdc42, the polarity Rho GTPase in all eukaryotes. As a result, Cdc42 will become activated and further activate the MAPK pathway through its effector Pak1, a p21-activated kinase (PAK). In turn, downstream MAPK Spk1 will lead to the activation of Ste11 (Kjaerulff et al., 2005), resulting in a feedback loop that ensures cells stay in the sexual differentiation program.

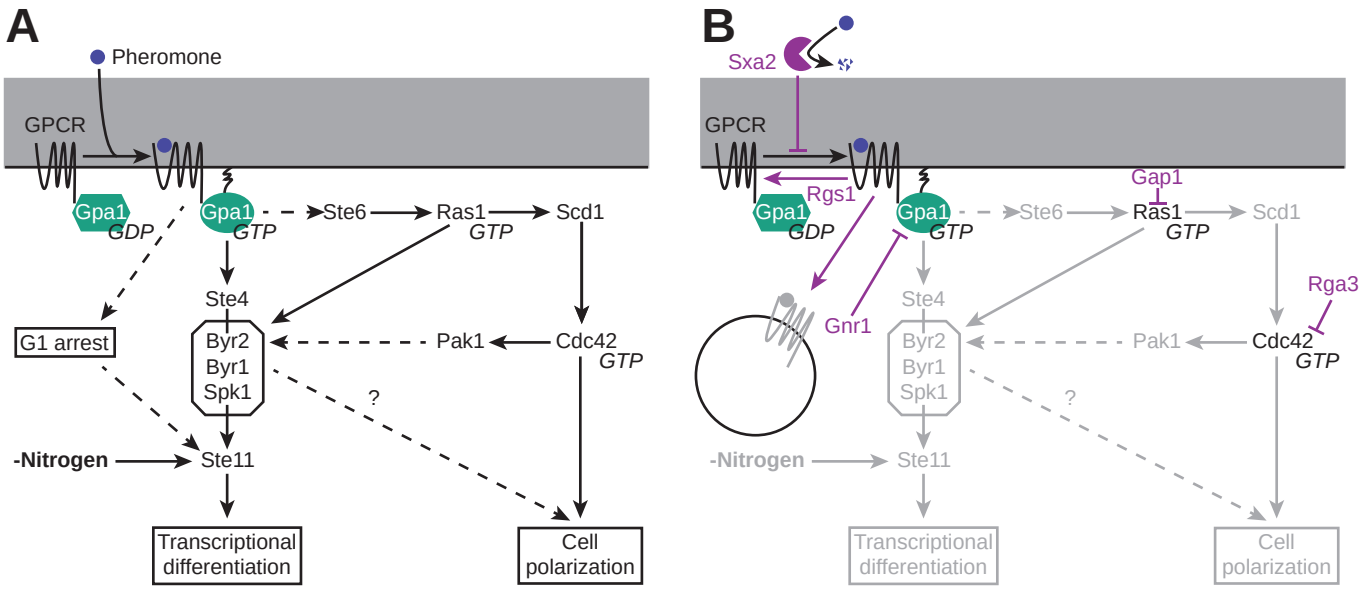

Figure 1.3 Pheromone signaling in *S. pombe* (adapted from Sieber et al., in press)
A. Upon nitrogen starvation, Gα-GTP acts as the main inducer of the pheromone signaling pathway. Activation of Ras1, through its GEF Ste6, induces both the MAPKKK Byr2 (and its scaffold Ste4) and Cdc42 activity through its GEF Scd1. In addition to its key role in cell polarization, Cdc42 also activates Pak1 and thus the MAPK cascade, which triggers Ste11-dependent transcriptional differentiation. **B.** Scheme of pheromone signaling in *S. pombe* as in (B) on which negative controls that prevent hyperactivation of pheromone signaling are indicated.

Regulation of the pheromone signaling pathway is essential for several reasons. First, premature activation would lead to unregulated fusion events, which in a cell under high turgor pressure, could lead to cell lysis (Dudin et al., 2016; Merlini et al., 2018; Seike et al., 2019). Second, pheromone signaling hyperactivation can increase the proportion of sister cell (two daughters just formed after mother cell division) mating (Bendezú & Martin, 2013), which reduces genetic mixing and defeats the purpose of sex. The cell avoids the overactivation of the pheromone signaling pathway in several ways (Figure 1.3B). First, *h+* cells secrete the protease Sxa2, which degrades extracellular P-factor, thereby helping shape the pheromone gradient (Imai & Yamamoto, 1992; Ladds et al., 1996). Second, both receptors cytoplasmic tails

signal for receptor internalization, thereby interrupting the signaling. In addition, Mam2 cytoplasmic tail also recruits Rgs1, a regulator of G-protein signaling which inhibits Gpa1, which also results in signaling interruption (Croft et al., 2013; Hirota et al., 2001). Third, the putative Gβ Gnr1 interacts with Gpa1 which also results in inhibition of pheromone signaling (Goddard et al., 2006).

1.1.3 Polarizing growth towards a mating partner

Decoding shallow chemical gradients along a cell of only a few μm is a biological challenge, as over so short a distance differences in concentration are minimal, representing only a few % between the front and back of the cell (Wu, 2005). Bacteria and mammalian cells have evolved different strategies to tackle this issue. The bigger mammalian cells evolved complex machineries to be able to sense those very small differences in the chemoattractant concentration. They then transduce it into a much steeper intracellular gradient which serves as the basis for polarization. In contrast, the much smaller bacterial cell uses a process of temporal comparison of chemical concentration to regulate runs and tumbles by its flagella.

S. pombe cells, instead, use a trial-and-error mechanism to orient their polarization apparatus towards the gradient by the use of dynamic polarity patches, which contain both the sensing and secretion apparatuses (Bendezú & Martin, 2013; Merlini et al., 2016; Merlini et al., 2018). The polarity patch is mainly composed of the active form of Cdc42, its GEF Scd1 and its scaffold Scd2. In addition, it contains some of the pheromone signaling machinery, such as the Gα Gpa1 and the active form of Ras1. It also contains the secretion machinery including type V myosin Myo52, the Rab GTPase Ypt3 and the exocyst complex (Merlini et al., 2016). Rapid assembly and disassembly of the polarity patch leads to exploration of the cell periphery (Figure 1.4A). At low pheromone concentration, Ras1 GTPase Activating Protein (GAP, inhibitor of GTPases, favors hydrolysis of GTP into GDP) Gap1 strongly inhibit Ras1, which leads to the patch destabilization (Merlini et al., 2016; Merlini et al., 2018). Gap1 is not the sole negative input as Cdc42 GAP Rga3 also contributes (Gallo Castro & Martin, 2018). Instead, at high pheromone concentration induced by the presence of a mating partner, Ste6 induction leads to Ras1 activation which in turns activates Cdc42 and stabilizes the polarity patch (Figure 1.4B) (Merlini et al., 2016).

Once the patch is stabilized, Cdc42 strong activation results in polarized growth, or shmooing, towards the cell partner through several mechanisms likely similar to what happens in interphase cells. First, Cdc42 mediates the activation of the exocyst complex, leading to cell-wall hydrolases delivery at the shmoo tip (Estravís et al., 2011; Zhang et al., 2001). The exocyst complex is a conserved eukaryotic 8-subunit complex (Sec3, Sec5, Sec6, Sec8, Sec10, Sec15, Exo70 and Exo84) implicated in the tethering of secretory vesicles to the plasma membrane prior to SNARE-mediated fusion (Wu & Guo, 2015). Second, Cdc42 activates the actin cables which support long range polarized transport which then coalesce at the shmoo tip. Studies have shown that those two mechanisms are not mutually dependant (Bendezú & Martin, 2011). In particular, Cdc42 is required for glucan synthases Bgs1 and Bgs4 transport to the plasma membrane, which are therefore also recruited to the shmoo tip. Bgs4 is responsible for most of the β-D-glucan that forms the cell wall during growth, while Bgs1 is primarily involved at the septum but also contributes (Cortés et al., 2005; Cortés et al., 2002; Cortés et al., 2007). Both the actin cables and the exocyst contribute to their accumulation at the shmoo tip. A combination of all those Cdc42 effects will lead to cell wall remodelling, which, due to internal turgor pressure, will drive local cell wall expansion and subsequent

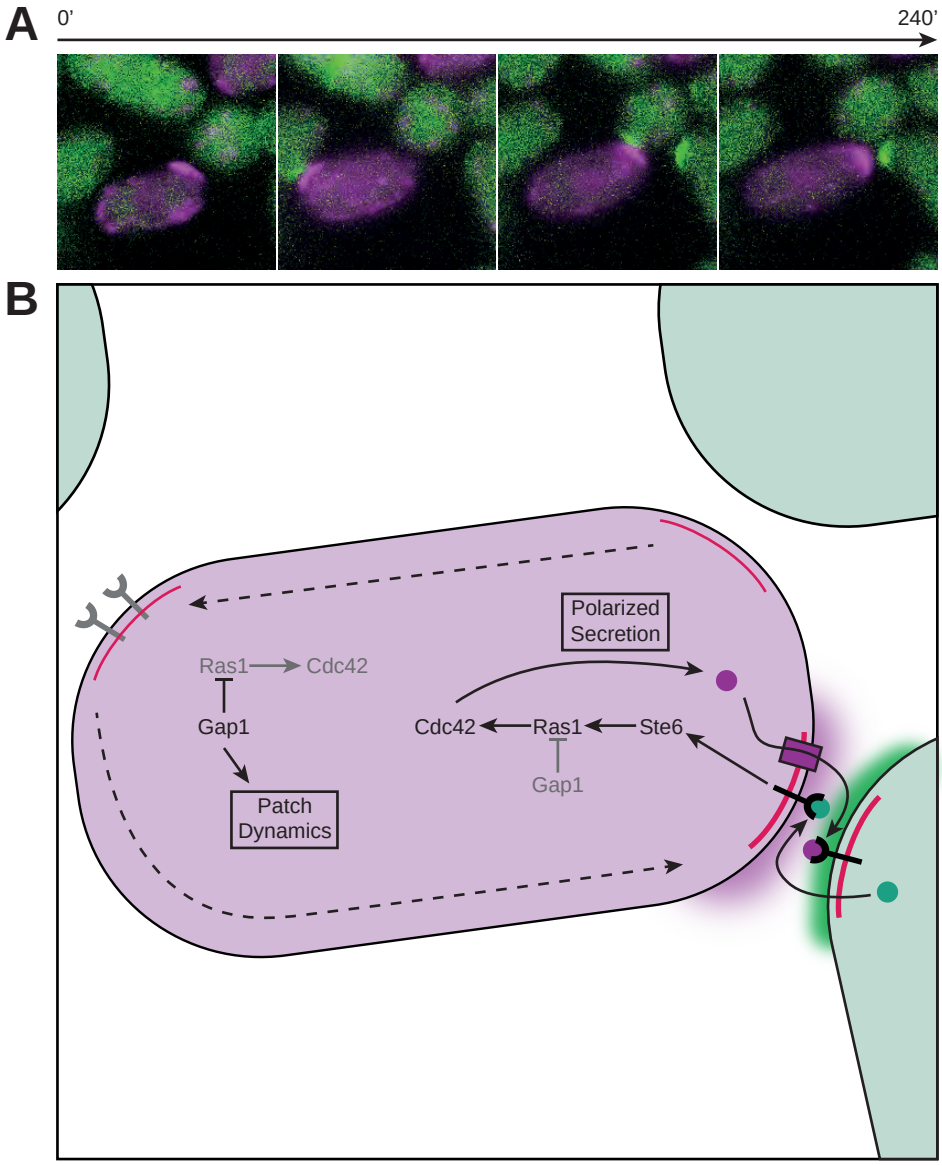

Figure 1.4 Dynamics of the polarity patch in *S. pombe* (adapted from Sieber et al., in press)
A. Assembly-disassembly of the polarity patch with Cdc42 activity (Scd2-mCherry, magenta) in a fission yeast *h-* cell surrounded by *h+* mating partners with labelled polarity patches (Scd2-GFP, green). **B.** The polarity patch moves by assembly-disassembly around the cell, regulated by a competition between positive and negative signaling. When pheromone concentration is low, inhibition by Gap1 leads to disassembly of the patch. In proximity of the patch of a partner, high pheromone concentration overcomes GAP inhibition and triggers signaling via Ras1 and Cdc42, thus supporting local secretion of the components of the pathway, including pheromones. This positive feedback loop between the mating partners ensures patch stabilization and polarized growth.

formation of the shmoo. While those shmoos can occasionally extend over several micrometers, especially in fusion defective strains, the vast majority of cell pairing happens at close range.

1.1.4 Mating Partners Fusion

After cell pairing, cells encased in a cell wall such as yeast must additionally digest their cell wall to put their membrane in contact for cell-cell fusion to occur. This is especially dangerous as these cells are under important turgor pressure, such that any unregulated cell-wall digestion event would lead to lysis

(Hall & Rose, 2019). For example, fission yeast autocrine cells which have been modified to coexpress a pheromone receptor pair and therefore 'believe' that a partner is here, lyse if the sexual differentiation program is launched through nitrogen starvation (Dudin et al., 2016). The cell-wall digestion process is then carefully controlled and involves several steps (Figure 1.5A).

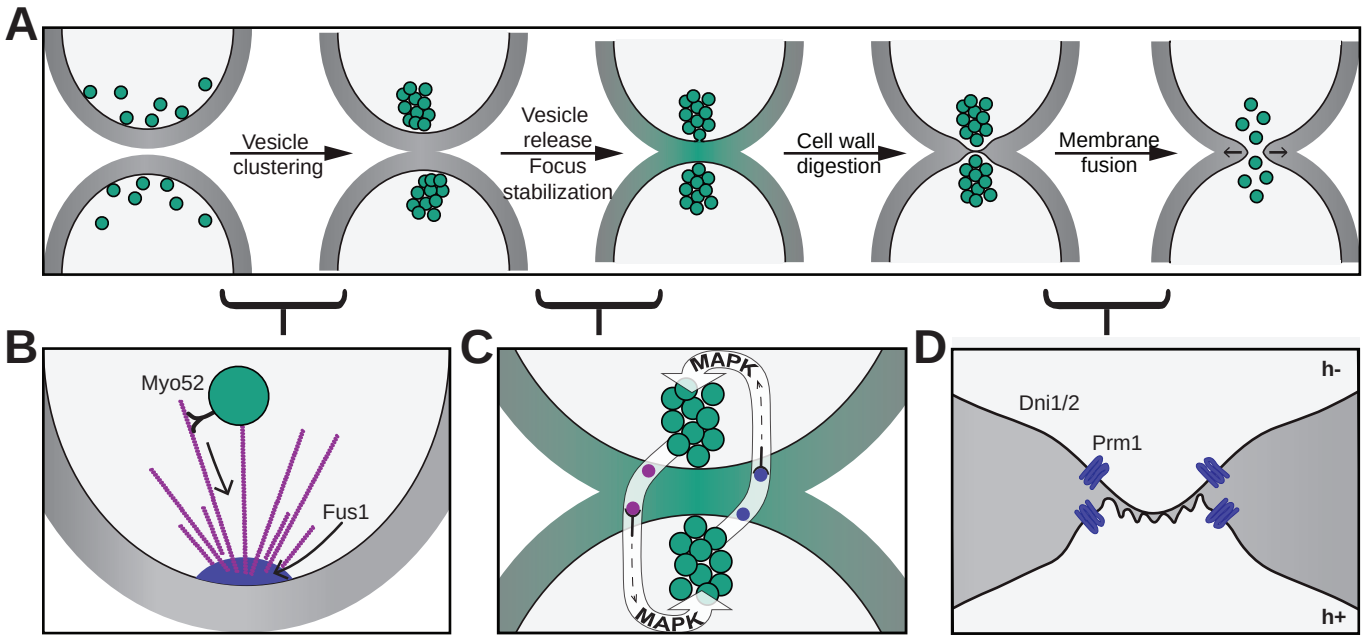

Figure 1.5 Cell-cell fusion in *S. pombe* (adapted from Sieber et al., in press)
A. After polarization of partner cells towards each other, clustering of secretory vesicles at facing positions and release of their content (green) leads to cell wall (grey) digestion. Plasma membranes fuse and the fusion pore expands. Individual panels highlight specific steps. **B.** the mating-specific formin Fus1 (blue) nucleates the fusion focus, an actin aster underlying the clustering of the vesicles brought by Myo52. **C.** Fusion focus stabilization relies on a positive feedback loop, driven by local pheromone secretion and MAPK signaling. This leads to local cell wall digestion. **D.** As the cell wall is digested, fission yeast pairs exhibit a morphological asymmetry, where the *h-* cell membrane protrudes into a wavy, less tense *h+* cell membrane. Prm1 is then important for membrane fusion.

Cell wall digestion involves the clustering and subsequent release of cell-wall hydrolases containing secretory vesicles at the zone of cell-cell contact. This clustering is mediated through a specialized actin structure called the fusion focus in each partner (Figure 1.5B). This structure is nucleated by the mating-specific formin Fus1 and consists of an aster of actin filaments whose barbed ends are likely concentrated at the region of contact between the two cells, which allows directional transport of the secretory vesicles, principally through cellular motor Myo52, a type V myosin (Dudin et al., 2015). As cell-wall hydrolases are delivered and the cell wall is degraded, the distance between each fusion focus is gradually reduced until they join upon fusion (Dudin et al., 2015). Fus1 is essential for cell-wall digestion but is otherwise dispensable for the previous polarization steps.

At the early steps of cell-wall degradation, the actin fusion focus is quite diffuse and is gradually focalized as the process continues. This focalization relies on several mechanisms. First and foremost, Fus1, which itself forms a tight cluster at the region of cell-cell contact through unknown mechanisms, as the nucleator of this actin structure, is strictly required, as in its absence Myo52 decorates the entire shmoo tip (Dudin et al., 2015). Myo52 may even participate in delivering Fus1 to the zone of cell-cell contact, thereby participating in a feedback loop helping focusing actin filaments. Second, both the second type V

myosin Myo51 and associated coiled-coiled proteins Rng8 and Rng9 control the fusion focus coalescence likely through tropomyosin cross-linking of actin filaments (Dudin et al., 2017; Kurahashi et al., 2002), as the absence of Rng8 and Rng9 results in the formation of multiple Myo52 dots at the cell-cell contact site. Then, Myo52 and Myo51 have distinct functions, with Myo52 mainly involved in polarized transport while Myo51 plays a more structural role. Additional actin binding proteins also contribute to the fusion focus focalization, such as profilin Cdc3 (Petersen et al., 1998a) and Calmodulin Cam22 (Dudin et al., 2015).

As cells begin digesting their cell wall, an important regulation is established to ensure the proper timing and place of the digestion to avoid cell lysis, which relies on a feedback loop mechanism between the pheromone signaling pathway components and fusion focus assembly proteins (Figure 1.5C) (Dudin et al., 2016). Indeed, pheromone signaling pathway components, including pheromone receptors, active Ras1 GTPase and components of the MAPK cascade, all concentrate at the fusion focus (Dudin et al., 2016; Merlini et al., 2018). As the actin focalizes in the fusion focus, transported signaling pathway components are further enriched at the zone of cell-cell contact, which further increases the sexual response and leads to further focalization of fusion focus assembly proteins, stabilizing the structure spatially. Then, this feedback loop induces a very biased spatial patterning which is proposed to result in local enrichment of cell-wall hydrolases over cell-wall synthesis, leading to cell-wall digestion (Martin, 2016). Additionally, the feedback loop leads to a new cell-pairing state, where the cells are irreversibly engaged in the fusion process (Dudin et al., 2016). In this committed state, in opposition to the preceding uncommitted state, wash out of external pheromones will not block fusion.

Once the cell-wall is degraded, membranes are put in apposition and membrane fusion occurs (Figure 1.5D). The mechanism of membrane fusion is poorly understood in fungi, but is likely to be mediated by accessory proteins and specific membrane composition to overcome the repulsive forces generated by reducing the gap between two charged membranes (Hernández & Podbilewicz, 2017). In fact, the shmoo tip has been showed to be enriched in ergosterol and phosphatidylinositol 4,5-bisphosphate (Jin et al., 2008; Proszynski et al., 2006), and defects in the ergosterol synthesis pathway have been linked in both *S. cerevisiae* and *Neurospora crassa* to membrane fusion defects (Aguilar et al., 2010; Jin et al., 2008; Weichert et al., 2020). However, to date, no fusogen (defined by being essential and sufficient to promote cell-cell fusion, as removing it in its dedicated cell type would abolish fusion and introducing it in another cell type would be sufficient to promote fusion) has been identified in fungal cell-cell fusion, while such proteins have been extensively described in vesicular or viral fusion (Segev et al., 2018). Instead, plasma membrane fusion requires Prm1, a 4-pass transmembrane protein (Figure 1.5D) (Curto et al., 2014; Heiman & Walter, 2000). Its absence blocks fusion in more than 95% of the pairs and cells form big membrane blebs into the other partner. Aberrant cell-wall persists in between those blebs but is likely resulting from a rapid repair response. Prm1 has been proposed to mediate lipid microdomain formation at the zone of cell-cell contact to promote membrane fusion. Pheromone receptors have also been proposed to promote membrane fusion through heterotypic interaction (Shi et al., 2007). However, those proteins are essential for the earlier mating steps, so that point mutants block cell-cell fusion before cell-wall removal. Membrane tension just before fusion has been shown by electron microscopy to be asymmetric in *S. pombe* (Muriel et al., 2021), as the *h+* partner forms membrane waves while the *h-* partner protrudes into the *h+* (Figure 1.5D). This is

likely the result of an overall asymmetry during the fusion process that starts at the pheromone level (Seike et al., 2019) and results in an unbalanced symmetry between exocytosis and endocytosis in each partner.

After membrane fusion, a succession of events occurs. First, a poorly understood pore expansion mechanism takes place, leading to a zygote with a continuous cytosol in a seamless envelope (Merlini et al., 2013). Next, karyogamy happens, with the two nuclei merging together, forming the diploid zygote (Polakova et al., 2014). Meiosis ensues and leads to the formation of 4 haploid nuclei (Yamamoto, 1996). Those nuclei mature into spores by a process called sporulation (Shimoda, 2004), whereby the nuclei are enclosed in a newly synthetized forespore membrane around which cell-wall is deposited. They stay enclosed in the mother envelope, and the lot is called an ascus. This an extremely resistant stage in which the cell can stay for extended periods of time, ensuring survival until favorable conditions return (Coluccio et al., 2008; Egel, 1977). Upon return to rich media conditions, the spores will germinate (Hatanaka & Shimoda, 2001), thereby rupturing the maternal envelope, resulting in 4 genetically shuffled haploid cells, whose newly acquired genetic diversity will help in adapting to the new environment (Waxman & Peck, 1999).

1.2 Actin Cytoskeleton

The actin cytoskeleton provides the driving force for establishing the astonishing morphological diversity and dynamics of organisms from all domains of life, by supporting a vast array of functions, such as motility, cell division, vesicle motion, and cell shape. Here, I will first present how monomeric actin (G-actin) assembles into filaments. Next, I will provide an overview of the most common of numerous Actin Binding Proteins (ABPs) that control actin assembly in space and time. As this work will mostly center on formin and capping protein, I will give them particular attention. Then, I will discuss how those ABPs assemble together with Filamentous actin (F-actin) to form higher degree structures with specific functions. Last, I will present current knowledge on how those actin networks all interact together through competition for ABPs or monomeric actin.

1.2.1 Actin assembly

Actin is one of the most conserved proteins among eukaryotes, with usually about 90% identity between sequences of actin from different species (Gunning et al., 2015). Small differences in actin sequence can result in significant functional differences. For example, in vertebrates, there is 6 isoforms of actin, each encoded by a specific gene, which are nearly identical, except for a few amino acid substitutions, which have distinct functions and localizations (Vedula & Kashina, 2018). Similarly, plants have 10 or more actin genes, with some specialized for reproductive tissues and others for vegetative tissues (Kijima et al., 2016; Kijima et al., 2018; Slajcherová et al., 2012). Actin is also one of the most abundant proteins in the cell, with levels reaching way beyond 50 µM (Koestler et al., 2009). Monomeric actin is a small 375 amino acids polypeptide composed of two main domains divided into two subdomains each (Figure 1.6) (Holmes et al., 1990). In a deep cleft between the domains, actin is carrying a tightly associated molecule of ATP or ADP with its accompanying cation, usually magnesium (Estes et al., 1992). G-actin is a very poor ATPase, so that no significant hydrolysis occurs in the cell (Rould et al., 2006). The two halves of the protein

flanking the nucleotide binding cleft have similar folds but no sequence similarity, suggesting that a very ancient duplication formed the original actin gene, followed by divergence of the two halves (Pollard, 2016). Overall, while having the shape of a flattened globule, actin is slightly asymmetrical.

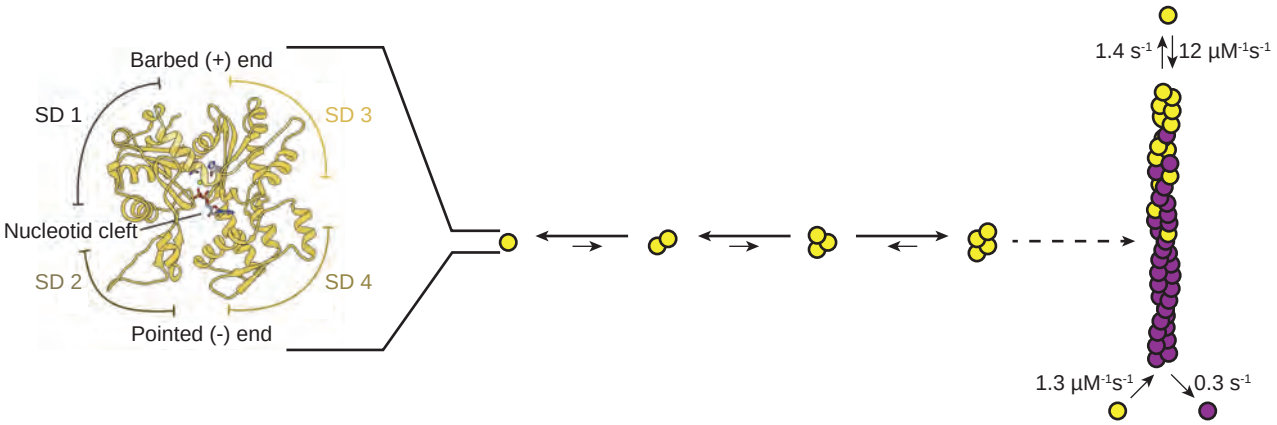

Figure 1.6 Monomeric actin assembly into filamentous actin (adapted from Merino et al., 2020 and Alberts et al., 2014)
(Left) Illustration of monomeric actin domain architecture consisting of four subdomains (SD) and a central nucleotide binding cleft. (Middle) Monomeric ATP-actin (yellow) assemble spontaneously into very unstable dimers and trimers. Addition of a new subunit to the trimer stabilizes the filament which leads to fast elongation at both ends. (Right) Differential monomeric affinity for both ends coupled to ATP hydrolysis (GDP-actin in magenta) leads to preferential polymerization at the barbed end. Relevant kinetic rates are indicated.

Actin subunits assemble head-to-tail to form a tight right-handed helix (Holmes et al., 1990), forming a structure about 8 nm wide called F-actin, slightly changing conformation in the process (Oda et al., 2009). Because the asymmetrical actin subunits all point in the same direction, filaments are polar and have structurally different ends, called pointed end (minus) and barbed end (plus) (Alberts et al., 2014). Within the filament, the subunits are positioned with their nucleotide binding cleft directed toward the minus end. While actin can spontaneously polymerize, dimers and trimers are highly unstable which causes a significant delay in spontaneous actin assembly (Figure 1.6) (Cooper et al., 1983). To shortcut this issue, subunits can be assembled into an initial nucleus or seed, where subunits are stabilized and can then elongate rapidly by addition of more subunits at both ends (Alberts et al., 2014). This process is called nucleation. Once nucleated, in a solution the filament can readily elongate by addition of new subunits at a k_{on} rate dependent on G-actin concentration, while dissociating from it at a concentration-independent rate k_{off}. At high G-actin concentration, this leads to rapid elongation, consuming G-actin until the critical concentration, $C_c=k_{off}/k_{on}$, is reached, where dissociation exactly balances out association.

Because the filament is polar, the two ends behave differently with the minus end being much less dynamic than the plus end (Pollard, 2017). The latter then has much greater kinetic rate constants k_{on} and k_{off}. However, if all the subunits in the filament are in the same nucleotide state, the free energy difference between a polymer of n subunits and n+1 subunits is the same at both ends, and hence the equilibrium constant as well, as the starting and finishing points of the reaction are the same. This means that the ratios between k_{off} and k_{on} at each end are the same in this case, even though their absolute value differ.

However, as the catalytic activity of monomeric actin is enhanced upon incorporation into F-actin as a result of the change in conformation (Blanchoin & Pollard, 2002), the ATP hydrolysis and subsequent Pi

release half time fairly exceeds the incorporation speed at the plus end (Pollard, 2017), such as the plus end is statistically more often in an ATP bound state. In contrast, slower assembly dynamics at the minus end results in a mostly ADP bound state, such as the critical concentrations at both ends are now different, the minus end being greater, as G-actin has a preferential affinity for ATP-bound actin ends (Figure 1.6) (Alberts et al., 2014). Thus, there is a certain range of G-actin concentration where the minus end will shrink while the plus end grows. This property is called treadmilling. At a specific concentration in this range, depolymerisation at the minus end will exactly balance polymerization at the plus end such as the polymer maintains a constant length but experiences a net flux of subunits through the polymer, which requires constant energy consumption in the form of ATP hydrolysis.

F-actin assembly can be perturbed by the use of chemical inhibitors to study their role *in vivo* (Alberts et al., 2014). For example, drugs belonging to the sponge-derived Latrunculin family inhibit F-actin assembly by inducing depolymerisation through binding actin subunits (Spector et al., 1989). Similarly, Cytochalasin B, discovered in fungi, inhibits F-actin assembly by inducing depolymerisation through capping F-actin plus ends (MacLean-Fletcher & Pollard, 1980). In contrast, Phalloidin from Amanita mushrooms stabilizes the filament by binding along its sides, which inhibit actin dynamics (Cooper, 1987).

1.2.2 Actin binding proteins

In the cell, actin filaments behaviour is dramatically altered by ABPs. Collectively, they control the pool of monomeric actin available for polymerization, they sever, destabilize or stabilize filaments, they cap barbed ends or pointed ends to terminate elongation, they nucleate assembly of new filaments, they promote their elongation, they cross-link filaments, and anchor them to the membrane (Figure 1.7). In this section, I will present an overview of the most common ABPs and their function relative to actin.

1.2.2.1 Monomer binders

In most cells, the concentration of monomeric actin vastly exceeds the critical concentration. Cells manage this prowess thanks to a specific set of ABPs which sequester actin monomers, rendering polymerization less favorable (Figure 1.7), an action similar to the drug Latrunculin.

Profilin is one of those ABPs. It is essential for the viability of most eukaryotes, including in *S. pombe* (Balasubramanian et al., 1994). It is present at high concentrations in the cell, and has a high affinity for actin monomers. This means that in the cell, most of the G-actin is bound to profilin. Profilin binds to the barbed end of the actin monomer, thereby blocking the site that would normally associate at the pointed end while leaving the monomer free to bind at the barbed end. If it does indeed bind to the barbed end filament, the resulting conformation change lowers the affinity of actin for profilin, which then dissociates rapidly from the barbed end (Courtemanche & Pollard, 2013). However, high profilin concentration can slow elongation and even promote dissociation of the terminal subunit. Many organisms contain several profilin isoforms, which they differentially express depending on cell types (Honoré et al., 1993; Staiger et al., 1993). The small differences between profilin isoforms are harvested to fulfil different functions (Di Nardo et al., 2000; Kovar et al., 2000; Murk et al., 2012; Neidt et al., 2009). Other activities than the monomer sequestering property of profilin are essential for viability, such as its ability to bind proline

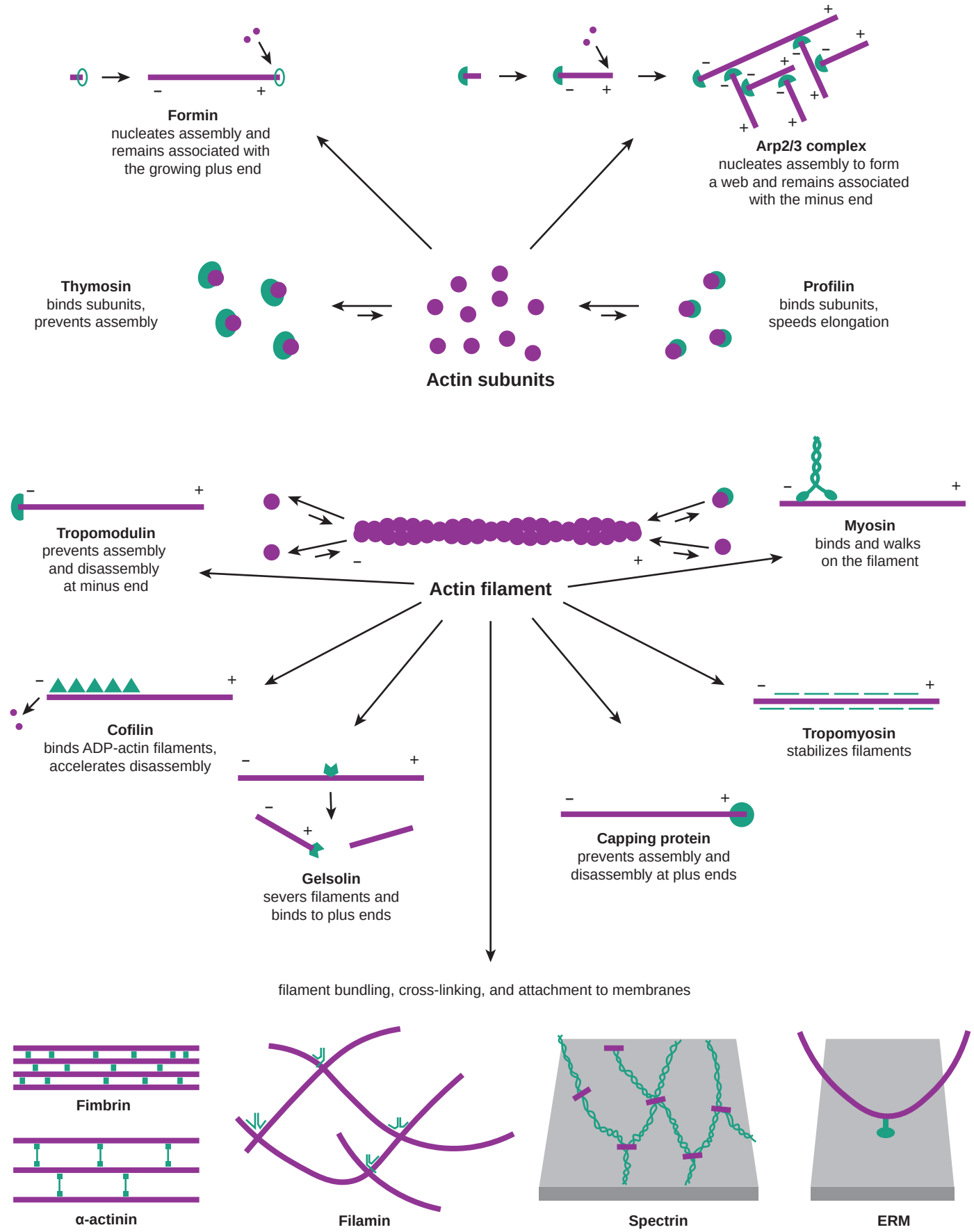

Figure 1.7 Actin binding proteins (adapted from Alberts et al., 2014)
Some of the major accessory proteins of the actin cytoskeleton. An example of each major type is shown. Each of these is discussed in the text. However, most cells contain more than a hundred different actin-binding proteins, and it is likely that there are important types of actin-associated proteins that are not yet recognized.

rich tracks at a site distant from its actin binding site (Archer et al., 1994), or its ability to promote G-actin nucleotide exchange. Profilin encourages the latter by inducing a slight conformation change on G-actin upon binding that opens the nucleotide cleft (Neidt et al., 2009; Porta & Borgstahl, 2012).

In some mammalian cells, such as leukocytes and platelets, the main monomer sequester is a small peptide called thymosin-β4 (Safer et al., 1991). Thymosin-β4 caps the monomer at both ends, thereby completely inhibiting polymerization (Xue et al., 2014). Its binding site on G-actin is then partially overlapping with profilin's, so that they are mutually exclusive. However, thymosin-β4 affinity for actin is lower than profilin's, which can easily recover G-actin by competition and render it available for barbed end polymerization (Crockford et al., 2010).

1.2.2.2 Filamentous actin cappers

Controlling the length of the actin filament is key for many cellular processes, with the most spectacular example being the muscle unit sarcomere, where arrays of F-actin of equal lengths are key for its function. Such result is achieved by the use of filament end cappers (Figure 1.7).

Capping protein (CP) is conserved through the eukaryotic kingdom and is present at high concentrations in the cell. Several variants exist in mammals with different characteristics (Casella & Torres, 1994), while only one is present in *S. cerevisiae* or *S. pombe*. It binds tightly to the barbed end of actin filaments where it prevents polymerization or depolymerisation (Wear et al., 2003). CP is a heterodimer of α and β subunits (Figure 1.8A). Despite very low sequence similarity, α and β subunits exhibit a striking structure similarity, resulting in a CP with a pseudo 2-fold rotational symmetry (Yamashita et al., 2003). Each subunit has 3 subdomains that form the body of the subunit and a C-terminal extension. The 3 subdomains are a N-terminal bundle of antiparallel helices, a β-strands middle domain and an antiparallel β-sheet at the C-terminus, tightly aligned between the two subunits, followed by long α-helixes. The full protein then resembles a mushroom, with the N terminus forming the stalk and the rest of the protein forming the cap. Both subunits tightly interact together and each of them is unstable in absence of the other (Sizonenko et al., 1996).

The flexible C-terminal extensions are called tentacles (Figure 1.8A) and are not involved in dimerization but are responsible for most of the actin affinity (Kim et al., 2004). Indeed, CP binding to actin can be recapitulated in a 2-step model (Figure 1.8B) (Narita et al., 2006). First, the β-body and α-tentacle contact the last two protomers of the actin filament barbed end through electrostatic interaction and together determine the on-rate. Second, hydrophobic interactions between the β-tentacle and the last actin protomer determine the off-rate. Thus, even though both tentacles are involved in the strength of actin binding, the α-tentacle alone is able to cap as it is the only one binding in the cleft between the last 2-protomers that would receive the incoming monomer. Losing both tentacles abolishes all interaction with actin (Kim et al., 2004; Wear et al., 2003), while losing the α-tentacle results in a 5000-fold reduction in affinity *in vitro*. Losing the β-tentacle, however, has a less severe impact with a 300-fold reduction in affinity *in vitro*.

While CP contacts actin through its mushroom-like cap, it contacts most of its inhibitors through its stalk, where a few specific amino-acids interact with what is called a Capping Protein Interaction (CPI) motif (Hernandez-Valladares et al., 2010). CP interaction with CPI motif containing proteins is necessary for CP function *in vivo* (Edwards et al., 2015) as its disruption through the use of specific CP mutants that

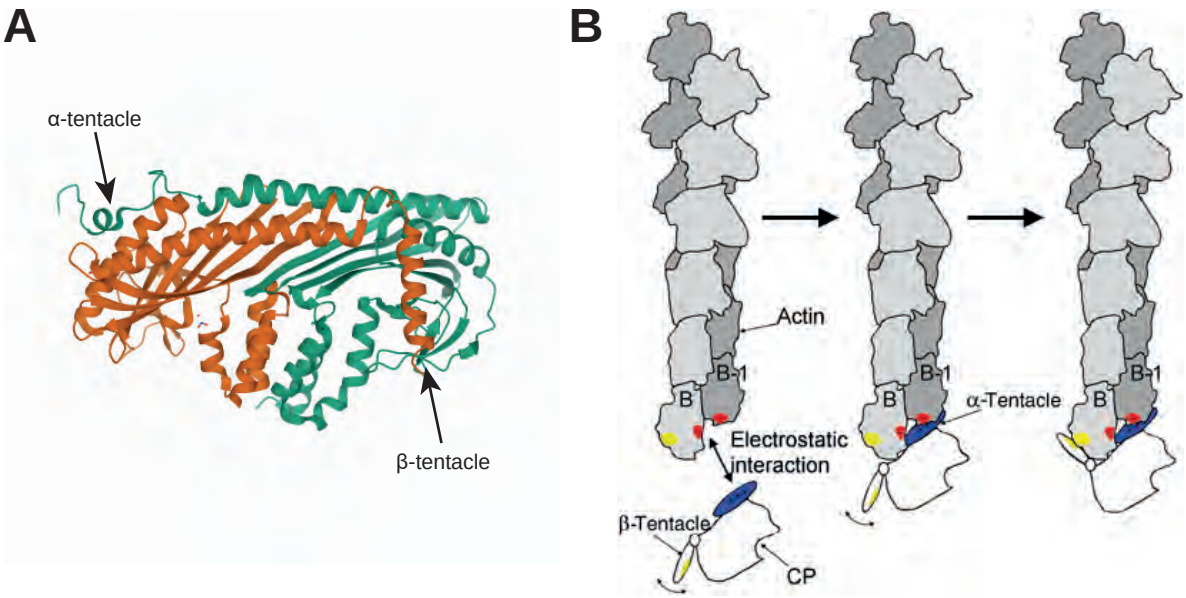

Figure 1.8 Capping protein structure and binding to actin filament barbed end (adapted from Yamashita et al., 2003 and Narita et al., 2006)
A. Crystal structure of chicken actin filament capping protein CapZ. α-subunit is in green and β-subunit is in orange. (PDB 1IZN) **B.** Model for the binding of CP to the actin filament barbed-end. (Left) First, the basic residues on the α-tentacle (blue) and the acidic residues on the bottom of the actin filament (red) attract each other. This interaction should determine the on-rate of the binding. The unbound β-tentacle (yellow) is freely mobile, due to the flexibility at the basal part. (Middle) Second, the α-tentacle binds to the bottom of the actin filament. The β-tentacle remains freely mobile, and searches for its binding position on the actin filament. (Right) The β-tentacle binds to the hydrophobic cleft (yellow) on the outer surface of the end protomer B. This binding reduces the off-rate of the binding, and thereby stabilizes the binding.

retain full ability to bind and cap actin filaments but that lose the capacity to bind the CPI motif produce phenotypes equivalent to the loss of CP in human cells. In binding to the stalk of CP, CPI-motif containing proteins induce a conformational change that lowers CP's affinity for the barbed end. CPI motif containing proteins are a set of otherwise unrelated proteins such as CARMIL or twinfilin (Johnston et al., 2018).

In addition, some factors inhibit CP through steric hindrance of its interaction with actin, because their binding site overlap with the F-actin binding site. One such factor is the vertebrate V-1 or myotrophin (Taoka et al., 2003), which sequesters CP by binding to its actin binding site with high affinity. However, biochemical studies have found that V-1 is not able to actively remove CP from the barbed end and is only acting preventively (Bhattacharya et al., 2006). Another of those factors is phosphatidylinositol 4,5-bisphosphate ($PI_{4,5}P2$). Similarly to V-1, $PI_{4,5}P2$ binds to a basic patch on CP that overlaps with the actin-binding site (Kim et al., 2007). $PI_{4,5}P2$ inhibition of CP may require CP binding to a $PI_{4,5}P2$ membrane cluster. While some debate is still ongoing regarding that issue, $PI_{4,5}P2$, like V-1, is believed not to be able to directly uncap CP from barbed ends but rather prevents it from happening in the first place (Kuhn & Pollard, 2007). The physiological relevance of the interaction of CP with phospholipids is largely unknown, as CP mutations affecting $PI_{4,5}P2$ binding also affect actin binding, rendering these studies difficult (Edwards et al., 2014).

Tropomodulin, instead, is exclusively a pointed end capper (Weber et al., 1994). Tropomodulins are metazoans specific proteins (Yamashiro et al., 2012). The protein wraps around the three last protomers of

the actin filament pointed end and blocks polymerization or depolymerisation at that end (Rao et al., 2014). Tropomodulin is a leaky cap, as it dissociates and reassociates from the pointed end quickly (Weber et al., 1999). It is best known for its function in the capping of the extremely long-lived actin filaments in the sarcomere of skeletal muscle cells (Gokhin & Fowler, 2011), where interaction with the N-terminus of two tropomyosin molecules strengthen its activity (Colpan et al., 2013).

1.2.2.3 Filamentous actin severers

Another important class of ABPs are proteins that sever actin filaments into many smaller filaments, thereby generating a lot of new filament ends, whose fate then depends on the presence of other ABPs. The two main actin filament severing proteins are the tiny cofilin and the large multidomain proteins of the gelsolin family (Figure 1.7).

ADF/Cofilin is present ubiquitously in eukaryotes at high concentration. Most organisms express a single cofilin gene which is essential for viability. Mammals, in contrast, have three isoforms (Poukkula et al., 2011). Contrary to profilin, cofilin has a higher affinity for ADP-actin, in its monomeric or filamentous form, than ATP-actin or ADP-Pi actin (Cao et al., 2006). Additionally, cofilin enhances the rate of the ɣ-phosphate dissociation (Blanchoin & Pollard, 1999). As hydrolysis occurs stochastically as a function of time in the filament, cofilin is then a timer of the age of the filament. Its binding to the filament locks it in a tighter helical twist (McGough et al., 1997). Filaments completely decorated with cofilin are more flexible (McCullough et al., 2011) than bare filaments and quite stable (Andrianantoandro & Pollard, 2006). However, at boundaries between bare and cofilin-decorated domains as it happens *in vivo*, due to the non-homogenous state of ATP hydrolysis, the differential structural properties make the junction very unstable (Tanaka et al., 2018; Wioland et al., 2019). Cofilin is regulated *in vivo* through several mechanisms, such as binding with $PI_{4,5}P2$ or phosphorylation of its Ser3 residue (Pollard, 2016). Other members of the cofilin/ADF family exist and are widespread in eukaryotes, though none of them is quite as essential as cofilin itself (Poukkula et al., 2011). One such member, twinfilin, consist of a tandem repeat of cofilin domains.

The large proteins of the gelsolin superfamily are defined by the presence of two to six homologous gelsolin domains (Nag et al., 2013). High levels of cytosolic Ca^{2+} release the protein from an autoinhibited state by inducing large scale conformational changes. Once activated, they both sever F-actin and cap its barbed ends. Gelsolins have two binding sites for actin, with one exposed on the surface of the filament and another hidden between adjacent subunits. Mammalians have 8 members with specific expression patterns and functions, including bona fide gelsolin, villin, adversin or CapG (Nag et al., 2013). Some of these specific functions are conferred by additional domains, and for example villin is able to bundle actin filaments. The rest of the function specificity is conferred by variation in strength of typical gelsolin functions. Invertebrates express different members such as severin (Yin et al., 1990).

1.2.2.4 Filamentous actin stabilizers

A number of ABPs bind to the side of actin filaments and, like phalloidin, stabilize the filament by reducing monomer exchange and stiffening the filament. Such ABPs include tropomyosin (Figure 1.7) and nebulin.

Tropomyosin is an elongated coiled coiled dimer that binds to the side of actin filaments, simultaneously contacting several actin subunits (Sodek et al., 1972). Vertebrate tropomyosins span six or seven actin subunits while yeast tropomyosins are shorter with *S. cerevisiae* and *S. pombe* isoforms contacting 4 or 5 subunits (Skoumpla et al., 2007). Tropmoyosin molecules associate head to tail to form continuous tropomyosin cables that wraps around both sides of the F-actin filament helix (von der Ecken et al., 2015). Tropomyosin association stabilizes and stiffens the actin filament (Hitchcock-DeGregori et al., 1988; Kojima et al., 1994). In addition, tropomyosin association regulates interaction with other ABPs (Gunning et al., 2008; Pollard & Lord, 2014), which is important for muscle contraction, for example. Tropomyosin is regulated through acetylation including in *S. pombe* (Skoumpla et al., 2007). Genes for one or more tropomyosins are present in fungi and animals but not in amoebas or plants. These different tropomyosins are expressed at different locations (Lin et al., 1988) and fulfil different functions (Drees et al., 1995; Gunning et al., 2008).

Nebulin is a giant protein specific to skeletal muscle cells of more than 6000 aminoacids which contacts up to 200 actin monomers simultaneously. The full protein spans the entire length of the sarcomere thin filament and is thought to act as ruler, controlling its length (McElhinny et al., 2003). Nebulin structural characteristics help stabilize the actin filament by reducing actin turnover and depolymerisation (Chen et al., 1993; Pappas et al., 2010).

1.2.2.5 Filamentous actin nucleators and polymerases

Spontaneous actin assembly is limited by the assembly of the first monomers, because small oligomers are very unstable (Figure 1.6). *In vitro*, there is a lag phase until some of those oligomers are stabilized and can then elongate. *In vivo*, however, the lag phase is bypassed by the use of specific ABPs called nucleators. Three types exist: Arp2/3, which forms branched actin networks and binds at the pointed end, formins, which form linear actin networks and bind to the barbed end (Figure 1.7), and WH2-domain-based nucleators such as Spire, Cordon-bleu, or Leimodin.

Arp2/3 was the first nucleation factor characterized (Machesky et al., 1994). It is highly conserved in virtually all eukaryotes (Goley & Welch, 2006). It is a 7-subunit oligomer that binds to the side of pre-existing filaments at a ~70° angle and nucleates a new filament branch. At its core are the two Actin Related Proteins Arp2 and Arp3, which are evolutionary related to actin and share about 45% identity with it (Robinson et al., 2001). They retain a structure similar to monomeric actin especially at the barbed end while they are held at the pointed end by the accessory subunits, ArpC1-5. The complex is intrinsically inactive because the accessory subunits of the complex hold Arp2 and Arp3 apart such as they don't resemble a filament barbed end. Upon binding to the side of a mother filament, a conformational change brings them closer together such as they form the daughter filament seed (Rouiller et al., 2008) which is then free to elongate at its barbed end.

Arp2/3 is activated by a myriad of Nucleation Promoting Factors (NPFs), each in a specific context (Rottner et al., 2010). Most of them, such as proteins of the Wiskott–Aldrich Syndrome Protein (WASP) family, harbour a WCA domain, which consists of one or more Wasp Homology 2 motifs (WH2) that bind actin monomers and a connector region and peptide (CA) that binds the Arp2/3 complex. Binding of the CA domain to the Arp2/3 complex induces a significant conformational change that renders it nucleation

competent (Goley et al., 2004), while the WH2 domains deliver G-actin to the barbed end of the primed complex (Chereau et al., 2005). The branching nucleation process mediated by Arp2/3 can be inhibited by the CK-666 drug (Nolen et al., 2009), which stabilizes the inactive state of the Arp2/3 complex (Hetrick et al., 2013).

WH2-domain based nucleators are a family of nucleators containing three or more repeats of the WH2 domain and nucleate actin by tethering three or more actin monomers in either a single-stranded long-pitch multimer or a short pitch trimer, which form the actin nucleus (Dominguez, 2016). Spire was the first of these proteins to be characterized (Baum & Kunda, 2005; Quinlan et al., 2005) and contains 4 sequential WH2 domains. It forms a single strand nucleus of 4-actin monomers. It interacts with formins to enhance its nucleation activity while simultaneously reducing that of the formin (Vizcarra et al., 2011). Cordonbleu contains three WH2 domains repeats located at the C-terminus of the protein (Ahuja et al., 2007), with a long linker in between the second and the third repeat, whose length has been shown to be important for Cordonbleu function. Cordonbleu has a nucleation activity when its concentration relative to that of the actin is low, but sequesters monomers when the ratio increases (Husson et al., 2011).

Last but not least, formins are homodimeric proteins that nucleate the growth of linear F-actin at the barbed end (Pruyne et al., 2002). They consist in two highly conserved actin assembly domains, the Formin Homology domains 1 and 2 (FH1 and FH2, Figure 1.9A), flanked by two less well conserved N- and C-terminal regulatory regions (Higgs, 2005). Most organisms express different formins, which fulfil different functions, from two in *S. cerevisiae* (Breitsprecher & Goode, 2013), 3 in *S. pombe* (Kovar et al., 2011), through 6 in the nematode *Caenorhabditis elegans* or the fruit fly *Drosophila melanogaster* (Higgs & Peterson, 2005), to about 15 in mammals (Schönichen & Geyer, 2010) and at least 21 in the plant *Arabidopsis thaliana* (Blanchoin & Staiger, 2010).

The protein dimerizes head-to tail through dimerization domains within its FH2 domain (Xu et al., 2004). The FH2 domain can be divided into 4 subdomains, lasso, knob, coiled-coiled and post (Figure 1.9B). A flexible linker separates the lasso and the knob. When free of actin, these two halves are relatively close together and are stretched apart thanks to the flexible linker to allow the FH2 dimer to wrap around an actin filament barbed end (Otomo et al., 2005). Each FH2 monomer contains 2 actin binding sites. The first site is located in the knob region, and is characterized by an invariant isoleucine residue. The second site is located on the lasso/post region and is characterized by two invariant lysine residues. When each actin binding site is engaged, the FH2 domain contacts several actin subunits, which explains how formins stabilize the energetically unfavorable dimer and trimer states (Baker et al., 2015; Pring et al., 2003). Formins differ vastly in their potency as actin nucleators, with some formins even proposed not to act as nucleators such as *S. pombe* For3 (see subsection 1.3.2).

The FH2 dimer then stays processively associated with the barbed end as it elongates, making it a leaky cap. Formins then populates two states, an open state, that is polymerization competent, and a closed state (Vavylonis et al., 2006). Depending on their affinity for actin, some formins will spend most of their time in the closed state like *S. pombe* Cdc12, while others will be mainly in the open state, like mDia1. Two main models have been proposed for how formins go from one state to another (Courtemanche, 2018). In the stair-stepping model, both the FH2 domains of the dimer are bound to the last 2 actin protomers, leaving the post of one FH2 domain free to interact with an upcoming actin (open state). Once that monomer

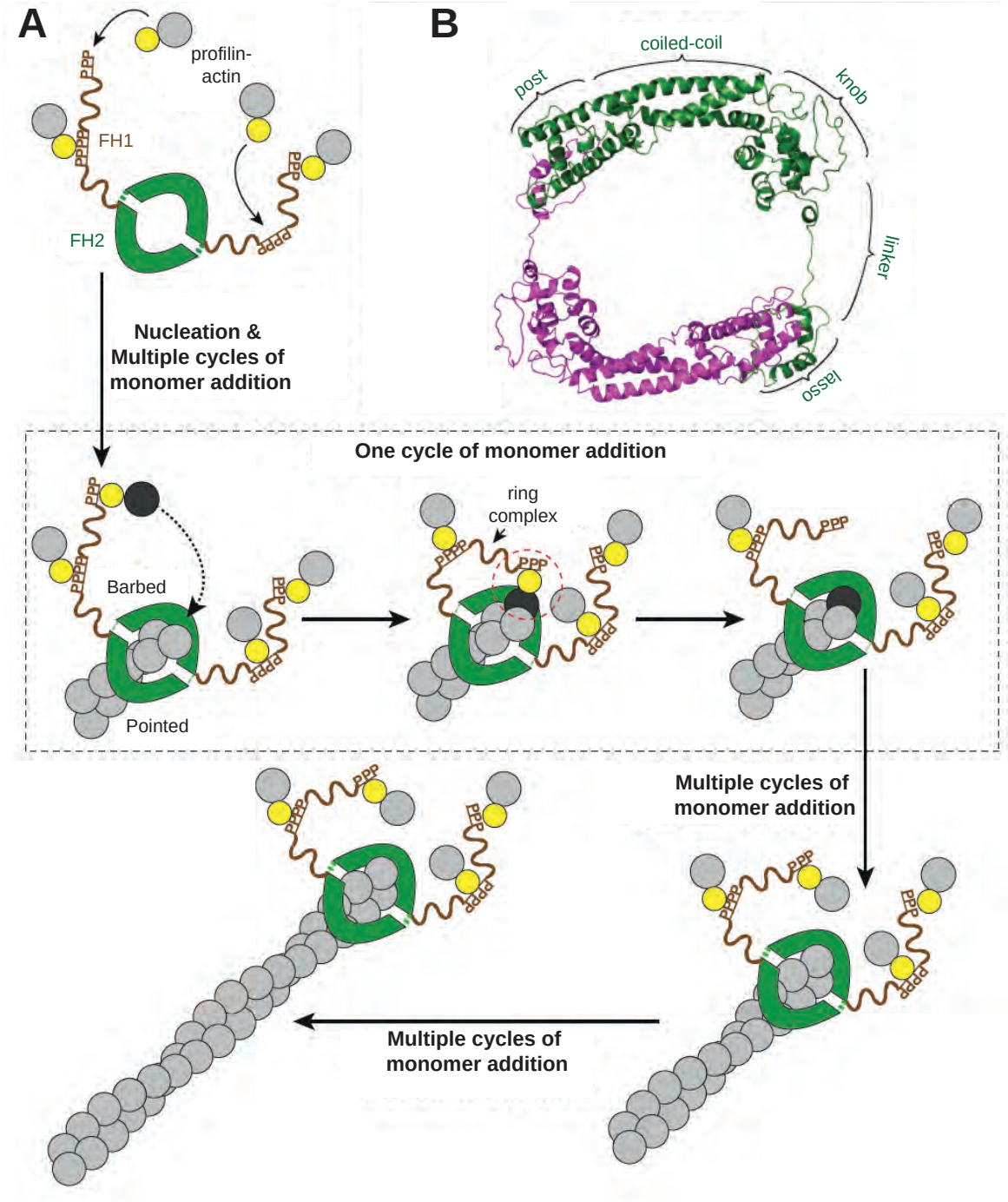

Figure 1.9 Formin-mediated assembly of profilin-actin and formin structure (adapted from Bonnie Jayne Scott PhD manuscript)

A. Working model for profilin-actin assembly in the presence of formin. Formins nucleate actin filaments with varying efficiency by stabilizing the dimer. Upon filament nucleation or association with a preassembled filament, the formin FH2 domain dimer remains processively associated with the elongating barbed end while profilin binds multiple proline-rich tracks in the FH1 domain which directs the rapid addition of profilin-actin monomers. FH1-bound profilin-actin forms a 'ring complex' by binding to the FH2-associated barbed end. The red-dashed circle indicates a favorable interaction of profilin and/or profilin-actin with the FH2 domain. Profilin and the FH1 domain then dissociate together or separately from the barbed end for subsequent rounds of elongation. **B.** Structure of the FH2 domain. Ribbon diagram of the Bni1 FH2 domain crystal structure (residues 1350-1760; PDB 1Y64) as seen in the co-crystal with actin (Otomo et al., 2005). The FH2 domain forms a tethered homodimer in the shape of a donut. The two subunits are shown in green and purple and labels indicate approximate positions of the lasso, flexible linker, knob, coiled-coil, and post regions of the green subunit.

binds, both actin binding sites are then occupied leaving the formin in a closed state. The trailing FH2 then steps forwards, returning the formin in an open conformation and the cycle continues. In the stepping second model, both the FH2 domains always have both their actin binding sites occupied, and formins only move forward as a new monomer is added.

FH1 domains are flexible tails extending from the FH2 dimer which contain a variable number of proline rich tracks which directly bind profilin-actin (Figure 1.9A). For example, *Mus musculus* mDia1 contains 14 tracks while *S. pombe* Fus1 contains only one. Flexibility allows FH1-bound profilin-actin to interact with and bind to the FH2 domain-associated barbed end (Paul & Pollard, 2008; Vavylonis et al., 2006). This transforms formins into actin polymerases, the rate of which is dependent not only on the number and quality of proline rich tracks but also on their spacing relative to their associated FH2 domain (Courtemanche & Pollard, 2012; Paul & Pollard, 2008; Scott et al., 2011).

The N-terminal region of most formins is a regulation hub. The most common mode of diaphanous formin (a certain subtype of formins homolog to vertebrate mDia formins) regulation is based on the interaction between a Diaphanous Autoinhibitory Domain (DAD) and a DAD-Interacting Domain (DID) (Alberts, 2001). The DID domain is present in the N-terminal regulatory region and the DAD on the C-terminal regulatory region. When interacting, they inhibit actin binding. Their interaction is released following binding of a Rho GTPase, whose binding site overlaps with the DID on the N-terminal regulatory region (Rivero et al., 2005). Multiple Rho GTPases regulate different formins in different subcellular locations, thereby determining when and where nucleation takes place (Breitsprecher & Goode, 2013). Post-translational modifications such as phosphorylation (Cheng et al., 2011; Iskratsch et al., 2013; Staus et al., 2011; Wang et al., 2009) or farnesylation (Chhabra et al., 2009) are also known to regulate formin activity.

Besides nucleation and elongation, some formins harbour additional properties. For example, some formins, like *S. pombe* Cdc12, *Mus musculus* mDia1 or *S. cerevisiae* Bni1 are mechanosensitive, meaning their elongation rate is sensitive to the mechanical stress exerted (Courtemanche et al., 2013; Jégou et al., 2013; Zimmermann et al., 2017). Some formins such as *S. pombe* Fus1, *Arabidopsis thaliana (A. thaliana)* AFH1 or *Mus musculus* INF2 have been shown to mediate actin filament bundling (Michelot et al., 2005; Scott et al., 2011). Other formins have been shown to promote interaction with microtubules (Gaillard et al., 2011). Some formins have been shown to mediate F-actin severing (Chhabra & Higgs, 2006; Harris et al., 2004).

In addition to formins which act as barbed end actin polymerases on top of their role as F-actin nucleators, proteins of the ENA/VASP family act solely as F-actin polymerases (Breitsprecher, Kiesewetter, et al., 2011). They do so thanks to their tandem WH2 motifs (Hansen & Mullins, 2010) and their proline rich track regions (Ferron et al., 2007). *In vitro*, contrary to formins, profilin appears dispensable for ENA/VASP-mediated filament elongation (Samarin et al., 2003).

1.2.2.6 Cross-linkers and membrane linkers

A large family of ABPs establish physical connection in between distinct actin filaments, or in between actin filaments and the membrane to establish higher degree structures (Figure 1.7) (Matsudaira, 1994). Two or more Actin-Binding Domains (ABDs) either in the same monomeric protein or in the two subunits

of a dimeric protein are necessary to connect actin filaments. The distance between the two ABDs varies considerably between different actin cross-linkers. In proteins where that distance is short, binding results into actin bundles. When the distance between the two ABDs is greater, binding results into a looser, gel-like array. The density of the resulting array controls accessibility to additional ABPs.

For example, fimbrin (Bretscher, 1981) consists of two continuous ABDs and induces closely packed actin filaments (a few nanometers apart) in both parallel and antiparallel bundles (Skau et al., 2011). Similarly, fascin is a small protein resulting in tightly packed crosslinking (Tilney et al., 1998). α-actinin acts as a dimer and its two subunits are oriented in opposite orientation. A linker separates the two binding sites by about 30nm, creating a looser bundle of actin filaments in an antiparallel orientation. The different spacings they induce make fimbrin and α-actinin mutually exclusive (Winkelman et al., 2016). Filamin forms a dimer which separates its two ABDs through a flexible V-shape linker, so that the filaments it crosslinks are almost at right angle to one another (Alberts et al., 2014; Popowicz et al., 2006). The result is a loose, highly viscous gel. In addition to actin, filamin interacts with a great variety of cellular partners which confers it a great functional diversity. Spectrin, first identified in red blood cells (Yu et al., 1973), is a long, flexible, heterotetrameric protein which consists of 4 elongated subunits (2 α subunits and 2 β) (Zhang et al., 2013), with a separation of about 200nm between its ABDs. It forms a two-dimensional weblike network. Spectrin also contains separate binding sites for membrane proteins so that it links the crosslinked actin filament network to the membrane (Bennett & Baines, 2001; Machnicka et al., 2014). Other proteins can similarly mediate F-actin membrane targeting, such as the proteins of the ERM family, a name derived from its first three members, ezrin, radixin and moesin (Fehon et al., 2010).

1.2.2.7 Filamentous actin molecular motors

There are three types of molecular motors on cytoskeletal polymers: dyneins, kinesins, and myosins. While the first two types interact with microtubules, myosins interact with F-actin. Myosins are a superfamily of proteins separated into many different classes, some of which are specific to certain subdivisions of the tree of life (Foth et al., 2006; Odronitz & Kollmar, 2007). Myosins use the energy of ATP hydrolysis to move alongside filaments and have been implicated in an ever-expanding list of cellular functions (Figure 1.7) (Masters et al., 2017). They are roughly separable in three domains. At the N-terminus sits the catalytic motor domain containing the actin binding site and the ATP binding and hydrolysis site. Following is a lever arm region containing one to six IQ motifs (IQxxxRGxxxR) which binds myosin light chains or associated proteins such as calmodulin, thereby regulating the motor function. The C-terminal region, the tail, is the most variable region and mediates the different functions of the different classes. They typically consist of a helical coiled coiled region for dimerization and/or a cargo or membrane binding domain (Krendel & Mooseker, 2005). Most organisms express different myosins genes, with some of them further diversified through alternative splicing. For example, humans express 38 myosin genes spread into 12 classes (Masters et al., 2017) while *S. pombe* expresses 5 myosin genes spread into 3 classes (East & Mulvihill, 2011). Covering all of the myosin classes is beyond the scope of this introduction, and because this manuscript deals principally with *S. pombe*, only the 3 classes present in *S. pombe* will be developed, as they are the most important classes throughout the eukaryotic kingdom. All *S. pombe* myosins are directional plus end motors but minus end directed myosins exist (Inoue et al., 2002; Wells et al., 1999).

Class I myosins, including *S. pombe* Myo1, are a class of myosins whose discovery arrived after the discovery of conventional class II myosins and uncovered the diversity of myosins (Pollard & Korn, 1973). Since then, representatives have been identified in all animal and fungi studied so far (Odronitz & Kollmar, 2007). They are monomeric myosins, with one or two calmodulin-binding IQ domains and a tail region containing pleckstrin homology domains mediating binding to membrane phospholipids (Feeser et al., 2010; Masters et al., 2017). Both *pombe*'s and *cerevisiae*'s class I myosins play a role in stimulating Arp2/3 complex-dependent actin polymerization (East & Mulvihill, 2011) and are regulated through phosphorylation.

Class II myosins, including *S. pombe* Myo2 and Myp2, are the first and most extensively studied myosins (Huxley, 1969). In mammals, they provide the contractile force in muscle cells where they form the heavy filaments in the highly specialized sarcomere units (Masters et al., 2017). In non-muscle cells, they are also involved in the formation of contractile networks such as the stress fibers, or the cytokinetic contractile ring. They are dimeric motors and each subunit interacts with two light chains (essential and regulatory; Cdc4 and Rlc1 in *pombe*, respectively) through their lever arm region which contains 2 IQ sites each. Their C-terminus consist of long coiled-coiled α-helices which assemble to form the dimer. They are regulated through phosphorylation in addition of the light chains.

Class V myosins, including *S. pombe* Myo51 and Myo52, are amongst the most evolutionary conserved myosins. They act as dimers and walk along actin cables to transport molecular cargoes throughout the cell. For example, Chicken Myo5a can slide actin filaments up to 400 $nm.s^{-1}$. They consist in their N-terminal motor domain, a long neck region containing up to 6 IQ motifs, and a tail containing a coiled-coiled domain mediating dimerization followed by a cargo binding domain. Their activity is regulated by light chains and calmodulin associating with the IQ motifs.

1.2.3 Actin networks

F-actin associates with a specific set of ABPs to create higher order actin networks. They can be divided roughly into 4 main subtypes: branched (or dendritic) networks, parallel networks, contractile networks, which are often antiparallel, and gel-like networks (Figure 1.10).

1.2.3.1 Dendritic actin networks

Branched actin networks provide the force for migration or vesicle internalization. At the leading edge of migrating cells is the lamellipodium, a flat two dimensional branched network nucleated by Arp2/3, with the barbed ends oriented towards the membrane, which provides the force to move forward (Figure 1.10) (Svitkina, 2018). The lamellipodium is a very dynamic structure, where actin is constantly disassembled at the back to be reassembled upfront, producing an apparent retrograde flow of the actin protomers, which seem to move backwards as new subunits are added upfront. The molecular machinery controlling the lamellipodium includes the Arp2/3 complex and its activators including the member of the WASP family WAVE and cortactin, capping protein and ADF/coffilin. The shape of the actin network resulting from all these ABPs is particularly adapted to force generation, with its short filaments, which don't buckle (Kovar

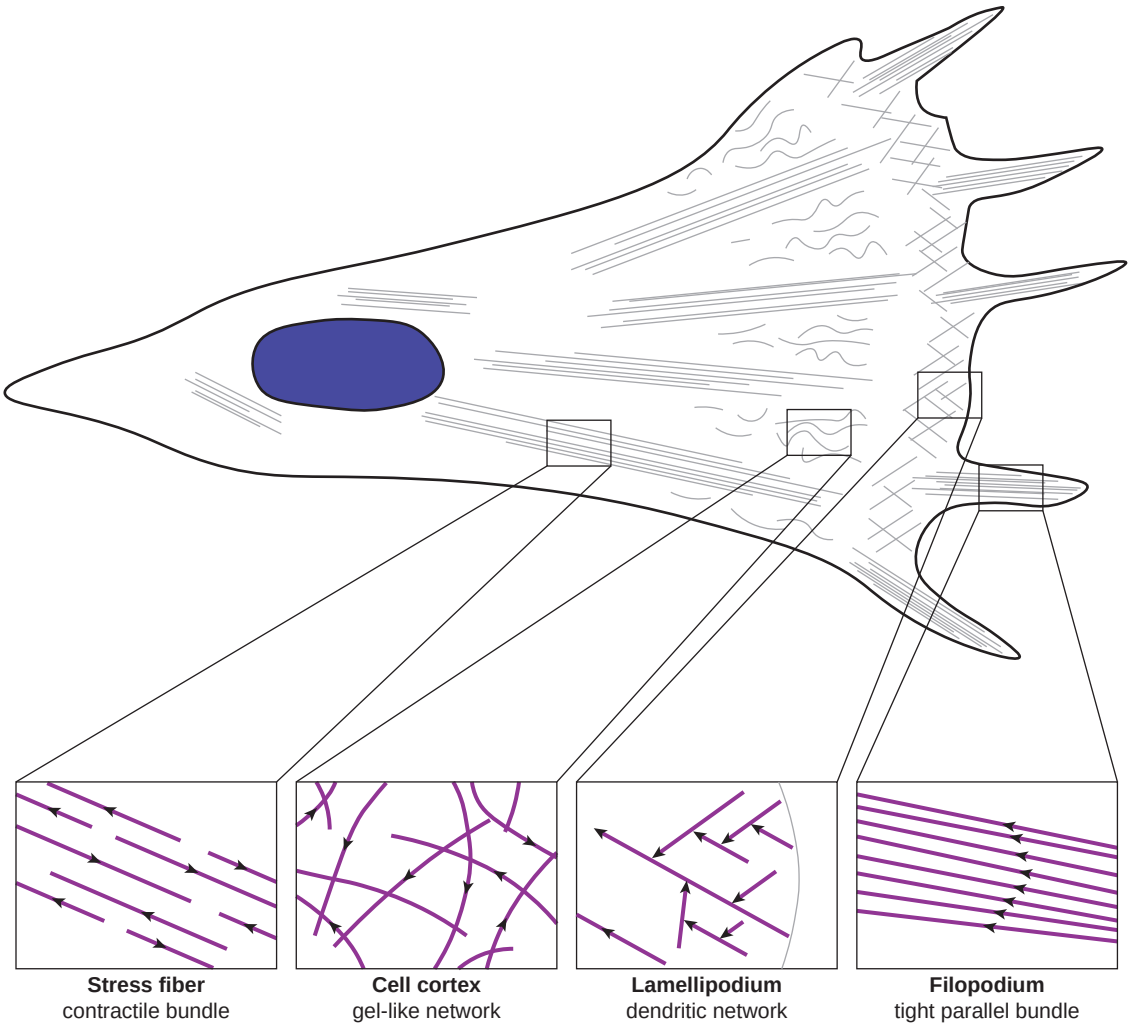

Figure 1.10 Actin arrays in a cell (adapted from Alberts et al., 2014)
A fibroblast crawling in a tissue-culture dish is shown with four areas enlarged to show the arrangement of actin filaments. The actin filaments are shown in magenta, with arrowheads pointing toward the minus end. Stress fibers are contractile and exert tension. The actin cortex underlies the plasma membrane and consists of gel-like networks or dendritic actin networks that enable membrane protrusion at lamellopodia. Filopodia are spike-like projections of the plasma membrane that allow a cell to explore its environment.

& Pollard, 2004), are crosslinked, and branch from a mother filament which provides anchoring, and which show a characteristic angle relative to the membrane (Mogilner & Oster, 2003).

Similarly, cells assemble branched actin networks for cellular uptake, through clathrin mediated endocytosis (Collins et al., 2011). Invagination of the membrane, bud neck constriction and vesicle scission are all energetically unfavorable mechanisms which require force, some of which is generated by the underlying 3-dimensional branched network, called the actin patch, best studied in *S. cerevisiae* (Kaksonen et al., 2005). As for the lamellipodium, barbed ends localize at the membrane in the actin patch. The actin machinery includes the nucleator Arp2/3 and its NPFs located at the membrane, capping protein, disassembly proteins such as cofilin and coronin, cross-linker fimbrin, and Class I myosins, also located at the membrane through recruitment by phospholipids (Galletta et al., 2010; Girao et al., 2008). Capping protein and disassembly proteins together ensure a fast turnover of actin subunits within the network. In mammals, but not in yeast, actin patches further require a particular protein called dynamin, which is both a regulator and a molecular motor (Song & Schmid, 2003). F-BAR proteins which sense and bind

membrane curvature emerge as linkers between the actin network and the membrane, as they have been shown to regulate NPFs (Boettner et al., 2009; Soulard et al., 2005; Takano et al., 2008).

1.2.3.2 Parallel actin networks

Parallel actin networks mediate membrane protrusions and tracks for myosin-mediated intracellular transport. Filopodia are finger-like protrusions formed at the leading edge of migrating cells, such as fibroblasts, and consist of a bundle of crosslinked parallel actin filaments which span the entire length of the filopodium, with their barbed end oriented towards the filopodial tip (Figure 1.10) (Small et al., 1978). Filopodia can be very long lived but are still very dynamic as constant assembly occurs at the tip and constant disassembly occurs at the back. As a result, even though the whole filopodium grows forward, individual actin protomers exhibit a retrograde flow towards the cell interior (Mallavarapu & Mitchison, 1999). Both formins and ENA/VASP accumulate at the filopodial tip and control nucleation and elongation of the filament and their relative importance is dependent on the cell type (Lebrand et al., 2004; Yang et al., 2007). Their presence excludes capping protein through competition (Svitkina et al., 2003). Class X myosin helps deliver ABPs and actin subunits to the filopodial tip (Kerber & Cheney, 2011), as diffusion in those long structures is unfavorable (Mogilner & Rubinstein, 2005). Filament buckling which would impede force production is overcome by fascin crosslinking, which increase the collective stiffness of the network (Vignjevic et al., 2006). The lateral link to the membrane is provided by proteins of the ERM family and also contributes to the network stiffness (Niggli & Rossy, 2008). ADF/cofilin helps accelerate actin turnover (Breitsprecher, Koestler, et al., 2011).

Microvilli are another type of finger-like protrusions of bundled filaments. They are present on the apical surface of the non-motile intestinal epithelial cells. They help increase the membrane surface area for nutrient intake optimization. They are of uniform length and diameter with 20 to 30 parallel actin filaments with their barbed ends oriented towards the tip, and their actin molecular machinery is very similar to the one of filopodia (Brown & McKnight, 2010), except that in their case, class I myosins make the link between the membrane and the actin network (Nambiar et al., 2010), the crosslinkers are fimbrin and villin, and the actin filament turnover rate is much lower than in filopodia.

Yeast cells primarily use actin cables of bundled parallel filaments to support polarized transport of molecular components throughout the cell (Moseley & Goode, 2006), while mammals primarily do it by using their microtubule cytoskeleton. These cables extend throughout the long axis of the cell and serve as tracks for the transport by class V myosins of numerous cargoes, such as secretory vesicles, organelles, and mRNA to the site of polarized growth (Mishra et al., 2014). Individual filaments within the structure don't span the whole cable and are crosslinked and stabilized by tropomyosin to form the total length of the structure. Actin filaments barbed ends are all oriented towards the site of growth. Formins nucleate those actin cables with the help of their Rho GTPase activator. Cables are not static and experience constant assembly at the barbed end and disassembly at the pointed end. Actin cables are also long since recognised in plants and their molecular components resemble the ones used in yeast (Huang et al., 2005; Michelot et al., 2006; Nagai & Rebhun, 1966; Ye et al., 2009).

1.2.3.3 Contractile actin networks

The best studied example of contractile actin network is the skeletal muscle unit sarcomere, whose microscopic unit contraction addition result in macroscopic muscle contraction (Alberts et al., 2014). Sarcomeres assemble in a symmetric and stereotypic manner with virtually no variation between units. Class II myosins assemble in antiparallel bundles with multiple heads on each side of the symmetry line, forming the thick filament. The thick filament is anchored to both sides of the sarcomere in the Z disc, composed of capping protein and α-actinin, by the molecular spring protein titin. On each side of the sarcomere, actin filaments of controlled length and inverse orientation form the thin filaments. They are anchored to the sides of the sarcomere in the Z-disc through their barbed ends where capping protein impedes elongation, and they are capped by tropomodulin on their pointed end, toward the center of the sarcomere. They are stabilized by the extremely long side binding protein nebulin. Tropomyosin and troponin also bind to the side of the actin filament and regulate myosin head binding to the actin filament through Ca^{2+} regulation of their conformation, covering or not the myosin binding site on actin. Calcium entry serves as the signal for contraction and as myosins move towards the plus ends of thin filaments, the length of the sarcomere is decreased. Addition of all those individual reductions result in the macroscopic muscle contraction.

Stress fibers are another example of mammalian contractile networks which are observed in non-muscle cells (Tojkander et al., 2012). They are bipolar, bundled actomyosins networks which contract to provide tension (Figure 1.10). They often contact focal adhesions. Their structural organization resembles the one of sarcomeres but is much less stereotypic and much more dynamic. Their actin molecular machinery includes Class II myosins, tropomyosin and α-actinin but excludes capping protein or tropomodulin. Formins and their Rho GTPase activators are involved in the nucleation of stress fibers and proteins of the ENA/Vasp family participate in their elongation (Smith et al., 2010).

The actomyosin cytokinetic ring is an antiparallel actin network conserved from metazoans to yeast which provides the force for cell division (Glotzer, 2017). Its components include formins, class II myosins, Rho GTPases which activate formins and or/myosins, bundling protein α-actinin, tropomyosin and cofilin. In addition, some components bridge the actin network to the membrane, such as proteins from the ERM family, F-BAR proteins, or Myosin II association with phospholipids. Anillin acts as a scaffold in binding both F-actin and a number of those regulators (Zhang & Maddox, 2010).

1.2.3.4 Gel-like actin networks

The contractile actin cortex in metazoan cells is a thin layer of cross-linked filaments that provides structural resistance and shapes the membrane of eukaryotic cells devoid of a cell wall (Figure 1.10) (Chugh & Paluch, 2018). Their molecular machinery includes class II myosins, which provide tension to the network, mixed Arp2/3 and formin nucleators, whose relative proportion is dependent on the cell type, capping protein and cofilin which control filament length and ensure that the network is dynamic, actin cross linkers whose type differs depending on the cell type and actin-membrane linkers, including ERM proteins and class I myosins (Biro et al., 2013). The type of crosslinker used, which can be mixed, is important in regulating the physical properties of the resulting cortex (Ennomani et al., 2016). For example, red

blood cells use spectrin, which crosslinks actin filaments more than 200nm apart, and the resulting actin network is strong yet highly flexible, which allows the cell to withstand squeezing through blood vessels and recover their shapes afterward (Mohandas & Gallagher, 2008).

1.2.4 Actin networks and actin binding proteins interaction

How multiple actin networks with distinct localization, function and architecture manage to self-assemble within a common cytosol, from the same common pool of monomeric actin and ABPs is a fascinating and emerging question in the actin field (Boiero Sanders et al., 2020; Kadzik et al., 2020; Michelot & Drubin, 2011). The question is still far from being answered, but several studies have shed light along the years on a number of mechanisms governing this fundamental actin cytoskeleton property.

The answer begins at the level of actin itself. As mentioned above, several organisms exhibit multiple actin genes, which can be differentially spliced and lead to different isoforms, but also additionally modified by post-translational modifications (Gunning et al., 2015; Herman, 1993; Terman & Kashina, 2013; Vedula & Kashina, 2018), so that virtually every eukaryote has different actin forms, even single-celled organsims such as yeast. These different forms are differentially expressed between different cell types, or differentially localized within the same cell type (DeNofrio et al., 1989; Kijima et al., 2018; Kislauskis et al., 1993; Perrin & Ervasti, 2010; Slajcherová et al., 2012). They exhibit differences in term of actin assembly (Drazic et al., 2018; Perrin & Ervasti, 2010) and are functionally different so that they are not interchangeable (Fyrberg et al., 1998; Kandasamy et al., 2002).

Next, the nucleator contributes in conferring to the network its specific identity. Through their nucleation mechanism, Arp2/3 and fomins induce networks of different architectures, branched and linear respectively. Their presence, or that of their activators, has been shown to be sufficient in cell extracts to induce the formation of a network of similar architecture (Miao et al., 2013; Michelot et al., 2010). *In vivo*, forced localization of the activator at an ectopic cellular location triggers the formation of ectopic actin networks (Levskaya et al., 2009; Wagner & Glotzer, 2016). This property has been exapted by pathogens such as *Shigella* or *Listeria*, which express activators of the Arp2/3 complex at their surface to produce dendritic comet tails which allow them to move inside their host cells (Welch et al., 1997). Distinct formins are not equivalent as they have distinct regulations and actin assembly properties so that they dictate the formation of actin networks of distinct properties. A formin specificity can even be dictated by the actin track itself, as for the human formins DIAPH3, which favors β-actin over ɣ-actin filaments (Chen et al., 2017), and INF2, which was shown to be inhibited by actin acetylation (A et al., 2020; A et al., 2019). In addition, the nucleator is likely to influence the conformation of the actin filament it nucleates, as it has been demonstated for Arp2/3 (Rouiller et al., 2008). Overall, these results suggest that the specific nucleator that assembles an actin network confers to it specific mechanical properties and architecture (Reymann et al., 2010).

As all nucleators compete for the same cytosolic actin pool, competition drives G-actin sorting to the different structures they nucleate, such that the networks are in homeostasis (Burke et al., 2014). Indeed, a number of examples show that inhibition of a specific actin network results in overaccumulation of actin in competing networks and vice versa. In *S. pombe*, inhibition of Arp2/3 leads to an excess of formin-assembled F-actin, while disruption of formins results in an increase in Arp2/3-mediated patch

density (Burke et al., 2014). Similarly, in *S. cerevisiae*, overexpression of the Arp2/3 activator Las17 results in overaccumulation of actin in patches and decreases actin incorporation in formin-nucleated actin cables (Gao & Bretscher, 2008). In mice fibroblasts, inhibition of Arp2/3-mediated networks leads to both the disappearance of lamellipodia and to an increase in filopodia formation, likely by incorporation of the released actin monomers by formin or Ena/VASP (Rotty et al., 2015; Wu et al., 2012). Because profilin is bound to most of the G-actin in the cell, it influences this competition (Suarez et al., 2015). Profilin has been showed to favor formin-nucleated networks over Arp2/3-nucleated networks through several mechanisms. First, it increases the rate of formin elongation up to 15-fold (Kovar et al., 2006; Romero et al., 2004). Second, it inhibits nucleation by Arp2/3 (Rotty et al., 2015). As a result, manipulations of the Actin/Profilin ratio displace the balance between the different networks, such as high ratios favor Arp2/3 based networks and low ratios favor linear networks, while overexpression of both actin and profilin leads to a very similar distribution (Suarez et al., 2015). Capping protein also regulates actin homeostasis by limiting the amount of monomeric actin incorporated into Arp2/3-based networks (Amatruda et al., 1990).

ABPs are able to harvest the differences between actin filaments produced by different actin forms or by the use of different nucleators to selectively bind distinct actin networks. Indeed, a number of studies have showed that some ABPs exhibit preferences for certain actin forms. For example, in *A. thaliana*, some profilin isoforms specifically avoid one form of actin (Kijima et al., 2016). In addition, in the same organism, the phenotypes that arise from artificially expressing the wrong actin form in one cell type can be rescued by simultaneously expressing the cognate profilin and cofilin isoforms, arguing that they have acquired specificity in each cell type (Kandasamy et al., 2007). In chicken, profilin shows higher affinity for β- and ɣ-actin than α-actin (Ohshima et al., 1989). Gelsolin, capping protein and profilin show a differential affinity towards arginylated and non-arginylated forms of actin (Saha et al., 2010). Other studies have showed that ABPs loading onto the filament depends on the architecture and the mechanical properties of the network, conferred by the nucleator. For example, myosins are highly sensitive to the network architecture, selecting preferentially antiparallel networks (Reymann et al., 2012). Tropomyosins will preferentially bind to linear networks over branched networks and will go as far as being selective for particular formin-mediated networks (Blanchoin et al., 2001; Gateva et al., 2017; Johnson et al., 2014). In *S. pombe*, acetylated and non-acetylated forms of tropomyosins respectively bind the actin network generated by Cdc12 and For3, and if the localization of Cdc12 and For3 is artificially switched, the localization of the two tropomyosins forms will also be switched (Johnson et al., 2014). Crosslinkers will bind to the network when the spacing between two filaments is favorable (Winkelman et al., 2016). Network architecture will also affect ADF/cofilin binding, which will be more effective in promoting disassembly in branched rather than linear networks (Gressin et al., 2015). Furthermore, some ABPs are able to act as mechanosensors such as the mechanical state of the network will influence their binding (Schiffhauer et al., 2016).

These initial differences in ABP loading, combined with cooperative loading onto actin filaments, affect the recruitment of additional ABPs through competition. One strong clue of that is an experiment conducted by (Brawley & Rock, 2009), where they observed the recruitment of three types of myosins to actin networks extracted from cells. They observed that the different myosins were sorting to distinct actin networks, demonstrating that actin networks have specific binding properties and recruit ABPs selectively in absence of cell-signaling. Along the years, a lot of groups have offered more examples of this property,

with strong emphasis on tropomyosin. Indeed, most tropomyosins exhibit end-to-end cooperativity which promotes their cooperative loading (or unloading) along the whole actin filament (Christensen et al., 2017). In addition, tropomyosin coating controls the access of a lot of ABPs onto the filament, in an isoform dependent manner (Gateva et al., 2017; Jansen & Goode, 2019). Combination of the two properties gives tropomyosin an important role in controlling the filament's access. For example, tropomyosin's presence excludes fimbrin or ADF/cofilin (Christensen et al., 2017), and regulates myosin loading and activity onto the filament (Clayton et al., 2010; Coulton et al., 2010; Gateva et al., 2017). Similarly, crosslinking proteins loading is somewhat cooperative as the loading of one crosslinking protein sets the perfect environment for the loading of another. This results in crosslinking proteins of different size excluding each other (Freedman et al., 2019; Winkelman et al., 2016). In turn, crosslinking controls the access to the network of different ABPs. For example, the obligate dimer myosin X is selectively recruited to actin bundles over single filaments, while cofilin has the reverse selectivity (Michelot et al., 2007; Nagy et al., 2008). In fact, myosin and cofilin compete with each other for F-actin binding and myosin can even displace cofilin in some cases (Elam et al., 2013; Wiggan et al., 2012). Another great example of how ABPs compete with each other and influence their respective loading onto actin filaments is formin and capping protein competition. Since they both bind the barbed end of the filament, they compete with each other for binding to that filament (Harris et al., 2004; Zigmond et al., 2003). This competition is mediated by the formation of a decision complex, where both proteins bind the barbed end, and results in a reduction in both proteins' affinity for the barbed end (Bombardier et al., 2015; Shekhar et al., 2015).

Of course, all those events don't occur in an orderly manner but simultaneously, providing feed-back loop mechanisms that ensure the particular identity of an actin network. This also means that the removal of a given ABP from one actin network can be amplified and may result in the global relocation of ABPs from other actin networks (Skau & Kovar, 2010). The deletion phenotype will then not only stem from the absence of the ABP but also from the mislocalization of other ABPs.

1.3 Actin in *S.pombe*

Fission yeast has a relatively simple actin cytoskeleton composed of 4 well segregated actin networks: Arp2/3 nucleated actin patches which support endocytosis, For3 nucleated actin cables which support long range polarized transport, Cdc12 nucleated cytokinetic ring which supports cytokinesis, and Fus1 nucleated actin fusion focus, which supports cell-cell fusion (Figure 1.11) (Kovar et al., 2011).

1.3.1 Actin patches

Endocytosis is a molecular process resulting in the internalization of cargo molecules from the extracellular environment to the cell interior. It requires deformation then invagination of the membrane, followed by neck scission. Because of important turgor pressure, this process is strictly dependent on actin in yeast, in opposition to mammalian cells (Conibear, 2010). In *S. pombe*, endocytosis mainly occurs at the cell tips or at the center of dividing cells, i.e. where active growth is happening (Gachet & Hyams, 2005). Extensive study in budding yeast revealed a very stereotypic assembly of the endocytic and subsequent

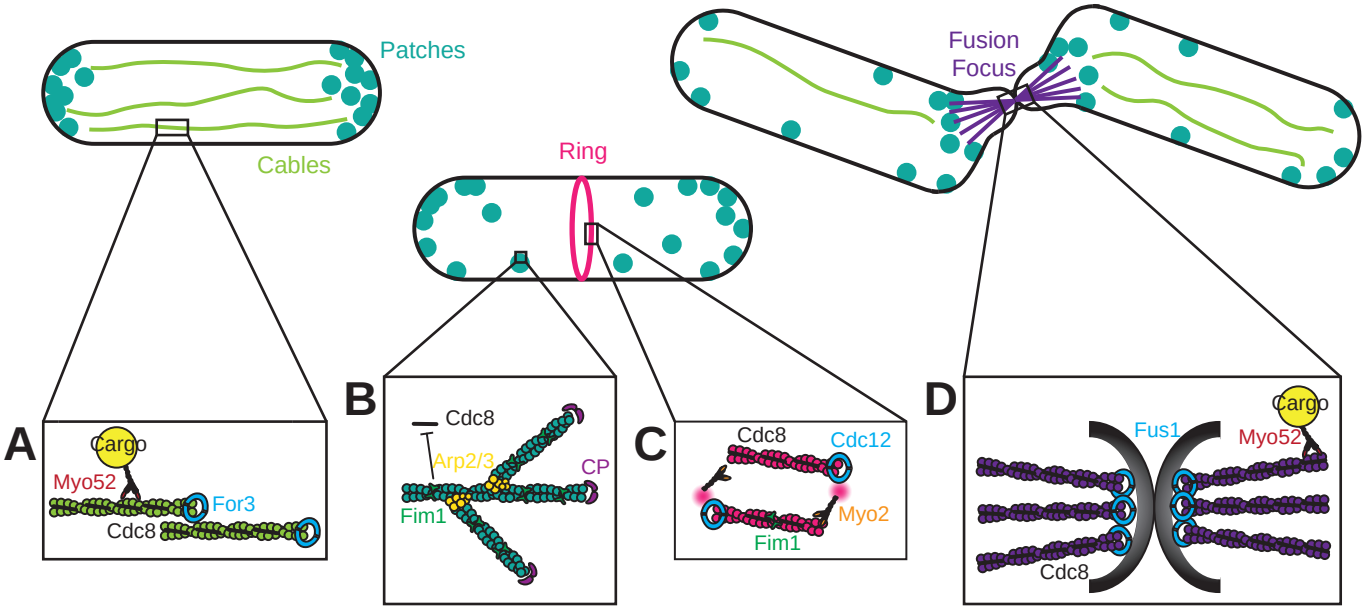

Figure 1.11 *S. pombe*'s four actin networks (adapted from Kovar et al., 2011)
S. pombe possesses 4 actin networks : cables, patches, ring and fusion focus. **A.** Actin cables are parallel actin bundles nucleated by formin For3, decorated by tropomyosin Cdc8, along which directionally walks the molecular motor class V myosin Myo52. **B.** Actin patches are branched actin networks nucleated by Arp2/3, capped by capping protein (CP) and heavily decorated by actin crosslinker fimbrin Fim1, whose high concentration excludes tropomyosin. **C.** The cytokinetic ring is a contractile antiparallel actin network nucleated by formin Cdc12, decorated by Cdc8 and Fim1 at low concentration, and rendered contractile by class II myosin Myo2. **D.** The actin fusion focus is a concentric aster of actin filaments nucleated by the formin Fus1, decorated by Cdc8, along which Myo52 directionally walks.

actin assembly machinery (Kaksonen et al., 2003; Kaksonen et al., 2005), which is conserved in *pombe* (Sirotkin et al., 2010).

First, the initial membrane invagination is mediated by the early coat components, clathrin, scaffold protein Ede1, Yap18, Ent1 and Syp1. Clathrin is a conserved three-legged protein that auto assembles to form lattice-like coats (Royle, 2006). Yap18 is involved in clathrin cage assembly and binds late coat component Pan1. Ent1 belongs to the conserved epsin family which are membrane sensing proteins (Sakamoto et al., 2004). Syp1 is an F-BAR protein which binds to lipids and deforms the membrane (Ahmed et al., 2010). Clustering of all those molecules lead to membrane deformation.

Next, late coat components, adaptor proteins including End4 and Pan1 in *S. pombe*, accumulate at the deformed membrane site and provide the link to the subsequent actin assembly components. End4 localization to patches is actin independent. It uses its C-terminal tail to recruit actin (Castagnetti et al., 2005). Pan1 contains domains expected to bind both actin and Arp2/3 (Duncan et al., 2001). Together, those components recruit the actin machinery components.

Arp2/3 activation is a concerted effort by Pan1, Wsp1 and Myo1 (Lee et al., 2000; Sirotkin et al., 2010). Wsp1 is a member of the WASP family and acts as the principal activator (Galletta et al., 2008). Myo1 is a class I myosin which localizes at the base of the invagination and stays there until internalization of the vesicle (Sirotkin et al., 2005). It is a weaker activator than Wsp1, because it lacks the necessary WH2 domain (Sun et al., 2006), but its localization suggests that it could be important to activate Arp2/3 in a distinct region that Wsp1. Pan1, which is recruited 20 s before Arp2/3, is also not sufficient to promote full Arp2/3 activation by himself.

Once Arp2/3 is activated, it nucleates branched actin filaments at their pointed end which make the basis of the actin network (Figure 1.11B). Capping protein caps the barbed end of the filaments, maintaining them short, and thus able to mediate force without buckling (Berro & Pollard, 2014). Fim1 bundles and crosslinks actin filaments, thereby also contributing to the strength of the actin network. Fim1 concentration is extremely high, with 900 molecules for about 150 actin filaments containing ~7000 actin subunits (Sirotkin et al., 2010). Such a concentration is determinant in excluding tropomyosin, which would otherwise prevent patch internalisation and actin turnover (Skau & Kovar, 2010). The network assembly happens as a rapid burst which results in patch internalization (Sirotkin et al., 2005). Afterwards, it is quickly disassembled by the coordinated action of cofilin, Aip1 and coronin (Gandhi et al., 2009; Lin et al., 2010).

1.3.2 Actin cables

Actin cables are polarized tracks for class V myosin-directed delivery of vesicles or organelles cargos at growth sites. They are long bundles of short, parallel actin filaments with barbed ends oriented towards the nearest cell tip (Figure 1.11A) (Kamasaki et al., 2005).

The assembly site is established by a crosstalk with microtubules (Martin, 2009). The polarity factor complex composed of Tea1 and Tea4 is transported to the microtubules plus ends via the +TIP complex and translocated to the cell cortex by Mod5 receptor. There, it is able to recruit the polarity factors making up the polarisome complex, including For3, Cdc42, Bud6 and Pob1.

For3 is the formin assembling the actin cable filaments (Martin & Chang, 2006). It is characterized by a very poor *in vitro* nucleation rate (1 filament per 170 dimers), a medium *in vitro* elongation rate of 10 subunits per second per µM of actin (Table 1.1) (Scott et al., 2011) and a canonical auto-inhibition mechanism through interaction of its N-terminal DID domain and its C-terminal DAD domain (Martin et al., 2007). Rho GTPase Cdc42 is the master regulator of polarity (Rincón et al., 2014). It interacts with and participates in relieving the autoinhibition of For3 (Martin et al., 2007). Bud6 is an actin monomer binding protein which binds For3 C-terminus and participates in fully activating For3. Additionally, Bud6 contributes in increasing For3 poor *in vitro* nucleation efficiency *in vivo* by recruiting actin monomers (Graziano et al., 2011). Pob1 interacts with Cdc42 through its C-terminal pleckstrin homology domain, and with For3 through its N-terminal sterile alpha motif and contributes to For3 localization at the cell tips (Rincón et al., 2009). Establishment of the polarity site is further reinforced by feedback loops involving Cdc42 (Martin, 2009).

Table 1.1 *In vitro* actin assembly properties of *S. pombe* formins

Formin	Nucleation efficiency	Elongation rate (subunits.s^{-1}.μM^{-1})	Dissociation rate (s^{-1})
Cdc12	one filament per two to three dimers	10–12	$4.7–7.0 \times 10^{-5}$
For3	one filament per 170 dimers	10	3.6×10^{-5}
Fus1	one filament per two dimers	5	6.5×10^{-4}

Formin nucleation efficiency (filaments per dimer), barbed-end elongation rate (in the presence of profilin), and dissociation rate from the barbed end were determined in (Scott et al., 2011), with in vitro biochemical assays.

Once activated, For3 stays at the cell cortex only a few seconds before moving towards the cell interior with the elongating actin cable, experiencing a retrograde flow (Martin & Chang, 2006). Thus, For3 is nucleation competent only transiently, as moving away from its activators would partially inactivate it. Other For3 molecules will then nucleate the assembly of new filaments which will be crosslinked into the bundle and will mediate the progressive flow of the old filament inward. Both the transient activation of For3 and its native poor nucleation rate may be key in creating this actin cable architecture, where asynchronous nucleation events must take place. If all nucleation events took place simultaneously, this would result into a thick and short bundle unable to fulfil its function (Kovar et al., 2011).

Besides For3, very few proteins have been identified to be bona fide components of the actin cables, in contrast to the actin patch. This may be because cables are notoriously difficult to image in *S. pombe*, so that mutants with minor effects would be difficult to investigate. In addition, any other accessory protein concentration might be very low, further adding to the difficulty. Both Cdc8 and Crn1 have been shown to decorate actin cables and contribute to their stability (Pelham & Chang, 2001). Furthermore, Myo51 plays a structural role in maintaining the architecture and dynamics of the actin cables in addition of their role in transporting cargo (Lo Presti et al., 2012). Interestingly and despite its importance in the actin network architecture, the bundler of actin cables hasn't yet been identified in *S. pombe*.

1.3.3 Cytokinetic ring

Cytokinesis is the process whereby two daughter cells physically separate after mitosis in the mother cell. It relies on the formation and subsequent constriction of a specialised actin structure, the actomyosin ring (Pollard & Wu, 2010), which is essentially a contractile bundle of antiparallel actin filaments (Figure 1.11C).

Extensive research on the process has led to multiple models for cytokinesis along the years, the primary one being the search-capture-pull release (SCPR) model (Lee et al., 2012; Vavylonis et al., 2008; Wu et al., 2006). In this model, several proteins accumulate in ~140 pre-cytokinetic nodes distributed around the cell middle (Laplante et al., 2016), including Mid1, Cdc15, Cdc12 and Myo2. Mid1 is the first protein to be recruited to the nodes and dictates the nodes position (Sohrmann et al., 1996). Cdc15 is a F-BAR protein that self assembles into filaments thought to mediate membrane deformation (Roberts-Galbraith et al., 2010). It helps recruit Cdc12 which it binds directly (Carnahan & Gould, 2003) and acts as a scaffold in recruiting additional proteins which help stabilize the ring (Roberts-Galbraith et al., 2009; Roberts-Galbraith et al., 2010). Formin Cdc12 nucleates actin filaments which will radiate in random directions from the nodes. On average, there are 4 Cdc12 dimers per node (Laplante et al., 2016). Cdc12 is an excellent nucleator with an efficiency of one filament per 2/3 dimers *in vitro* (Table 1.1) (Scott et al., 2011), which means that there is an average of 2 actin filaments per node. This high nucleation efficiency has been shown to be instrumental in Cdc12's ability to mediate the formation of the actomyosin ring (Homa et al., 2021). Once nucleated, Cdc12 is able to elongate the actin filament while staying processively associated to the barbed end with an *in vitro* elongation rate of 10 to 12 subunits per second per µM of actin (Table 1.1) (Scott et al., 2011). Some of those filaments will be captured, and subsequently pulled, by class II myosin Myo2 on another node, which is an actin plus end directed motor. Thus, Myo2's action will bring the two nodes closer together as it will walk towards Cdc12 bound barbed end. Cdc12 is mechanosensitive so that when it experiences the tension resulting from Myo2's capture, its elongation rate decreases, which helps in coalescing the ring

(Zimmermann et al., 2017). The node connection is then severed by severing ABPs such as cofilin and the cycle starts over, ultimately resulting into a fully formed ring.

Additional ABPs accumulate at the actomyosin ring and cooperate in mediating its specific architecture. Tropomyosin stabilizes Cdc12-nucleated filaments and enhances its *in vitro* elongation rate two-fold, while simultaneously encouraging its dissociation from the barbed end (Skau et al., 2009). α-actinin Ain1 and Fimbrin Fim1 help bundle and crosslink the filaments within the network. Cdc12 itself bundles actin filaments in a regulated manner (Bohnert, Grzegorzewska, et al., 2013). Once the actomyosin ring is fully formed, its constriction is coupled with septum formation so that the process will ultimately result in cell separation (Proctor et al., 2012; Sipiczki & Bozsik, 2000).

1.3.4 Fusion focus

Relatively little is known concerning the fourth *S. pombe* network compared to actin patches, actin cables, and actomyosin ring. Fusion focus formation exclusively occurs during mating, following nitrogen starvation, and, as mentioned earlier, supports cell-cell fusion, in a manner strictly dependent on the formin Fus1. It forms a couple of hours prior to fusion and disassembles quickly afterwards (Dudin et al., 2015).

Several factors indicate that it consists of an aster of filaments whose barbed ends coalesce in a restricted area at the zone of contact between the two cells (Figure 1.11D). First, actin markers and linear actin network marker tropomyosin Cdc8 localize in a large focus at the region of contact between the two cells (Dudin et al., 2015). Second, both the barbed end binding formin Fus1 and plus end motor myosin Myo52 localize in a tight spot in the actin foci, at the cell-cell contact zone (Dudin et al., 2015). Third, actin filaments were observed by transmission electron microscopy and adopted a roughly aster-like shape (Muriel et al., 2021), even though actin structures are hard to preserve and detect with this method.

Fus1 is specifically expressed during mating and localizes at the zone of cell-cell contact via a specific domain in its N-terminal regulatory region, through an unknown mechanism (Petersen et al., 1998b), and acts as the nucleator of the actin fusion focus (Dudin et al., 2015). It has been shown to be a very good nucleator *in vitro* with an efficiency of 1 filament per 2 dimers, a quite poor elongator with an elongation rate of 5 subunits per second per µM of actin (Table 1.1; for comparison, worm formin CYK-1 elongates at a rate of 60 sub.s-1.µM (Neidt et al., 2008)), and to be able to bundle filaments (Scott et al., 2011). Whether these properties are transposable *in vivo* or required for the specific architecture and functionality of the fusion focus is unknown.

Other ABPs decorate the fusion focus and contribute to its particular architecture and function. Class V myosin Myo52 is the main molecular motor responsible for the polarized delivery of glucanases supported by the structure. Myo51 partially overlaps in that function but mainly has a structural role in coalescing the fusion focus, in association with Rng8, Rng9 and Cdc8 (Dudin et al., 2017). Tropomyosin itself is likely to influence the network in several ways and has been showed to be essential for fusion (Kurahashi et al., 2002). First, it likely stabilizes the filaments within the fusion focus, reducing exchange of actin subunits and stiffening it, as it does for the other linear actin networks. Second, it has been shown to enhance the elongation rate of several mammalian and yeast formins (Skau et al., 2009; Wawro et al., 2007). Third, tropomyosin has been shown to regulate class V myosins processivity on actin filaments (Clayton et al., 2014; Clayton et al., 2010; Hodges et al., 2012). Class I Myosin light chain Calmodulin Cam2 also localizes

at the fusion focus, suggesting Myo1 could have a role, even though it doesn't localize as a tight spot at the fusion focus but rather in a broader area at the shmoo tip (Dudin et al., 2015). Coronin Crn1 also localizes at the fusion focus and is likely helping in ensuring actin turnover.

In the microscopy screen for fusion defective mutants that unravelled Myo51 and associated proteins Rng8 and Rng9 role, other actin related proteins showed up, such as Acp2 (capping protein β-subunit), Slm1, Twinfilin, Yap18, and Vrp1 (Dudin et al., 2017), which interacts with Myo1, WASP protein Wsp1, and actin monomers and is involved in the formation of the Arp2/3-nucleated actin network. In fact, all of those proteins and Crn1 are involved in the formation of the actin patches, which decorates a broad zone at the shmoo tip during fusion (Dudin et al., 2015), suggesting that competition between this actin network and the fusion focus might be important for fusion.

We then began this work by investigating that suggested competition, by studying capping protein relevance to cell-cell fusion. Our findings are presented in chapter 2 of this work. These results made us interested in Fus1 more directly, and we investigated the importance of its actin assembly properties first, as presented in chapter 3, and of its N-terminal regulatory region next, as presented in chapter 4.

2. Capping protein insulates Arp2/3-assembled actin patches from formins

Adapted from:

Capping Protein Insulates Arp2/3-Assembled Actin Patches from Formins

Ingrid Billault-Chaumartin and Sophie G. Martin

Published in Current Biology, October 2019

2.1 Introduction

Cells simultaneously contain several actin-based structures that need to be tailored to their specific function, with a specific architecture, size, life-time, and set of actin binding proteins. The specific architecture is defined in part by the nucleator that assembles it (Campellone & Welch, 2010; Kovar et al., 2011): Arp2/3 promotes the assembly of branched structures, whereas other nucleators, in particular formins, assemble linear ones. The dendritic networks assembled by Arp2/3 generate pushing forces against membranes, for instance in the lamellipodium of migrating cells, to drive the movement of intracellular bacteria, or to promote internalization of endocytic vesicles in yeast actin patches. Formin-nucleated actin structures consist of linear filaments, which can be bundled in parallel or antiparallel manner for protrusive or contractile force generation, for instance in filopodia or cytokinetic contractile ring, or which underlie long-range myosin-based transport.

The principles that allow a cell to assemble distinct functional actin structures at the same time are just beginning to be understood. First, because the building blocks for assembly of diverse actin structures are the same, competition is an important factor. For instance, diverse filamentous actin (F-actin) structures are in competition for a limited pool of actin monomers (Burke et al., 2014). This competition is modulated by G-actin associated profilin, which favors F-actin assembly by formins and other nucleators over Arp2/3 (Rotty et al., 2015; Suarez et al., 2015). Second, the structure's identity may be conferred, at least in part, by the specific actin nucleator that assembles it. For instance, formins promote the formation of more flexible filaments (Papp et al., 2006), which favor tropomyosin association (Skau et al., 2009). Different formins were recently proposed to promote association of distinct tropomyosin isoforms on filaments (Johnson et al., 2014). Third, self-assembly principles likely govern the segregation of specific actin-binding proteins to diverse structures. For instance, competition between fimbrin and tropomyosin for F-actin binding, together with their individual cooperative loading on actin filament, drives their association to distinct actin structures (Christensen et al., 2017). This is manifested *in vivo* by preferential association of tropomyosin to formin-assembled structures and fimbrin to Arp2/3-nucleated actin patches (Clayton et al., 2010; Skau & Kovar, 2010).

An important factor that helps limit actin filament growth is capping protein (CP). CP is present in cells in μM concentration, similar to the concentration of actin filament barbed ends, and binds the barbed end

to arrest dynamics (Edwards et al., 2014). CP forms a heterodimer of structurally similar α- and β-subunits, both of which harbor a mobile C-terminal extension, called the tentacle, which strongly contributes to barbed end binding (Narita et al., 2006; Wear et al., 2003; Yamashita et al., 2003). CP lacking both tentacles still forms a stable complex but does not bind actin, with the α-tentacle playing a more critical role than the β-tentacle, both *in vitro* and *in vivo* (Kim et al., 2004; Wear et al., 2003). CP activity is further regulated by interaction with binding partners bearing a capping protein interaction (CPI) motif (Hernandez-Valladares et al., 2010). Indeed, CP carrying surface mutations that block CPI motif binding retain capping activity *in vitro*, but lose localization and function *in vivo*, indicating that binding partners are required for its activity *in vivo* (Edwards et al., 2015). Furthermore, the Aim21/Tda2 complex, which binds CP through the same surface residues, modulates CP recruitment and activity at actin patches in *S. cerevisiae* (Farrell et al., 2017; Shin et al., 2018). By keeping filaments short, CP promotes Arp2/3 branching and plays a major role in the force production of dendritic networks (Akin & Mullins, 2008). Indeed, absence of CP *in vivo* leads to loss of the lamellipodium in migrating cells (Iwasa & Mullins, 2007; Mejillano et al., 2004), and excess actin filaments in yeast actin patches, which exhibit a longer lifetime (Berro & Pollard, 2014; Kaksonen et al., 2005; Kim et al., 2006; Kim et al., 2004).

As formins and capping proteins both interact with the barbed end of actin filaments but promote opposite activities – i.e. filament extension vs. capping – they compete with each other *in vitro* (Harris et al., 2004; Kovar et al., 2003; Moseley et al., 2004; Zigmond et al., 2003). Interestingly, recent single-molecule work has shown that formin and CP can simultaneously bind the filament barbed end, forming a ternary 'decision complex' intermediate (Bombardier et al., 2015; Shekhar et al., 2015). Evidence for competition *in vivo* comes from work in the fission yeast *Schizosaccharomyces pombe*, in which deletion of capping protein ameliorates the function of a hypomorphic formin cdc12 allele for cell division (Kovar et al., 2005). CP may also compete with formins and ENA/VASP to control filopodial shape (Sinnar et al., 2014). Indeed, competition of CP with ENA/VASP is also well established *in vitro*, where ENA/VASP protects actin barbed ends against CP (Bear & Gertler, 2009; Kaksonen et al., 2003; Martin, 2016; Sirotkin et al., 2010), and *in vivo*, where this competition controls the formation of filopodia and other F-actin structures (Aghamohammadzadeh & Ayscough, 2009; Amatruda & Cooper, 1992; Mejillano et al., 2004; Nakano & Mabuchi, 2006). Whether such competition contributes to actin structure identity has not been explored.

The fission yeast cell represents a simple system in which to dissect the mechanisms by which distinct actin structures are formed. Indeed, this cell contains only four actin structures, actin patches, cables, ring and focus, each of which fulfils a specific function (Martin, 2016; Kovar et al., 2011). Arp2/3 nucleates the assembly of actin patches around invaginating endocytic vesicles. The actin patch, marked in particular by fimbrin Fim1, reproducibly assembles in a stereotypical manner (Kaksonen et al., 2003; Sirotkin et al., 2010) and is thought to provide force for vesicle internalization (Aghamohammadzadeh & Ayscough, 2009). CP localizes to actin patches (Kovar et al., 2005; Amatruda & Cooper, 1992; Nakano & Mabuchi, 2006), where it limits actin incorporation and helps force production (Kim et al., 2004; Berro & Pollard, 2014; Kaksonen et al., 2005; Kim et al., 2006). Interestingly, although active CP is a heterodimer, deletion of the α- and β-subunit (Acp1 and Acp2, respectively) do not produce exactly the same phenotype (Berro & Pollard, 2014). Three formins nucleate distinct structures formed of linear filaments: Cdc12 promotes the assembly of the actin contractile ring for cell division; For3 assembles linear actin filaments bundled

in cables that underlie long-range myosin-based transport for polarized cell growth; Fus1 is expressed specifically during cell mating and nucleates the assembly of the fusion focus, an aster-like actin structure that concentrates secretory vesicles transported by the myosin V Myo52 (Dudin et al., 2015; Petersen et al., 1995). These vesicles carry cell wall hydrolases such as Agn2 and Eng2, whose local secretion drives cell wall digestion for cell fusion. Besides Fus1, the coalescence of the fusion focus requires the action of tropomyosin Cdc8 (Kurahashi et al., 2002), and a visual screen revealed Cdc8 functions together with the type V myosin Myo51 and associated proteins to organize the focus in a single structure (Dudin et al., 2017). This same screen identified the deletion of *acp2* to have fusion focus defects.

Starting from the hypothesis that CP and formin Fus1 compete during fusion focus assembly, we discovered that CP protects actin patches against formin activity. In the absence of CP, formin Fus1 binds uncapped barbed ends in actin patches, forming ectopic foci that divert secretory vesicles away from the site of cell-cell contact and compromise cell fusion. Similarly, in proliferating cells lacking CP, the formins For3 and Cdc12 are ectopically recruited to actin patches, which exhibit a dual identity manifested by co-decoration with fimbrin and tropomyosin. Thus, CP ensures actin structure identity by insulating Arp2/3-assembled structures against formins.

2.2 Capping protein is required for efficient cell-cell fusion

To investigate the role of CP in cell fusion, we first assessed the fusion efficiency of strains lacking one or both CP subunits (*acp1Δ*, *acp2Δ*, *acp1Δacp2Δ*). After 12 hours of starvation, these strains exhibited a reduced fraction of fused zygotes compared to WT, which increased 36 hours post starvation (Figure 2.1A), indicating that the absence of CP causes a cell fusion delay. We measured the duration of the fusion process, from initial formation of the fusion focus marked by the type V myosin Myo52 in both partner cells (Dudin et al., 2015) to cytoplasmic mixing. Cytoplasmic mixing was defined by entry in the M-cell of cytosolic GFP expressed in P-cells under control of the *map3* promoter. The process lasted significantly longer in CP-lacking cells (Figure 2.1B,C). We also observed that the fusion focus persisted significantly longer post-fusion in CP-lacking cells (Figure 2.1B,D). Both phenotypes were clear in all mutant combinations, but strongest in *acp2Δ* single mutant. Thus, CP promotes the fusion process, since its absence causes fusion delay and persistence of the fusion focus after fusion.

2.3 Formin Fus1 and F-actin excessively accumulate at the fusion site in the absence of capping protein

Consistent with CP preventing filament barbed-end extension, previous work reported that Arp2/3-assembled actin patches lacking CP accumulate more actin (Berro & Pollard, 2014; Nakano & Mabuchi, 2006). To investigate the organization of F-actin during fusion, we first used GFP-CHD as F-actin marker (Karagiannis et al., 2005; Martin & Chang, 2006). Like in interphase cells, actin patches appeared brighter in *acp1Δ* and *acp2Δ* than WT cells during mating (Figure 2.2A) (Berro & Pollard, 2014). *acp2Δ*, *acp1Δ* and *acp1Δacp2Δ* cells also displayed slightly more F-actin at the position of the fusion focus (Figure 2.2A,D).

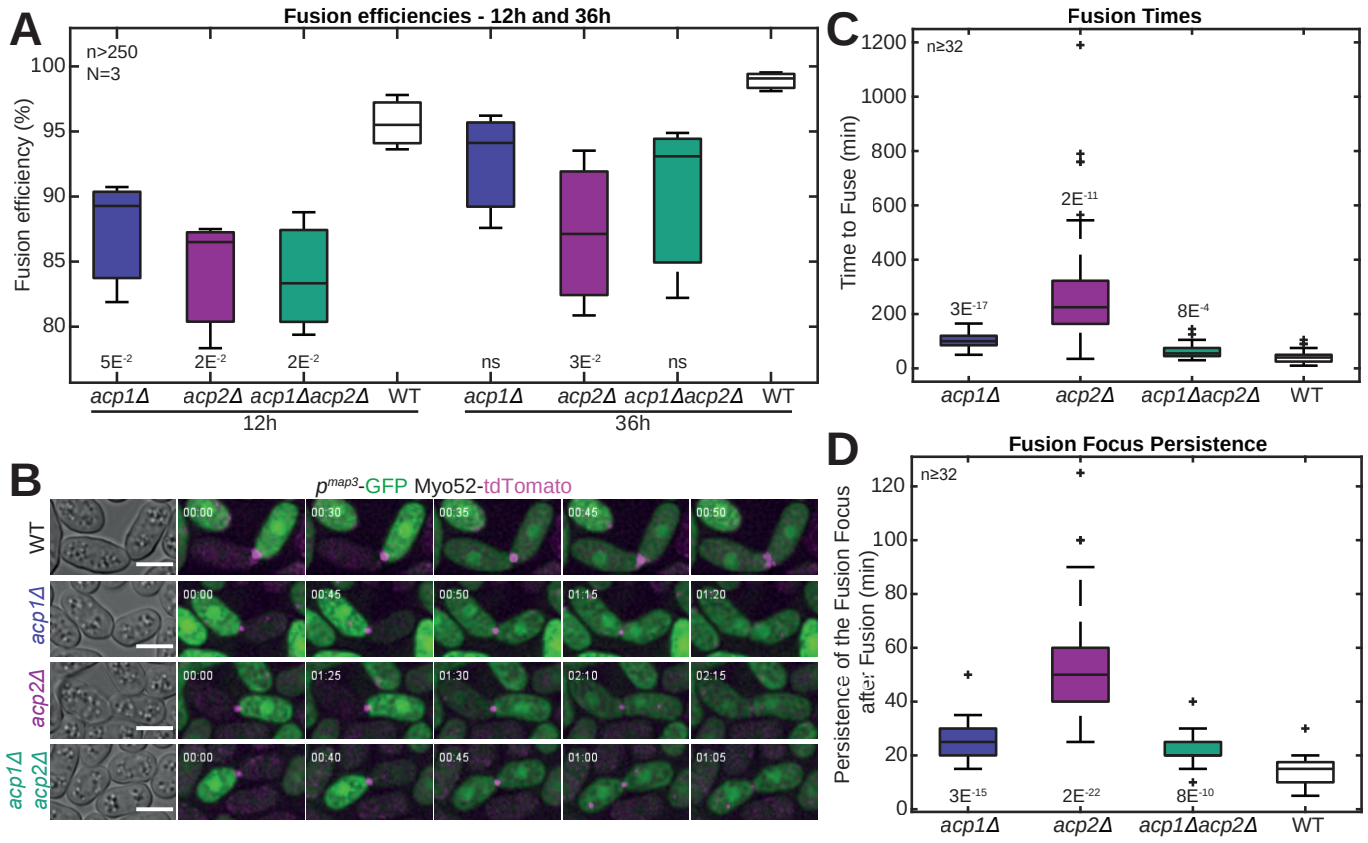

Figure 2.1 CP deletion leads to fusion delay and fusion focus persistence after fusion
A. Fusion efficiencies 12h and 36h after nitrogen removal in indicated strains. **B.** Time-lapse images and timing of Myo52-tdTomato and cytosolic GFP expressed in P-cells under *map3* promoter in WT and *acp2Δ*, showing the subsequent steps of the fusion process : beginning of the fusion process (Myo52 focus appearance), last time point before fusion, first time point after fusion, last time point exhibiting a fusion focus post-fusion, disappearance of the fusion focus. **C.** Fusion times (from Myo52 focus appearance to first post-fusion time point) in indicated strains. **D.** Fusion focus persistence times (from first post-fusion time point to Myo52 focus disappearance) in indicated strains. All indicated p-values are relative to WT. Time in hour:min. Bars are 5 µm.

Because GFP-CHD measurements at the fusion site cannot distinguish between F-actin in the fusion focus or in surrounding patches, we probed the localization of specific fusion focus components. Fus1 accumulated approximately 4-fold more in *acp2Δ*, *acp1Δ* and *acp1Δacp2Δ* cells than in WT cells at the fusion focus (Figure 2.2B,E). Global Fus1-sfGFP fluorescence levels also increased 1.6-fold (Figure 2.2G). Tropomyosin Cdc8, which preferentially binds formin-assembled filaments (Arai et al., 1998; Balasubramanian et al., 1992; Coulton et al., 2010; Kurahashi et al., 2002; Skau et al., 2009), increased about 2-fold at the fusion focus of *acp2Δ* compared to WT cells (Figure 2.2C and 2F). Thus, the absence of capping protein leads to increased F-actin and associated proteins at the fusion focus.

The dramatic Fus1 increase in *acp2Δ* fusion foci is consistent with the proposed competition between formins and CP for barbed-end binding (Bombardier et al., 2015; Kovar et al., 2005; Shekhar et al., 2015). We note that CP total levels were mildly increased in *fus1Δ* (1.1-fold; Figure 2.3A,B). To probe the hypothesis that CP promotes cell fusion by limiting Fus1-driven actin polymerization at the fusion focus, we tested whether 1) Fus1 overexpression mimics loss of CP, 2) reducing Fus1 activity ameliorates fusion efficiency in absence of CP, and 3) CP localizes to the fusion focus. First, Fus1 overexpression had no effect on fusion duration, fusion focus persistence, or ectopic Myo52 foci (Figure 2.3C,E; see below regarding ectopic foci).

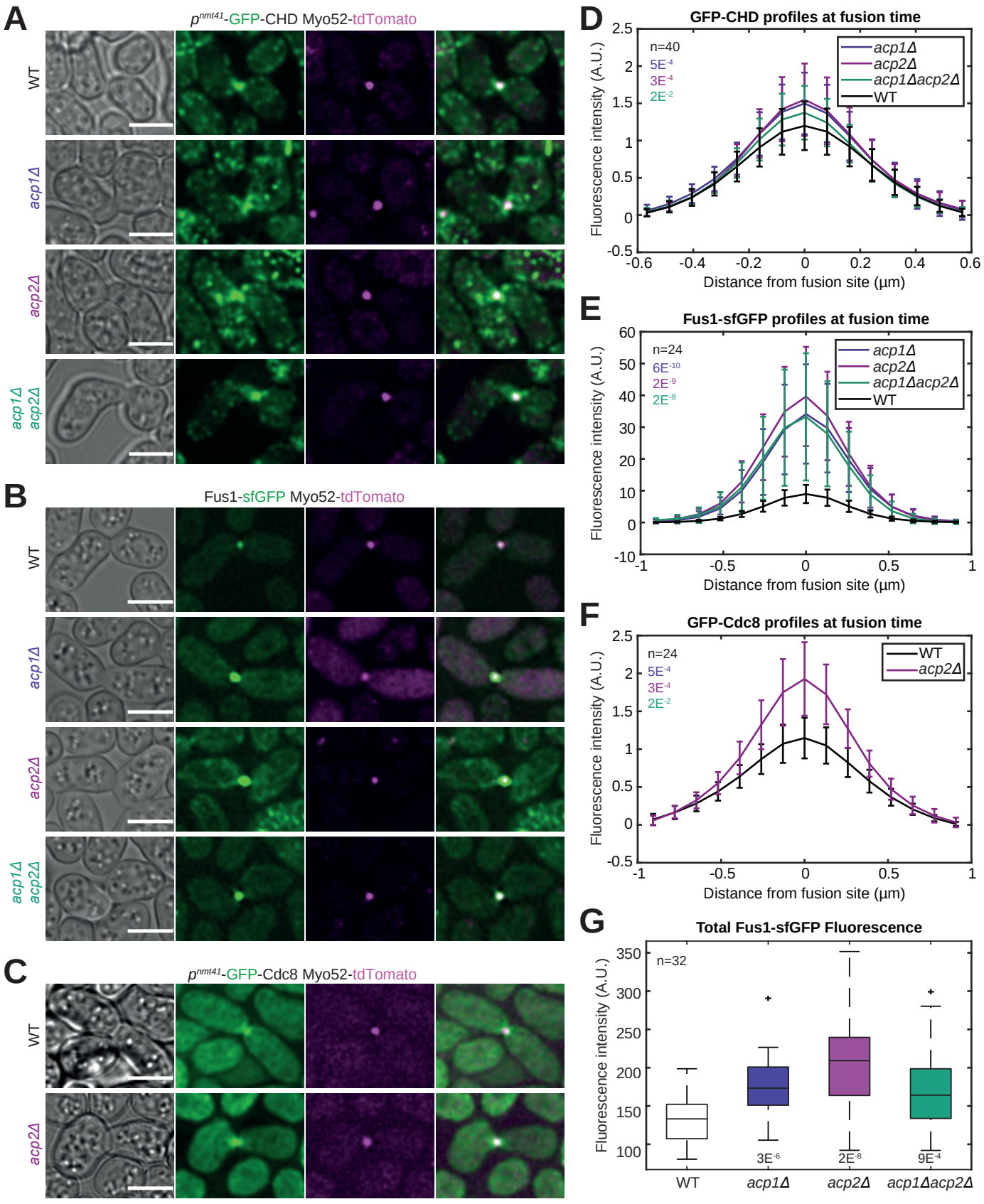

Figure 2.2 CP deletion leads to increased actin, tropomyosin and Fus1 at the fusion focus
A-C. Myo52-tdTomato and (A) GFP-CHD labeling F-actin, (B) Fus1-sfGFP, (C) GFP-Cdc8 in WT, *acp1Δ*, *acp2Δ* and *acp1Δacp2Δ* at fusion time. **D-F.** Profiles of the bleach-corrected fluorescence intensities around the fusion focus at fusion time in the strains as in A-C. (D) GFP-CHD profiles. (E) Fus1-sfGFP profiles. (F) GFP-Cdc8 profiles. **G.** Boxplot of total Fus1 fluorescence intensity in fusing cells, in WT and *acp2Δ*. All p-values are relative to WT. Bars are 5 μm.

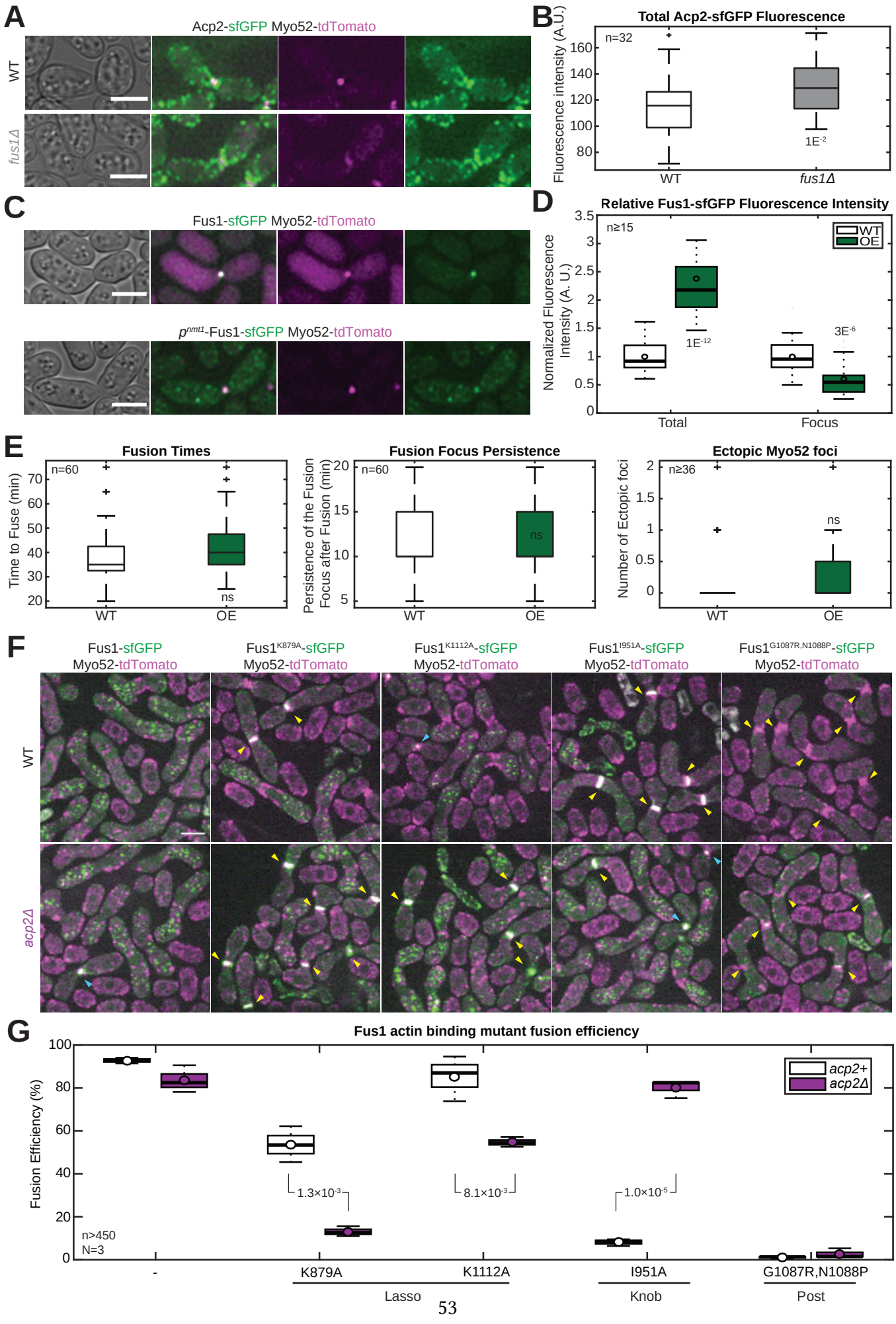
A
Acp2-sfGFP Myo52-tdTomato
WT
fus1Δ
B
Total Acp2-sfGFP Fluorescence
n=32
Fluorescence intensity (A.U.)
160
140
120
100
80
1E-2
WT
fus1Δ
C
Fus1-sfGFP Myo52-tdTomato
pnmt1-Fus1-sfGFP Myo52-tdTomato
D
Relative Fus1-sfGFP Fluorescence Intensity
n≥15
WT
OE
Normalized Fluorescence Intensity (A. U.)
3.5
3
2.5
2
1.5
1
0.5
0
1E-12
3E-6
Total
Focus
E
Fusion Times
n=60
Time to Fuse (min)
70
60
50
40
30
20
ns
WT
OE
Fusion Focus Persistence
n=60
Persistence of the Fusion Focus after Fusion (min)
20
15
10
5
ns
WT
OE
Ectopic Myo52 foci
n≥36
Number of Ectopic foci
2
1.5
1
0.5
0
ns
WT
OE
F
Fus1-sfGFP Myo52-tdTomato
Fus1K879A-sfGFP Myo52-tdTomato
Fus1K1112A-sfGFP Myo52-tdTomato
Fus1I951A-sfGFP Myo52-tdTomato
Fus1G1087R,N1088P-sfGFP Myo52-tdTomato
WT
acp2Δ
G
Fus1 actin binding mutant fusion efficiency
Fusion Efficiency (%)
100
80
60
40
20
0
acp2+
acp2Δ
1.3×10-3
8.1×10-3
1.0×10-5
n>450
N=3
-
K879A
K1112A
I951A
G1087R,N1088P
Lasso
Knob
Post

Figure 2.3 Weak increase in CP fluorescence in *fus1Δ* and no effect of Fus1 overexpression (previous page) **A.** Myo52-tdTomato and Acp2-sfGFP in WT and *fus1Δ* at fusion time. **B.** Boxplot of total fluorescence intensities in fusing cells in strains as in (A). **C.** Myo52-tdTomato and Fus1-sfGFP at fusion time, in strains expressing Fus1 either from endogenous locus or, in addition, under the *nmt1* promoter. **D.** Boxplot of total and fusion focus fluorescence intensities normalized to WT in fusing cells in strains as in (C). Note that the quantified levels of overexpressed Fus1-sfGFP do not represent all Fus1 in the cell, as endogenous Fus1 is not tagged. **E.** Boxplots of fusion times, fusion focus persistence, and ectopic Myo52 foci in WT and Fus1-overexpressing strains. **F.** Spinning-disk confocal images of Myo52-tdTomato and WT or mutant Fus1-sfGFP, as indicated, in WT and *acp2Δ*. Yellow arrowheads point to unfused cell pairs, with a broad Fus1 and Myo52 distribution at the contact zone. Blue arrowheads point to fusion foci. **G.** Fusion efficiencies at 9h after nitrogen removal in WT or *acp2Δ* strains carrying WT or mutant *fus1*, as indicated. All p-values are relative to WT, except where indicated. Bars are 5 µm.

However, the overexpression increased total Fus1 but not Fus1 at the fusion focus (Figure 2.3D). Thus, Fus1 overexpression does not directly mimic loss of CP. Second, we constructed four Fus1 alleles mutated in the FH2 domain. While all mutants abolished actin assembly *in vitro* (Scott et al., 2011), they showed different phenotypes when introduced as sole copy at the native genomic locus of otherwise wildtype cells. Fus1^{K879A} and Fus1^{K1112A}, which carry mutations in the FH2 lasso, were partly fusion-competent, whereas Fus1^{I951A} and Fus1^{G1087R,N1088P}, which carry mutations in the FH2 knob and post, respectively, almost completely blocked cell fusion. Combining these fus1 alleles with *acp2Δ* genotype did not systematically ameliorate the fusion phenotype (Figure 2.3F,G). In particular, the two hypomorphic lasso mutants compromised fusion further in *acp2Δ*. By contrast, the fusion-incompetent fus1^{I951A} allele permitted high levels of fusion in *acp2Δ*. This reveals an allele-specific suppression, where Fus1 knob, but not lasso mutants compromise competition with CP. This finding is consistent with the recently proposed steric clash between the FH2 knob and the CPβ tentacle (Shekhar et al., 2015). Third, Acp1 and Acp2 tagged with sfGFP localized prominently to actin patches, but neither were detected at the fusion focus in either wildtype cells or cells lacking the other CP subunit (see Figure 2.7A, C, D, F). Thus, CP is largely absent from the fusion focus, suggesting that competition with Fus1 principally takes place elsewhere.

2.4 Absence of capping protein leads to reduced levels of myosin V and cargoes at the fusion focus and formation of ectopic foci

Despite higher Fus1 levels, myosin Myo52 was reduced about 2-fold at the fusion focus in *acp2Δ* compared to WT cells (Figures 2.1B and 2.4F). A similar reduction was observed in *acp1Δ* and *acp1Δ acp2Δ* cells (Figure 2.1B and 2.4F). Similarly, exocytic vesicles marked by the exocyst subunits Exo84 and Exo70, the Rab11-homologue Ypt3, and the glucanase cargoes Agn2 and Eng2, were all reduced at the focus at fusion time in CP-lacking strains (Figure 2.4A-E, G-K). Since these glucanases are responsible for degrading the cell wall for fusion (Dudin et al., 2015), their reduced accumulation at the focus is the likely cause of the *acp2Δ* fusion delay. This view was further reinforced by Correlative Light Electron Microscopy images that confirmed that *acp2Δ* mating cells close to fusion have less vesicles at the shmoo tip than WT cells (Figure 2.5). Interestingly, the shmoo tip was also rather devoid of ribosomes in those cells compared to

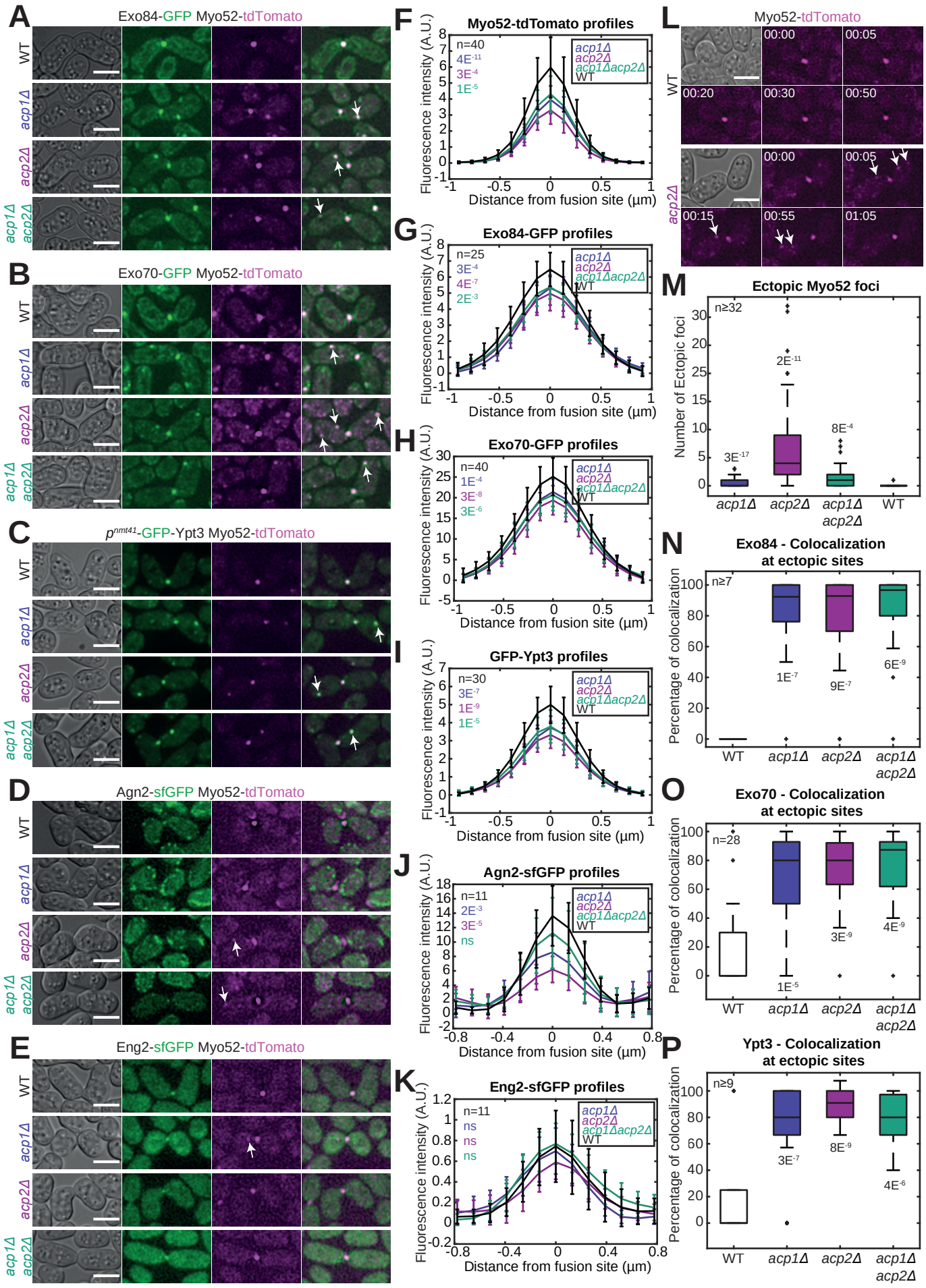
A
Exo84-GFP Myo52-tdTomato
WT
acp1Δ
acp2Δ
acp1Δ acp2Δ
B
Exo70-GFP Myo52-tdTomato
C
p^nmt41-GFP-Ypt3 Myo52-tdTomato
D
Agn2-sfGFP Myo52-tdTomato
E
Eng2-sfGFP Myo52-tdTomato
F
Myo52-tdTomato profiles
n=40
4E-11
3E-4
1E-5
acp1Δ
acp2Δ
acp1Δacp2Δ
WT
Fluorescence intensity (A.U.)
Distance from fusion site (µm)
G
Exo84-GFP profiles
n=25
3E-4
4E-7
2E-3
H
Exo70-GFP profiles
n=40
1E-4
3E-8
3E-6
I
GFP-Ypt3 profiles
n=30
3E-7
1E-9
1E-5
J
Agn2-sfGFP profiles
n=11
2E-3
3E-5
ns
K
Eng2-sfGFP profiles
n=11
ns
ns
ns
L
Myo52-tdTomato
00:00
00:05
00:20
00:30
00:50
00:00
00:05
00:15
00:55
01:05
M
Ectopic Myo52 foci
n≥32
2E-11
8E-4
3E-17
Number of Ectopic foci
acp1Δ
acp2Δ
acp1Δ acp2Δ
WT
N
Exo84 - Colocalization at ectopic sites
n≥7
1E-7
9E-7
6E-9
Percentage of colocalization
O
Exo70 - Colocalization at ectopic sites
n=28
1E-5
3E-9
4E-9
P
Ypt3 - Colocalization at ectopic sites
n≥9
3E-7
8E-9
4E-6

Figure 2.4 CP deletion leads to reduced vesicular markers at the fusion focus (previous page)
A-E. Myo52-tdTomato and (A) Exo84-GFP, (B) Exo70-GFP, (C) GFP-Ypt3, (D) Agn2-sfGFP, (E) Eng2-sfGFP in WT, *acp1Δ*, *acp2Δ* and *acp1Δ acp2Δ*, before fusion time. White arrows highlight ectopic foci. Note that these images, selected to show ectopic foci, stem from various timepoints during time-lapse imaging, for which specific timing in the fusion process and photobleaching may mask the difference in fusion focus intensity. **F-K.** Profiles of the bleach-corrected fluorescence intensities around the fusion focus at fusion time in the strains shown in A-E. (F) Myo52-tdTomato. (G) Exo84-GFP. (H) Exo70-GFP. (I) GFP-Ypt3. (J) Agn2-sfGFP. (K) Eng2-sfGFP. **L.** Time-lapse images of Myo52-tdTomato in WT and *acp2Δ* during the fusion process. White arrows show ectopic Myo52 foci. Time in hour:min. **M**. Number of time frames at which a Myo52 ectopic focus was observed during the fusion process in time-lapse imaging as in (L). **N-P.** Boxplots of the colocalization of Myo52 with (G) Exo84, (H) Exo70, and (I) Ypt3 at ectopic sites in WT, *acp1Δ*, *acp2Δ*, and *acp1Δ acp2Δ* strains. All p-values are relative to WT. Bars are 5 µm.

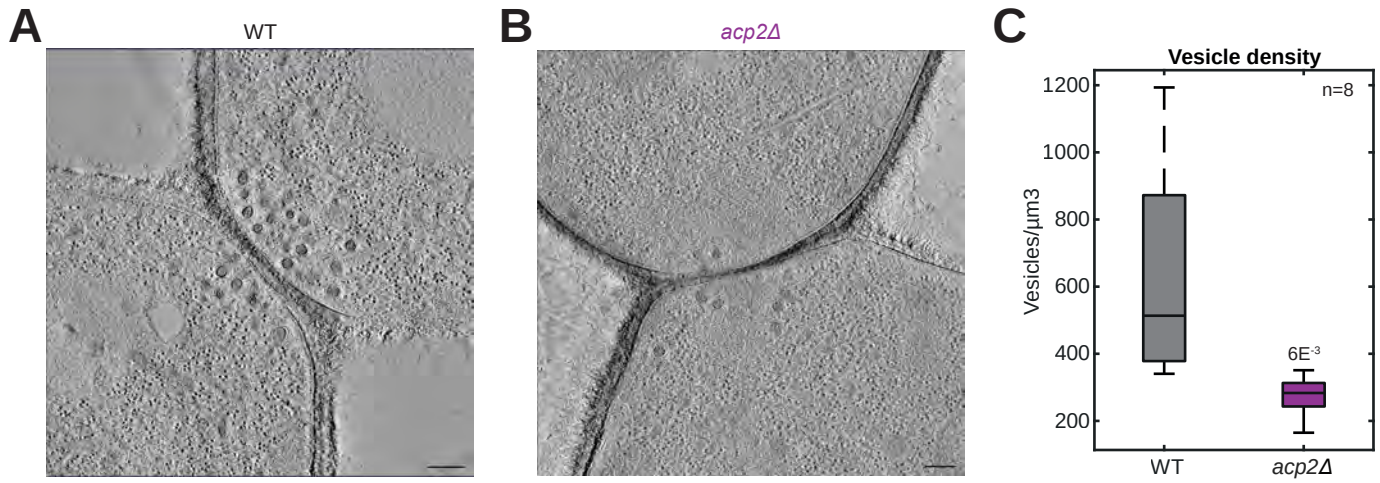

Figure 2.5 CP deletion leads to reduced vesicle numbers at the region of contact between the two mating cells
A. Virtual z-slices through electron tomograms taken at the contact site of cell pairs during the fusion process as identified by light microscopy. WT and *acp2Δ h90* strains were labelled with Myo52-tdTomato and Fus1-sfGFP. Cell pairs in fusion were identified by light microscopy on 300-nm sections after high-pressure freezing and freeze substitution, as described in (Muriel et al., 2021). Scale bars are 100 nm. **B.** Density of vesicles within a half-cylinder of 1 µm diameter centered at the center of the cells' contact zone. p-value is relative to WT.

the WT, which suggests molecular crowding. Because all actin markers were increased at that zone, their over-accumulation could explain this molecular crowding.

Why do the actin-rich *acp2Δ* fusion foci accumulate fewer exocytic vesicles? We noticed that *acp2Δ* cells frequently form Myo52 foci away from the fusion focus (Figure 2.4L). Such ectopic foci formed in both P- and M-cells, repeatedly during the fusion process. In time-lapse imaging at 5 min intervals, *acp2Δ* cells displayed on average 7 timepoints with ectopic foci, *acp1Δ* and *acp1Δ acp2Δ* cells displayed 1, and we barely found any for WT cells with this set-up (a single ectopic focus in 32 mating pairs; Figure 2.4M). Camera upgrade (which happened in the course of the project) or spinning disk imaging revealed more ectopic foci in all backgrounds, including WT (see Figure 2.7J and 2.6A, respectively). The rare, transient ectopic foci detected in WT mating pairs suggest that the *acp2Δ* behaviour exists but is normally repressed in WT cells. These ectopic foci extensively colocalized with Exo84, Exo70 and Ypt3 (Figure 2.4A-C, N-P). We could not detect glucanases at ectopic foci, likely because of low expression levels and reduction of function by sfGFP tagging (Figure 2.4D-E). These results suggest that the formation of ectopic foci is the cause of the reduced Myo52 and cargoes at the fusion focus.

2.5 Myo52 ectopic foci form at actin patches

Higher-speed time-lapse spinning-disk imaging at 1 s intervals showed Myo52 ectopic foci did not appear randomly: they did not break-off from the fusion focus; instead they formed and stayed at remote locations at the cell periphery, occasionally moving back and fusing with the fusion focus (Figure 2.6A). The colocalization with exocytic markers stood true at this higher temporal resolution (Figure 2.6B). Thus, ectopic foci are nucleated at remote location in absence of CP.

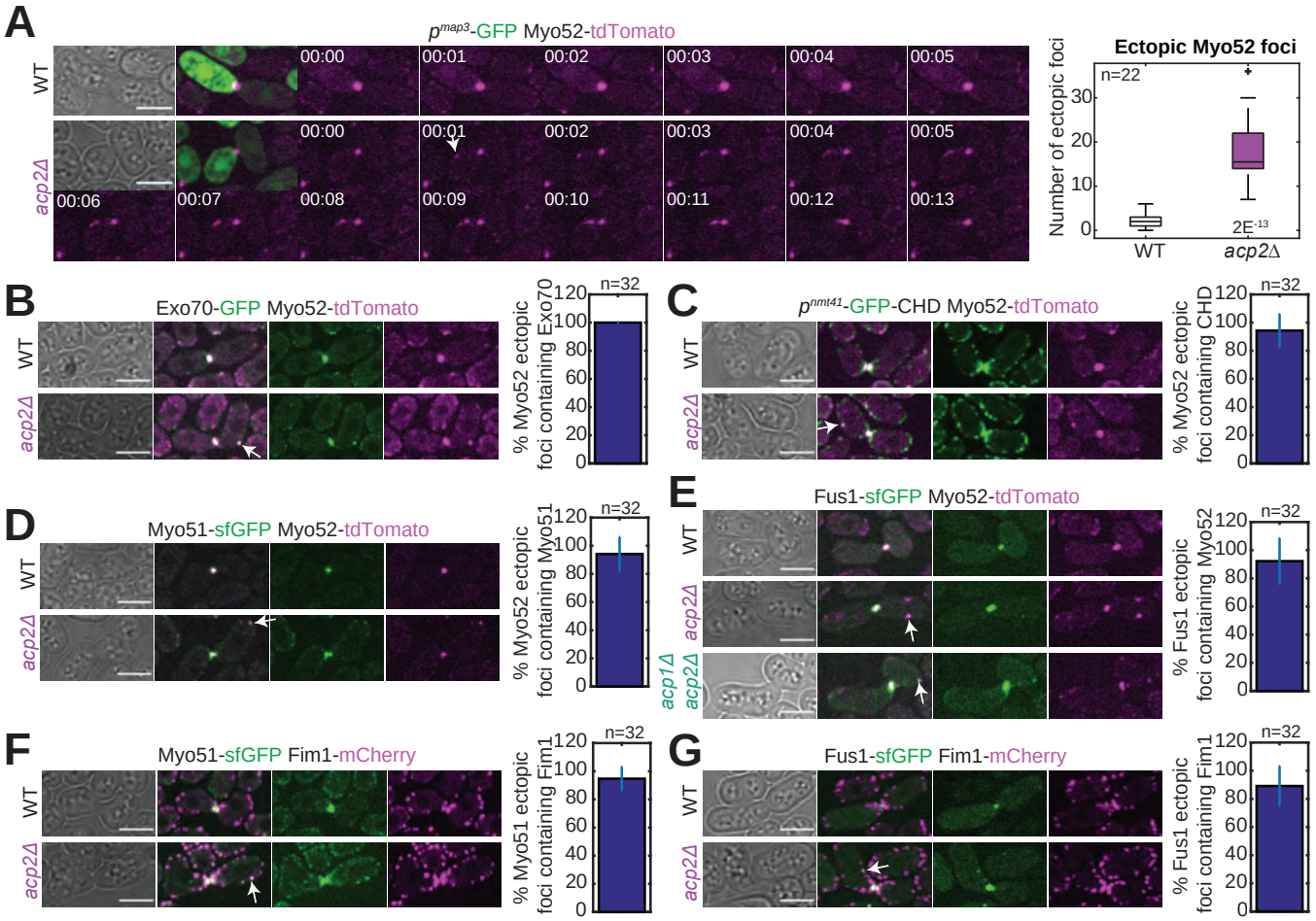

Figure 2.6 Myo52 ectopic foci form at actin patches
A. Spinning-disk confocal time-lapse images of Myo52-tdTomato and cytosolic GFP expressed under the *map3* promoter (shown only for first timepoint) in WT and *acp2Δ* before fusion time. The white arrow marks an ectopic Myo52 focus that forms at 1s and then moves towards the fusion focus. Time in min:sec. (Right) Number of time points, acquired at 1s interval during 3min, displaying a Myo52 ectopic focus. **B-E.** Spinning-disk confocal images of Myo52-tdTomato and (B) Exo70-GFP, (C) GFP-CHD, (D) Myo51-sfGFP, (E) Fus1-sfGFP in WT, *acp2Δ* and *acp1Δ acp2Δ* before fusion time. **F-G.** Spinning-disk confocal images of strains expressing Fim1-mCherry and (F) Myo51-sfGFP or (G) Fus1-sfGFP in WT and *acp2Δ* before fusion time. The bar plots to the right of the images show the proportion of ectopic foci colocalizing with indicated markers, of which an example is shown with a white arrow. Bars are 5 µm.

Interestingly, GFP-CHD as F-actin marker revealed that >90 % of ectopic foci colocalized, at least transiently, with what looked like actin patches (Figure 2.6C). Ectopic foci also colocalized with Myo51 (Figure 2.6D), a second type V myosin that normally associates with tropomyosin and decorates linear actin structures (Dudin et al., 2017; Lo Presti et al., 2012; Wang et al., 2014). Whereas Myo51 principally decorates the fusion focus in WT cells, in *acp2Δ* it additionally localized to actin patches marked by the

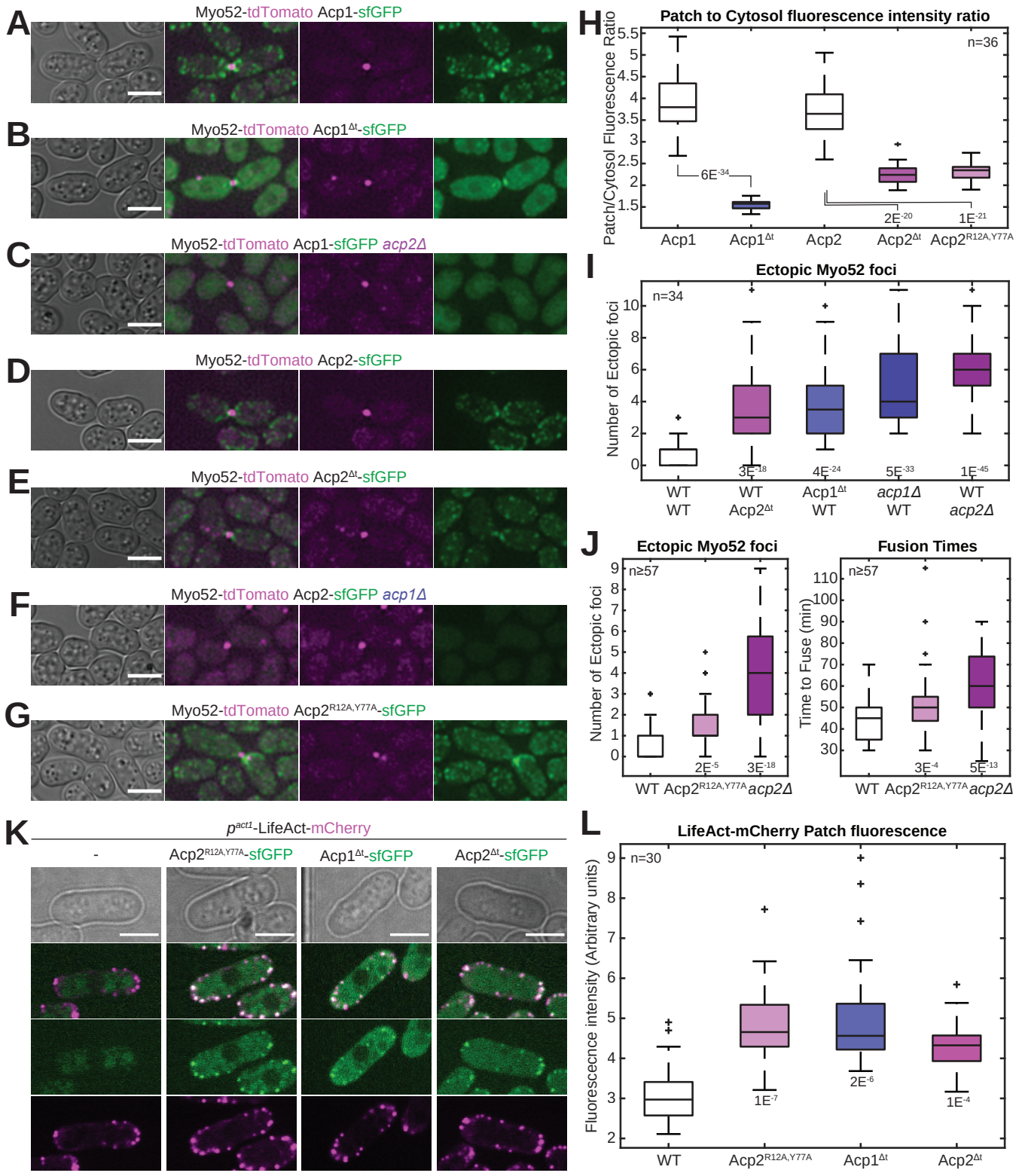

Figure 2.7 CP recruitment to actin patches and barbed end binding are required to protect against ectopic foci

A-G. Myo52-tdTomato and sfGFP-tagged Acp1 and Acp2, in WT, lacking its tentacle (Δt), carrying mutated CPI-interacting residues (R12A,Y77A), or in absence of the other subunit at fusion time, as indicated. Bars are 5 µm. **H.** Acp1-sfGFP or Acp2-sfGFP patch-to-cytosol fluorescence intensity ratios in fusing cells of strains as in (A-G). **I.** Number of time frames at which a Myo52 ectopic focus was observed during the fusion process in time-lapse imaging of strains as in (A-F). **J.** Ectopic foci (as in I) and fusion times for WT (*acp2-sfGFP*), *acp2*^{R12A,Y77A}*-sfGFP* and *acp2Δ* strains. **K.** Spinning-disk confocal microscopy images of LifeAct-mCherry under the actin promoter alone or in combination with Acp2^{R12A,Y77A}-sfGFP, Acp1$^{\Delta t}$-sfGFP and Acp2$^{\Delta t}$-sfGFP as described above in interphase cells during exponential growth. **L.** Boxplots of LifeAct-mCherry patch fluorescence intensity in the strains shown in (A). In (I-J) and (L), all p-values are relative to WT. Bars are 5 µm.

actin bundler Fim1 (Skau et al., 2011; Wu et al., 2001) (Figure 2.6F). Importantly, the more sensitive spinning-disk microscopy also revealed Fus1 in Myo52 ectopic foci (Figure 2.6E), which colocalized with Fim1 (Figure 2.6G). In *acp1Δacp2Δ* double mutant, Fus1 also colocalized with Myo52 ectopic foci (Figure 2.6E). Thus, the absence of CP leads to recruitment of formin Fus1 and type V myosin to Arp2/3-nucleated actin patches.

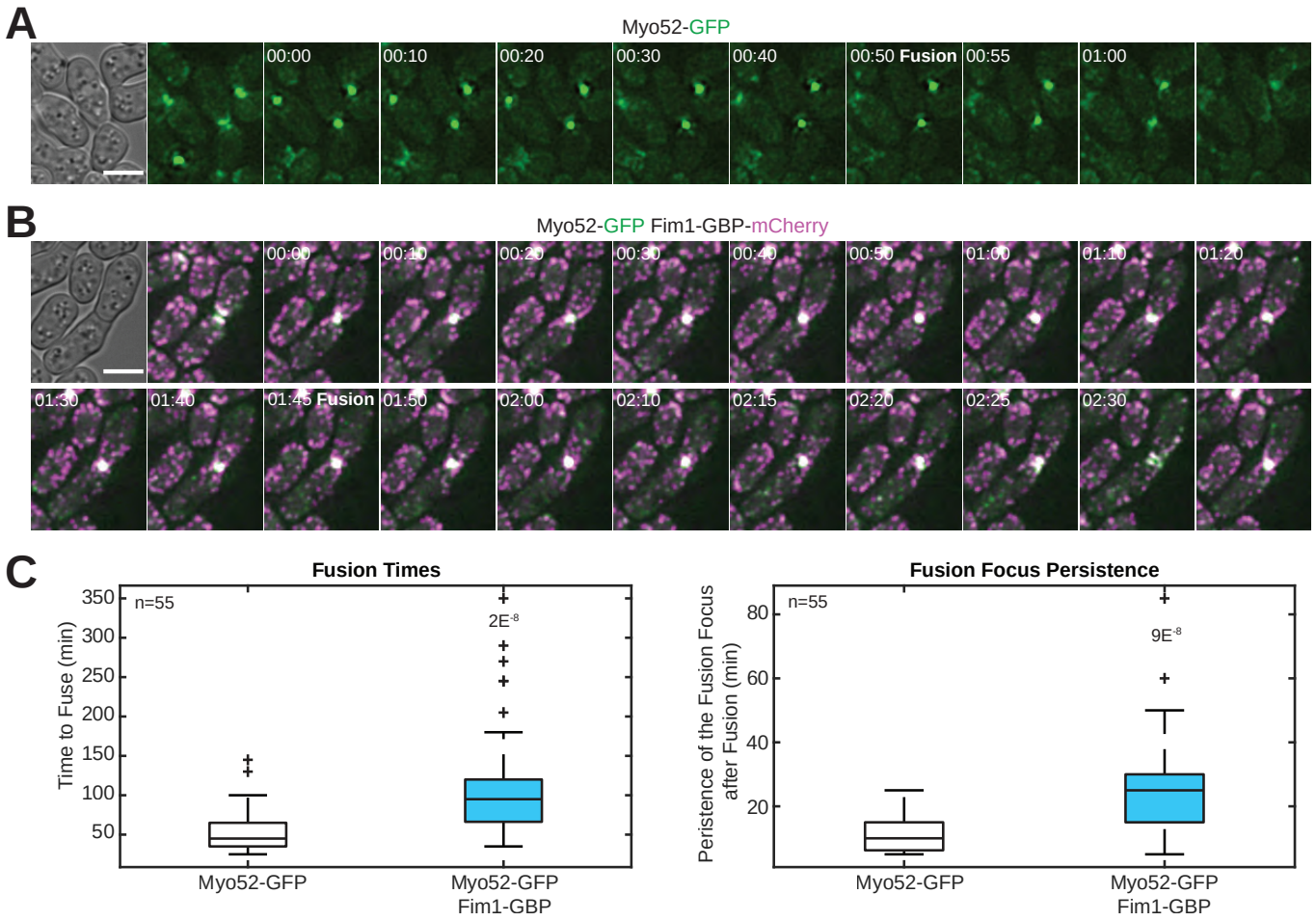

Figure 2.8 Forced recruitment of Myo52 to actin patches delays fusion
A-B. Time-lapse images of a strain expressing Myo52-GFP alone (A) or in combination with Fim1-GBP-mCherry (B) from beginning to disappearance of the fusion focus. The beginning is defined as the first formation of the focus in both cells. The fusion point is highlighted and is defined as the peak Myo52-GFP fluorescence intensity at the focus. Time in hour:min. Bars are 5 µm. **C.** Boxplots of the above-mentioned strains fusion times and focus persistence times.

Fus1 likely binds exposed filament barbed ends at actin patches in absence of CP, and nucleates ectopic foci. To investigate whether CP's capping function is required to protect patches from Fus1, we deleted Acp1 and Acp2 tentacles ($Acp1^{\Delta t}$ and $Acp2^{\Delta t}$) to reduce CP affinity for actin barbed ends. These truncations compromised actin patch localization, with $Acp2^{\Delta t}$ retaining better localization than $Acp1^{\Delta t}$ (Figures 2.7B, E, H), in agreement with previous *in vitro* work (Wear et al., 2003). They also showed more frequent ectopic Myo52 foci than WT cells, in an order consistent with their retained actin-binding capacity (Figure 2.7B, E, I). We also generated $Acp2^{R12A,Y77A}$, predicted not to bind the CPI motif (Edwards et al., 2015). $Acp2^{R12A,Y77A}$ localized inefficiently to patches (Figure 2.7G, H), and exhibited ectopic foci and increased fusion times, to levels intermediate between WT and *acp2Δ* cells (Figure 2.7J). The reduced localization of $Acp1^{\Delta t}$, $Acp2^{\Delta t}$

and Acp2^{R12A,Y77A} to actin patches was not due to reduced F-actin content in the patches, which instead exhibited increased LifeAct-mCherry fluorescence (Figure 2.7K-L), like *acp2Δ* cells (Berro & Pollard, 2014). These results indicate that localization of CP to patches is necessary to prevent the formation of ectopic foci.

Finally, to test whether ectopic foci cause the fusion delay by diverting vesicles away from the cell-cell contact zone, we artificially recruited Myo52-GFP to patches labelled with Fim1-GBP-mCherry by using the high affinity between GFP-Binding Protein (GBP) and GFP (Figure 2.8A-B). This led to fusion delay and focus persistence after fusion, replicating the *acp2Δ* phenotypes (Figure 2.1B-D and Figure 2.8C).

We conclude that during fusion, CP insulate actin patches from Fus1. This ensures Fus1 activity is restricted, and myosin V-driven cargoes are directed, to the site of cell-cell contact.

2.6 Uncapped actin patches recruit formins and acquire a dual identity in interphase cells

To test whether CP more generally protects actin patch identity, we investigated the influence of CP deletion in interphase cells. In absence of CP, actin patches are dispersed both in *S. cerevisiae* (Sizonenko et al., 1996) and in *S. pombe* (Berro & Pollard, 2014; Nakano & Mabuchi, 2006), and *S. pombe* cells also exhibit weak actin cables (Kovar et al., 2005; Nakano & Mabuchi, 2006). Remarkably, markers normally associated with formin-nucleated actin cables were perturbed in *acp2Δ*: Myo51, which labels cable-like structures in WT cells (Lo Presti et al., 2012), formed punctate structures that colocalized with Fim1 in *acp2Δ* cells (Figure 2.9A); Myo52, which mainly localizes to cell tips in WT cells, formed dots that coincided with Myo51 and Fim1 patches in *acp2Δ* (Figure 2.9B-C); Tropomyosin Cdc8, which stabilizes actin cables and is largely absent from actin patches in WT cells, formed foci that colocalized with Fim1 in *acp2Δ* (Figure 2.9D). The co-incidence of fimbrin and tropomyosin is particularly remarkable given recent data showing that competition between these two proteins drives their sorting to distinct Arp2/3 and formin-nucleated networks, respectively (Christensen et al., 2017). Thus, actin patches assume a dual identity in absence of CP both during mating and during vegetative growth.

Because Fus1 is not expressed during mitotic growth (Petersen et al., 1995), we monitored the localization of For3 and Cdc12 formins. For3, which only occasionally overlapped with actin patches in WT cells, was prominently present at actin patches in *acp2Δ* mutants (Figure 2.9E). By contrast, in *fim1Δ* cells, in which tropomyosin also decorates patches (Skau & Kovar, 2010), For3 was largely absent from patches like in wildtype cells (Figure 2.9F). In *acp2Δ* cells, disruption of patches with the Arp2/3 inhibitor CK-666 or F-actin depolymerization with Latrunculin A restored For3 localization to cell poles (Figure 2.9E). Arp2/3 inhibition also promoted Fim1 re-localization to cell poles, which is likely due to excess formin-assembled cables (Burke et al., 2014), as complete actin depolymerization rendered Fim1 cytosolic (Figure 2.9E). Thus, uncapped actin patches ectopically recruit For3. Cdc12 also formed ectopic foci at actin patches in *acp2Δ* cells (Figure 2.9G). These ectopic foci were distinct from the previously-reported spot of Cdc12 (Chang, 1999), which occurs also in WT cells, does not coincide with patches, has a longer life-time, and is more intense (Figure 2.9G). We conclude that formins are recruited to uncapped actin patches.

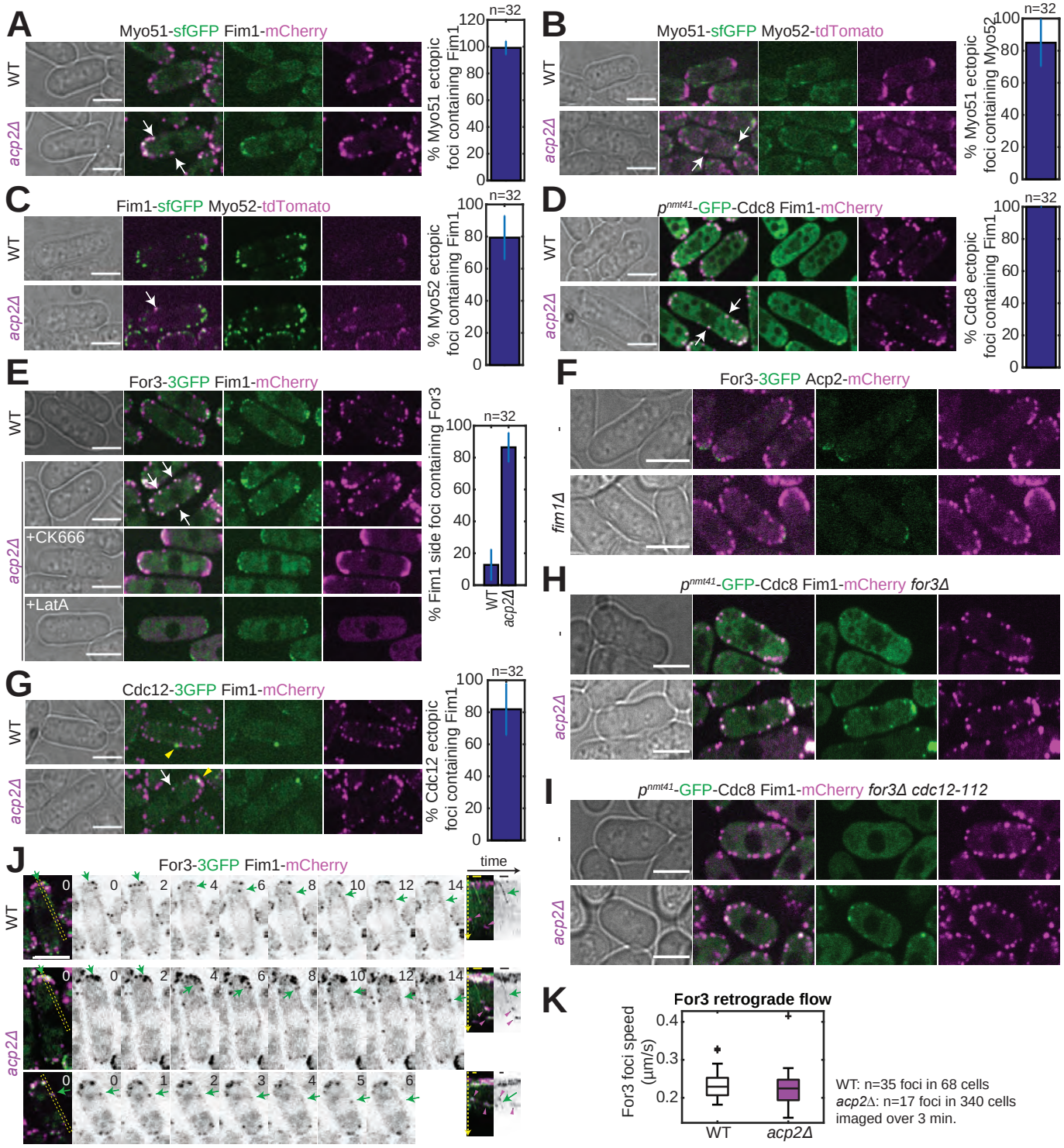

Figure 2.9 CP insulate actin patches from Myo52 and actin cable markers in interphase cells

A-E. Spinning-disk confocal images of (A) Fim1-mCherry and Myo51-sfGFP, (B) Myo52-tdTomato and Myo51-sfGFP, (C) Myo52-tdTomato and Fim1-sfGFP, (D) Fim1-mCherry and GFP-Cdc8, (E) Fim1-mCherry and For3-3GFP, in WT and *acp2Δ* interphase cells. In (E), bottom panels show *acp2Δ* treated with 500 μM CK-666 for 5 min or 200 μM Latrunculin A for 5 min. White arrows highlight colocalization events in *acp2Δ*, which rarely occur in WT cells. The proportion of colocalization at ectopic sites along the cell sides is shown with the bar plot on the right. **F.** Spinning-disk confocal images of For3-3GFP and Acp2-mCherry in WT and *fim1Δ* cells. **G.** Spinning-disk confocal images of Fim1-mCherry and Cdc12-3GFP, in WT and *acp2Δ* interphase cells. White arrows highlight colocalization events in *acp2Δ*, which do not occur in WT cells. Yellow arrowheads point to Cdc12 spots. The proportion of colocalization at ectopic sites along the cell sides is shown with the bar plot on the right. **H-I.** Spinning-disk confocal microscopy images of Fim1-mCherry and GFP-Cdc8 in interphase cells during exponential growth in (H) *for3Δ* and (I) *for3Δ cdc12-112* at 36°C, in otherwise WT and *acp2Δ* backgrounds. **J.** Spinning-disk confocal time-lapse images of

Fim1-mCherry and For3-3GFP (green and grey) showing retrograde flow in WT (top) and *acp2Δ* cells (bottom two panels). The bottom panel shows an example of retrograde flow starting at a lateral actin patch. Kymographs of the yellow dashed boxed region are shown on the right. Green arrows point to For3-3GFP retrograde flow. Purple arrowheads in kymographs show lateral actin patches on which For3 localizes in *acp2Δ* but not WT cells. **K.** For3 retrograde flow rate. Time in seconds. Bars are 5 μm.

To address whether formins are active at patches, we first tested whether their inactivation would alleviate the localization of tropomyosin at *acp2Δ* actin patches. However, deletion of for3 by itself led to significant Cdc8 enrichment on actin patches, likely because actin cytoskeleton homeostasis is perturbed in absence of actin cables (Figure 2.9H). Therefore, not surprisingly, Cdc8 also localized to actin patches in *for3Δ acp2Δ* and *cdc12-112 for3Δ acp2Δ* mutants (Figure 2.9H-I). We then directly probed for For3 activity by observing its retrograde flow, which depends on actin assembly in cables (Martin & Chang, 2006). For3 retrograde flow occurred at similar rates in WT and *acp2Δ* cells, though fewer movements were observed in *acp2Δ*, consistent with the weak actin cables (Figure 2.9J-K) (Kovar et al., 2005; Nakano & Mabuchi, 2006). Interestingly, For3 retrograde movements could be observed to initiate from actin patches, indicating cable assembly from the patches (Figure 2.9J). We conclude that, independently of the specific formin, CP insulates actin patches from formins, restricting their activity to the proper location.

2.7 Discussion

How cells simultaneously assemble functionally diverse actin structures of distinct identity within a common cytosol is a debated question. Arp2/3 and formins respectively assemble branched and linear actin structures decorated by largely distinct actin-binding proteins. A hallmark of formins is their ability to promote barbed-end growth against the growth-arrest function of capping protein (CP), a feature demonstrated in numerous *in vitro* studies (Bombardier et al., 2015; Harris et al., 2004; Kovar et al., 2003; Moseley et al., 2004; Shekhar et al., 2015; Zigmond et al., 2003). However, how CP may prevail against formins *in vivo* was largely unexplored. Here, we have shown that CP protects Arp2/3-assembled actin patches against formins, thus preserving their identity and restricting formins to their proper location.

Our interest in CP arose from the cell fusion delay of *acp2Δ* cells. For fusion, cells locally digest their cell wall by concentrating the exocytosis of secretory vesicles containing cell-wall hydrolases at the site of cell-cell contact (Dudin et al., 2015). In WT cells, this is achieved by the Fus1-assembled actin fusion focus. By contrast, in cells lacking CP, despite strong Fus1 accumulation at the fusion site, secretory vesicles are frequently diverted away from the fusion site to ectopic Fus1 foci at actin patches. This correlates with a reduction in secretory vesicles at the fusion focus, which likely explains the fusion delay. Indeed, the forced diversion of Myo52 to actin patches also yields extended fusion times. Thus, the fusion defect of CP mutants likely results from diversion of secretory vesicles to ectopic sites, rather than from excessive actin assembly at the fusion site. Because CP mutants exhibit longer actin patch lifetimes (Berro & Pollard, 2014), which may lead to slower endocytosis, the fusion delay may also partly result from reduced recycling of the pheromone receptor from the plasma membrane (Dudin et al., 2016).

This raises the question of where CP acts – in formin-assembled structures or at Arp2/3-assembled patches. We argue that the formin-CP competition happens throughout the cell, with distinct outcome:

in formin-assembled structures, the formin wins and CP is largely dispensable; at actin patches, CP dominates and insulates this structure against formins. These distinct outcomes are reflected in the exclusive localization of CP at patches and restriction of formins to other cellular locations. The occasional ectopic foci detected in WT cells illustrate that CP patch protection against formins is an active process that can transiently fail even in WT cells.

CP-formin competition is best revealed by alteration of Fus1 and/or CP function. At the fusion focus, the competition is exposed by Fus1 FH2 mutations. A first observation is that FH2 mutations compromise fusion to various extent *in vivo*, although they all fully abrogated actin assembly *in vitro* (Scott et al., 2011). The poor predictive value of the *in vitro* activity may be due to high local Fus1 concentration in the focus, which likely exceeds the concentrations tested *in vitro*. A second observation is the strong allele-specific suppression by *acp2Δ* of the fusion defect of fus1^{I951A}, which carries a mutation in the knob. This allele-specific suppression is consistent with the proposed structural arrangement of the formin-CP ternary complex at the barbed end, which shows a steric clash between the formin knob and CPβ (Shekhar et al., 2015). The I951A mutation likely favors the binding of CPβ, thus promoting capping function in the ternary complex, which is relieved upon CPβ deletion. In the cell, the inability of Fus1^{I951A} to assemble a fusion focus must be due to CP competing with the formin at the fusion site. Further evidence for competition at this location comes from increased Fus1 intensity at the fusion focus and the extended focus lifetime in CP mutants. This suggests that small amounts (below detection levels) of CP may compete with Fus1 in the fusion focus, although the increased Fus1 intensity may also be due to Fus1 recruitment to adjacent patches. We conclude that some Fus1-CP competition can take place at the fusion site, where Fus1 normally dominates.

Our data indicate that the principal sites of formin-CP competition are actin patches, where CP efficiently outcompetes Fus1 (Figure 2.10). In WT cells, CP is strongly enriched at actin patches and prevents formin binding. In cells lacking CP function, all three formins localize to actin patches. The strength of CP protection against formins largely scales with its barbed end binding affinity as measured *in vitro* (Wear et al., 2003), with acp2$^{\Delta t}$ showing fewer ectopic foci than acp1$^{\Delta t}$, and *acp1Δ* or *acp2Δ*. When CP is absent from patches, these acquire characteristics of linear actin structures: they are decorated by myosin V Myo51 and tropomyosin, which normally preferentially associate with actin cables, ring and focus (Arai et al., 1998; Balasubramanian et al., 1992; Coulton et al., 2010; Dudin et al., 2017; Kurahashi et al., 2002; Lo Presti et al., 2012; Skau et al., 2009; Wang et al., 2014); they also accumulate the myosin V Myo52, which erroneously transports its cargoes to these locations. The coincidence of tropomyosin and fimbrin at patches devoid of CP is striking given recent findings that competition between these actin-binding proteins drives their specific association with formin- and Arp2/3-assembled structure *in vitro*, respectively (Christensen et al., 2017; Clayton et al., 2010; Skau & Kovar, 2010). Importantly, For3 is absent from tropomyosin-decorated *fim1Δ* patches, indicating that formins localize to patches because of a specific defect in capping rather than a global change in actin cytoskeleton homeostasis. We conclude that, in absence of CP, actin patches acquire a double identity.

One important question is whether the double identity of CP-devoid patches arises from ectopic formin activity or simply from uncapping. This question is difficult to address because any perturbation in actin structures will perturb homeostasis (Burke et al., 2014). For instance, formin deletion frees G-actin and

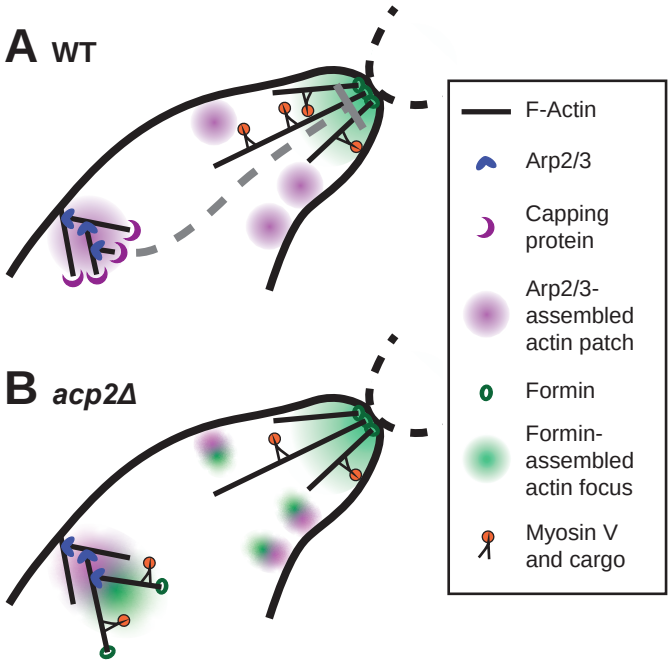

Figure 2.10 CP insulates Arp2/3-assembled actin patches from formins
A-B. Summary sketches of the findings presented in this study, showing the behavior of the different actin networks and their ABPs in (A) WT cells and (B) *acp2Δ* cells.

tropomyosin, which now incorporate in actin patches. Conversely, actin patch disruption enhances formin-assembled structures, now more permissive for fimbrin association. However, two observations argue for formin activity at CP-devoid patches. First, during mating, Myo52 was not present at all actin patches, but was always there when Fus1 was. This argues that Fus1 activity is the driving force for vesicular cargo recruitment. Second, the For3 retrograde flow from patches indicates assembly of cables from this location (Martin & Chang, 2006). As a side note, while the mechanism and function of For3 retrograde flow remain unknown, it occurred, and at similar rates, in *acp2Δ* cells, indicating that flow is not due to arrest of For3-dependent filament elongation upon formation of a ternary formin-CP complex. Together, these observations indicate that patch-localized formins actively assemble linear actin filaments.

An interesting observation is that *acp2Δ* cells consistently displayed stronger phenotypes not only than *acp1Δ*, but also than *acp1Δ acp2Δ* double mutants. Berro and Pollard also previously noted that the phenotypes of *acp2Δ* and *acp1Δ* are not identical (Berro & Pollard, 2014). We note that our data show a quantitative, but not qualitative, difference between these genotypes. It is formally possible that the stronger phenotype of *acp2Δ* cells is due to a CPβ function partly unrelated to capping activity. However, the weaker phenotype of *acp1Δ acp2Δ* instead indicates that Acp1 not bound by Acp2 enhances the phenotype. One interpretation is that, while formins gain access to actin barbed ends in absence of Acp2, they may gain better access if Acp1 is still present. Because Acp1 still weakly binds the actin barbed end in absence of Acp2 *in vitro* (Kim et al., 2004), its presence may somehow help recruit formins to the barbed end. This interpretation predicts an interaction between formins and CPα, a hypothesis consistent with human INF2 formin association with CPα (Rollason et al., 2016).

Because CP-formin competition yields distinct outcomes at the sites of formin action and Arp2/3-assembled patches, one question is what defines the competition outcome. Part of the answer comes from

the Acp2^{R12A,Y77A} allele, carrying mutations in the CPI-binding residues, which compromises CP localization to actin patches. This finding agrees with previous data in human cells that CP localization relies on interaction with CPI-containing proteins (Edwards et al., 2015). The specific CP-binding partners are unknown in *S. pombe*, but may involve the homologue of *S. cerevisiae* Aim21, which binds CP through the CPI-binding residues and contributes to its localization to actin patches (Farrell et al., 2017), though this finding was not reproduced in a second study (Shin et al., 2018). Consistent with this hypothesis, deletion of *S. pombe* Aim21 was identified in our genome-wide screen to have fusion defects (Dudin et al., 2017). The phenotype of acp2^{R12A,Y77A} cells indicates that CP recruitment to actin patches by pre-localized partners is required to protect them against formin activity. Thus, barbed end-independent recruitment of CP may tip the CP-formin competition in favor of CP in Arp2/3-assembled structures.

The findings described in our study present the CP-formin competition in a new light, where CP protects Arp2/3 structures against ectopic localization of formins. In fission yeast *acp2Δ* cells, formin localization to actin patches has important consequences on cellular organization: during mating, Fus1 diverts cargoes away from the fusion site, slowing the fusion process; in interphase cells, For3 activity at patches may cause the previously noted actin cables disorganization and partial loss of cell polarity, leading to actin patch depolarization (Berro & Pollard, 2014; Kovar et al., 2005); in dividing cells, the reason for the cytokinetic defect of cells lacking CP (Kovar et al., 2005) may also be the titration of Cdc12 to actin patches. As CP is ubiquitous in eukaryotic cells, it likely protects the identity of Arp2/3 actin assemblies and prevents formin ectopic activity in a vast range of organisms.

3. Mating specific fusion focus formin Fus1 actin assembly properties are uniquely tailored to its function

3.1 Introduction

Formins are a large family of conserved proteins that act both as nucleators and elongators of actin filaments (Breitsprecher & Goode, 2013; Courtemanche, 2018). They are involved in a large variety of cellular processes such as polarization, motility, or division (Bohnert, Willet, et al., 2013; Goode & Eck, 2007; Pollard & O'Shaughnessy, 2019; Skau & Waterman, 2015). They consist of two highly conserved Formin Homology (FH) domains flanked by less well conserved N- and C-terminal regulatory regions (Rivero et al., 2005). The FH2 domain acts as a dimer which processively binds the elongating actin filament barbed end (Paul & Pollard, 2009), while the FH1 domain extrudes from the FH2 dimer as a flexible proline-rich track and binds profilin-actin to feed it to the elongating filament. The number and quality of proline-rich tracks, but also their spacing in relationship to the FH2 dimer will then dictate elongation speed (Courtemanche & Pollard, 2012; Scott et al., 2011; Vidali et al., 2009). For example, fission yeast formins For3, Cdc12 and Fus1 possess 4, 2 and 1 proline-rich tracks, respectively, but that doesn't scale perfectly with their respective *in vitro* elongation speed, as Cdc12 and For3 have a very similar elongation speed. However, both are better elongators than Fus1 with its one and only proline-rich track, which suggest that while elongation speed roughly scales up with the number of proline rich-tracks, those proline rich-tracks are not equivalent. In addition, replacing Cdc12 FH1 by Fus1's does not dictate an elongation speed equal to Fus1's and vice-versa, which further indicate that the elongation speed dictated by the FH1 domain are also dictated by the FH2 domain there are connected to. The regulatory regions, instead, regulate the specific activation at the right time and place, often through interaction with additional proteins, which explains their lower conservation (Breitsprecher & Goode, 2013). Additionnally, formins can have non canonical properties such as filamentous actin (F-actin) severing, F-actin bundling, mechanosensitivity or self-association properties (Bohnert, Grzegorzewska, et al., 2013; Courtemanche, 2018; Scott et al., 2011; Zimmermann & Kovar, 2019).

Most organisms express different formin genes, which will carry out specific functions. For example, while *Saccharomyces cerevisiae* possesses only 2 formins (Breitsprecher & Goode, 2013), *Arabidopsis thaliana* has at least 21 (Blanchoin & Staiger, 2010), and *Schizosaccharomyces pombe* (*S. pombe*) has 3, which organize distinct actin networks (Kovar et al., 2011). Indeed, For3 supports the formation of polarizing actin cables (Feierbach & Chang, 2001), Cdc12 supports the contractile cytokinetic ring (Chang et al., 1997), and Fus1 supports the formation of the fusion focus (Dudin et al., 2015), an aster of actin filaments specifically formed upon nitrogen starvation, which is necessary for the fusion step to form the diploid zygote. Attention has been given to regulated activation as the main factor explaining functional specificity of those different formins (Breitsprecher & Goode, 2013; Yonetani et al., 2008), but there is less information on how the

specific actin assembly properties of formins, such as their nucleation or elongation rates, which vary significantly between formins, or their additional actin-regulatory properties, can participate in functional specificity. Importantly, some formins, such as Cdc12 or Fus1, are thought not to be autoinhibited by a canonical N- to C-terminus interaction (Scott et al., 2011; Yonetani et al., 2008), which further reinforces the importance of studying other characteristics as to what makes a formin specific to its actin network. For example, recent findings by (Homa et al., 2021), have shed some light on the importance of Cdc12's specific actin assembly properties in supporting cytokinesis, but those findings have, as of now, not been generalized. All three *S. pombe* formins have been extensively studied *in vitro*, and their specific actin assembly rates are known (Scott et al., 2011), which makes *pombe* a good model organism to understand the specificities of each formin necessary to organize their own actin network.

Cell-cell fusion is a fundamental process heavily relying on actin assembly (Eitzen, 2003; Lanzetti, 2007). In *S. pombe*, cell-cell fusion occurs following mating inducing nitrogen starvation. During this processs, cells have to digest their cell wall to put their membrane in contact and coordinate spatially and temporally so that this doesn't lead to lysis due to the important internal turgor pressure. This is coordinated by a mating specific actin structure, the fusion focus, which consists of an aster of actin filaments assembled by Fus1 and forms at the region of contact between the two cells (Dudin et al., 2015). This structure supports directed release of glucanases-loaded secretory vesicles transported by Myosin V Myo52, which ultimately leads to cell-wall digestion. As cell-cell fusion is not a necessary step of the cell cycle, contrary to cytokinesis, it is a very convenient process to study the specific formin properties that have been selected to assemble a particular actin network, as changing those won't be lethal, which allow us to test the whole range of formin properties with no problematic impact on cell growth.

Using chimeras of the three different *pombe* formins to replace Fus1, we found specificities in both the N-terminal regulatory region of Fus1 and in its actin assembly domains which are essential to sustain fusion. This chapter brings about the necessary properties contained within Fus1 and then concentrates on the importance of Fus1 actin assembly domains FH1 and FH2 while the next chapter will focus on its N-terminal regulatory region.

3.2 Fus1 cannot be functionally replaced by any of the other *pombe* formins

To investigate whether Fus1 contains any essential property for fusion, we replaced Fus1 by either of the two other *pombe* formins, Cdc12 and For3. We did so by integrating them at the *ura4* locus under the *fus1* promotor in a *fus1Δ* strain (Figure 3.1A). The Fus1 version of that construct performed just as well as the WT in terms of both localization (Figure 3.1B) and fusion efficiency (Figure 3.1C), i.e. the proportion of fused cells amongst all mating pairs 24 hours after the process was started by removal of nitrogen. On the contrary, neither Cdc12 nor For3 were able to replace Fus1, as they were almost fully fusion deficient (Figure 3.1C) while they clearly mated (Figure 3.1B). Those results confirm that Fus1 is a formin well adapted to its function and cannot be replaced by another formin.

While this may be explained in part by the N-terminal regulatory regions of those formins, responsible for their localizations (Gao et al., 2010; Martin et al., 2007; Petersen et al., 1998b; Yonetani et al., 2008), the

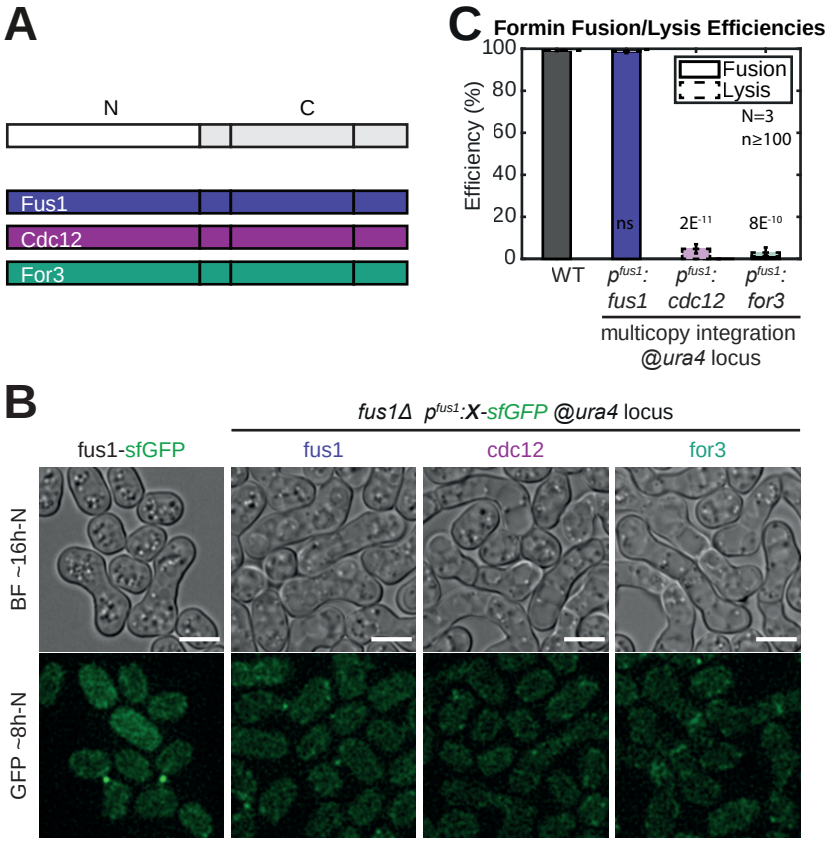

Figure 3.1 Fus1 cannot be functionally replaced by the other *S. pombe* formins
A. Scheme showing the different constructions used in the figure. **B.** Brightfield images ~16h post starvation and GFP fluorescence images ~8h post starvation of homothallic WT strains expressing Fus1-sfGFP at the endogenous locus or homothallic *fus1Δ* strains expressing Fus1, Cdc12 or For3 tagged with sfGFP at the *ura4* locus under the *fus1* promotor. **C.** Fusion and lysis efficiencies 24h after nitrogen removal in strains as in (B). All p-values are relative to WT. Bars are 5 µm.

lack of proper localization is not solely responsible for those findings. Indeed, the For3 construct localizes, as Fus1, at the region of contact between the two mating cells (Figure 3.1B). Instead, we also have to consider that those three formins possess a different array of actin assembly properties within their FH1 and FH2 domains (Table 1.1) that may account for some of the inability to support cell fusion. In order to understand to what extent Cdc12 and For3's inability to replace Fus1 stems from their different N-terminal regulatory region or FH1-FH2 domains, we decided to construct a set of chimeric formins where all three formins were cut right in between their N-terminal regulatory region and their FH1-FH2 actin assembly domains, resulting in two halves that we will call N and C, which we can assemble together keeping one or the other constant to answer those questions.

3.3 Both N-terminal regulatory region and FH1-FH2 actin assembly part of Fus1 are unique among other *pombe* formins

Using the set of chimeric formins that keep Fus1C constant while varying the N-part, we have a set of formins with all the required actin assembly properties for fusion (Figure 3.2A). However, only the control Fus1N-Fus1C, with a restriction site separating the two halves, was able to support fusion (Figure 3.2B-C).

Indeed, both Cdc12N-Fus1C and For3N-Cdc12C showed almost no fusion (Figure 3.2B-C), similarly to Cdc12 and For3 alone. Because N-terminal regulatory regions of formins are usually responsible for localization information (Gao et al., 2010; Martin et al., 2007; Petersen et al., 1998b; Rivero et al., 2005; Yonetani et al., 2008), an incorrect localization could be the direct explanation for those results. However, while Cdc12, which normally localizes to the cytokinetic nodes in interphase cells, indeed mislocalizes (Figure 3.2B), For3, which normally localizes to the cell poles in interphase cells, localizes to the region of contact between the two cells, but it does not show a normal distribution, as it has a wider distribution at the cell tip (Figure 3.2B). As such, localization probably isn't the only reason why this set of chimeric Formins are fusion incompetent. Together, those results show that Fus1 N-terminal region has specific properties required for cell fusion.

Reversely, using the set of chimeric formins that keep Fus1N constant while varying the C-part, we have a set of formins that should be localized properly but display a range of actin assembly properties (Figure 3.2A, Table 1.1). The control Fus1N-Fus1C, as earlier, was able to support fusion in a manner indistinguishable from the WT (Figure 3.2D-E). The other chimeric formins were instead able to support fusion to varying reduced degrees (Figure 3.2D-E), which indicates an importance of the actin assembly properties of the formin nucleating the fusion focus, but also stresses the relative importance of the N-terminal regulatory region as all those chimeras performed better than the ones lacking Fus1N. Indeed, the Fus1N-For3C chimera performed very poorly, with only 12% of the cells managing to fuse 24h post Nitrogen starvation and a very hazy localization at the region of contact between the two cells (Figure 3.2D-E). On the contrary, the Fus1N-Cdc12C chimera performed relatively well, with a fusion efficiency of more than 76% and a localization to the region of contact between the two cells more similar to the WT than the one of For3 (Figure 3.2D-E). Of note, Fus1N-Cdc12C chimera resulting focus intensity is stronger than in the WT and had a tendency to form two resolvable fusion foci further apart than in the WT (Figure 3.2D-E), where the two fusion foci in each partner are very early on not resolvable by conventional light microscopy and instead appear as one and only focus (Dudin et al., 2015).

While this difference between Fus1N-For3C and Fus1N-Cdc12C could be, and probably is partly, explained by the differences in actin assembly properties (Table 1.1), where Cdc12 is more similar to Fus1 than For3, the two chimeras respective localizations, with Cdc12, as Fus1, being able to form a condensed focus while For3 isn't, instead directed us to assess the importance of Cdc12 C-terminal oligomerization domain. Indeed, this domain has been shown to mediate Cdc12 self oligomerization and its removal to be detrimental for cytokinesis, the cellular process supported by Cdc12 (Bohnert, Grzegorzewska, et al., 2013). We then constructed a Fus1N-Cdc12C chimera lacking this oligomerization domain, Fus1N-Cdc12CΔolig (Figure 3.2A), which reduced the ability of the Fus1N-Cdc12C chimera to support fusion with a fusion efficiency of only 15% and resulted in a wider localization (Figure 3.2D-E). Those results suggest that there is a self-oligomerization property contained within Fus1C which is important for fusion that is not present within For3C. To test this theory, we added Cdc12 oligomerization domain to the Fus1N-For3C chimera (Figure 3.2A), resulting in a chimera much more potent than Fus1N-For3C in supporting fusion, with 53% of the cells managing to fuse, and the formation of a more condensed fusion foci (Figure 3.2D-E). Of note, the presence of Cdc12 oligomerization domain correlate with the presence of the double dot phenotype, as it is suppressed in Fus1N-Cdc12CΔolig and appears in Fus1N-For3C-Cdc12olig (Figure 3.2D).

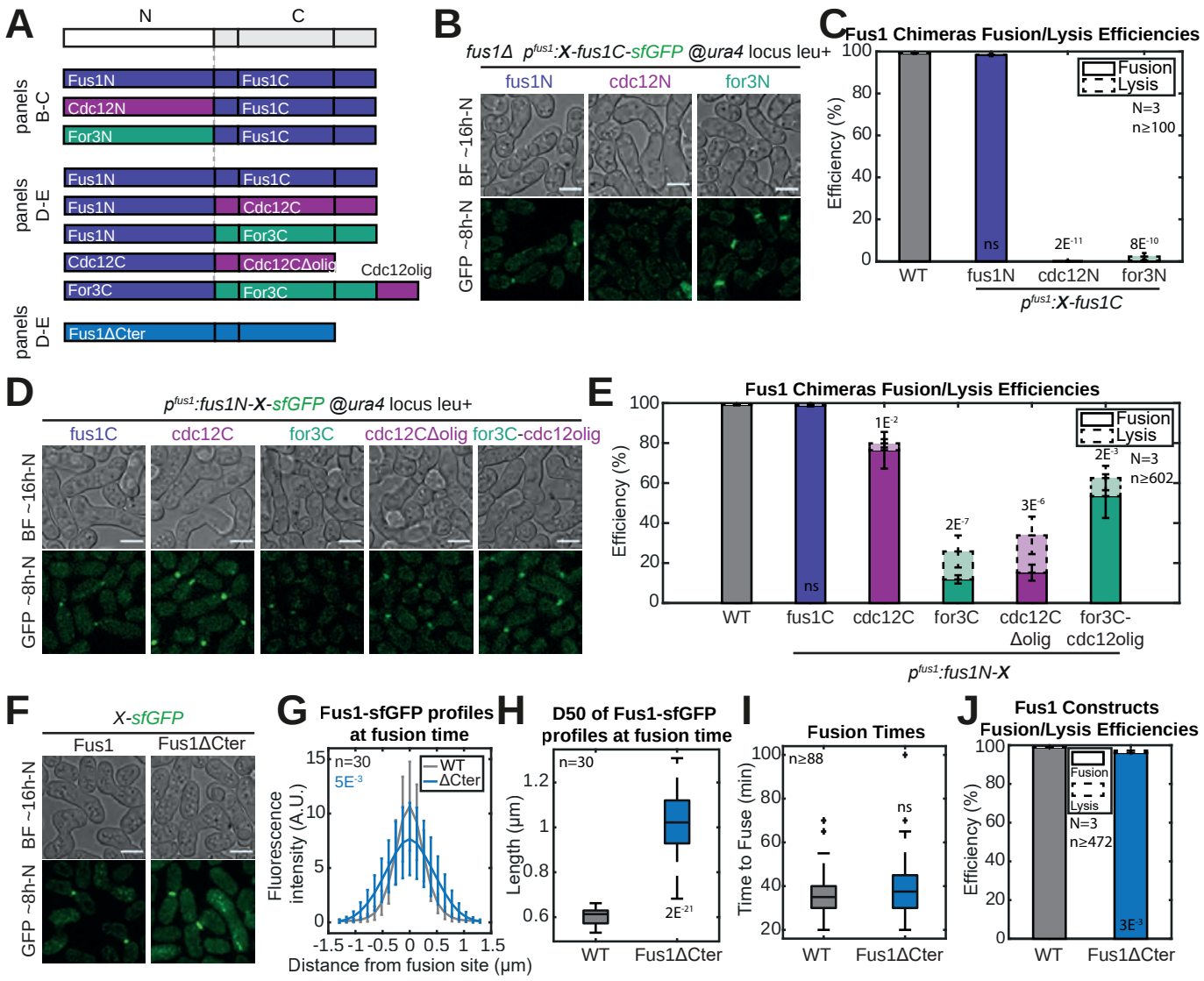

Figure 3.2 Both Fus1 N-terminal regulatory region and actin-assembly domains are crucial for fusion
A. Scheme showing the different constructions used in the figure. All were tagged C-terminally with sfGFP and expressed in homothallic *fus1Δ* strains under control of the *fus1* promotor at the *ura4* locus. **B.** Brightfield images ~16h post starvation and GFP fluorescence images ~8h post starvation of strains expressing the chimeric formins Fus1N-Fus1C, Cdc12N-Fus1C or For3N-Fus1C. Formins are cut between the N-terminal regulatory region and FH1 domain and the two halves are separated by a BamHI restriction site. **C.** Fusion and lysis efficiencies 24h after nitrogen removal in strains as in (B) compared to the WT. **D.** Brightfield images ~16h post starvation and GFP fluorescence images ~8h post starvation of strains expressing the chimeric formins Fus1N-Fus1C, Fus1N-Cdc12C, Fus1N-For3C, Fus1N-Cdc12CΔolig or Fus1N-For3C-Cdc12olig. Formins are cut in between the N-terminal regulatory region and FH1 domain and the two halves are separated by a BamHI restriction site. Cdc12olig is Cdc12 C-terminal domain known to oligomerize. **E.** Fusion and lysis efficiencies 24h after nitrogen removal in strains as in (D) compared to the WT. **F.** Brightfield images ~16h post starvation and GFP fluorescence images ~8h post starvation of strains expressing the formins Fus1 or Fus1ΔCter. Fus1ΔCter is cut just after the FH2 domain. **G.** Profiles of Fus1-sfGFP bleach-corrected fluorescence intensities around the fusion focus at fusion time in strains as in (F). p-values concern the fusion point site. **H.** Width at half maximum of the fluorescence profiles shown in (G). **I.** Fusion times in strains as in (F). **J.** Fusion and lysis efficiencies 24h after nitrogen removal in strains as in (F). All p-values are relative to WT. Bars are 5 μm.

This phenotype could explain the partial deficiency of the Fus1N-Cdc12C chimera and be interpreted as an excess of self-oligomerization.

Fus1C self-oligomerization property could be contained either in the actin assembly domains, or, similarly to Cdc12, in the C-terminal regulatory region. However, the C-terminal regulatory region of Fus1, contrary to Cdc12 is very short. Instead, previous studies have shown that Fus1 actin assembly domains are able to mediate actin bundling, which could be seen as functionally similar to Cdc12 self oligomerization property (Scott et al., 2011). However, to confirm that Fus1C self-assembly property is contained within its actin assembly domains, we decided to characterize a formin lacking the C-terminal regulatory extension, Fus1$^{\Delta Cter}$ (Figure 3.2A). While such a formin localized properly to the region of contact between the two cells, it did so in a more spread manner along the perpendicular axis of the mating pair than the full Fus1 (Figure 3.2F-H). However, it didn't cause any important increase in fusion time (Figure 3.2I) or reduction in fusion efficiency (Figure 3.2F and J), even though it seemed to exhibit cell wall remnants post-fusion (Figure 3.2F). In particular, the reduction in fusion efficiency for Fus1 is not at all comparable to the one observed for Cdc12. Hence, while Fus1$^{\Delta Cter}$ is not completely devoid of phenotypes, and could contain some self-assembly properties, Fus1 C-terminal regulatory region cannot account for the strength of Fus1C self-oligomerization property. Instead, those results suggest that the assembly properties contained within the FH1 and FH2 domains are an important factor in that regard.

Taken together, those results suggest that both the actin assembly domains, FH1 and FH2, and the N-terminal regulatory region of Fus1 are particularly tailored to Fus1 function in assembling the fusion focus. We will explore the importance of Fus1 actin assembly domains in section 3.5 to 3.8 of this chapter and the importance of Fus1 N-terminal regulatory region in chapter 4.

3.4 Both formin expression levels and leucine auxotrophy have important effects on fusion efficiency

In the process of making the set of chimeras with varying C-terminal moieties described in the previous part, we observed some discrepancies between different backgrounds. Chimeras expressed at the endogenous locus behaved quite differently than the set of chimeras presented previously. These seemed to be more strongly expressed but had a reduced mating efficiency (Figure 3.3A, Top right panel, compare to Figure 3.2D). Interestingly, endogenous insertions were in a leucine - (leu-) background, while the previous chimeras were in a leu+ background. In the lab, various people had experienced reduced mating efficiencies in leu- strains, but no proper assessment of leucine auxotrophy on fusion efficiency was done. We therefore decided to systematically investigate the influence of leucine auxotrophy and the site of chimera insertion on mating efficiency. For that, we introduced the set of 5 C-terminal chimeras at the endogenous or the *ura4* locus in a leu- or leu+ background and assessed fusion efficiency of the chimeras (Figure 3.3A-C). In both endogenous and *ura4* insertions, leu- chimeras seem to fuse strikingly less well than their leu+ counterpart (Figure 3.3A-C), which suggest a role of leucine auxotrophy not only in mating efficiency but also fusion efficiency. This was further confirmed by an increase in fusion time of the Fus1N-Fus1C strains in the leu- background compared to their leu+ counterpart, independently of the site of insertion (Figure 3.3H). While we do not fully understand the reason as to why this might be, we note two things. First, uracil and adenine auxotrophy didn't have the same impact (results not shown), but they encode nucleotides instead of aminoacids, and we do not have insights on any other auxotrophy. This

could be very interesting to investigate in the future as aminoacids auxotrophy has been linked to TOR pathway activation. Second, in comparing constructs in fusion, it is very important to compare strains with the same auxotrophies, which is what we did for this work.

In leu- cells, endogenous chimeras performed much better than the *ura4* inserted chimeras (Figure 3.3A-C). In fact, the *ura4* inserted Fus1N-Fus1C was not even able to completely support fusion (Figure 3.3B, 48% on average), and the 4 other chimeras were almost fully fusion deficient, while the endogenous Fus1N-Fus1C showed no significant difference from the WT (Figure 3.3C, 98,7% on average vs 99,1% for the WT). Because those chimeras were visibly expressed to different levels (Figure 3.3A Top panels), we quantified those differences in all the different backgrounds to understand if that could explain the differences in fusion efficiency. Fus1 fluorescence increases as the fusion process goes through and is maximal as fusion happens. As *S. pombe* mating is not synchronized, we chose to quantify Fus1 total cell intensity exactly as the fusion occurs, which is an easily identifiable step, by using time lapses, to have comparable data for all those cells. As Fus1N-Fus1C was the only chimera that fused, at least partially, in all backgrounds, we quantified only this one (Figure 3.3G). Both *ura4* locus insertion chimeras were expressed to similar levels (~0.7 A.U.) and were inferior to both endogenous insertion levels (~1.1 A.U.), which were also similar to each other (Figure 3.3G). Those results suggest that the *ura4* insertion of the chimera induces expression to levels inferior to an endogenous insertion, even though we used a quite extended version of the *fus1* promotor, using 1000bp upstream the start codon. In fact, this reduction in expression levels is not restricted to Fus1 expression since it was also suspected by other members of the lab (personal communication) for different proteins and might instead be attributed to genomic context. This suggests that Fus1 expression levels matter in fusion.

To understand expression levels influence on fusion, we expressed the set of 5 C-terminal chimeras at both the endogenous and the *ura4* locus in a leu- background and assessed their quantity and their fusion efficiency (Figure 3.3A,D and G). The Fus1N-Fus1C pendant of the set indeed showed an increased expression compared to the WT (1,5 A.U. vs 1,1 for the endogenously inserted, Figure 3.3G). This led to a minor and non-significant reduction in fusion efficiency for Fus1N-For3C, Fus1N-Cdc12CΔolig and Fus1N-For3C-Cdc12olig (4, 33 and 4% vs 7, 38 and 7%, respectively, Figure 3.3C-D), while Fus1N-Fus1C fusion efficiencies were indistinguishable (99%) and Fus1N-Cdc12C was mildly and non-significantly improved upon over expression (15% vs 8%). This suggests that fusion is more robust to a mild Fus1 overexpression (~1.4-fold) than it is to an underexpression.

We then expressed the full Fus1 under mating specific promotors of different strengths, *ste11* and *pak2* at the *ura4* locus in *fus1Δ* cells (Figure 3.3E), which respectively gave expression levels of 1.1 A.U., which was similar to endogenous Fus1 levels, and of 2.36 A.U., which was very superior to not only endogenous levels but also dual locus insertion (Figure 3.3G). Despite inducing similar levels to endogenously expressed Fus1, expression from the *ste11* promotor did not allow for a fully successful fusion efficiency (Figure 3.3F). It was, however, superior to the strain expressing Fus1 under the *fus1* promotor at the *ura4* locus, which was expressed to levels inferior to the WT (60% vs 48%). This could be explained by an overestimation of the expression levels, since we had to quantify fusing pairs only for comparison purposes, and while this is essentially all of them in the endogenously expressed strain, about 40% of the pairs do not fuse in the p^{ste11} background and as such, were not quantified. This could very well be because those pairs don't manage to

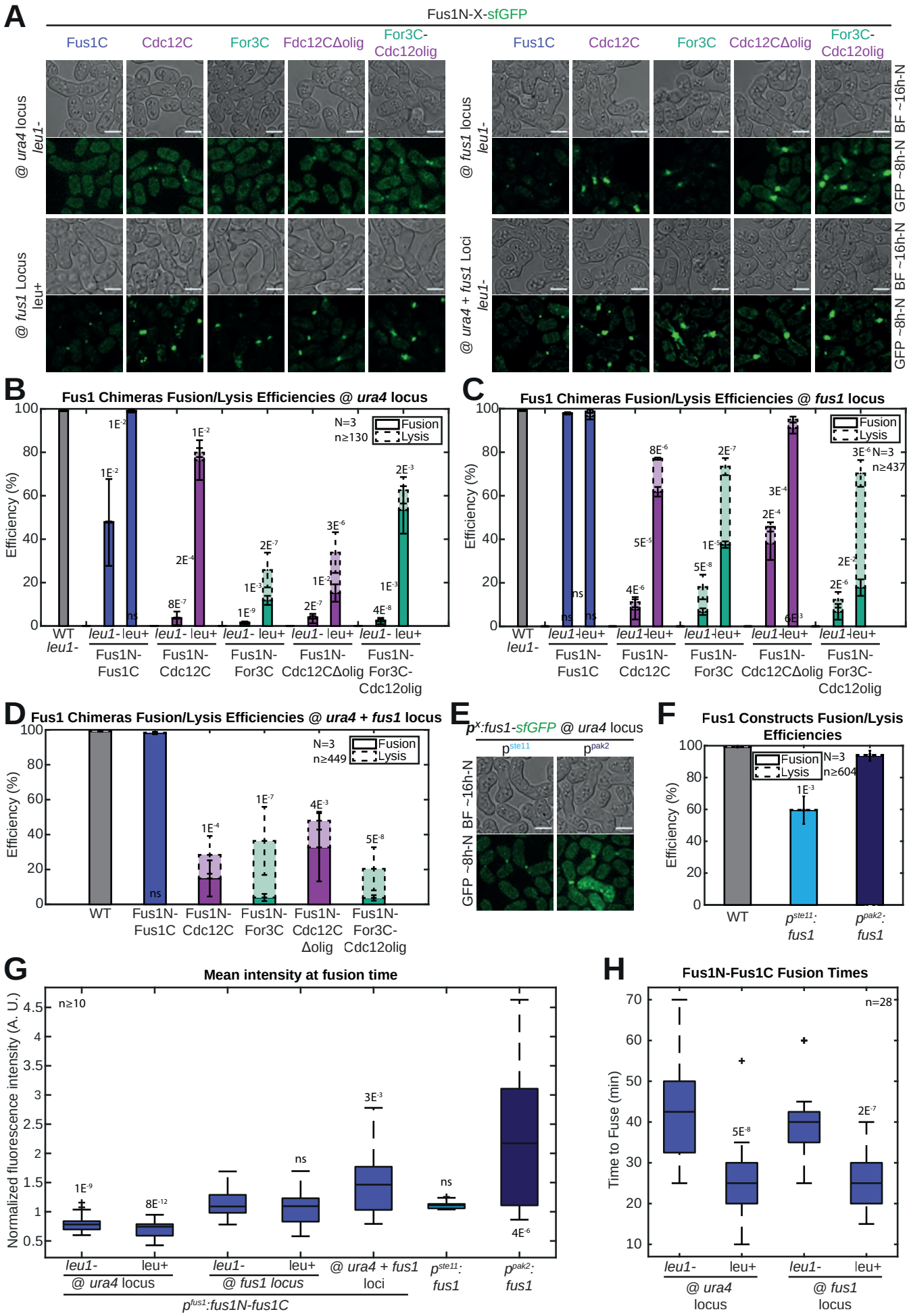
A
Fus1N-X-sfGFP
Fus1C
Cdc12C
For3C
Fdc12CΔolig
For3C-Cdc12olig
@ ura4 locus leu1-
@ fus1 Locus leu+
@ fus1 locus leu1-
@ ura4 + fus1 Loci leu1-
BF ~16h-N
GFP ~8h-N
B
Fus1 Chimeras Fusion/Lysis Efficiencies @ ura4 locus
Efficiency (%)
N=3
n≥130
Fusion
Lysis
WT leu1-
Fus1N-Fus1C
Fus1N-Cdc12C
Fus1N-For3C
Fus1N-Cdc12CΔolig
Fus1N-For3C-Cdc12olig
C
Fus1 Chimeras Fusion/Lysis Efficiencies @ fus1 locus
N=3
n≥437
D
Fus1 Chimeras Fusion/Lysis Efficiencies @ ura4 + fus1 locus
N=3
n≥449
E
p^x:fus1-sfGFP @ ura4 locus
p^ste11
p^pak2
F
Fus1 Constructs Fusion/Lysis Efficiencies
N=3
n≥604
p^ste11:fus1
p^pak2:fus1
G
Mean intensity at fusion time
Normalized fluorescence intensity (A. U.)
n≥10
@ ura4 locus
@ fus1 locus
@ ura4 + fus1 loci
p^fus1:fus1N-fus1C
H
Fus1N-Fus1C Fusion Times
Time to Fuse (min)
n=28

Figure 3.3 Leucine auxotrophy and formin expression levels have an impact on fusion efficiency (previous page)
A. Brightfield images ~16h post starvation and GFP fluorescence images ~8h post starvation of *fus1Δ* homothallic strains expressing the chimeric formins Fus1N-Fus1C, Fus1N-Cdc12C, Fus1N-For3C, Fus1N-Cdc12CΔolig or Fus1N-For3C-Cdc12olig tagged C-terminally with sfGFP under the *fus1* promotor either (top left) at the *ura4* locus in *leu1-* cells, (bottom left) at the endogenous locus in leu+ cells, (top right) at the endogenous locus in *leu1-* cells, or (bottom right) at both *ura4* and endogenous loci in *leu1-* cells. **B.** Fusion and lysis efficiencies 24h after nitrogen removal of the 5 chimeric formins as in (A) expressed at the *ura4* locus in *leu1-* or leu+ backgrounds compared to the WT. p-values between *leu1-* and leu+ bars compare the two backgrounds. p-values in top of each bar are relative to the WT. **C.** Fusion and lysis efficiencies 24h after nitrogen removal of the 5 chimeric formins as in (A) expressed at the endogenous locus in *leu1-* or leu+ backgrounds compared to the WT. p-values between *leu1-* and leu+ bars compare the two backgrounds. p-values on top of or inside each bar are relative to the WT. **D.** Fusion and lysis efficiencies 24h after nitrogen removal of the 5 Chimeric formins as in (A) expressed at both the *ura4* and endogenous loci compared to the WT. All strains are *leu1-*. **E.** Brightfield images ~16h post starvation and GFP fluorescence images ~8h post starvation of *fus1Δ* homothallic strains expressing Fus1 tagged C-terminally with sfGFP under the *ste11* or the *pak2* mating specific promotor at the *ura4* locus. All strains are *leu1-*. **F.** Fusion and lysis efficiencies 24h after nitrogen removal in strains as in (E) compared to the WT. **G.** Boxplot of the normalized mean total fluorescence intensity at fusion time of strains as indicated. **H.** Fusion times in strains expressing Fus1N-Fus1C as indicated. All p-values are relative to WT unless indicated otherwise. Bars are 5 μm.

reach the levels necessary for fusion. On the contrary, expression from the *pak2* promotor allowed for a much better fusion efficiency, just slightly, but significantly inferior to the endogenous and the dually expressed Fus1 (94%). This confirmed that fusion is more robust to increased than reduced formin levels but nevertheless hints at an optimum around Fus1 native levels. Taken together, those results show that in a leu- background, the increased expression obtained in endogenously inserted strains compared to the *ura4* inserted ones help increase fusion efficiency of all the 5 Chimeric formins tested here.

Similarly, in leu+ cells, the increased levels of the endogenous expression relative to the *ura4* expression induce a general increase (or stay constant at the very least) in the chimera's efficiency if we look at both the fusion and lysis proportions. Indeed, Fus1N-For3C, Fus1N-Cdc12CΔolig and Fus1N-For3C-Cdc12olig have increased overall efficiencies when we compare, in the leu+ background, the *fus1* to the *ura4* insertion (average efficiencies of 73 vs 26% – $p=6E^{-4}$, 95 vs 34% – $p=1E^{-3}$ and 70 vs 63% – ns, respectively ; Figure 3.3B-C) while both Fus1N-Fus1C, which was already maximal in the *ura4* background, and Fus1N-Cdc12C don't show any significant variation (average efficiencies of 99 vs 99% – ns and 80 vs 77% – ns, respectively ; Figure 3.3B-C). Those results confirmed than the higher quantity at which Fus1 is normally expressed, compared to a *ura4* insertion expression level, is optimized for proper fusion in all backgrounds.

However, this increase was strikingly more pronounced in strains lacking Cdc12olig, i.e. Fus1N-For3C and Fus1N-Cdc12CΔolig than in the other strains. In addition, the strains which expressed Cdc12olig, i.e. Fus1N-Cdc12C and Fus1N-For3C-Cdc12olig showed a reduced fusion efficiency in strains with higher expression (average fusion efficiencies of 62 vs 76% – ns and 18 vs 53% – $p=6E^{-3}$, respectively ; Figure 3.3B-C) but a rather increased lysis efficiency (15 vs 3% – $p=7E^{-4}$ and 52vs 9% – $p=1E^{-3}$, respectively ; Figure 3.3B-C). One explanation for those puzzling results is that Cdc12 oligomerization domain could become detrimental at high levels of expression. Indeed, at low overall formin quantities, Cdc12 oligomerization domain might help reach local concentration at the fusion site sufficient for fusion, thereby helping the chimeras that contain this domain to fuse more successfully. On the contrary, at normal overall formin quantities, it could instead start to be detrimental by inducing too high local levels, disorganizing the architecture of

the resulting actin network, probably causing the two dot phenotype and the high lysis percentages we observed in those strains. In fact, oligomerization properties such as Cdc12's are known to be concentration dependant (Kumari & Yadav, 2019), which could explain why the influence of quantity is reversed depending on the presence of Cdc12 oligomerisation domain.

Taken together, these results suggest that in addition to properties contained within the N-terminal regulatory region and the actin-assembly domains of Fus1, the formin expression levels and the auxotrophy background are relevant for proper fusion dynamics.

3.5 Fus1 actin elongation rate has to be maintained low for proper fusion dynamics

The C-terminal halves of the chimeras discussed in the previous part contain both the actin assembly domains and the C-terminal regulatory regions of the three formins. Even though we showed that the C-terminal regulatory region of Fus1 was dispensable for fusion, to understand the importance solely of the actin assembly domains, we constructed a set of chimeras keeping the C-terminal regulatory region constant (Figure 3.4A and 3.5A). The extensive *in vitro* characterisation of Fus1, Cdc12 and For3 allowed us to control for actin assembly parameters (Scott et al., 2011) (Table 1.1). We first assessed a set of constructs where we kept the FH2 domain of Fus1 constant and varied the FH1 domain, so as to obtain a gradation in Fus1 elongation speed while keeping the other actin assembly properties constant (Figure 3.4A-B). All those constructs localized properly as a single focus at the region of contact between the two cells (Figure 3.4B). While 24h post starvation, none of those constructs led to significantly less fusion than in the WT (Figure 3.4B,C), there was a clear correlation between the actin elongation speed measured *in vitro* and the duration of the fusion process *in vivo* (Figure 3.4D), whereby an increase in elongation speed relative to the native elongation speed of Fus1 induces a delay in fusion, with a fusion time of 40 minutes on average for the WT, 49 and 47 minutes for Fus1^{2FH1}-Fus1^{FH2} and Cdc12^{½FH1}-Fus1^{FH2}, respectively, which both have about twice the native elongation rate of the WT *in vitro*, and 62 minutes for Cdc12^{2FH1}-Fus1^{FH2}, which has about 3 times the native elongation speed of the WT.

This increase in elongation speed was paired with a visual change in the architecture of the fusion focus, as evidenced by LifeAct, which decorates indistinctively all actin filaments, or more specifically, tropomyosin Cdc8 tagging, which decorates preferentially linear actin networks, allowing us to see past the actin patches (Figure 3.4E). The mNeonGreen tagging, which is expressed from the endogenous *cdc8* promotor at the *leu1* locus, while the GFP tagged version was expressed from the conditional *nmt41* promotor at the same locus, both in addition of the endogenous Cdc8, was a kind gift from Pr. Mohan Balasubramanian and shown to behave in a less dominant negative manner than its GFP tagged counterpart, offered us a better signal over noise ratio. Indeed, the construct with twice the FH1 domain of Cdc12, that has the most important elongation speed, exhibited a bigger actin fusion focus than its WT counterpart, probably because its individual filaments are longer, which was slightly detrimental for fusion as it induced a delay in fusion.

Put together, those results suggest that the elongation speed of the formin working in fusion has to be maintained low to produce a functionally relevant fusion focus architecture.

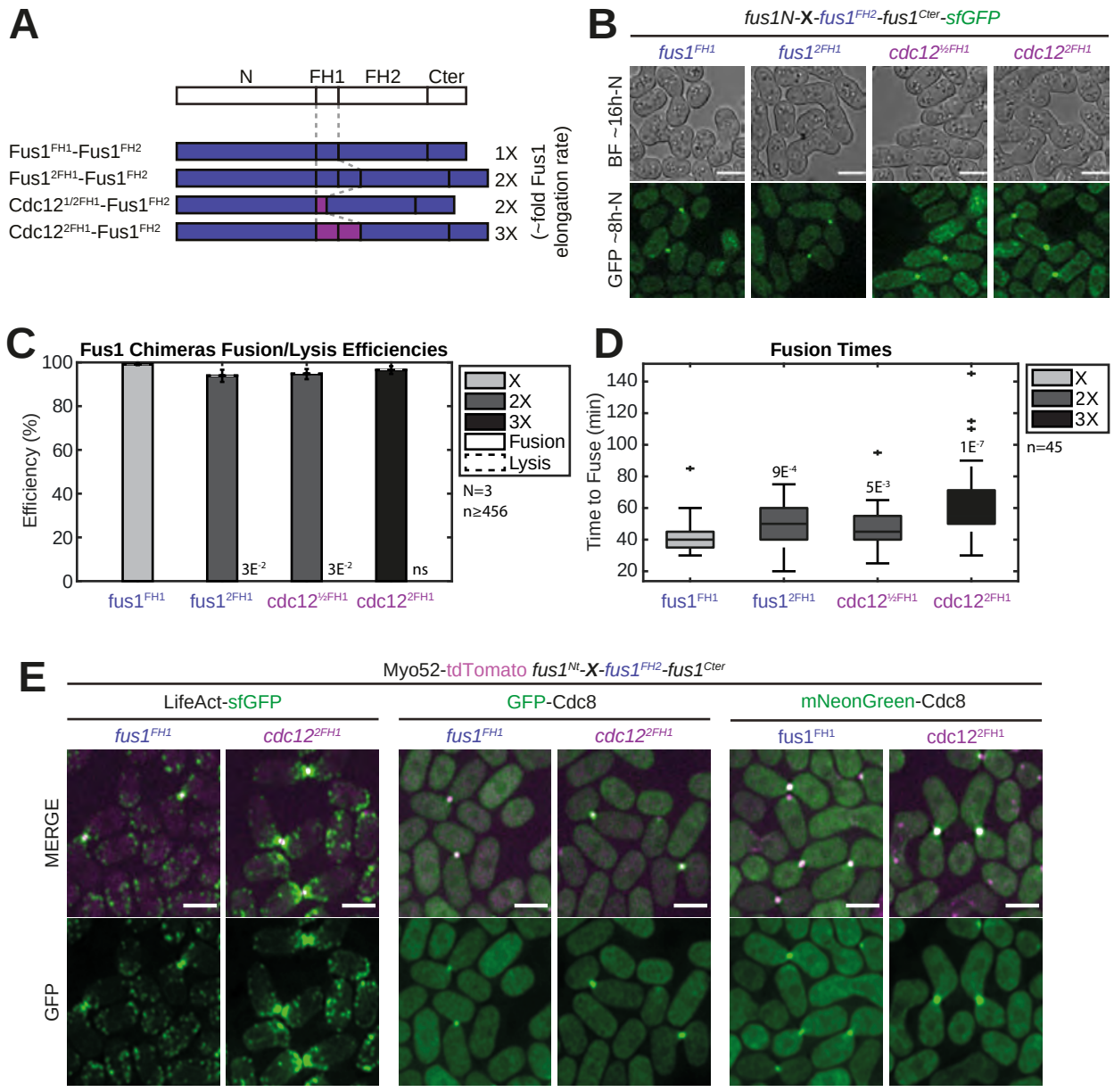

Figure 3.4 An increase in Fus1 actin elongation rate delays cell fusion
A. Scheme showing the different constructions used in the figure. All constructs were constructed seamlessly (no restriction sites separate domains) and are integrated at the endogenous *fus1* locus. As they keep their N- and C-terminal regulatory parts and their FH2 actin assembly domain constant, they are referred to only by their variable FH1 domain. Indicative actin filament elongation rates as measured *in vitro* on FH1-FH2 fragments by (Scott et al., 2011) are shown on the right, as multiple of Fus1 elongation rate. **B.** Brightfield images ~16h post starvation and GFP fluorescence images ~8h post starvation of homothallic strains expressing chimeric formins with Fus1^{FH1}, Fus1^{2FH1}, Cdc12^{½FH1} or Cdc12^{2FH1} tagged C-terminally with sfGFP. **C.** Fusion and lysis efficiencies 24h after nitrogen removal in strains as in (B). **D.** Fusion times in strains as in (B). **E.** Merge and GFP fluorescence images ~8h post starvation of homothallic strains expressing Myo52-tdTomato and either (left) LifeAct-sfGFP, (middle) GFP-Cdc8, or (right) mNeonGreen-Cdc8, in strains expressing untagged chimeric formins with Fus1^{FH1} or Cdc12^{2FH1}. All p-values are relative to WT. Bars are 5 µm.

3.6 Fus1 actin assembly properties are tailored to its function

We then set to examine chimeras with different FH2 domains. *In vitro* studies showed that For3 has a nucleation rate vastly inferior to Fus1. Regarding elongation speed, For3 is a better elongator than Fus1,

as its elongation speed is about twice the native Fus1 speed. Using the For3 chimera (Figure 3.5A-B) and the set of Fus1 FH2 chimeras with varying FH1s and elongation speeds (Figure 3.4A-B), we can control for elongation speed and assess the importance of the nucleation rate. Thus, for a matched elongation speed (Fus1^{2FH1}-Fus1^{FH2} or Cdc12$^{1/2FH1}$-Fus1^{FH2}), and all regulatory regions being kept unchanged, the For3 chimera performs comparatively very poorly, with an average of 13% of the mating pairs managing to fuse compared to more than 94% for the two comparable Fus1 chimeras (Figure 3.5C and 3.4C), suggesting the

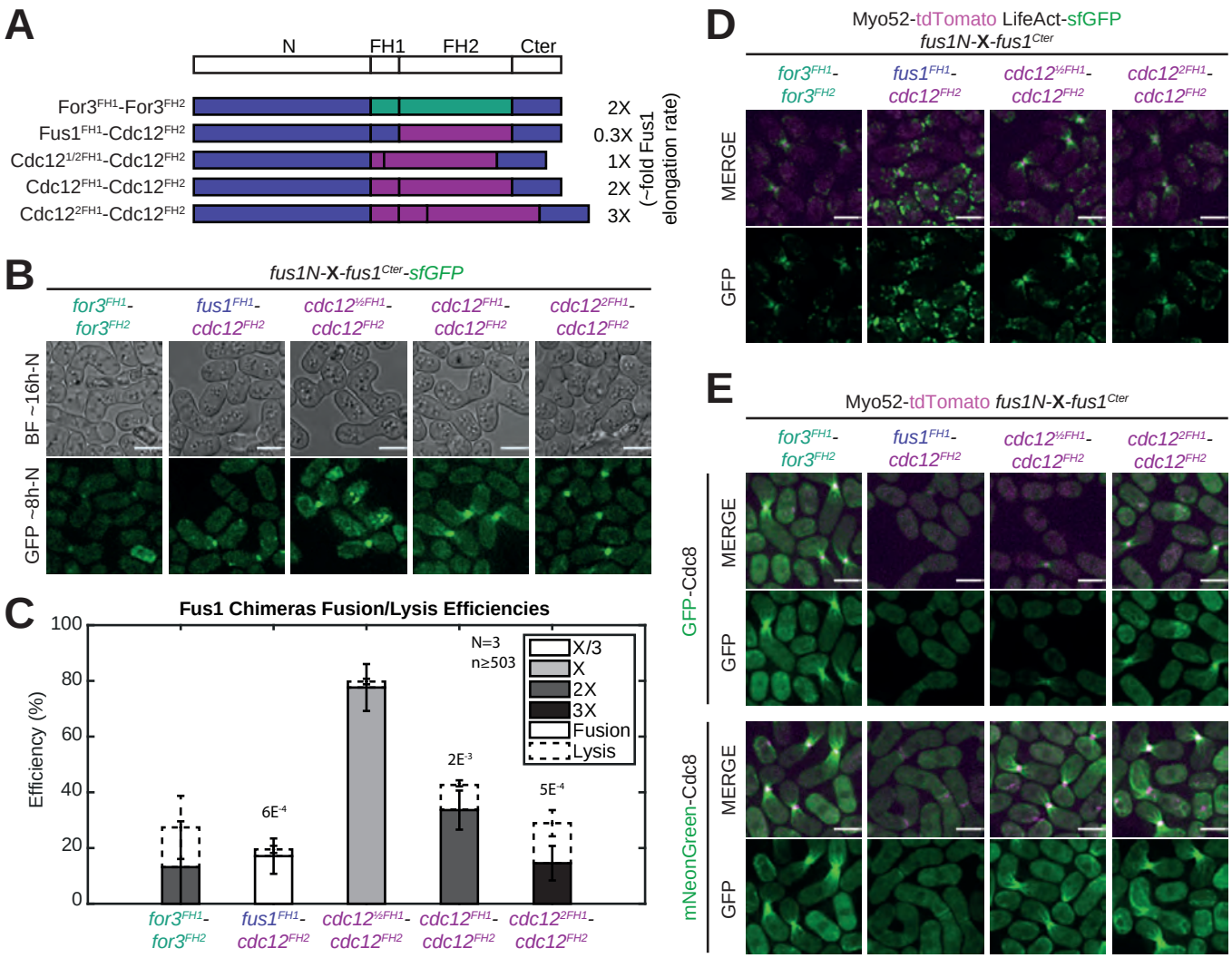

Figure 3.5 Low elongation and nucleation rates are detrimental for cell fusion
A. Scheme showing the different constructions used in the figure. All constructs were constructed seamlessly (no restriction sites separate domains) and are integrated at the endogenous *fus1* locus. As they keep their N- and C-terminal regulatory parts constant, they are referred to only by their variable FH1 and FH2 domains. Indicative actin filament elongation rates as measured *in vitro* on FH1-FH2 fragments by (Scott et al., 2011) are shown on the right, as multiple of Fus1 elongation rate. Note that For3 exhibits very low nucleation rates (Table 1.1). **B.** Brightfield images ~16h post starvation and GFP fluorescence images ~8h post starvation of homothallic strains expressing the chimeric formins shown in (A) tagged C-terminally with sfGFP. **C.** Fusion and lysis efficiencies 24h after nitrogen removal in strains as in (B). **D.** Merge and GFP fluorescence images ~8h post starvation of homothallic strains expressing Myo52-tdTomato and LifeAct-sfGFP in strains expressing the untagged chimeric formins shown in (A). **E.** Merge and GFP fluorescence images ~8h post starvation of homothallic strains expressing Myo52-tdTomato and either (top) GFP-Cdc8, or (bottom) mNeonGreen-Cdc8, in strains expressing the untagged chimeric formins shown in (A). Bars are 5 µm.

importance of a high nucleation rate in assembling the fusion focus. This finding is further confirmed by the perturbed fusion focus actin architecture in those strains, with a very long fusion focus from which form cable-like extensions, evidenced by various actin probing (Figure 3.5D-E). Importantly, the only difference between this For3 chimera and the previous Fus1N-For3C chimera (Figure 3.3A, top right panel) is the C-terminal regulatory region which in this case is the one of Fus1, and in the other the one of For3, and this led to virtually no difference, meaning than the poor ability of For3 in replacing Fus1 can be explained solely by its different actin assembly properties.

Using Cdc12 FH2 domain and varying FH1 domains, we were able to construct strains with a wider range of *in vitro* elongation rates than those obtained with Fus1 FH2. *In vitro* studies showed that Cdc12 has a nucleation rate very close to the native nucleation rate of Fus1 (Table 1.1). Then, using Cdc12 FH2 is probably keeping the nucleation speed unchanged *in vivo*, permitting us to test for an optimum elongation speed in fusion (Figure 3.5A). The $Cdc12^{FH1}$-$Cdc12^{FH2}$ chimera, with twice the native elongation speed of Fus1 functions at an average of 33% in supporting fusion. Importantly, bringing the Cdc12 chimera to an elongation speed equivalent to the native Fus1 using half the FH1 domain of Cdc12 (Figure 3.5A) led to an important increase in fusion efficiency, with an average of 78% (Figure 3.5B-C), while further decreasing it ($Fus1^{FH1}$-$Cdc12^{FH2}$) or further increasing it ($Cdc12^{2FH1}$-$Cdc12^{FH2}$) led to a decreased fusion efficiency, of 17 and 15 % on average, respectively, demonstrating a clear optimum for the native elongation speed of Fus1. This is further supported by the resulting fusion focus architecture of those strains where the poorest elongator is barely able to form a proper aster and the better one forms cable like structures and accumulates actin to an extent very different from the native Fus1 (Figure 3.5D-E), which is evidenced best by looking at mNeonGreen Cdc8 tagging.

Putting those constructs together and comparing them to their Fus1 counterpart, the chimeras with Cdc12 FH2 perform comparatively worse while both the elongation and nucleation speeds are matched. This suggests that there is a property present within the FH2 domain of Fus1 which is absent from the FH2 domain of Cdc12 and critical for proper fusion (For the clearest example, look at $Cdc12^{2FH1}$-$Fus1^{FH2}$ and $Cdc12^{2FH1}$-$cdc12^{FH2}$ in Figure 3.4C and 3.5C which has the same FH1 and a matched elongation and nucleation speed and perform at 97 and 15%, respectively). Thus, taken collectively, those results show that the actin assembly properties of Fus1 are tailored to its function in assembling the fusion focus in at least three ways: a relatively low elongation speed (about 5 subunits.s^{-1}.mM^{-1}), a relatively high nucleation speed (one filament per two to three dimers) and an additional specific property.

3.7 The specific property contained within the FH2 domain of Fus1 is conserved

To understand what that specific property might be and pinpoint it to a few aminoacids, we first needed to understand whether it was conserved. To ask that question we replaced the FH2 domain of *pombe* Fus1 by the FH2 domains of 2 of the 3 other *Schizosacharromyces* species. We did this replacement in an otherwise WT Fus1 context such that only the FH2 domain is exchanged. However, as seen above, elongation rates conferred by $Fus1^{FH1}$ vary depending on the linked FH2 domain. To control for changes in elongation rates, we thus also performed the replacement in constructs containing $Cdc12^{2FH2}$ (Figure 3.6A),

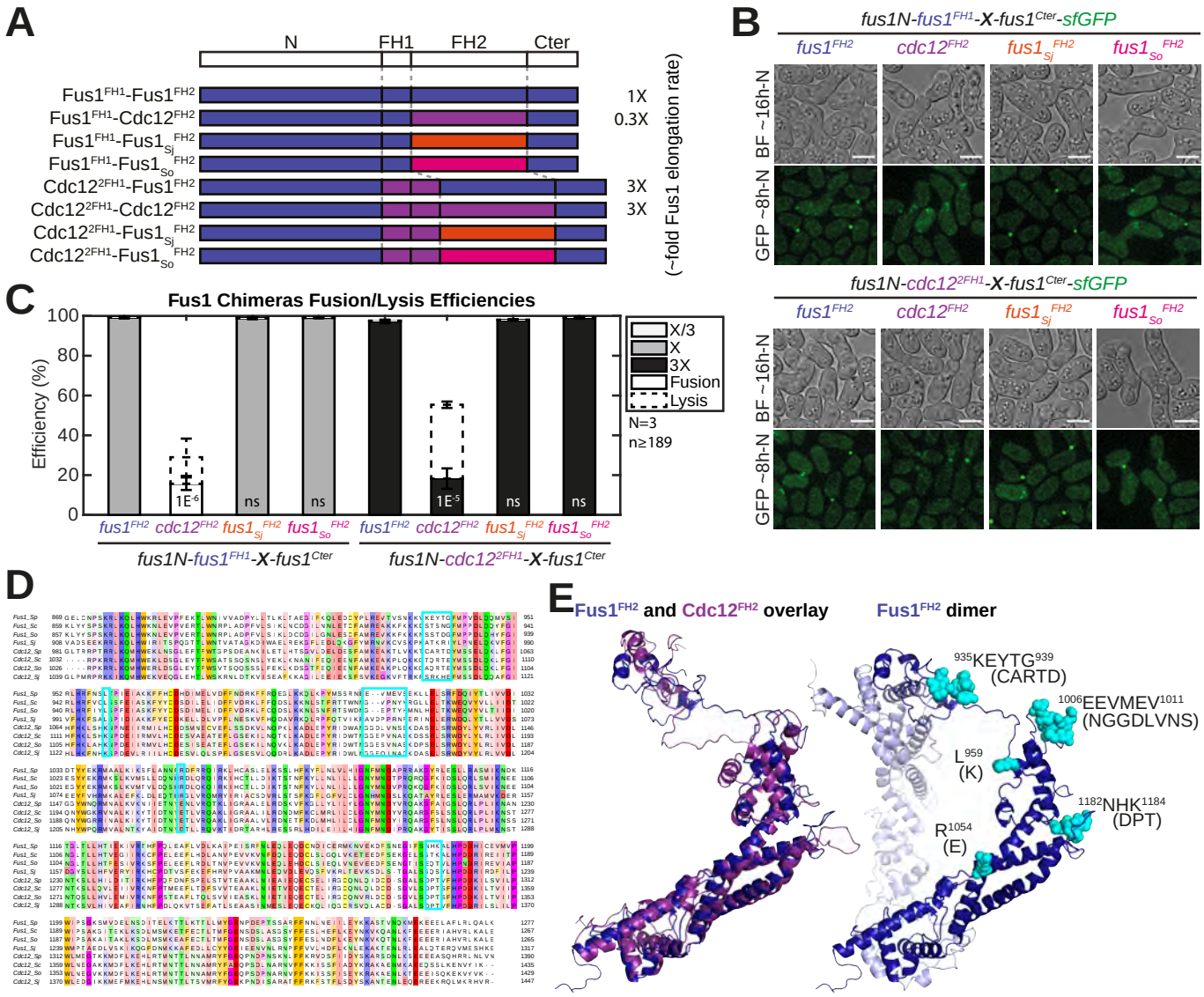

Figure 3.6 Fus1 FH2 specific property is conserved within the *Schizosaccharomyces* clade

A. Scheme showing the different constructions used in the figure. All constructs were constructed seamlessly (no restriction sites separate domains) and are integrated at the endogenous *fus1* locus. As they keep their N- and C-terminal regulatory parts constant, they are referred to only by their FH1 and FH2 domains. Where known, indicative actin filament elongation rates as measured *in vitro* on FH1-FH2 fragments by (Scott et al., 2011) are shown on the right, as multiple of Fus1 elongation rate. **B.** Brightfield images ~16h post starvation and GFP fluorescence images ~8h post starvation of homothallic strains expressing C-terminally sfGFP-tagged chimeric formins with either (top) variable FH2 domains and Fus1^{FH1} or (bottom) variable FH2 domains and Cdc12^{2FH1}. **C.** Fusion and lysis efficiencies 24h after nitrogen removal in strains as in (B). p-values of strains with Fus1^{FH1} chimeras are relative to Fus1^{FH1}-Fus1^{FH2}, p-values of strains with Cdc12^{2FH1} chimeras are relative to Cdc12^{2FH1}-Fus1^{FH2}. **D.** ClustalO alignment of Cdc12 and Fus1 FH2 domains from *Schizosaccharomyces* species (Sp = *S. pombe*; Sc = *S. cryophilus*; So = *S. octosporus*; Sj = *S. japonicus*). The turquoise boxes highlight mutated residues. **E.** (Left) Overlay of Fus1 and Cdc12 FH2 domain structures, which were constructed by homology modelling with murine FMNL3. (Right) Dimeric Fus1 FH2 homology model with mutated residues shown in turquoise. Residues were selected in regions that were unlikely to disrupt the formin FH2 dimerization or actin binding, were surface-exposed and had a charge difference between Cdc12 and Fus1 or were in variable loops. Bars are 5 µm.

which support similar elongation rates whether coupled to Fus1 or Cdc12 FH2. With its faster elongation rate, this background is also sensitized to changes in FH2 domain function, as shown by the vast difference in fusion efficiencies for constructs with Fus1 or Cdc12 FH2 domains. We then assessed whether those

FH2 domains would behave like a Cdc12 FH2 or a Fus1 FH2, meaning if it would have or not Fus1 specific property.

Both the *japonicus* and *octosporus* FH2 domains were able to replace *pombe* FH2 in both the Fus1^{FH1} and the Cdc12^{2FH2} backgrounds with localizations (Figure 3.6B) and fusion efficiencies (Figure 3.6C) equivalent to the WT, which suggest that the property we are looking for is conserved within the *Schizosaccharomyces* clade. We then aligned *Schizosaccharomyces* Cdc12 and Fus1 protein sequences and looked for residues or regions which were conserved in Fus1 among the *Schizosaccharomyces* species but different in Cdc12 and resulted in local charge difference (Figure 3.6D). We found a lot of those residues and decided to construct the structure of Fus1 FH2 by homology modelling, in collaboration with Justyna Iwaszkiewicz from the Swiss Institute of Bioinformatics in Lausanne, to locate those residues and eliminate those which were likely to affect actin binding or homodimerization (Figure 3.6E). We found 2 such residues, L959K and R1054E. Similarly, we obtained the structure of Cdc12 FH2 by homology modelling and superimposed it to the one of Fus1 to find regions with charge difference between the two unlikely to affect the overall structure. We found 3 such regions, located in flexible loops, KEYTG935-939CARTD, EEVMEV1006-10011NGGDLVNS and NHK1182-1184DPT. However, those stretches of amino-acids were poorly conserved among the *Schizosaccharomyces* clade (Figure 3.6D). While this low conservation strongly indicates that these amino-acids stretches are not involved in conventional actin binding, as those amino-acids are extremely conserved throughout evolution, it also is an argument against those regions being involved in the specific property we're looking to pinpoint, since it is conserved. However, as an equivalent structure can be mediated by different amino-acids, especially one of a flexible nature, we still decided to keep these 3 regions in for further analysis. Hence, We identified two residues and three poorly conserved loop regions that are possibly supporting the specific property we are looking for.

Thus, the specific property contained within the FH2 domain of Fus1 and absent in Cdc12 which is critical for fusion is likely conserved within the *Schizosaccharomyces* clade and we found a set of 5 mutations that could lead to the loss of this function.

3.8 Mutations in Fus1 FH2 domain recapitulate the cell fusion deficiencies observed with Cdc12 FH2

We introduced these mutations in both the WT and the Cdc12^{2FH1} backgrounds (Figure 3.7A). In the WT background, none of those mutations had any significant impact on fusion efficiency (Figure 3.7B-C), as expected if actin assembly property such as elongation rate, nucleation efficiency, actin binding affinity, or Fus1 dimerization was left unchanged. However, in the Cdc12^{2FH1} background, while most mutations had only a slight or no effect on fusion efficiencies, Fus1(R1054E) FH2 behaved strikingly similarly to Cdc12 FH2 (Figure 3.7B-C), with a severely reduced fusion efficiency but also largely increased amounts of lysis, also present in the Cdc12^{2FH1}-Cdc12^{FH2} strain. This suggests that this mutant has lost the property present in Fus1 FH2 and now behaves like a Cdc12-like FH2. Encouraged by those results, we introduced the opposite mutation in Cdc12 FH2 and while this led to a slight rescue of the fusion efficiency in the Cdc12^{2FH1} background (Figure 3.7E-G), that wasn't enough to recover WT levels. However, this property is likely supported by several amino acids or stretches of amino acids, among which could even be some of

the mutations tested here as we see a small effect of the KEYTG935-939CARTD mutation for example, and while mutating one will easily disrupt the full property, one might need to identify all the amino acids involved to introduce it in a distinct FH2 domain.

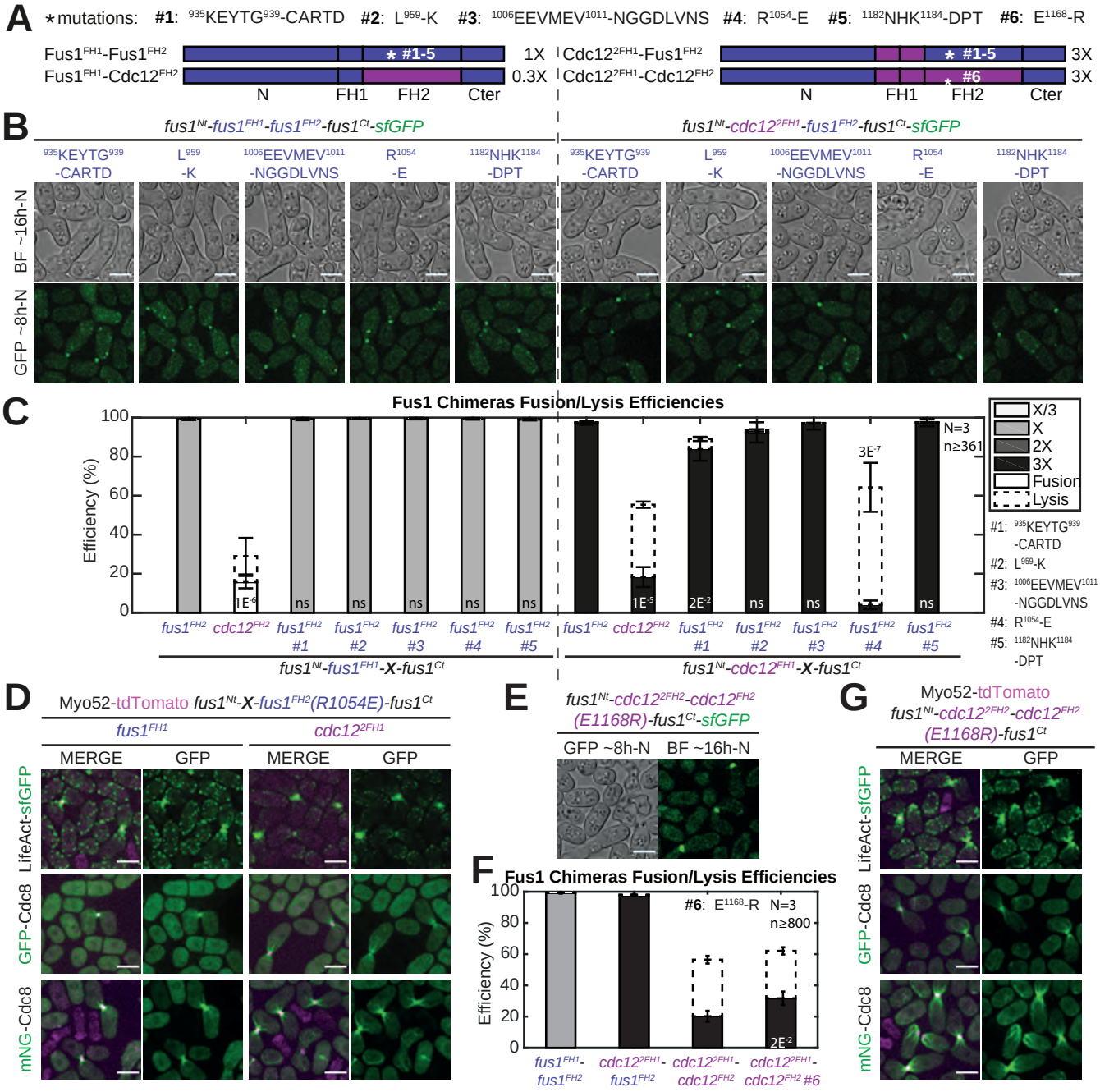

Figure 3.7 The R1054E mutation in Fus1 FH2 domain recapitulates the cell fusion deficiencies observed with Cdc12 FH2

A. Scheme showing the different constructions used in the figure. All constructs were constructed seamlessly (no restriction sites separate domains) and are integrated at the endogenous *fus1* locus. The 5 mutations described in Figure 3.6 (#1 KEYTG935-939CARTD, #2 L959K, #3 EEVMEV1006-1011NGGDLVNS, #4 R1054E and #5 NHK1182-1184DPT) were introduced in chimera with either $Fus1^{FH1}$ (left) or $Cdc12^{2FH1}$. The latter shows identical elongation rate when combined with either $Fus1^{FH2}$ or $Cdc12^{FH2}$ (as indicated on the right from measurements in vitro on FH1-FH2 fragments by (Scott et al., 2011)). The reverse #4 mutation (#6 E1168R) was introduced in the $Cdc12^{2FH1}$-$Cdc12^{FH2}$ chimera. **B.** Brightfield images ~16h post starvation and GFP fluorescence images ~8h post starvation of homothallic strains expressing either (left) Fus1-sfGFP with either of the 5 mutations or (right) sfGFP-tagged chimeric formin

Cdc12^{2FH1}-Fus1^{FH2} with either of the 5 mutations. **C.** Fusion and lysis efficiencies 24h after nitrogen removal in strains as in (B) compared to the non-mutated controls. p-values are relative to the non-mutated Fus1 controls. Chimeras with Cdc12^{FH2} are shown for information, but note that Fus1^{FH1}-Cdc12^{FH2} (left) cannot be used for comparison due to its lower elongation rate. **D.** Merge and GFP fluorescence images ~8h post starvation of homothallic strains expressing Myo52-tdTomato and either (top) LifeAct-sfGFP, (middle) GFP-Cdc8 or (bottom) mNeonGreen-Cdc8 in strains expressing the untagged mutated formins Fus1^{FH1}-Fus1$_{R1054E}{}^{FH2}$ or Cdc12^{2FH1}-Fus1$_{R1054E}{}^{FH2}$. Note the extended actin, compared to unmutated equivalents in Figure 3.4E. **E.** Brightfield images ~16h post starvation and GFP fluorescence images ~8h post starvation of homothallic strains expressing the chimeric formin Cdc12^{2FH1}-Cdc12$_{E1168R}{}^{FH2}$ tagged C-terminally with sfGFP. **F.** Fusion and lysis efficiencies 24h after nitrogen removal in strains as in (E) compared to the non-mutated controls. **G.** Merge and GFP fluorescence images ~8h post starvation of homothallic strains expressing Myo52-tdTomato and either (top) LifeAct-sfGFP, (middle) GFP-cdc8 or (bottom) mNeonGreen-cdc8 in strains expressing the untagged chimeric formin Cdc12^{2FH1}-Cdc12$_{E1168R}{}^{FH2}$. Bars are 5 µm.

Because of its important effect on fusion efficiency, we set to investigate the architecture of the R1054E mutant fusion focus (Figure 3.7D). Strikingly, in the Cdc12^{2FH1} background, we see cable-like structures originating from the fusion focus, as in the Cdc12^{2FH1}-Cdc12^{FH2} strain, which are absent from the Cdc12^{2FH1}-Fus1^{FH2} strain (compare Figure 3.7D, right panel, to Figure 3.5D-E, right panel and Figure 3.4E). Similarly, albeit to a lesser extent, this is also true for the WT background (Figure 3.7D, left panel), although we don't have the Cdc12 counterpart to compare since it doesn't have a matched elongation speed. Thus, Fus1(R1054E) FH2 not only behaves like a Cdc12 FH2 in terms of fusion and lysis efficiency, but the fusion focus architecture it creates also resemble a lot the one induced by a Cdc12 FH2. Put together, those results suggest that R1054 is one of the amino acids involved in the property that makes Fus1 so well equipped to support fusion.

Together, thanks to chimeras between the different *pombe* formins that allowed us to control for different parameters, we have shown that Fus1 actin assembly domains properties are particularly well tailored to its function. Indeed, we showed that its relatively low elongation rate is optimal for fusion focus architecture, that reducing its natively high nucleation rate is detrimental and that it also contains an additional property within its FH2 which we demonstrated is essential for fusion, conserved within the *Schizosaccharomyces* clade, and absent from *pombe* Cdc12 FH2. We have found amino-acids which are good candidates to support this function.

3.9 Discussion

How cells simultaneously assemble functionally diverse actin structures from a common cytosolic actin pool is a multifaceted question. Specific actin nucleators confer part of the structure's identity. In particular, Arp2/3 promotes branched F-actin networks in opposition to formins which promote the formation of linear F-actin networks. However, formin-nucleated actin networks exist in a wide variety of sizes and shapes, which are dependent on the specific formin which nucleates the network. While activation at the proper time and place plays a definite and well-studied role, less light has been shed on how the other specificities of each formin contribute to its specific actin network architecture, which could help understand the need for multiple formin isoforms. *S. pombe*, with only 3 different and well segregated linear actin networks, the cables supporting polarized transport in the cell, the cytokinetic ring, and the mating specific fusion focus, respectively nucleated by For3, Cdc12 and Fus1, is a good model organism

to tackle those questions. Here we have shown that both actin assembly properties specific rates and non-conventional additional specific properties play a role in conferring Fus1-nucleated fusion focus its specific architecture.

On one part, building on knowledge of *S. pombe* three formins *in vitro* elongation and nucleation rates, we used chimeric formins to show that Fus1 actin assembly properties are particularly well tailored to its function. Indeed, changes in actin assembly properties as assessed *in vitro* led to change *in vivo* in actin fusion focus architecture which correlated with fusion impairment.

First, Fus1 relatively low elongation rate is optimal for fusion focus architecture. Indeed, Increasing it, as in the Cdc12^{2FH1}-Fus1^{FH2} chimera, leads to a bigger actin aster unable to achieve proper fusion, probably because of a loss of spatial resolution. Importantly, chimeras with a high elongation rate have a relatively higher percentage of lysed mating pairs, as exemplified by Cdc12^{FH2} chimeras, which show increasing amounts of lysis as the elongation rate is increased by switching FH1 domains. In the context of cells attempting cell fusion, this could be interpreted as unsuccessfully aligned cell wall digestion apparatuses. Similarly, reducing Fus1 native elongation rate also leads to fusion defects as in the Fus1^{FH1}-Cdc12^{FH2} chimera, likely because it leads to filaments too short to produce a functional actin structure. Such fusion focus would fail to support Myo52-based vesicular transport concentration, leading to an unsuccessful cell wall digestion.

Second, Fus1 high nucleation rate is probably the basis for proper focalization of the downstream components, as lowering it, as in the For3 chimera, leads to a very spread actin network, therefore losing in spatial information, and again, leading to high lysis percentages. It has even been suggested that For3 may not nucleate (Scott et al., 2011) but use filaments from actin patches to elongate them, which may contribute to the more distributed localization of For3. Importantly, while those actin assembly parameters have been controlled for *in vitro*, we cannot exclude that cellular context, especially specific interactors, regulate those parameters *in vivo*, as for example, budding yeast nucleation promoting factor Bud6 interacts with formin Bni1 to enhance nucleation by recruiting actin monomers (Graziano et al., 2011). On a similar note, other actin assembly parameters are of crucial importance *in vitro*, but of a very moderate importance *in vivo*, such as the processivity, in relation to the dissociation rate. Indeed, *in vivo*, actin structures are temporally regulated by other actin interacting proteins which either sever the actin filaments or actively unload the formin (Shekhar et al., 2016). Capping protein is one of those proteins, as it has been shown to be in competition with formins for the barbed end of actin filaments (see chapter 2), forming a ternary complex which lower the affinity of both proteins for the barbed end (Billault-Chaumartin & Martin, 2019; Shekhar et al., 2015). However, we hope that general trends are conserved.

Fus1 nucleation rate relevance to fusion is to put in relation with Fus1 expression levels, which we have shown are also tailored to Fus1 function in assembling the fusion focus as the combination of both the nucleation rate and the number of formin molecules will dictate the number of filaments that will assemble at the fusion focus. This is a very general finding that can probably be generalized to other actin structures than the fusion focus and other formins than Fus1. Indeed, we have demonstrated that single integration at the *ura4* locus of Fus1 under its promotor led to reduced expression levels compared to endogenous expression. Strikingly, that led to a generally reduced capacity in supporting fusion. Theoretically, we could imagine that a Fus1 construct with a specifically increased nucleation rate would perform better in this

background than expressed at endogenous level, as the combination of both the increased nucleation rate and reduced number of formin dimers would lead to a resulting number of actin filaments within the fusion focus more similar to the WT situation than when the chimera is endogenously expressed. Additional work would have to be done to assess this theory. Why the *ura4* insertion leads to reduced expression levels compared to the endogenous locus could be explained by several reasons. First, even though we used a quite extensive *fus1* promotor, it could be that it isn't sufficient in providing the endogenous strength. Second, genomic context is important for expression levels as heterochromatin or histone occupancy and modifications are known to modulate access of polymerases or transcription factors to the DNA (Klemm et al., 2019; Tsompana & Buck, 2014). It could then be that chromatin accessibility is reduced at the *ura4* locus compared to the *fus1* locus during the mating process. As chromatin is remodelled upon starvation, this isn't a trivial problem to tackle (Alfredsson-Timmins et al., 2009).

In the process of unravelling the reduced Fus1 expression levels when expressed at the *ura4* locus, we have discovered an implication of leucine auxotrophy in fusion, whereby strains prototroph for leucine fused considerably faster and better than their leu- counterpart. While we didn't conduct a systematic evaluation of all the auxotrophy effects, we note than neither uracil or adenine auxotrophies had similar effects, but those are nucleotides while leucine is an amino acid. It would be interesting to test if this effect is specific to leucine or instead is shared by other amino acid auxotrophies, especially as amino acid auxotrophies have been linked to the TOR pathway. Besides offering a new direction for further research, the leucine auxotrophy effect reminded us of the importance of using an identical background, especially in mating, when comparing different strains. In addition, those findings can be put to profit by using the leu- background as a sensitized background to expose more modest phenotypes.

On another part, we showed that Fus1 also contains an additional property within its FH2 domain which we demonstrated is essential for fusion, conserved within the *Schizosaccharomyces* clade, and absent from Cdc12. Losing this function probably leads to the formation of the long cable-like structure emanating from the region of contact between the two cells induced by chimeras containing Cdc12 or For3 FH2 domains. Remarkably, mutation of a single amino-acid with the FH2 domain of Fus1, R1054, to its Cdc12 counterpart E, converts Fus1 into a formin that assembles long cable-like structures emanating from the fusion focus similar to Cdc12 or For3 chimeras. We believe bundling is a good candidate for what this function may be for two reasons. First, our data with N-C chimeras has showed that Fus1C contains oligomerization properties that could be replaced by Cdc12 oligomerization domain at certain concentrations. Because Fus1 binds F-actin, self-oligomerization could be functionally similar to actin bundling. Second, previous work in the field has demonstrated that Fus1 is able to bundle actin filaments, and that this ability is contained within its actin assembly FH1-FH2 domains (Scott et al., 2011). *In vitro* work is needed to invalidate or confirm that theory. However, Fus1 putative bundling could be at least partially indirect and instead be mediated by accessory proteins, in which case *in vitro* work will fail to demonstrate such property. Then, one could use chimeras between Fus1 and other formins known to directly bundle actin such as *Mus musculus* mDia2 (Alfredsson-Timmins et al., 2009) or *S. cerevisiae* Bnr1 (Moseley & Goode, 2005), or fusions with known actin bundlers such as Fim1 to assess this theory instead. Alternatively, it could be that this specific property isn't bundling and is mediated by a specific interactor and that we have just found the

residues involved in that interaction. In any case, further work will be needed to assess with certainty the nature of Fus1 specific property.

Of note, *S. cerevisiae*, which has only 2 formins, Bni1 and Bnr1, which have partially overlapping functions (Moseley & Goode, 2005), probably use one or both of them to assemble an actin structure functionally similar to *pombe*'s fusion focus (Merlini et al., 2013), which raises the question of the need of an additional formin in *pombe*. Bni1, which localizes at the bud tip, assembles the actin cables and the cytokinetic actomyosin ring, with a relatively low nucleation efficiency of one filament per 20 dimers and a relatively fast elongation rate of 20-25 subunits.s^{-1}.mM^{-1} *in vitro* (Moseley & Goode, 2005). However, Bni1 poor *in vitro* nucleation rate is alleviated *in vivo* by cooperation with Bud6 (Graziano et al., 2011). For comparison, Cdc12 and Fus1 are both potent nucleators with efficiencies of one per 2 dimers and elongators at a rate of 10 and 5 subunits.s^{-1}.mM^{-1}, respectively (Table 1.1). In contrast, Bnr1, which localizes at the bud neck, is a 10 times more potent nucleator than Bni1, with an efficiency of 1 filaments per 2 dimers, while its elongation speed is less than half that of Bni1, and it has been shown to bundle actin filaments (Moseley & Goode, 2005). Those different actin assembly properties have been proposed to tailor those two formins to their particular roles, but no systematic analysis as the one presented here has been conducted. In particular, more robust actin nucleation activity may be required at the bud neck, where Bnr1 is positioned throughout the cell cycle. Comparing those two formins to Fus1 necessary properties for fusion yields a clear winner. Bnr1 high nucleation rate, slower elongation rate, and bundling activity result in strikingly similar properties to Fus1 and would be an excellent choice to confirm bundling capacity of Fus1 by swapping their actin assembly domains. However, the fact that it would be particularly well suited to assemble the fusion focus in *pombe* doesn't necessarily mean Bnr1 is fulfilling the homologous function in *S. cerevisiae*, as those two organisms are morphologically different and might then need different actin assembly properties for a similar function. In addition, while we're not yet sure which formin functions for the later stages of cell fusion, Bni1 has clearly been identified as being responsible for the early polarization steps (Matheos et al., 2004). As initial polarization is needed to reach the later cell-cell fusion step, implication in this last step is hard to distinguished from the first, which has hindered progress in that specific matter.

The fact that formins may be tailored to their role not only by specific regulation in time and space but also through their specific actin assembly properties is an emerging problematic, which doesn't seem to be specific to Fus1. A recent study on Cdc12 arrived to similar results (Homa et al., 2021). Beyond *pombe*, (Vidali et al., 2009) have shown that *Physcomitrella patens* formin For2 extremely rapid elongation rate was critical for the formation of apical F-actin necessary for polarized growth. A 2018 review by (Courtemanche, 2018) have called this problematic the most challenging remaining questions about formins. With this work, we have provided new insights in answering this challenging question.

4. Fus1 N-terminal regulatory region has self-assembly properties necessary for fusion

4.1 Introduction

Formins form a large family of proteins conserved from yeast to humans (Breitsprecher & Goode, 2013; Courtemanche, 2018). They act dually as nucleators and processive elongators of actin filaments. They consist of very conserved actin assembly domains which are inserted in between divergent N- and C-terminal regulatory domains (Rivero et al., 2005). These regulatory domains confer to the formin its localization and account for a large portion of their regulation. They support a vast array of functionally distinct actin networks involved in countless biological processes such as polarity, migration, or division (Bohnert, Willet, et al., 2013; Goode & Eck, 2007; Pollard & O'Shaughnessy, 2019; Skau & Waterman, 2015).

In most organisms, those different functions are supported by different formin genes. For example, mammals express 15 formins isoforms, the fruit fly *Drosophila melanogaster* 6, and *Schizosaccharomyces pombe* (*S. pombe*) expresses 3, Cdc12, For3 and Fus1, which support segregated and specific cellular functions (Kovar et al., 2011). Understanding the functional specificity of all these different formins in their respective organism is a work in progress. We have shown in the previous part of this work that their respective actin assembly properties, such as their elongation rate or nucleation efficiencies are part of the answer in tailoring those formins to their specific function. However, regulation of the activity of those formins at the proper time and place in the cell is also an important factor.

How formins activity is modulated by their regulatory regions is still an open question. Most diaphanous related formins are autoinhibited by interaction between their N-terminal DID and C-terminal DAD domains, which is relieved by Rho-GTPase binding, whose binding site partially overlap with the DID domain. Mammalian mDia1 and mDia2 (Staus et al., 2011), human FHOD1 (Schulte et al., 2008), *S. pombe* For3 (Martin et al., 2007) or *Saccharomyces cerevisiae* (*S. cerevisiae*) Bni1 and Bnr1 (Dong et al., 2003) are all at least partially regulated in this way. Diversity in the Rho-GTPase partner confer some of the specificity (Evangelista et al., 1997; Tolliday et al., 2002). However, some formins are known not to be canonically inactivated even though they contain putative DID and DAD sequences, such as Cdc12 (Yonetani et al., 2008) or mammalian formins INF2 and FRL2 (Chhabra et al., 2009; Vaillant et al., 2008). Still others lack those domains altogether such as the animal formin FMN. Hence, different mechanisms of regulation must exist. For example, both *S. cerevisiae* Bni1 and human FHOD1 are, in addition to their canonical inactivation, regulated through phosphorylation (Takeya et al., 2008; Wang et al., 2009). *S. cerevisiae* Bud6 interacts with and modulates Bni1 nucleation activity (Graziano et al., 2011; Moseley & Goode, 2005). Similarly, in *S. pombe*, Bud6 interacts with For3 and promotes For3-mediated actin assembly by correctly localizing For3 and relieving autoinhibition (Martin et al., 2007). *S. cerevisiae* formin Bnr1 harbors at least two separate localization sequences that independently target the formin *in vivo* (Gao et al., 2010), suggesting that a combination of cues and binding partners control formin recruitment. Moreover, mDia1 and mDia2 directly

bind phospholipid membranes (Gorelik et al., 2011; Ramalingam et al., 2010). This diversity of mechanisms is just the tip of the iceberg and more and more varieties emerge along the years.

In *S. pombe*, while Cdc12 and For3 regulation mechanisms have received a fair amount of attention (Martin et al., 2007; Yonetani et al., 2008), Fus1 N-terminal regulatory region (Fus1N) importance in modulating Fus1 localization and activity has not been elucidated. Fus1 nucleates the actin fusion focus, a mating-specific actin structure which serves as a basis for myosin V Myo52 dependant concentration of cell-wall hydrolases necessary for cell-cell fusion (Dudin et al., 2015). Fus1N has been found to recruit Fus1 to the shmoo tip of mating pairs (Petersen et al., 1998b), but we lack information as to its specific regulation. However, in the chapter 3 of this work, we have showed that Fus1N region cannot be functionally replaced by any of the other *pombe*'s formins N-terminal regulatory region, suggesting its mode of regulation might be rather unique.

Fus1 N-terminal sequence harbors a large disorganized region (see section 4.3). Recently, more and more attention has been given to intrinsically disorganised regions in proteins and their ability to mediate Liquid-Liquid Phase Separation (LLPS) (Alberti et al., 2019; Franzmann & Alberti, 2019; Guillen-Chable et al., 2021; Hyman et al., 2014; Pak et al., 2016). Intrinsically disordered regions are portions of a protein which lack stable secondary and tertiary structures. They are abundant in the eukaryotic kingdom, where they contribute to the cellular complexity by participating in the vast majority of signaling and regulation events (Wright & Dyson, 2015; Xie et al., 2007). LLPS is the process whereby a well-mixed solution of macromolecules such as proteins spontaneously separates into two phases: a dense and a dilute phase. The dense phase has liquid-like properties and enriches certain macromolecules while others are depleted, allowing the dense phase to function as a compartment (Alberti et al., 2019). One of the best studied protein known to mediate LLPS is mammalian FUS (Fused in Sarcoma) (Li et al., 2021). It has been associated with neurodegenerative diseases such as Amyotrophic Lateral Sclerosis, or ALS, where mutations shift FUS from its physiological reversible phase separation self-association mechanism to a fibrillar, pathological aggregation (Chen et al., 2019). FUS study has allowed to unravel a lot of the properties dictating LLPS in proteins, such as the sequence determinants, including aromatic/hydrophobic residues distributed across the protein. Intrinsically disordered regions have been shown to be enriched in such sequence determinants (Pak et al., 2016).

In this part, we merged those two divergent areas of biology to unravel some of the puzzling properties existing within Fus1N which are essential for fusion. We found that Fus1N, likely by self-interaction, is recruited to the fusion focus in presence of the full length Fus1. When artificially expressed in interphase, it formed cytosolic clusters, which are dependent on its C-terminal low complexity region and resistant to treatments known to dissolve LLPS mediated condensates. We showed that this low complexity region was essential for fusion and could be functionally replaced by domains known to mediate oligomerization or LLPS, such as the LLPS FUS subdomain. The ability of the construct to rescue Fus1 was inversely proportional to the *in vivo* self-interaction strength of the construct, suggesting that Fus1N rather solid interphase self-interaction is regulated in mating to obtain a relatively liquid agglomeration property.

4.2 Fus1 N-terminal regulatory region likely has self-association properties and is lysogenic

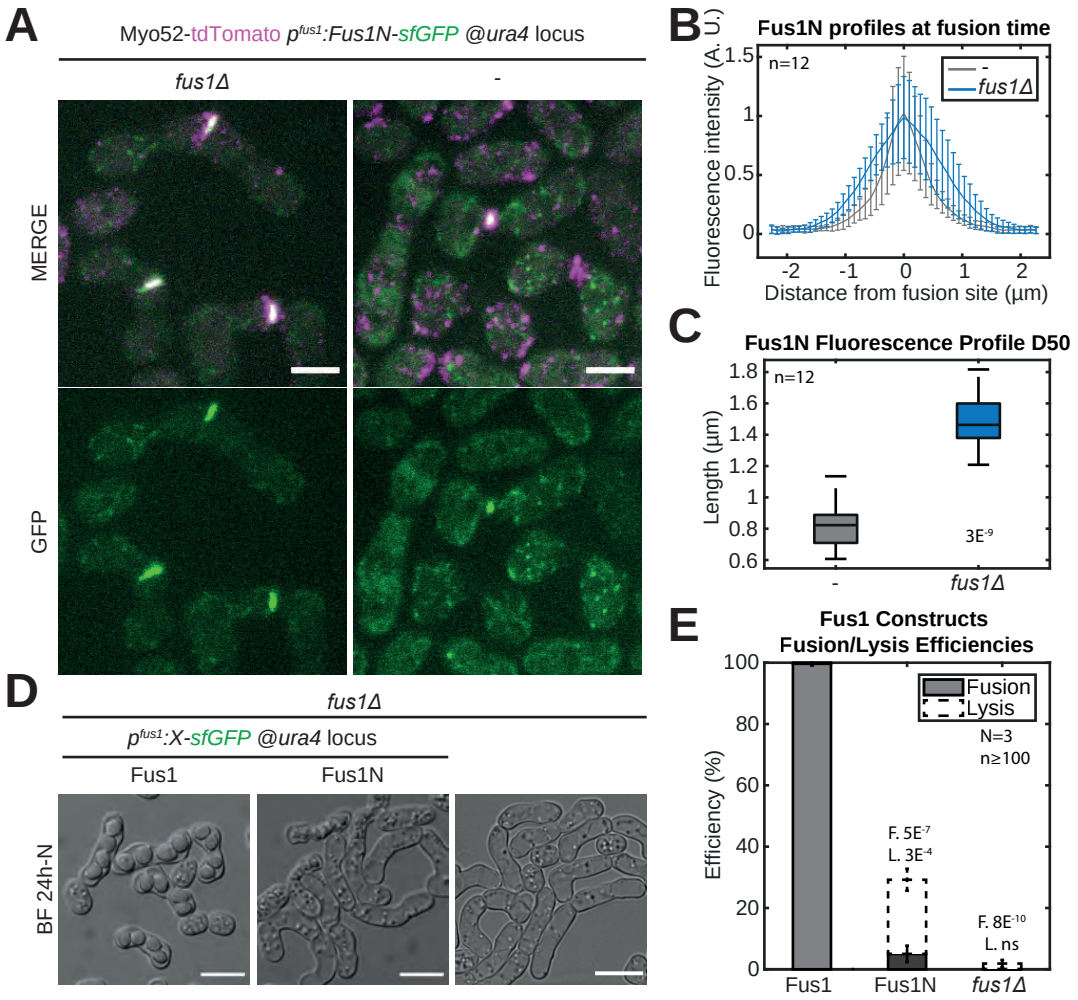

Figure 4.1 Fus1N is mediating self-assembling, lysogenic and fusogenic properties
A. Merge and GFP fluorescence images ~8h post starvation of homothallic strains expressing Myo52-tdTomato and Fus1N ($Fus1^{1\text{-}792}$) tagged with sfGFP under control of the *fus1* promotor at the *ura4* locus in WT or *fus1Δ* cells. **B.** Profiles of Fus1N-sfGFP fluorescence intensities along the fusion focus perpendicularly to the mating pair long axis at the time of Myo52-tdTomato maximal fluorescence intensity, which corresponds to fusion time for fusing pairs, in strains as in (A). **C.** Width at half maximum of the fluorescence profiles shown in (B). p-values are relative to Fus1N expressed in the WT background. **D.** Brightfield images ~16h post starvation of homothallic *fus1Δ* cells and cells expressing or not Fus1 or Fus1N tagged with sfGFP under the *fus1* promotor at the *ura4* locus. **E.** Fusion and lysis efficiencies 24h after nitrogen removal in strains as in (D). p-values are relative to WT. Bars are 5 µm.

We showed in the previous chapter that Fus1 N-terminal regulatory region contains some of the properties necessary for fusion. Thus, we became interested in Fus1 N-terminal regulatory region independently of the rest of the formin, which we will name Fus1N subsequently. When expressed in a *fus1Δ* background, Fus1N localizes to the region of contact between two mating cells (Figure 4.1A). This is consistent with previous data indicating that Fus1N has localization information (Petersen et al., 1998b). Fus1N distribution was quite wide along the zone of cell-cell contact. By contrast, when expressed in addition of the WT Fus1, Fus1N localizes, as the WT Fus1, in a focalized dot at the region of contact between the two

cells (Figure 4.1A), typical of a functional fusion focus. The width of Fus1N distribution was reduced by almost two-fold in presence of endogenous Fus1 (Figure 4.1B-C), which we showed by recording Fus1N fluorescence profiles perpendicularly to the mating pair long axis (Figure 4.1B), and measuring the width at half maximum intensity, or D50 (Figure 4.1C). Because Fus1N is recruited to the focus in presence of full-length Fus1, this suggests that Fus1 N-terminal regulatory region may have self-interaction properties.

Because Fus1N doesn't contain actin assembly properties, it is not surprising that, when expressed alone, it is almost fully fusion incompetent (Figure 4.1D-E). Surprisingly, some cells managed to fuse (5% on average), which suggests a weak fusogenic activity independent of direct actin assembly properties. Strikingly, Fus1N also induces a rather high lysis percentage of the mating pairs (24% on average, Figure 4.1D-E). In a fusion context, where cells that are under tremendous turgor pressure try digesting their cell wall, this again can be interpreted as failed and misplaced fusion attempts and reinforce the fusogenic characterisation of Fus1N.

Put together, those results suggest that Fus1N is likely to self-associate and contains intrinsic fusogenic properties. However, there are alternative ways to explain Fus1N recruitment to the fusion focus in presence of the full length Fus1 than self-association. For example, Fus1N binding to the fusion focus could be through another protein. Alternatively, it could also be that, because Fus1N alone does not support fusion, the cell never gets to the point where Fus1(N) would be forming a focus. In other words, we don't know if the change in distribution is part of the cause of the fusion defect, or if, instead the fusion defect is the cause of the wider distribution.

4.3 Fus1N contains separable cell tip-localization and cluster forming properties

To understand the unique Fus1N properties we expressed it in interphase cells under the *nmt1* promotor and performed a structure function analysis. Processing by domain analysis tools ODiNPred (Dass et al., 2020), IUPred3 (Erdős et al., 2021) and PONDR (Romero et al., 2001) and previous literature reviewing found that Fus1N contains a GBD/FH3 domain roughly from its 100th to 500th amino acids (Petersen et al., 1998b), which is followed by a disordered region (Figure 4.2A). The GBD/FH3 domain is found among other formins and is thought to perform a dual role in targeting the formin not solely but partly to Rho GTPases and controlling the activity of the formin (Rivero et al., 2005). Protein disordered regions have received a lot of attention over the past decade (Babu, 2016) and a lot of them have been showed to mediate weak protein-protein interactions that underlie the phenomenon of liquid-liquid phase-separation (Rana et al., 2021).

The full Fus1N$^{1\text{-}792}$ fragment has a dual localization to both cell tips and cytosolic clusters (Figure 4.2A-B). Shortening this fragment C-terminally led to a progressive loss of those cytosolic clusters, as exemplified by Fus1N$^{1\text{-}730}$ and Fus1N$^{1\text{-}500}$ (Figure 4.2A-B), suggesting that the formation of those cytosolic clusters is dictated by the disordered region. Reversely, shortening Fus1N from the N-terminus led to the progressive loss of the tip localization, as exemplified by Fus1N$^{93\text{-}792}$, Fus1N$^{140\text{-}792}$ and Fus1N$^{191\text{-}792}$ (Figure 4.2A-B), suggesting that the N-terminal part of Fus1N contains tip localization information. If cut from both sides,

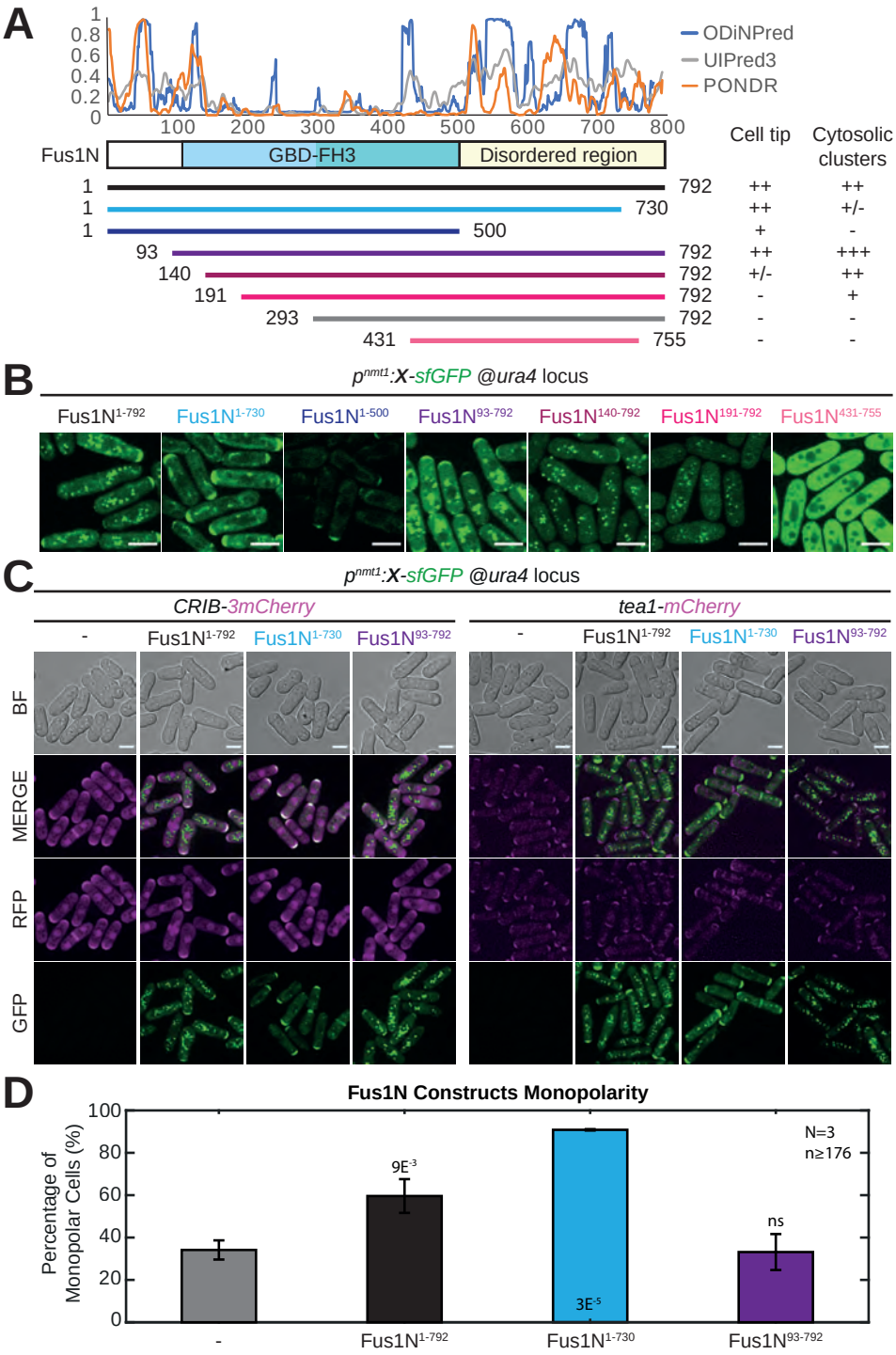

Figure 4.2 Fus1N contains independent tip localization and cluster forming determinants
A. Scheme of Fus1N with predicted domain organization and fragments tagged at their C-terminus with sfGFP and expressed from the *ura4* locus under the repressible *nmt1* promotor. Summary of their localization is shown to the right. The top graph shows the disorder index predicted by 3 prediction tools (Dass et al., 2020; Erdős et al., 2021; Romero et al., 2001). **B.** GFP fluorescence images of selected constructs from (A). **C.** Brightfield, merge, RFP and GFP fluorescence images of interphase cells expressing either (left) the polarity marker CRIB-3mCherry or (right) Tea1-mCherry in WT cells or in cells expressing Fus1N$^{1-792}$, Fus1N$^{1-730}$ or Fus1N$^{93-792}$. **D.** Monopolarity of the strains as in (C), assessed as the localization of CRIB on a single snapshot. Of note, even WT bipolar cells will sometimes appear as monopolar using this assay, because they are either before NETO or at a time point in CRIB oscillations where only one tip is decorated. All p-values are relative to WT. Bars are 5 µm.

Fus1N becomes homogenously cytosolic, losing both localizations, (Fus1N$^{431-755}$, Figure 4.2A-B) showing that those two localizations are independent.

Interestingly, Fus1N tip localization, which is often restricted to one of the two cells tips, seems to be a polarisation signal, as cells become monopolar when the tip localization is strong. Both Myo52 (See Figure 4.3A for an example in Fus1N), the motor supporting cargo transportation (Hammer & Sellers, 2011), and CRIB, a marker for active Cdc42 (Tatebe et al., 2008), the master polarity Rho GTPase, colocalize with the Fus1N decorated TIP while Tea1, a cell end marker linked to microtubules (Behrens & Nurse, 2002) seems to be restricted to the other tip (Figure 4.2C). The extensiveness of the monopolarity seems to correlate with the strength of the tip localization and requires the first 93 aa of Fus1 as Fus1N$^{1-730}$, which almost exclusively localizes to the tip with strong intensity (Figure 4.2B), shows a stronger percentage of monopolar distribution of CRIB on asynchronous cells than Fus1N$^{1-792}$, which itself shows a stronger monopolar percentage than Fus1$^{93-792}$ and the WT (Figure 4.2D), which progressively lose tip accumulation.

Put together with the previous mating observations, which brought about a likely self-association property of Fus1N, those results drove us to explore in detail Fus1N clusters interphase behaviour.

4.4 Fus1N clusters behave in a more solid manner than their tip localised counterpart

To investigate the possible phase separation behaviour of the Fus1N clusters, we subjected them and the full Fus1, as well as Myo52 tagged in the same cell, to treatments hindering weak interactions (Alberti et al., 2019). It is interesting to note that while Myo52 colocalize with Fus1N at the tips, it does not colocalize with Fus1N clusters. We used either 1,6-hexanediol exposure or high temperature treatments. Indeed, the aliphatic alcohol 1,6-hexanediol is widely used for disrupting liquid-liquid phase separation (LLPS) condensates *in vitro* and *in vivo* (Shi et al., 2021). It contains a hydrophobic group that is composed of 6 hydrogenated carbon atoms, which interferes with the hydrophobic interactions, and consequently affect hydrophobicity-dependent LLPS condensates. Similarly, as phase separation is exquisitely sensitive to changes in physicochemical conditions, even small differences in temperature can lead to different outcomes (Alberti et al., 2019). Upon 20% 1,6-hexanediol exposure, Fus1N and Myo52 tip localization was dissipated, while Fus1N clusters, although weakened, were still visible (Figure 4.3A, 1st and 2nd columns). This suggests that they are more solid than their tip localized counterpart. Similarly, at 37°C, while Myo52 localization is severely hindered with its tip localization barely visible, Fus1N localization is almost non affected (Figure 4.3A, 1st and 3rd columns). We conclude that high temperature treatment as we performed it is a less severe treatment than the 1,6-hexandiol treatment and that, whether at tips or in clusters, Fus1N localizes in a quite stable manner, but more stably so in clusters.

When artificially expressed in interphase cells, the full length Fus1 formed cytosolic clusters similar to the Fus1N clusters described above, which did not colocalize with Myo52. Fus1 did not decorate cell tips like Fus1N, and instead formed a dense focus at one of the cell ends, which seemed to polarize the cells, as the cells were thinner at the focus containing end (Figure 4.3A, 4th column). This focus resembled the fusion focus that Fus1 normally forms during mating, as it recruited the Myo52 motor. This suggests Fus1 is active when expressed in mitotic cells. As for Fus1N, Fus1 treatments with 1,6-hexanediol or high temperature

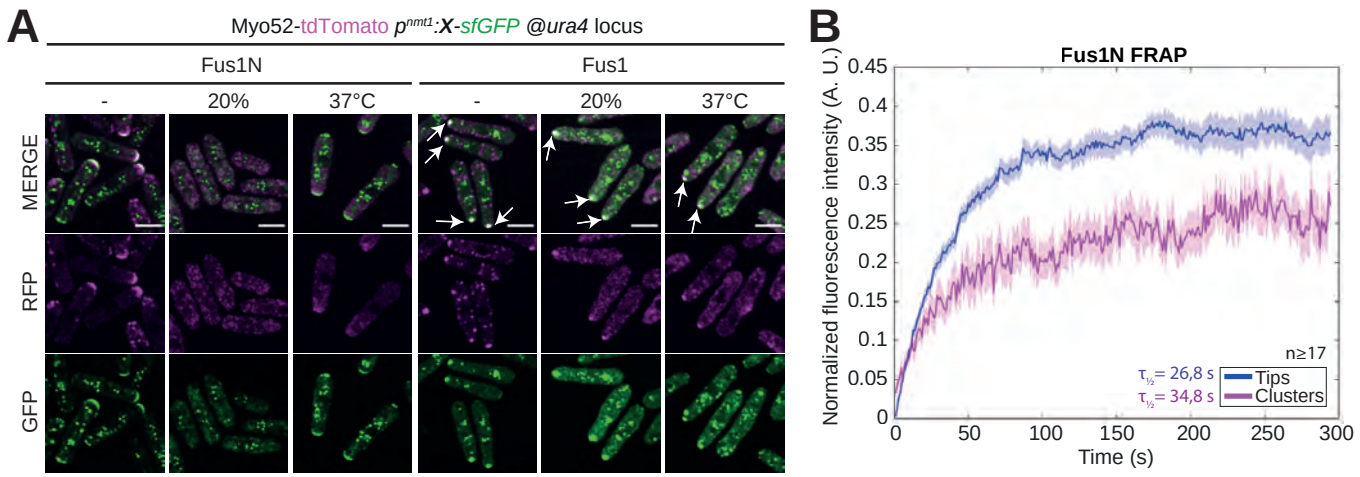

Figure 4.3 Fus1 forms stable clusters and focus-like structures in interphase cells
A. Merge, RFP and GFP fluorescence images of interphase cells expressing Myo52-tdTomato and either (left) Fus1N or (right) full length Fus1, both tagged C-terminally with sfGFP at the *ura4* locus under the *nmt1* promotor. Inside each panel, images show untreated cells (left) or cells after treatment with 20% 1,6-hexanediol treatment for 5 minutes (middle) or after 6h at 37°C and imaging at 40°C (right). **B.** FRAP recovery of cells as in (A). The data was scaled relative to the mean pre-bleaching value of each streain. The half-time recovery was calculated from fitting the mean of all profiles to an exponential recovery equation for each strain (see material and methods). Bars are 5 µm.

did not disrupt Fus1 cytosolic clusters although it increased cytosolic signal, whereas Myo52 clusters, likely on vesicles in the cytosol, were largely disrupted (Figure 4.3A, 5th and 6th columns). Interestingly, even in the more severe 1,6-hexandiol treatment, the Myo52 recruited to the Fus1 fusion focus-like structure was not disturbed (Figure 4.3A, 5th and 6th columns). This suggests that this structure is probably strengthened by actin polymerisation, potentially trapping Myo52.

The differential resistance of Fus1N localized at cell tips or in cytosolic clusters to treatments hindering weak interactions prompted us to perform a FRAP experiment on both of them and extract their half-time recovery (Figure 4.3B). Indeed, when localized in clusters, Fus1N shows a 35s half-time recovery, for only 27 s when it localizes to tips, which confirms that Fus1N clusters are less dynamic than their tip localized counterpart. Taken together, those results show that Fus1 localization in clusters, which is dictated by its low complexity region, confers to Fus1 a quite solid behaviour.

4.5 Fus1 low complexity region is essential for fusion

To investigate the relevance of the Fus1 cluster formation in mating, we removed by progressive chunks the low complexity region from the full-length Fus1 at the endogenous locus and assessed the ability of those strains to fuse (Figure 4.4A-B). Strikingly, the ability to fuse was correlated with the extent of the domain that we removed, with Fus1$^{\Delta 501\text{-}749}$ fusing better than Fus1$^{\Delta 501\text{-}791}$, which itself fuses better than Fus1$^{\Delta 492\text{-}791}$, which is not only almost fully fusion deficient but induces a lot of lysis in mating pairs (Figure 4.4A-B).

Interestingly, removing more and more of this low complexity region from Fus1 also led to an increasingly less focalized fusion focus (Figure 4.4A,C), with length at half maximum intensity going increasingly from 0.58 µm in average for Fus1 to 1,14 for Fus1$^{\Delta 492\text{-}791}$, where the full low complexity region is deleted

(Figure 4.4C). Because of internal turgor pressure, reduced spatial precision of cell wall digestion due to a wider distribution of the underlying structure concentrating secretory vesicles could very easily lead to lysis, and indeed, the two measures correlate (Figure 4.4B-C).

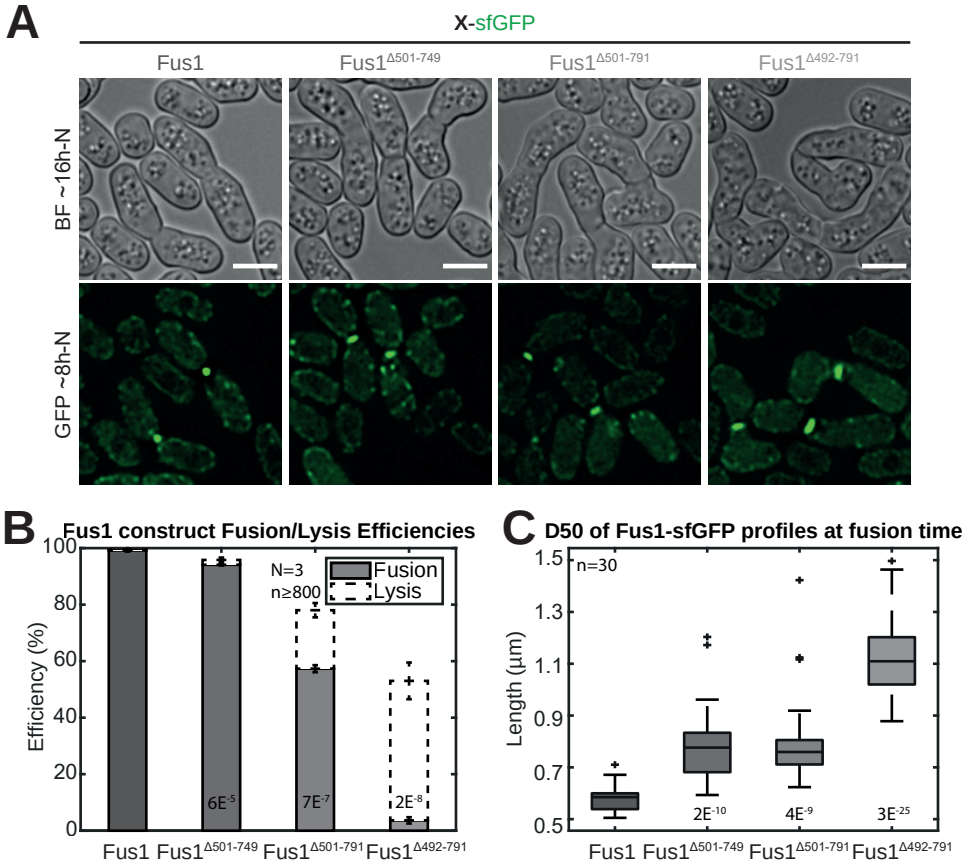

Figure 4.4 Fus1N cluster forming region is essential for fusion
A. Brightfield images ~16h post starvation and GFP fluorescence images ~8h post starvation of homothallic strains expressing Fus1, Fus1$^{\Delta 501\text{-}749}$, Fus1$^{\Delta 501\text{-}791}$ or Fus1$^{\Delta 492\text{-}791}$ tagged C-terminally with sfGFP. **B.** Fusion and Lysis efficiencies 24h after nitrogen removal in strains as in (A). **C.** Width at half maximum of the GFP-fluorescence profiles of strains as in (A), taken at the region of contact between the two mating cells, perpendicularly to the mating pair long axis, at the time of Myo52-tdTomato maximal fluorescence intensity, which corresponds to fusion time for fusing pairs. All p-values are relative to WT. Bars are 5 µm.

Hence, Fus1 contains a region that cannot be predicted to form any structural domain but when expressed in interphase forms quite solid clusters, and when removed in mating cells leads to fusion impairments correlated with a loss in fusion focus focalization. Taken together, those findings strongly indicate that this low complexity region dictate Fus1N self-assembling property, and that this property is essential for proper fusion.

4.6 Fus1 low complexity region can be functionally replaced by self-assembling domains

To test the hypothesis that Fus1 low complexity region mediates self-assembly properties essential for mating, we swapped Fus1 low complexity region by domains known to self-assemble, either by LLPS

mechanisms, or by light induced oligomerization (Figure 4.5A). FUS is one of the best studied LLPS-forming domains (Hofweber et al., 2018; Levone et al., 2021; Murray et al., 2017; Patel et al., 2015; Reber et al., 2021). It is known to form LLPS induced foci which are sensitive to 1,6-hexandiol or increase in temperature (Li et al., 2021). The strength of FUS self-interaction is regulated by phosphorylation, and a phosphomimetic version of FUS, FUS^{12E}, induces a more liquid version, as it discourages phase separation and aggregation (Monahan et al., 2017). $CRY2_{PHR}$ is a light sensitive protein domain from *Arabidopsis thaliana* that is used in optogenetics studies (Kennedy et al., 2010). Upon blue light exposure, it is able to bind its partner, CIB1, but it also oligomerizes (Che et al., 2015; Kennedy et al., 2010). This last property has been studied independently, and a mutant exists, CRY2olig, where those properties have been optimized to induce a stronger clustering (Taslimi et al., 2014). Interestingly, $CRY2_{PHR}$ oligomerization property has been used to induce light-dependent LLPS by hooking it to a LLPS-mediating domain and increase local concentration by light activation (Shin et al., 2017). By using these four domains, FUS, FUS^{12E}, $CRY2_{PHR}$ (subsequently called CRY2) and CRY2olig, we hoped to have a range in the strength of the self-assembling interaction, as we had no idea where the Fus1 low complexity region would fall in that regard.

Strikingly, by replacing Fus1 low complexity region by FUS or FUS^{12E}, we were able to fully rescue $Fus1^{\Delta 492\text{-}791}$ fusion defects, specifically the fusion efficiency and the focalization of the fusion focus (Figure 4.5A-B). Similarly, when using CRY2, and to a lesser extent, CRY2olig, we were able to partly rescue fusion efficiency upon light exposure, while they were almost fully fusion incompetent in the dark (Figure 4.5A,C). Interestingly, while fusion efficiency was similar to $Fus1^{\Delta 492\text{-}791}$ in the dark, there was almost no lysis, very similarly to a *fus1Δ* strain (Figure 4.5C). One hypothesis is that CRY2 interferes with Fus1N interaction with partners, which could explain both why CRY2 strains supress lysis and and why they don't support complete fusion in the light. However, we have, as of now, no data to support this hypothesis. Nonetheless, we showed that the self-aggregative properties of Fus1 low complexity region can be replaced by heterologous self-assembling domains that provide complete function, which shows both that Fus1 low complexity region indeed functions as a self-assembling region and that no other essential function can be assigned to this region.

To try and understand the underlying cause for the different efficiencies of FUS and CRY2 in restoring Fus1 function, we observed the localization of the constructs (Figure 4.5A). While all localized to the fusion site, CRY2 constructs accumulated to a greater extend at fusion time than their FUS or WT counterparts, with a fusion focus intensity of 15 and 11 A.U. for CRY2 and CRY2olig respectively, compared to 8 for WT and FUS, and 9 for FUS^{12E} (Figure 4.5D). This prompted us to FRAP the Fus1 foci in near fusing cells in each of those strains to compare their recovery time, which would give us a measure of how dynamic are those foci (Figure 4.5E). The half-time recoveries were increasing progressively in the following order : WT, FUS^{12E}, FUS, CRY2, CRY2olig, meaning that the molecules in those fusion foci are increasingly less mobile. The plateau of recovery (scaled to pre-FRAP intensity) was also different for each construct, as it is likely strongly influenced by the distribution and intensity of the different constructs. Importantly, the fusion efficiencies were inversely proportional to mobility of Fus1 inside the fusion focus, which suggest that having a more solid fusion focus is detrimental for fusion.

Additionally, we noticed that CRY2 containing fusion foci were often positioned at a larger distance than in WT cells (Figure 4.5A), similarly to Cdc12olig containing strains in Figure 3.2 and Figure 3.3, which

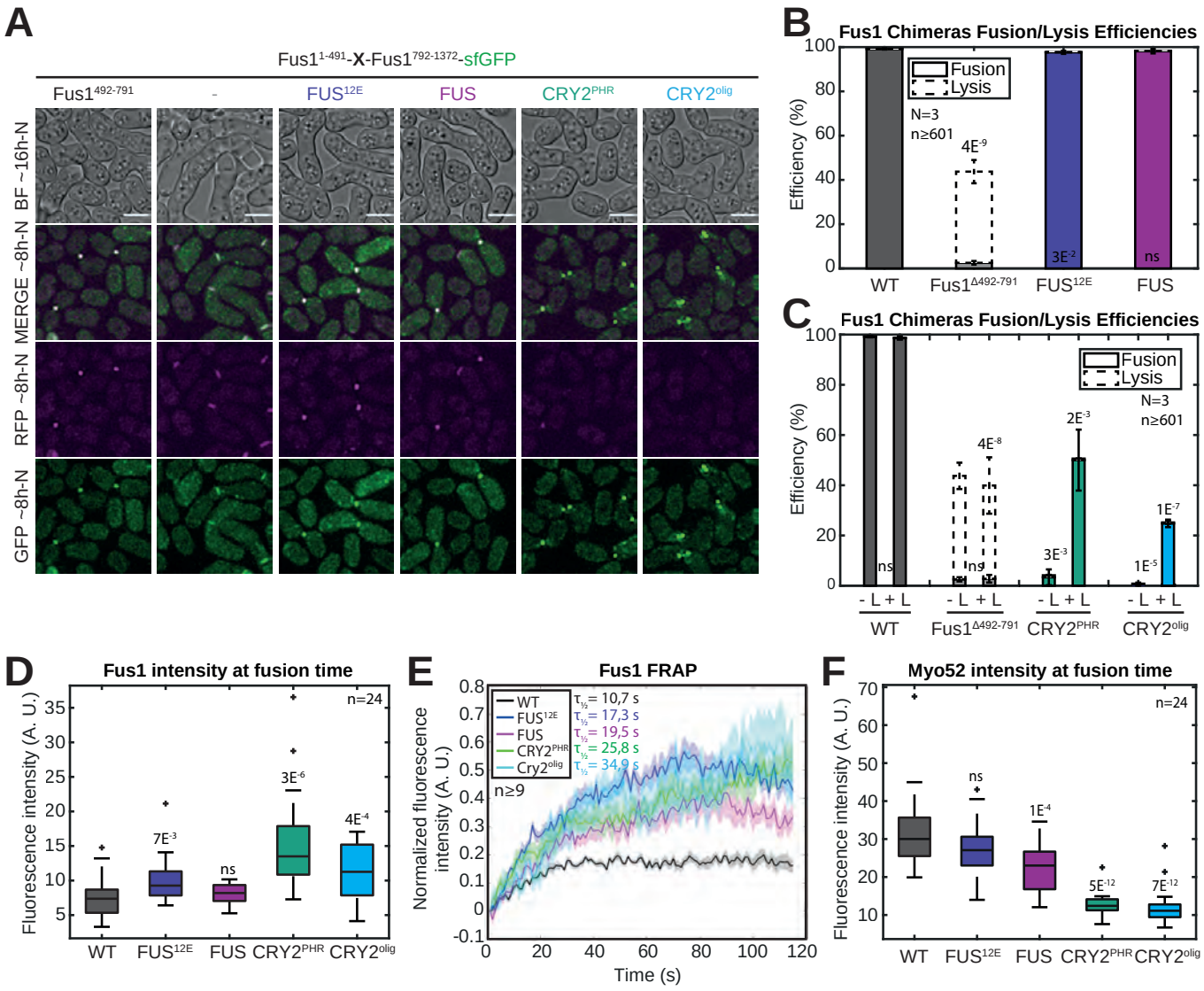

Figure 4.5 Fus1 cluster forming region can be functionally replaced by heterologous self-associating domains

A. Brightfield images ~16h post starvation and merge, RFP and GFP fluorescence images ~8h post starvation of homothallic strains expressing Myo52-tdTomato and sfGFP-tagged Fus1 constructs in which the disordered region is either intact, absent, or replaced by FUS^{12E}, FUS, CRY2 or CRY2olig. We used the N-terminal region of FUS (fused in sarcoma), know to self-associate through a LLPS mechanism (Li et al., 2021), or a mutated version (FUS^{12E}) that confers more liquid properties than its WT counterpart (Monahan et al., 2017). CRY2 is the codon optimized version of *Arabidopsis thaliana* CRY2 PHR domain, known to oligomerize upon light activation (Che et al., 2015), a characteristic enhanced in CRY2olig (Taslimi et al., 2014). Images stem from an overnight 5-minute time lapse movie started ~4h after Nitrogen removal. Hence, cells have been exposed to UV light every 5 minutes for several hours. **B.** Fusion and lysis efficiencies 24h after nitrogen removal in strains expressing either WT Fus1, Fus1 lacking its disordered region (Δ501-749), or with the region replaced by FUS^{12E} or FUS as in (A). p-values are relative to WT. **C.** Fusion and lysis efficiencies 24h after nitrogen removal under continuous white light exposure (+L) or in the dark (-L) in strains expressing either WT Fus1, Fus1 lacking its disordered region (Δ501-749), or with the region replaced by CRY2 or $CRY2_{olig}$ as in (A). p-values between -L and +L bars compare the two conditions. p-values at the top of each bar are relative to the WT. **D.** Boxplot of the max Fus1 fluorescence intensity at fusion time in strains as in (A). **E.** FRAP recovery of cells as in A. The data was scaled relative to the mean pre-bleaching value of each strain. The half-time recovery was calculated from fitting the mean of all the cells to an exponential recovery equation for each strain (see material and methods). **F.** Boxplot of the max Myo52 fluorescence intensity at fusion time in strains as in (A). Bars are 5 µm.

was not the case in WT or FUS strains that are close to fusion. Interestingly, the mating pairs that do manage to fuse are the ones that manage to form one non-resolvable focus (Bottom cell in Figure 4.5A, CRY2 strain), as for Cdc12olig containing strains. We reasoned that the extensivity to which CRY2 and CRY2olig oligomerize make it lose its interaction to the partners that localizes it to the region of contact between the two cells, and this is most probably partly responsible for the poor resulting fusion efficiency.

Interestingly, we saw that Myo52 maximal intensity at fusion time was inversely correlated with the half time recovery of Fus1 (Figure 4.5A,F). One tempting hypothesis to explain this anticorrelation is that as the Fus1 focus becomes more solid because of a self-aggregation property of increased strength, molecular crowding impedes other proteins to enter the structure, especially the Myo52 decorated vesicles that bring to the region of contact between the two cells the glucanases necessary for cell wall hydrolysis (Dudin et al., 2015).

Put together, those results show that Fus1 low complexity region behaves in mating as a self-assembling domain, the strength of which probably has to be low in order to allow for other proteins to enter the resulting fusion focus.

4.7 Discussion

How formins are regulated by their regulatory regions is still an open question. Most Diaphanous-related formins are autoinhibited by interaction of their N-terminal DID and C-terminal DAD domain. This inhibition is relieved through interaction at the right time and place by a Rho GTPase binding partner. However, some formins like Cdc12 or Fus1 are not believed to be canonically inhibited and hence rely on other mechanisms to be regulated. Here, we showed that Fus1 N-terminal region (Fus1N) not only contains essential localization information, but also cluster-forming information that is essential for fusion and quite unique among formins.

Indeed, when artificially expressed in interphase cells, Fus1N was dually localized at the poles, which was dictated by its N-terminal portion, and in clusters, which was dictated by its C-terminal portion, predicted to be disorganized. Those clusters were extremely resistant to treatments hindering weak interactions such as 1,6-hexanediol or high temperature, while the Fus1N tip-localized population was more sensitive. This was rather surprising as 1,6-hexanediol at the concentration we used has very severe effects on the cell who will die in a matter of minutes and dissolves almost anything (Düster et al., 2021), as exemplified in our case by Myo52 dispersion. Similarly, when we performed FRAP (Fluorescence Recovery After Photo Bleaching) on those cells, Fus1N clusters recovered faster than their tip localized counterpart. Both recovered only partially. However, and in contradiction to the very solid behaviour suggested by the response to the 1,6-hexanediol treatment, both recoveries were very fast, in a matter of 30 s, which suggest instead a quite dynamic behaviour. These conflicting pieces of data can be reconciled by hypothesizing that Fus1N forms a dense seed surrounded by a more liquid layer. Then, the external layer will be quickly dissolved and will quickly recover, bringing about the fast FRAP recovery time. In contrast, the dense layer will not dissolve upon hexanediol and high temperature treatments, and will make it appear as the clusters are not sensitive to such treatments, even though the surrounding layer did dissolved and contributed to

the observed rise in cytosolic signal in those cells post-treatment. These dense seeds will never recover after photobleaching and explain the only partial observed recovery.

Fus1N self-association properties were shown to be necessary for fusion. Indeed, removing the region leading to cluster formation in interphase cells led to virtually fusion incompetent cells in mating. In addition, this region could be functionally replaced by domains known to mediate self-interaction, attesting that Fus1 cluster forming region's sole function is to mediate self-interaction. This could help reach extremely high local concentrations that could explain why some Fus1 actin assembly mutants which were shown to be fully unable to assemble actin *in vitro* are partially functional *in vivo* such as Fus1^{K879A} and Fus1^{K1112A}.

The efficiency with which self-assembling domains replaced Fus1N cluster forming region was inversely proportional to the speed of recovery after photobleaching, meaning it correlated with how dynamic the Fus1 focus was, with highly dynamic FUS strains performing better than relatively less dynamic CRY2 strains. This suggests that the Fus1 focus needs to be maintained rather lose to allow for cell-wall hydrolases containing vesicles as well as monomeric actin, profilin and other necessary actin binding proteins, to enter the underlying actin structure. Another piece of evidence in that regard, is provided by electron microscopy of *acp2Δ* mating pairs (Figure 2.5). Those cells assemble an excess of Fus1, actin and tropomyosin at the region of contact between the two cells and exhibited a shmoo tip from where ribosomes were excluded, indicating molecular crowding at this zone. In addition, those cells showed fusion defects resulting mainly from Myo52 reduced accumulation at the fusion focus. While other indirect mechanisms were leading to that reduced accumulation in this case, one could propose that excessive Fus1 and F-actin recruitment could also be partly responsible for Myo52 exclusion, through increased steric occupancy. Because strains which formed a less dynamic focus, such as the CRY2 harbouring strains, similarly showed a reduced accumulation of Myo52 at the fusion focus, it would be very interesting to perform electronic microscopy on the deficient CRY2 harbouring strains and assess for ribosomal exclusion.

Because we showed that Fus1N cytosolic clusters were rather resistant to perturbations while the Fus1 foci must instead be quite dynamic to allow proper fusion, we suspected that Fus1 self-assembly properties could be regulated during mating. Another indication of a possible regulation of the strength of those clusters is found in expressing Fus1 too early in mating cells, using an inducible promotor. Such cells fail to accumulate Fus1 principally at the fusion focus and instead form clusters of high intensity in the cytosol (Figure 2.3C), and while they fuse relatively well when the early induced Fus1 copy is expressed in addition to the endogenously expressed Fus1, they don't manage to reach WT fusion levels when expressed as the sole copy (data not shown). This strongly indicates that early induced Fus1 is dysregulated and forms solid clusters which block Fus1 in a state where it isn't accessible to mating-induced regulation. One way to confirm that hypothesis would be to compare Fus1 FRAP behaviour in interphase to its behaviour in mating. We cannot directly compare our FRAP results between Fus1N in interphase and Fus1 in mating for two reasons. First, the rest of the protein might influence Fus1N self-interaction strength. Second, intensity levels reached by mating-induced Fus1 are vastly inferior to its Fus1N interphase overexpressed counterpart, which rendered using the same FRAP settings impractical. The same conclusion unfortunately stands true for the full length overexpressed Fus1. Trying different promotors to artificially express Fus1 in interphase cells will likely alleviate this issue but the clusters might then be more difficult to follow over

time. Proteins subjected to LLPS, as FUS, of which we also used a phosphomimetic version shown to behave in a more liquid manner, have been shown to mediate regulation of the strength of their self-interaction property through phosphorylation. It is then a seductive hypothesis that Fus1 self-interaction properties regulation may occur through phosphorylation by mating specific partners. Phosphoproteomics upon synchronized mating and fusion would help identify putative phosphorylation sites.

We also showed that Fus1N contains some intrinsic fusogenic properties, as, when expressed alone some pairs managed to fuse. This view was further reinforced by the very high lysis percentage, which, in a context of cell wall digestion, suggest an active but misplaced digestion apparatus. How could such lysogenic property be mediated by a formin fragment lacking its actin assembly domains? One hypothesis is that Rho1, which is known to mediate activation of glucan synthases (Arellano et al., 1996), binds Fus1N. Formins usually bind Rho GTPases as part of their canonical activation process through their G binding domain. While we have no evidence that Fus1 is activated through the conventional pathway, this region could still effectively bind a specific Rho GTPase and have evolved to fulfil a different function. Interestingly, preliminary proteomics conducted on a Fus1N immunoprecipitation retrieved Rho1 as one of its significant hits. If Fus1N indeed binds Rho1, it could titrate it away from the membrane at the region surrounding the future fusion site, downregulating cell wall synthase activity and ensuring that glucanase exocytosis exceeds the synthesis by glucan synthases at this specific point. Indeed, while glucan synthesis is needed at the shmoo tip for the early steps of polarization, once cells reach each other, the balance between cell wall formation and degradation should eventually be tipped in favor of cell wall degradation if the partner membranes are to be put in contact. Fus1 binding to Rho1 would provide the necessary tipping. However, in a cell where actin fusion focus mediated focalization of exocytosis doesn't happen, Fus1N titrating Rho1 away would result in a balance still tipped in favor of degradation but with much less spatial resolution, thereby leading to lysis. As such, Fus1 would perform the dual function of concentrating cell wall degradation while restricting its synthesis and act as the principal spatial information encoder.

5. Conclusion and Perspectives

Filamentous actin (F-actin), which forms by successive addition of monomeric actin (G-actin), provides the force for many of the cellular processes, ranging from cell motion, membrane deformation such as filopodia or lamellipodia, to cytokinesis, cellular uptake and long ranged cell-transport (Rottner et al., 2017). Cells need structurally different actin networks to fulfil those different functions. For example, a branched, capped, crosslinked actin network is required for cellular uptake. For long-ranged transport, instead, long linear actin bundles are required. For cellular fusion, an aster of actin filaments, which concentrate at one point the uptake from the whole shmoo tip, seems instead very adapated for its specific function. For cell division, however, an interconnected circular band is required. Each network is characterized not only by its architecture but also by the proteins that associate with it, the actin bindings proteins (ABPs), of which each network has its specific set. One of the most important ABPs are the nucleators. Indeed, while F-actin assembly can occur spontaneously, the assembly of the first three protomers is a slow limitating step that is sped up in the cell by the use of specific nucleators. In *Schizosaccharomyces pombe*, the model organism we used for this study, the previously mentioned networks each have their specific nucleators : Arp2/3 for the actin patches supporting endocytosis, For3 for the actin cables supporting polarized transport, Fus1 for the fusion focus and Cdc12 for the cytokinetic ring.

How cells assemble these architecturally different actin networks from a common cytosolic pool is one of the fundamental questions which the actin field tries to tackle (Boiero Sanders et al., 2020). The mechanisms governing this process are just beginning to be understood, but several elements were already clear before this work. First, as the common cytosolic pool of monomeric actin is limited, competition likely governs most of the segregation. For example, inhibiting the Arp2/3 complex in *Schizosaccharomyces pombe* not only depletes the endocytic patches but also induces a dramatic increase of the actin incorporated in the remaining networks (Burke et al., 2014). Such competition is in part regulated by profilin, a strong G-actin binder, which favors one type of nucleators, the formins, over Arp2/3 (Suarez et al., 2015). Second, the structure identity is probably also conferred in part by the specific nucleator that assembles it. For example, formins nucleate linear filaments while Arp2/3 nucleates branched filaments; Different formins promote the association of distinct tropomyosin isoforms to their respective networks, with tropomyosin itself showing preference for linear filaments over branched filaments (Johnson et al., 2014) ; Formins regulation by Rho GTPases and Arp2/3 activation by WASP proteins help spatially restrict their cognate actin networks to the proper time and place. Third, self-assembly principles are also probably involved in segregating the ABPs specific to each actin network. For example, competition between Tropomyosin, Fimbrin and ADF/Cofilin drives their sorting to distinct actin filament networks (Christensen et al., 2017).

This study offers some new aspects in response to the question. First, we showed that capping protein (CP), which limits filament growth on actin patches, has also to be seen in a different light, where it insulates actin patches barbed end from ectopic formin activity. Indeed, both CP and formin bind the same barbed end of the actin filament and have even been shown to compete in a ternary complex (Shekhar et al., 2015). Probably through recruitment by other ABPs, CP wins that competition at endocytic patches, which restricts the formins to their respective actin network. This sheds light not only on the self-assembly principles afore-mentioned but also raises a new focus. The question of the insulation of the different actin

networks once they have formed, though intrinsically connected to the question of how those distinct actin networks form from the same cytosolic pool, was until now left largely unexplored. Since CP and formins are ubiquitous in eukaryotic cells, those principles are likely to expand to other organisms than *S. pombe*. Second, we showed that the specific actin assembly properties of Fus1 were a key determinant of its resulting actin network architecture. Specifically, we showed that the combination of a high nucleation rate, a relatively low elongation rate, and an additional actin assembly property which we believe is bundling is essential to form a fusion focus of the required architecture. Similarly, recent studies have shown that Cdc12's high nucleation rate, high elongation rate and mechanoinhibition were important in organizing a cytokinetic ring of the proper architecture (Homa et al., 2021; Zimmermann et al., 2017). Third, we confirmed that the N-terminal regulatory part of formins is of importance in regulating a formin. While the canonical diaphanous formin is autoinhibitted through interaction of its N-terminal DID domain and its C-terminal DAD domain, which is relieved upon binding of a Rho GTPase, which binding site partially overlaps with the DID domain, some formins such as Cdc12 or Fus1 are not thought to be regulated as such. Instead, we showed that the C-terminal regulatory domain of Fus1 was largely dispensable for fusion, while the N-terminal regulatory region contained a cluster forming disorganized region essential for fusion. In addition, we showed that the cluster forming property of this region seems to be regulated upon mating, which is when Fus1-nucleated actin fusion focus needs to be assembled. Finally, this work on dissecting Fus1 shows that self-aggregation is important. Self-aggregation will lead to high local concentration, which can be a way to "compete" by creating a favorable local environment in a common cytosol. This gave a new and exciting direction in studying the numerous ways formins can be regulated in time and place.

Another important finding of this study is its multiple insights on how *in vitro* findings don't always directly translate *in vivo*. Indeed, we showed that a collection of four formin actin binding mutants, which all fully abrogated actin assembly *in vitro*, had a range of *in vivo* activity, with one of them functioning as high as 90% of the WT capacity in fulfilling its function. This can be in part explained by local *in vivo* concentrations that vastly exceeds what is tested *in vitro*. This can also be partially explained by the conveniency use of muscle actin in most of those studies, while it is known that different actin isoforms behave differently (Ti & Pollard, 2011). Other studies have to a various extent raised that point. For example, (A et al., 2020) showed that post-translational modification of actin itself played a role in formin regulation. (Graziano et al., 2011) have shown that budding yeast nucleation promoting factor Bud6 interacts with formin Bni1 to enhance *in vitro* nucleation rate by recruiting actin monomers. All of those findings helped reminding us how important is the back and forth conversation between *in vitro* and *in vivo* work in the actin field. Understanding why some *in vitro* findings cannot be reproduced *in vivo* raises new and exciting questions which can, in turn, be explored *in vitro*.

6. Materials and Methods

6.1 Strain, oligo and plasmid tables

6.1.1 Strain table

GENOTYPE	FIGURES	SOURCE	STRAIN
h90 myo52-tdTomato:natMX ura4-D18:p^{map3}:GFP:ura4+ leu1-32 ade6-M210	2.1 2.4 2.6	Lab Stock	YSM2535
h90 myo52-tdTomato:natMX ura4-D18:p^{map3}:GFP:ura4+ acp1Δ::kanMX leu1-32 ade6-M210	2.1	Lab Stock	YSM3307
h90 myo52-tdTomato:natMX ura4-D18:p^{map3}:GFP:ura4+ acp2Δ::kanMX leu1-32 ade6-M210	2.1 2.4 2.6	Lab Stock	YSM2955
h90 myo52-tdTomato:natMX ura4-D18:p^{map3}:GFP:ura4+ acp1Δ::kanMX acp2Δ::kanMX leu1-32 ade6-M210	2.1	This Work	YSM3308
h90 myo52-tdTomato:natMX leu1-32:p^{nmt41}:GFP-CHD:leu1+ ura4-D18 ade6-M216	2.2 2.6	Lab Stock	YSM2515
h90 myo52-tdTomato:natMX leu1-32:p^{nmt41}:GFP-CHD:leu1+ acp1Δ::hphMX ura4-D18 ade6-M216	2.2	This Work	YSM3309
h90 myo52-tdTomato:natMX leu1-32:p^{nmt41}:GFP-CHD:leu1+ acp2Δ::bleMX ura4-D18 ade6-M216	2.2 2.6	This Work	YSM3310
h90 myo52-tdTomato:natMX leu1-32:p^{nmt41}:GFP-CHD:leu1+ acp1Δ::hphMX acp2Δ::bleMX ura4-D18 ade6-M216	2.2	This Work	YSM3311
h90 myo52-tdTomato:natMX fus1-sfGFP:kanMX ura4- leu1-32 ade6-M216	2.2 2.3 3.1 3.2 3.3 3.4 3.6 3.7 4.4 4.5	This Work	YSM3312
h90 myo52-tdTomato:natMX fus1-sfGFP:kanMX acp1Δ::hphMX leu1-32 ade6-M210	2.2	This Work	YSM3313
h90 myo52-tdTomato:natMX fus1-sfGFP:kanMX acp2Δ::bleMX ura4- leu1-32 ade6-M210	2.2 2.5	This Work	YSM3314
h90 myo52-tdTomato:natMX fus1-sfGFP:kanMX acp1Δ::hphMX acp2Δ::bleMX ura4- leu1-32 ade6-M210	2.2	This Work	YSM3315
h90 myo52-tdTomato:natMX leu1-32:p^{nmt41}:GFP-cdc8:ura4+	2.2	This Work	YSM3316
h90 myo52-tdTomato:natMX leu1-32:p^{nmt41}:GFP-cdc8:ura4+ acp2Δ::bleMX ade6-M216	2.2	This Work	YSM3317
h90 myo52-tdTomato:natMX acp2-sfGFP:kanMX ade6-M216	2.3 2.7	This Work	YSM3355
h90 myo52-tdTomato:natMX acp2-sfGFP:kanMX fus1Δ::hphMX ade6-M216	2.3	This Work	YSM3433
h90 myo52-tdTomato:natMX ura4+:p^{nmt1}:fus1-sfGFP leu1-32 ade6-M210	2.3	This Work	YSM3328
h90 myo52-tdTomato:natMX fus1^{K879A}-sfGFP:kanMX ura4- leu1-32 ade6-M210	2.3	This Work	YSM3318

GENOTYPE	FIGURES	SOURCE	STRAIN
h90 myo52-tdTomato:natMX fus1^{I951A}-sfGFP:kanMX ura4- leu1-32 ade6-M210	2.3	This Work	YSM3319
h90 myo52-tdTomato:natMX fus1^{GN1087,1088RP}-sfGFP:kanMX ura4- leu1-32 ade6-M210	2.3	This Work	YSM3320
h90 myo52-tdTomato:natMX fus1^{K1112A}-sfGFP:kanMX ura4- leu1-32 ade6-M210	2.3	This Work	YSM3321
h90 myo52-tdTomato:natMX fus1^{K879A}-sfGFP:kanMX acp2Δ::bleMX ura4- leu1-32 ade6-M210	2.3	This Work	YSM3322
h90 myo52-tdTomato:natMX fus1^{I951A}-sfGFP:kanMX acp2Δ::bleMX ura4- leu1-32 ade6-M210	2.3	This Work	YSM3323
h90 myo52-tdTomato:natMX fus1^{GN1087,1088RP}-sfGFP:kanMX acp2Δ::bleMX ura4- leu1-32 ade6-M210	2.3	This Work	YSM3324
h90 myo52-tdTomato:natMX fus1^{K1112A}-sfGFP:kanMX acp2Δ::bleMX ura4- leu1-32 ade6-M210	2.3	This Work	YSM3325
h90 myo52-tdTomato:natMX exo84-GFP:kanMX ura4- leu1-32 ade6-M210	2.4	This Work	YSM3329
h90 myo52-tdTomato:natMX exo84-GFP:kanMX acp1Δ::hphMX ura4- leu1-32 ade6-M210	2.4	This Work	YSM3330
h90 myo52-tdTomato:natMX exo84-GFP:kanMX acp2Δ::bleMX ura4- leu1-32 ade6-M216	2.4	This Work	YSM3331
h90 myo52-tdTomato:natMX exo84-GFP:kanMX acp1Δ::hphMX acp2Δ::bleMX ura4- leu1-32 ade6-M216	2.4	This Work	YSM3332
h90 myo52-tdTomato:natMX exo70-GFP:kanMX ura4- leu1-32 ade6-M216	2.4 2.6	This Work	YSM3333
h90 myo52-tdTomato:natMX exo70-GFP:kanMX acp1Δ::hphMX ura4- ade6-M216	2.4	This Work	YSM3334
h90 myo52-tdTomato:natMX exo70-GFP:kanMX acp2Δ::bleMX ade6-M216	2.4 2.6	This Work	YSM3335
h90 myo52-tdTomato:natMX exo70-GFP:kanMX acp1Δ::hphMX acp2Δ::bleMX ade6-M216	2.4	This Work	YSM3336
h90 myo52-tdTomato:natMX ura4+:p^{nmt41}:GFP-ypt3 leu1-32 ade6-M210	2.4	This Work	YSM3337
h90 myo52-tdTomato:natMX ura4+:p^{nmt41}:GFP-ypt3 acp1Δ::hphMX leu1-32 ade6-M216	2.4	This Work	YSM3338
h90 myo52-tdTomato:natMX ura4+:p^{nmt41}:GFP-ypt3 acp2Δ::bleMX leu1-32 ade6-M216	2.4	This Work	YSM3339
h90 myo52-tdTomato:natMX ura4+:p^{nmt41}:GFP-ypt3 acp1Δ::hphMX acp2Δ::bleMX leu1-32 ade6-M210	2.4	This Work	YSM3340
h90 myo52-tdTomato:natMX agn2-sfGFP:kanMX	2.4	Lab Stock	YSM2571
h90 myo52-tdTomato:natMX agn2-sfGFP:kanMX acp1Δ::hphMX ura4- ade6-M216	2.4	This Work	YSM3341
h90 myo52-tdTomato:natMX agn2-sfGFP:kanMX acp2Δ::bleMX	2.4	This Work	YSM3342
h90 myo52-tdTomato:natMX agn2-sfGFP:kanMX acp1Δ::hphMX acp2Δ::bleMX ura4- leu1-32	2.4	This Work	YSM3343

GENOTYPE	FIGURES	SOURCE	STRAIN
h90 myo52-tdTomato:natMX eng2-sfGFP:kanMX	2.4	Lab Stock	YSM2572
h90 myo52-tdTomato:natMX eng2-sfGFP:kanMX acp1Δ::hphMX ura4-ade6-M216	2.4	This Work	YSM3344
h90 myo52-tdTomato:natMX eng2-sfGFP:kanMX acp2Δ::bleMX	2.4	This Work	YSM3345
h90 myo52-tdTomato:natMX eng2-sfGFP:kanMX acp1Δ::hphMX acp2Δ::bleMX leu1-32 ade6-M216	2.4	This Work	YSM3346
h90 myo52-tdTomato:natMX fus1-sfGFP:kanMX	2.5	Lab Stock	YSM3888
h90 myo52-tdTomato:natMX myo51-sfGFP:kanMX ura4-294 leu1-32 ade6-M210	2.6 2.9	This Work	YSM3347
h90 myo52-tdTomato:natMX myo51-sfGFP:kanMX acp2Δ::bleMX ura4-leu1-32 ade6-M216	2.6 2.9	This Work	YSM3348
h90 fim1-mCherry:natMX myo51-sfGFP:kanMX	2.6 2.9	This Work	YSM3351
h90 fim1-mCherry:natMX myo51-sfGFP:kanMX acp2Δ::bleMX ade6-M210	2.6 2.9	This Work	YSM3352
h90 fim1-mCherry:natMX fus1-sfGFP:kanMX leu1-32	2.6	This Work	YSM3349
h90 fim1-mCherry:natMX fus1-sfGFP:kanMX acp2Δ::bleMX ura4- leu1-32	2.6	This Work	YSM3350
h90 myo52-tdTomato:natMX acp1-sfGFP:kanMX ura4- ade6-M216	2.7	This Work	YSM3326
h90 myo52-tdTomato:natMX acp1$^{\Delta 233-256}$-sfGFP:kanMX ura4-294 leu1-32 ade6-M210	2.7	This Work	YSM3353
h90 myo52-tdTomato:natMX acp1-sfGFP:kanMX acp2Δ::bleMX ura4-leu1-32 ade6-M216	2.7	This Work	YSM3354
h90 myo52-tdTomato:natMX acp2$^{\Delta 244-268}$-sfGFP:kanMX ura4-294 leu1-32 ade6-M210	2.7	This Work	YSM3356
h90 myo52-tdTomato:natMX acp2-sfGFP:kanMX acp1Δ::hphMX ade6-M216	2.7	This Work	YSM3357
h90 myo52-tdTomato:natMX acp2^{R12A,Y77A}-sfGFP:kanMX ura4- leu1-32 ade6-M216	2.7	This Work	YSM3358
h- leu1-32:p^{act1}:LifeAct-mCherry:leu1+ ade6-M216	2.7	Lab Stock	YSM3434
h- leu1-32:p^{act1}:LifeAct-mCherry:leu1+ acp2^{R12A,Y77A}-sfGFP:kanMX ade6-M216	2.7	This Work	YSM3435
h- leu1-32:p^{act1}:LifeAct-mCherry:leu1+ acp1$^{\Delta 233-256}$-sfGFP:kanMX ade6-M216	2.7	This Work	YSM3436
h- leu1-32:p^{act1}:LifeAct-mCherry:leu1+ acp2$^{\Delta 244-268}$-sfGFP:kanMX ade6-M216	2.7	This Work	YSM3437
h90 myo52-GFP:kanMX ura4- leu1-32	2.8	Lab Stock	YSM2520
h90 myo52-GFP:kanMX fim1-GBP-mCherry:bleMX ura4- leu1-32	2.8	This Work	YSM3359
h90 myo52-tdTomato:natMX fim1-sfGFP:kanMX ura4- leu1-32 ade6-M216	2.9	This Work	YSM3360
h90 myo52-tdTomato:natMX fim1-sfGFP:kanMX acp2Δ::bleMX ura4-leu1-32 ade6-M216	2.9	This Work	YSM3361
h90 fim1-mCherry:natMX leu1-32:p^{nmt41}:GFP-cdc8:ura4+	2.9	This Work	YSM3362
h90 fim1-mCherry:natMX leu1-32:p^{nmt41}:GFP-cdc8:ura4+ acp2Δ::bleMX	2.9	This Work	YSM3363

GENOTYPE	FIGURES	SOURCE	STRAIN
h90 fim1-mCherry:natMX for3-3GFP:ura4+ leu1-32 ade6-M216	2.9	This Work	YSM3364
h90 fim1-mCherry:natMX for3-3GFP:ura4+ acp2Δ::bleMX leu1-32 ade6-M216	2.9	This Work	YSM3365
h+ fim1-mCherry:natMX cdc12-3GFP:kanMX ura4- leu1-32	2.9	This Work	YSM3366
h+ fim1-mCherry:natMX cdc12-3GFP:kanMX acp2Δ::bleMX ura4- leu1-32	2.9	This Work	YSM3367
h- fim1-mCherry:natMX leu1-32:p^{nmt41}:GFP-cdc8:ura4+ for3Δ::bsdMX ade6-M216	2.9	This Work	YSM3368
h- fim1-mCherry:natMX leu1-32:p^{nmt41}:GFP-cdc8:ura4+ for3Δ::bsdMX acp2Δ::bleMX ade6-M216	2.9	This Work	YSM3369
h- fim1-mCherry:natMX leu1-32:p^{nmt41}:GFP-cdc8:ura4+ for3Δ::kanMX cdc12-112	2.9	This Work	YSM3370
h- fim1-mCherry:natMX leu1-32:p^{nmt41}:GFP-cdc8:ura4+ for3Δ::kanMX cdc12-112 acp2Δ::bleMX	2.9	This Work	YSM3371
h90 myo52-tdTomato:natMX fus1Δ::LEU2+ ura4-294:p^{fus1}:fus1-sfGFP:ura4+ leu1-32	3.1 4.1	Lab Stock	YSM2498
h90 myo52-tdTomato:natMX fus1Δ::LEU2+ ura4-294:p^{fus1}:cdc12-sfGFP:ura4+ leu1-32	3.1	Lab Stock	YSM2502
h90 myo52-tdTomato:natMX fus1Δ::LEU2+ ura4-294:p^{fus1}:for3-sfGFP:ura4+ leu1-32	3.1	Lab Stock	YSM2500
h90 myo52-tdTomato:natMX fus1Δ::LEU2+ ura4-294:p^{fus1}-fus1N1-792-fus1C793-1372-sfGFP:ura4+ leu1-32	3.2	Lab Stock	YSM2504
h90 myo52-tdTomato:natMX fus1Δ::LEU2+ ura4-294:p^{fus1}-cdc12N1-887-fus1C793-1372-sfGFP:ura4+ leu1-32	3.2	Lab Stock	YSM2512
h90 myo52-tdTomato:natMX fus1Δ::LEU2+ ura4-294:p^{fus1}-for3N1-714-fus1C793-1372-sfGFP:ura4+ leu1-32	3.2	Lab Stock	YSM2510
h90 myo52-tdTomato:natMX ura4+:p^{fus1}:fus1N^{1-792}-fus1$C^{793-1372}$-sfGFP fus1Δ::hphMX ade6-M210	3.2 3.3	This Work	IBC680
h90 myo52-tdTomato:natMX ura4+:p^{fus1}:fus1N^{1-792}-cdc12$C^{888-1841}$-sfGFP fus1Δ::hphMX ade6-M210	3.2 3.3	This Work	IBC745
h90 myo52-tdTomato:natMX ura4+:p^{fus1}:fus1N^{1-792}-for3$C^{715-1461}$-sfGFP fus1Δ::hphMX ade6-M210	3.2 3.3	This Work	IBC747
h90 myo52-tdTomato:natMX ura4+:p^{fus1}:fus1N^{1-792}-cdc12CΔolig$^{888-1451}$-sfGFP fus1Δ::hphMX ade6-M210	3.2 3.3	This Work	IBC749
h90 myo52-tdTomato:natMX ura4+:p^{fus1}: fus1N^{1-792}-for3$C^{715-1461}$-cdc12olig$^{1446-1841}$-sfGFP fus1Δ::hphMX ade6-M210	3.2 3.3	This Work	IBC751
h90 myo52-tdTomato:natMX fus1$^{\Delta 1278-1372}$-sfGFP:kanMX ura4-294 leu1-32 ade6-M210	3.2	This Work	IBC332
h90 myo52-tdTomato:natMX ura4+:p^{fus1}:fus1N^{1-792}-fus1$C^{793-1372}$-sfGFP fus1Δ::hphMX leu1-32 ade6-M210	3.3	This Work	IBC344

GENOTYPE	FIGURES	SOURCE	STRAIN
h90 myo52-tdTomato:natMX ura4+:p^{fus1}:fus1N$^{1-792}$-cdc12C$^{888-1841}$-sfGFP fus1Δ::hphMX leu1-32 ade6-M210	3.3	This Work	IBC347
h90 myo52-tdTomato:natMX ura4+:p^{fus1}:fus1N$^{1-792}$-for3C$^{715-1461}$-sfGFP fus1Δ::hphMX leu1-32 ade6-M210	3.3	This Work	IBC364
h90 myo52-tdTomato:natMX ura4+:p^{fus1}:fus1N$^{1-792}$-cdc12CΔolig$^{888-1451}$-sfGFP fus1Δ::hphMX leu1-32 ade6-M210	3.3	This Work	IBC349
h90 myo52-tdTomato:natMX ura4+:p^{fus1}:fus1N$^{1-792}$-for3C$^{715-1461}$-cdc12olig$^{1446-1841}$-sfGFP fus1Δ::hphMX leu1-32 ade6-M210	3.3	This Work	IBC353
h90 myo52-tdTomato:natMX fus1N$^{1-792}$-fus1C$^{793-1372}$-sfGFP:kanMX ura4-294 leu1-32 ade6-M210	3.3	This Work	IBC735
h90 myo52-tdTomato:natMX fus1N$^{1-792}$-cdc12C$^{888-1841}$-sfGFP:kanMX ura4-294 leu1-32 ade6-M210	3.3	This Work	IBC737
h90 myo52-tdTomato:natMX fus1N$^{1-792}$-for3C$^{715-1461}$-sfGFP:kanMX ura4-294 leu1-32 ade6-M210	3.3	This Work	IBC739
h90 myo52-tdTomato:natMX fus1N$^{1-792}$-cdc12CΔolig$^{888-1451}$-sfGFP:kanMX ura4-294 leu1-32 ade6-M210	3.3	This Work	IBC741
h90 myo52-tdTomato:natMX fus1N$^{1-792}$-for3C$^{715-1461}$-cdc12olig$^{1446-1841}$-sfGFP:kanMX ura4-294 leu1-32 ade6-M210	3.3	This Work	IBC743
h90 myo52-tdTomato:natMX fus1N$^{1-792}$-fus1C$^{793-1372}$-sfGFP:kanMX ura4-294 ade6-M210	3.3	This Work	IBC490
h90 myo52-tdTomato:natMX fus1N$^{1-792}$-cdc12C$^{888-1841}$-sfGFP:kanMX ura4-294 ade6-M210	3.3	This Work	IBC516
h90 myo52-tdTomato:natMX fus1N$^{1-792}$-for3C$^{715-1461}$-sfGFP:kanMX ura4-294 ade6-M210	3.3	This Work	IBC492
h90 myo52-tdTomato:natMX fus1N$^{1-792}$-cdc12CΔolig$^{888-1451}$-sfGFP:kanMX ura4-294 ade6-M210	3.3	This Work	IBC523
h90 myo52-tdTomato:natMX fus1N$^{1-792}$-for3C$^{715-1461}$-cdc12olig$^{1446-1841}$-sfGFP:kanMX ura4-294 ade6-M210	3.3	This Work	IBC494
h90 myo52-tdTomato:natMX fus1N$^{1-792}$-fus1C$^{793-1372}$-sfGFP:kanMX ura4+:p^{fus1}:fus1N$^{1-792}$-fus1C$^{793-1372}$-sfGFP fus1Δ::hphMX leu1-32 ade6-M210	3.3	This Work	IBC537
h90 myo52-tdTomato:natMX fus1N$^{1-792}$-cdc12C$^{888-1841}$-sfGFP:kanMX ura4+:p^{fus1}:fus1N$^{1-792}$-cdc12C$^{888-1841}$-sfGFP fus1Δ::hphMX leu1-32 ade6-M210	3.3	This Work	IBC539
h90 myo52-tdTomato:natMX fus1N$^{1-792}$-for3C$^{715-1461}$-sfGFP:kanMX ura4+:p^{fus1}:fus1N$^{1-792}$-for3C$^{715-1461}$-sfGFP fus1Δ::hphMX leu1-32 ade6-M210	3.3	This Work	IBC541

GENOTYPE	FIGURES	SOURCE	STRAIN
h90 myo52-tdTomato:natMX fus1N$^{1-792}$-cdc12CΔolig$^{888-1451}$-sfGFP:kanMX ura4+:p^{fus1}:fus1N$^{1-792}$-cdc12CΔolig$^{888-1451}$-sfGFP fus1Δ::hphMX leu1-32 ade6-M210	3.3	This Work	IBC543
h90 myo52-tdTomato:natMX fus1N$^{1-792}$-for3C$^{715-1461}$-cdc12olig$^{1446-1841}$-sfGFP:kanMX ura4+:p^{fus1}:fus1N$^{1-792}$-for3C$^{715-1461}$-cdc12olig$^{1446-1841}$-sfGFP fus1Δ::hphMX leu1-32 ade6-M210	3.3	This Work	IBC545
h90 myo52-tdTomato:natMX ura4+:p^{ste11}:fus1-sfGFP fus1Δ::hphMX leu1-32 ade6-M210	3.3	This Work	IBC584
h90 myo52-tdTomato:natMX ura4+:p^{pak2}:fus1-sfGFP fus1Δ::hphMX leu1-32 ade6-M210	3.3	This Work	IBC588
h90 myo52-tdTomato:natMX fus1$^{1-868}$-fus1$^{792-1372}$-sfGFP:kanMX ura4-294 leu1-32 ade6-M210	3.4	This Work	IBC366
h90 myo52-tdTomato:natMX fus1$^{1-791}$-cdc12$^{928-972}$-fus1$^{869-1372}$-sfGFP:kanMX ura4-294 leu1-32 ade6-M210	3.4	This Work	IBC506
h90 myo52-tdTomato:natMX fus1$^{1-791}$-cdc12$^{882-972}$-cdc12$^{882-972}$-fus1$^{869-1372}$-sfGFP:kanMX ura4-294 leu1-32 ade6-M210	3.4 3.6 3.7	This Work	IBC504
h90 myo52-tdTomato:natMX ade6+:p^{act1}:LifeAct-sfGFP:term^{ScADH1}:bsdMX fus1:kanMX ura4-294 leu1-32	3.4	This Work	IBC705
h90 myo52-tdTomato:natMX ade6+:p^{act1}:LifeAct-sfGFP:term^{ScADH1}:bsdMX fus1$^{1-791}$-cdc12$^{882-972}$-cdc12$^{882-972}$-fus1$^{869-1372}$:kanMX ura4-294 leu1-32	3.4	This Work	IBC701
h90 myo52-tdTomato:natMX leu1-32:p^{nmt41}:GFP-cdc8:ura4+ fus1:kanMX	3.4	This Work	IBC767
h90 myo52-tdTomato:natMX leu1-32:p^{nmt41}:GFP-cdc8:ura4+ fus1$^{1-791}$-cdc12$^{882-972}$-cdc12$^{882-972}$-fus1$^{869-1372}$:kanMX	3.4	This Work	IBC769
h90 myo52-tdTomato:natMX leu1-32:p^{cdc8}:mNeonGreen-cdc8:term^{cdc8}:termADH1:leu1+ fus1:kanMX ura4-294 ade6-M210	3.4	This Work	IBC646
h90 myo52-tdTomato:natMX leu1-32:p^{cdc8}:mNeonGreen-cdc8:term^{cdc8}:termADH1:leu1+ fus1$^{1-791}$-cdc12$^{882-972}$-cdc12$^{882-972}$-fus1$^{869-1372}$:kanMX ura4-294 ade6-M210	3.4	This Work	IBC648
h90 myo52-tdTomato:natMX fus1$^{1-791}$-for3$^{718-1265}$-fus1$^{1278-1372}$-sfGFP:kanMX ura4-294 leu1-32 ade6-M210	3.5	This Work	IBC384
h90 myo52-tdTomato:natMX fus1$^{1-868}$-cdc12$^{973-1390}$-fus1$^{1278-1372}$-sfGFP:kanMX ura4-294 leu1-32 ade6-M210	3.5 3.6 3.7	This Work	IBC525
h90 myo52-tdTomato:natMX fus1$^{1-791}$-cdc12$^{928-1390}$-fus1$^{1278-1372}$-sfGFP:kanMX ura4-294 leu1-32 ade6-M210	3.5	This Work	IBC386

GENOTYPE	FIGURES	SOURCE	STRAIN
h90 myo52-tdTomato:natMX fus1$^{1-791}$-cdc12$^{882-1390}$-fus1$^{1278-1372}$-sfGFP:kanMX ura4-294 leu1-32 ade6-M210	3.5	This Work	IBC382
h90 myo52-tdTomato:natMX fus1$^{1-792}$-cdc12$^{882-972}$-cdc12$^{882-1390}$-fus1$^{1278-1372}$-sfGFP:kanMX ura4-294 leu1-32 ade6-M210	3.5 3.6 3.7	This Work	IBC517
h90 myo52-tdTomato:natMX ade6+:p^{act1}:LifeAct-sfGFP:term^{ScADH1}:bsdMX fus1$^{1-791}$-for3$^{718-1265}$-fus1$^{1278-1372}$:kanMX ura4-294 leu1-32	3.5	This Work	IBC703
h90 myo52-tdTomato:natMX ade6+:p^{act1}:LifeAct-sfGFP:term^{ScADH1}:bsdMX fus1$^{1-868}$-cdc12$^{973-1390}$-fus1$^{1278-1372}$:kanMX ura4-294 leu1-32	3.5	This Work	IBC712
h90 myo52-tdTomato:natMX ade6+:p^{act1}:LifeAct-sfGFP:term^{ScADH1}:bsdMX fus1$^{1-791}$-cdc12$^{928-1390}$-fus1$^{1278-1372}$:kanMX ura4-294 leu1-32	3.5	This Work	IBC714
h90 myo52-tdTomato:natMX ade6+:p^{act1}:LifeAct-sfGFP:term^{ScADH1}:bsdMX fus1$^{1-791}$-cdc12$^{882-972}$-cdc12$^{882-1390}$-fus1$^{1278-1372}$:kanMX ura4-294 leu1-32	3.5	This Work	IBC716
h90 myo52-tdTomato:natMX leu1-32:p^{nmt41}:GFP-cdc8:ura4+ fus1$^{1-791}$-for3$^{718-1265}$-fus1$^{1278-1372}$:kanMX	3.5	This Work	IBC774
h90 myo52-tdTomato:natMX leu1-32:p^{nmt41}:GFP-cdc8:ura4+ fus1$^{1-868}$-cdc12$^{973-1390}$-fus1$^{1278-1372}$:kanMX	3.5	This Work	IBC778
h90 myo52-tdTomato:natMX leu1-32:p^{nmt41}:GFP-cdc8:ura4+ fus1$^{1-791}$-cdc12$^{928-1390}$-fus1$^{1278-1372}$:kanMX	3.5	This Work	IBC780
h90 myo52-tdTomato:natMX leu1-32:p^{nmt41}:GFP-cdc8:ura4+ fus1$^{1-791}$-cdc12$^{882-972}$-cdc12$^{882-1390}$-fus1$^{1278-1372}$:kanMX	3.5	This Work	IBC773
h90 myo52-tdTomato:natMX leu1-32:p^{cdc8}:mNeonGreen-cdc8:term^{cdc8}:termADH1:leu1+ fus1$^{1-791}$-for3$^{718-1265}$-fus1$^{1278-1372}$:kanMX ura4-294 ade6-M210	3.5	This Work	IBC654
h90 myo52-tdTomato:natMX leu1-32:p^{cdc8}:mNeonGreen-cdc8:term^{cdc8}:termADH1:leu1+ fus1$^{1-868}$-cdc12$^{973-1390}$-fus1$^{1278-1372}$:kanMX ura4-294 ade6-M210	3.5	This Work	IBC657
h90 myo52-tdTomato:natMX leu1-32:p^{cdc8}:mNeonGreen-cdc8:term^{cdc8}:termADH1:leu1+ fus1$^{1-791}$-cdc12$^{928-1390}$-fus1$^{1278-1372}$:kanMX ura4-294 ade6-M210	3.5	This Work	IBC650
h90 myo52-tdTomato:natMX leu1-32:p^{cdc8}:mNeonGreen-cdc8:term^{cdc8}:termADH1:leu1+ fus1$^{1-791}$-cdc12$^{882-972}$-cdc12$^{882-1390}$-fus1$^{1278-1372}$:kanMX ura4-294 ade6-M210	3.5	This Work	IBC652
h90 myo52-tdTomato:natMX fus1$^{1-868}$-Sjfus1$^{908-1317}$-fus1$^{1278-1372}$-sfGFP:kanMX ura4-294 leu1-32 ade6-M210	3.6	This Work	IBC628
h90 myo52-tdTomato:natMX fus1$^{1-868}$-Sofus1$^{857-1265}$-fus1$^{1278-1372}$-sfGFP:kanMX ura4-294 leu1-32 ade6-M210	3.6	This Work	IBC630

GENOTYPE	FIGURES	SOURCE	STRAIN
h90 myo52-tdTomato:natMX fus1$^{1\text{-}792}$-cdc12$^{882\text{-}972}$-cdc12$^{882\text{-}972}$-Sjfus1$^{908\text{-}1317}$-fus1$^{1278\text{-}1372}$-sfGFP:kanMX ura4-294 leu1-32 ade6-M210	3.6	This Work	IBC626
h90 myo52-tdTomato:natMX fus1$^{1\text{-}792}$-cdc12$^{882\text{-}972}$-cdc12$^{882\text{-}972}$-Sofus1$^{857\text{-}1265}$-fus1$^{1278\text{-}1372}$-sfGFP:kanMX ura4-294 leu1-32 ade6-M210	3.6	This Work	IBC627
h90 myo52-tdTomato:natMX fus1(KEYTG935-939CARTD)-sfGFP:kanMX ura4-294 leu1-32 ade6-M216	3.7	This Work	IBC619
h90 myo52-tdTomato:natMX fus1(L959K)-sfGFP:kanMX ura4-294 leu1-32 ade6-M216	3.7	This Work	IBC620
h90 myo52-tdTomato:natMX fus1(EEVMEV1006-1011NGGDLVNS)-sfGFP:kanMX ura4-294 leu1-32 ade6-M216	3.7	This Work	IBC622
h90 myo52-tdTomato:natMX fus1(R1054E)-sfGFP:kanMX ura4-294 leu1-32 ade6-M216	3.7	This Work	IBC634
h90 myo52-tdTomato:natMX fus1(NHK1182-1184DPT)-sfGFP:kanMX ura4-294 leu1-32 ade6-M216	3.7	This Work	IBC625
h90 myo52-tdTomato:natMX fus1$^{1\text{-}792}$-cdc12$^{882\text{-}972}$-cdc12$^{882\text{-}972}$-fus1$^{869\text{-}1372}$(KEYTG935-939CARTD)-sfGFP:kanMX ura4-294 leu1-32 ade6-M210	3.7	This Work	IBC609
h90 myo52-tdTomato:natMX fus1$^{1\text{-}792}$-cdc12$^{882\text{-}972}$-cdc12$^{882\text{-}972}$-fus1$^{869\text{-}1372}$(L959K)-sfGFP:kanMX ura4-294 leu1-32 ade6-M210	3.7	This Work	IBC611
h90 myo52-tdTomato:natMX fus1$^{1\text{-}792}$-cdc12$^{882\text{-}972}$-cdc12$^{882\text{-}972}$-fus1$^{869\text{-}1372}$(EEVMEV1006-1011NGGDLVNS)-sfGFP:kanMX ura4-294 leu1-32 ade6-M210	3.7	This Work	IBC613
h90 myo52-tdTomato:natMX fus1$^{1\text{-}792}$-cdc12$^{882\text{-}972}$-cdc12$^{882\text{-}972}$-fus1$^{869\text{-}1372}$(R1054E)-sfGFP:kanMX ura4-294 leu1-32 ade6-M210	3.7	This Work	IBC615
h90 myo52-tdTomato:natMX fus1$^{1\text{-}792}$-cdc12$^{882\text{-}972}$-cdc12$^{882\text{-}972}$-fus1$^{869\text{-}1372}$(NHK1182-1184DPT)-sfGFP:kanMX ura4-294 leu1-32 ade6-M210	3.7	This Work	IBC616
h90 myo52-tdTomato:natMX ade6+:p^{act1}:LifeAct-sfGFP:term^{ScADH1}:bsdMX fus1(R1054E):kanMX ura4-294 leu1-32	3.7	This Work	IBC762
h90 myo52-tdTomato:natMX leu1-32:p^{nmt41}:GFP-cdc8:ura4+ fus1(R1054E):kanMX	3.7	This Work	IBC771
h90 myo52-tdTomato:natMX leu1-32:p^{cdc8}:mNeonGreen-cdc8:term^{cdc8}:termADH1:leu1+ fus1(R1054E):kanMX ura4-294 ade6-M216	3.7	This Work	IBC759
h90 myo52-tdTomato:natMX ade6+:p^{act1}:LifeAct-sfGFP:term^{ScADH1}:bsdMX fus1$^{1\text{-}792}$-cdc12$^{882\text{-}972}$-cdc12$^{882\text{-}972}$-fus1$^{869\text{-}1372}$(R1054E):kanMX ura4-294 leu1-32	3.7	This Work	IBC764

GENOTYPE	FIGURES	SOURCE	STRAIN
h90 myo52-tdTomato:natMX leu1-32:p^{nmt41}:GFP-cdc8:ura4+ fus1$^{1-792}$-cdc12$^{882-972}$-cdc12$^{882-972}$-fus1$^{869-1372}$(R1054E):kanMX	3.7	This Work	IBC772
h90 myo52-tdTomato:natMX leu1-32:p^{cdc8}:mNeonGreen-cdc8:term^{cdc8}:termADH1:leu1+ fus1$^{1-792}$-cdc12$^{882-972}$-cdc12$^{882-972}$-fus1$^{869-1372}$(R1054E):kanMX ura4-294 ade6-M210	3.7	This Work	IBC760
h90 myo52-tdTomato:natMX fus1$^{1-792}$-cdc12$^{882-972}$-cdc12$^{882-1390}$(E1168R)-fus1$^{1278-1372}$-sfGFP:kanMX ura4-294 leu1-32 ade6-M210	3.7	This Work	IBC678
h90 myo52-tdTomato:natMX ade6+:p^{act1}:LifeAct-sfGFP:term^{ScADH1}:bsdMX fus1$^{1-792}$-cdc12$^{882-972}$-cdc12$^{882-1390}$(E1168R)-fus1$^{1278-1372}$:kanMX ura4-294 leu1-32	3.7	This Work	IBC766
h90 myo52-tdTomato:natMX leu1-32:p^{nmt41}:GFP-cdc8:ura4+ fus1$^{1-792}$-cdc12$^{882-972}$-cdc12$^{882-1390}$(E1168R)-fus1$^{1278-1372}$:kanMX	3.7	This Work	IBC782
h90 myo52-tdTomato:natMX leu1-32:p^{cdc8}:mNeonGreen-cdc8:term^{cdc8}:termADH1:leu1+ fus1$^{1-792}$-cdc12$^{882-972}$-cdc12$^{882-1390}$(E1168R)-fus1$^{1278-1372}$:kanMX ura4-294 ade6-M210	3.7	This Work	IBC776
h90 myo52-tdTomato:natMX ura4+:p^{fus1}:fus1N$^{1-792}$-sfGFP leu1-32 ade6-M210	4.1	This Work	IBC557
h90 myo52-tdTomato:natMX ura4+:p^{fus1}:fus1N$^{1-792}$-sfGFP fus1Δ::hphMX leu1-32 ade6-M210	4.1	This Work	IBC559
h90 myo52-tdTomato:natMX ura4-294:p^{fus1}:fus1N-sfGFP:ura4+ fus1Δ::LEU2+ ura4-294 leu1-32	4.1	Lab Stock	YSM2486
h90 myo52-tdTomato:natMX fus1Δ::LEU2+ ura4-294 leu1-32	4.1	Lab Stock	YSM2439
h90 myo52-tdTomato:natMX ura4+:p^{nmt1}:fus1N$^{1-792}$-sfGFP:term^{nmt} leu1-32 ade6-M210	4.2 4.3	This Work	IBC342
h90 myo52-tdTomato:natMX ura4+:p^{nmt1}:fus1N$^{1-730}$-sfGFP:term^{nmt} leu1-32 ade6-M210	4.2	This Work	IBC359
h90 myo52-tdTomato:natMX ura4+:p^{nmt1}:fus1N$^{1-500}$-sfGFP:term^{nmt} leu1-32 ade6-M210	4.2	This Work	IBC411
h90 myo52-tdTomato:natMX ura4+:p^{nmt1}:fus1N$^{93-792}$-sfGFP:term^{nmt} leu1-32 ade6-M210	4.2	This Work	IBC381
h90 myo52-tdTomato:natMX ura4+:p^{nmt1}:fus1N$^{140-792}$-sfGFP:term^{nmt} leu1-32 ade6-M210	4.2	This Work	IBC578
h90 myo52-tdTomato:natMX ura4+:p^{nmt1}:fus1N$^{191-792}$-sfGFP:term^{nmt} leu1-32 ade6-M210	4.2	This Work	IBC508
h90 myo52-tdTomato:natMX ura4+:p^{nmt1}:fus1N$^{293-792}$-sfGFP:term^{nmt} leu1-32 ade6-M210	4.2	This Work	IBC512

GENOTYPE	FIGURES	SOURCE	STRAIN
h90 myo52-tdTomato:natMX ura4+:p^{nmt1}:fus1N$^{431-755}$-sfGFP:$term^{nmt}$ leu1-32 ade6-M210	4.2	This Work	IBC415
h+ his5+:p^{act1}:CRIB-3mCherry:bsdMX ura4-D18	4.2	This Work	IBC396
h90 his5+:p^{act1}:CRIB-3mCherry:bsdMX ura4+:p^{nmt1}:fus1N$^{1-792}$-sfGFP:$term^{nmt}$ leu1-32	4.2	This Work	IBC435
h90 his5+:p^{act1}:CRIB-3mCherry:bsdMX ura4+:p^{nmt1}:fus1N$^{1-730}$-sfGFP:$term^{nmt}$ ade6-M210	4.2	This Work	IBC437
h90 his5+:p^{act1}:CRIB-3mCherry:bsdMX ura4+:p^{nmt1}:fus1N$^{93-792}$-sfGFP:$term^{nmt}$ leu1-32 ade6-M210	4.2	This Work	IBC571
h90 tea1-mCherry:kanMX ura4-D18 leu1-32	4.2	This Work	IBC568
h90 tea1-mCherry:kanMX ura4+:p^{nmt1}:fus1N$^{1-792}$-sfGFP:$term^{nmt}$ leu1-32	4.2	This Work	IBC431
h90 tea1-mCherry:kanMX ura4+:p^{nmt1}:fus1N$^{1-730}$-sfGFP:$term^{nmt}$ leu1-32	4.2	This Work	IBC433
h90 tea1-mCherry:kanMX ura4+:p^{nmt1}:fus1N$^{93-792}$-sfGFP:$term^{nmt}$ leu1-32 ade6-M210	4.2	This Work	IBC569
h90 myo52-tdTomato:natMX ura4+:p^{nmt1}:fus1-sfGFP:$term^{nmt}$ leu1-32 ade6-M210	4.3	This Work	IBC361
h90 myo52-tdTomato:natMX fus1$^{\Delta 501-749}$-sfGFP:kanMX ura4-294 leu1-32 ade6-M210	4.4	This Work	IBC303
h90 myo52-tdTomato:natMX fus1$^{\Delta 501-791}$-sfGFP:kanMX ura4-294 leu1-32 ade6-M210	4.4	This Work	IBC500
h90 myo52-tdTomato:natMX fus1$^{\Delta 492-791}$-sfGFP:kanMX ura4-294 leu1-32 ade6-M210	4.4 4.5	This Work	IBC372
h90 myo52-tdTomato:natMX fus1$^{1-491}$-FUS^{12E}-fus1$^{792-1372}$-sfGFP:kanMX ura4-294 leu1-32 ade6-M210	4.5	This Work	IBC730
h90 myo52-tdTomato:natMX fus1$^{1-491}$-FUS-fus1$^{792-1372}$-sfGFP:kanMX ura4-294 leu1-32 ade6-M210	4.5	This Work	IBC728
h90 myo52-tdTomato:natMX fus1$^{1-491}$-CRY2PHR-fus1$^{792-1372}$-sfGFP:kanMX ura4-294 leu1-32 ade6-M210	4.5	This Work	IBC722
h90 myo52-tdTomato:natMX fus1$^{1-491}$-CRY2olig-fus1$^{792-1372}$-sfGFP:kanMX ura4-294 leu1-32 ade6-M210	4.5	This Work	IBC724

6.1.2 Oligo table

NAME	SEQUENCE	ORIENTATION	PURPOSE
osm765	CAGCTCCAAATTTTGAAAGTAAAACCCCTAATTAGGGA ATAAATAAGTAGGCAGAGCACCTTGAAAAATAACTAGA TAGAATTCGAGCTCGTTTAAAC	R	WACH (Myo52 3')

NAME	SEQUENCE	ORIENTATION	PURPOSE
osm932	AATAAAAAGAGACAAACAGTCGTCCTTAAAGCTGAATG CATGCTTAAGCAGCTGGAGAATAACAATGAACTTAAGA GACGGATCCCCGGGTTAATTAA	F	WACH (Fus1 ORF)
osm933	TTTTATTAATTATAATTTCATTATAATTTGTTTAAGTCA TTTAATTGTCATTAAAAGTCATTAACATTTCAAACATCA GAATTCGAGCTCGTTTAAAC	R	WACH (Fus1 3')
osm1028	TTACAACTGCACATGCATTTCACCACACATAATATACG ATTTTCATAAATCGCATCCTTCGTAAAAATTATATGCAA ACGGATCCCCGGGTTAATTAA	F	WACH (Exo70 ORF)
osm1029	AGAAAAGTGAGAATGCCAGTACACCCACTTTAGTACTA TATTATGGAATTTCAAAGGACCCAAATTCATCATATTG AAGAATTCGAGCTCGTTTAAAC	R	WACH (Exo70 3')
osm1196	GATCACTGTAGGCAACGTAGCCGACAATGATGTACAGA ACTCGAGCGACGAAGAAAATCAAGTACCAAATGGTATT AAAGTTCGGATCCCCGGGTTAATTAA	F	WACH (Myo52 ORF)
osm1237	ACGGAATTAAAGGAAGCTAAAATTGATGCCATGCCGAT ATTACAGCGTCTTTTTGATGTTCATTCTAAAGATTTAAA ACGGATCCCCGGGTTAATTAA	F	WACH (Exo84 ORF)
osm1238	TTAAATTGTATTAAAAAAATAATGGGTCTTTCATGAAA TTTATATTCCATACCCTTATATAAAAACTGAAATCAAA ATGAATTCGAGCTCGTTTAAAC	R	WACH (Exo84 3')
osm1670	TTACGAGCAAAAAACCTTGTTTCTGTAATTATAGGACA TATTATTGATGGTTTCACCTTTTTTAGCTATTGCTTGTTA CGGATCCCCGGGTTAATTAA	F	WACH (Fus1 5')
osm1746	ACGGATTTCATGAAGTTATTGGTTAAAAGCGGCCTCTC AAATCCTCCAGCTAAAGAACCAGTCCATGACAACGAAA ATCGGATCCCCGGGTTAATTAA	F	WACH (Tea1 ORF)
osm1747	ATGTCATCGTCGAATATTTACACTATGTACAGTCCTTTC AACTAGTAAAGGAGATGCTTTCAAAATAGTTCCAAAGA GGAATTCGAGCTCGTTTAAAC	R	WACH (Tea1 3')
osm1772	CGTATCACGAGGCCCTTTCG	F	CLONING
osm2217	CCGGATCCTCCAAGGGTGAAGAGCTATTTACTGGGG	F	CLONING
osm2646	GGGGTACCCACACCATTCAGAATTAAGTTG	F	CLONING
osm2789	TATGGTCCATTAAATATTCTTGGTAACAATTCTGTTGTG CTATACAACTTCAACTTCTGCACCACTAGGATATCCTGG CGGATCCCCGGGTTAATTAA	F	WACH (Agn2 ORF)
osm2790	TGCCACCAAAAAGTAATGTAAACTTCAGTCATACCATC AGGATTGACTAATTTTGATCTCCACTTTTAGTTTATGGA AGAATTCGAGCTCGTTTAAAC	R	WACH (Agn2 3')

NAME	SEQUENCE	ORIENTATION	PURPOSE
osm2791	TTTACTGCTGATAAAATTGATAACGGAGCTAGTAAAAC CTGGTACTTAGCTATGGCTGCTGGTATGGGTGGATCAC CACGGATCCCCGGGTTAATTAA	F	WACH (Eng2 ORF)
osm2792	TCTATGTGTTGTTTTGAAATGGTTACATAATTTTGAAAC GAAAAGTAATGCTTCAGTTTTTCATTAGCTCCCTTGCCA GAATTCGAGCTCGTTTAAAC	R	WACH (Eng2 3')
osm2876	ATCAAATCACCACAACGAGCACAAGAAATGCTTGCAGG TTTATTATCTGGAAAATTGGCGCCTAAGGAGAATGAGA AACGGATCCCCGGGTTAATTAA	F	WACH (Cdc12 ORF)
osm2877	AGGGCAATCTTCCAACTAAACTAACTTCCAAAATTAGA AAAAAAAATTATGCAATGGTAGAAAGATTGCATCATTA ACGAATTCGAGCTCGTTTAAAC	R	WACH (Cdc12 3')
osm2878	ATCTTTATTTTGCCAGAAGATATTGTGGCCGTTCGTCCT CGGTTGGTCCTTCATTTTATTGGCAGTTTAATGGCCGTA CGGATCCCCGGGTTAATTAA	F	WACH (Fim1 ORF)
osm2879	CGCAATATAAGTAATTAAATTGGGAAAAACACATGTGT TAAATCGTTTCGTTAAAAGCTATAGTTAAGTCGAAACA AAGAATTCGAGCTCGTTTAAAC	R	WACH (Fim1 3')
osm3005	ACTGCGGCCGCATGATGACGGCTAGTTTTAAAGG	F	CLONING
osm3006	ACTCCCGGGTCTCTTAAGTTCATTGTTATTCTCC	R	CLONING
osm3007	ACTGCGGCCGCATGGCATCTAAAATGCCTGAAG	F	CLONING
osm3008	ACTCCCGGGTGTTTTTGGCGGTCATTTTCAAC	R	CLONING
osm3009	ACTGCGGCCGCATGCGAAATTCGTCAAAGGGAC	F	CLONING
osm3010	ACTCCCGGGTTTCTCATTCTCCTTAGGCGC	R	CLONING
osm3026	CTTGGATCCTCATATTTTCTATTTTAGAAAACCTC	R	CLONING
osm3027	TGAGGATCCAAGAAGTTATTGATGGGAATCC	F	CLONING
osm3028	CTGGGATCCATGGCGAAGGCGAGGAAG	R	CLONING
osm3029	CATGGATCCCAGATGTTTCCGACACCGTAG	F	CLONING
osm3030	TCGGGATCCTACTATTGTTGCTAACTGTTTCTGC	R	CLONING
osm3031	GTAGGATCCCGAACTTTGATATTCCTAATGATGC	F	CLONING
osm3091	CGGGGTACCGATCAGAAAATTATCGCCAT	F	CLONING
osm3416	GAATTGCGTCGTCAACTTCCAGTCACTCGCCAGAAAAT TAATTGGGAAAACGTTAGTGGCATCCGTATGAGAAATA CTCGGATCCCCGGGTTAATTAA	F	WACH (Acp1 ORF)
osm3417	AGGAAACAGCTTGAATCACCGTCTTAAAAAATATCGTC GCAAAAAAATTTCCAAAATTTATAAACACATATAAGTG TTGAATTCGAGCTCGTTTAAAC	R	WACH (Acp1 3')
osm3516	ACTGCGGCCGCTGATTTAACAAAGCGACTATAAGTC	R	CLONING
osm3521	ACTCCCGGGAGTAGAAGTGTTAGGAGCTTC	R	CLONING

NAME	SEQUENCE	ORIENTATION	PURPOSE
osm3570	CCTTACCATTTATTCCTTAATCAGCTTCGTTAGTATCTTT TTTACAACCAAATTACCAGTTTGGTATGTTAATTCATAC GGATCCCCGGGTTAATTAA	F	WACH (For3 5')
osm3571	TTTCAGACAAATCGTCAATGTATGTAATGTACAGATAT ACTGTTCTAAAAATCCATCCTAGAAAGAACAATGGAGC AAGAATTCGAGCTCGTTTAAAC	R	WACH (For3 3')
osm3773	ACTCCCGGGGCTCCTAACACTTCTACTAAATC	F	CLONING
osm3932	TTATCACTTGAAAATAATCATATATACGAAGAGCTTCG ACTTTCAGAGTTGATAAACTTATTGGCTAAAGCTACATT ACGGATCCCCGGGTTAATTAA	F	WACH (Myo51 ORF)
osm4021	CTTGGATCCTATGAACCTCAAAAGAATGCGTTG	R	CLONING
osm4503	TGCGGCATTGTCTTCACCATCCGTATTCGTTTCTTACCA TTCACCATTGTCCGCACCACATTATAGAAATTTCGAAA GCGGATCCCCGGGTTAATTAA	F	WACH (Acp1 5')
osm4504	CATTAAGGCCTCACTTTTATTCTGAGATCGCTATCCGGT TGTATTCTTTTGTTTAAAGCATTATATCATCAACTCACC CGGATCCCCGGGTTAATTAA	F	WACH (Acp2 5')
osm4505	CAATCTTTCTATGACTATTTTCGTTGAAGATGGAACGAA TACTATGAGAAGATCACGGAAAGAAAACAAAAAGCAA TCGAATTCGAGCTCGTTTAAAC	R	WACH (Acp2 3')
osm4577	GGAATAAGGGCGACACGG	F	ANALYTICAL
osm4641	ACTCGTTCCATTCAACCCGTTTCCGATGCCCAACCAAAT GATTCGGCTTTGCGTTCAGTTTTAAACGATCTTTCCATT CGGATCCCCGGGTTAATTAA	F	WACH (Acp2 ORF)
osm4819	TGGGTACCAAGCTTGGTTAGTTACAAAAATA	F	CLONING
osm4920	GAATATAGTATTAATGAGTACTAATATAAATTAAAAAT ATTGATCGGGTGTAACGTTTAATGATACTTGATAAAAA GCGAATTCGAGCTCGTTTAAAC	R	WACH (Myo51 3')
osm5328	GCTCAAGTCGAAAATGGAATTCAACAGTCCTTCAACGT TGAACTTTCTTCACTTAATGACAAAAAGTTTAAAGAATT GCGGATCCCCGGGTTAATTAA	F	WACH (Acp1 ORF*)
osm5329	GAGGAAATGGAAACTCGGATGCGCAACTTCCTCCAGGA TGTCTACTTTGGAAAAACTAAAGATATCATCAACCAGA CTCGGATCCCCGGGTTAATTAA	F	WACH (Acp2 ORF*)
osm5330	GCGGCCGCCATATGTTGTTCACTT	F	CLONING
osm5331	GCGGCCGCTTATTTCATGACCTT	R	CLONING
osm5432	GCATTAGATTTACTCGCACGATTAAACCC	F	SDM
osm5433	GGGTTTAATCGTGCGAGTAAATCTAATGC	R	SDM
osm5434	CCATGGAGCAATAAAGCTGATCCTCCTTTGG	F	SDM
osm5435	CCAAAGGAGGATCAGCTTTATTGCTCCATGG	R	SDM

NAME	SEQUENCE	ORIENTATION	PURPOSE
osm5449	AAAGTCGACTGTTGCTTTGAATCATATTAC	F	CLONING
osm5452	GATCCGCGGCCGATGTATTTACTGATTACTT	R	CLONING
osm5453	CTTCTAAACGGCTAGCTCAGCTTCATTGG	F	SDM
osm5454	CAATGAAGCTGAGCTAGCCGTTTAGAAGG	R	SDM
osm5455	CAAATGGTTAGTGCTCGTTTGCATAG	F	SDM
osm5456	CTATGCAAACGAGCACTAACCATTTGC	R	SDM
osm5457	GTCCTTCATATTCGTCCTTTTATGAATGATGC	F	SDM
osm5458	CATCATTCATAAAAGGACGAATATGAAGGACC	R	SDM
osm5459	GCTTCCATGATTGCTAATGACAAAACAG	F	SDM
osm5460	CCTGTTTTGTCATTAGCAATCATGGAAG	R	SDM
osm6064	CATATGGTCTGGGTATCT	R	CLONING
osm6183	GCCTTCCAACCAGCTTCTCT	R	ANALYTICAL
osm6396	ATGTACCAGGCGAAGCGCTTC	F	ANALYTICAL
osm6576	CTTGGATCCATCATTATTTGAATTACCAT	R	CLONING
osm6577	GAAGGATCCTCAAAACACAAGGTTTTTA	F	CLONING
osm6582	CTTGTTTAAACCAACATGCCTGTAAG	R	CLONING
osm6583	GAAGTTTAAACTGCTTTTGTGGTTATC	F	CLONING
osm7119	CTTCGTACGCTGCAGGTCGACACAGTATGTACGCCAC	F	INFUSION
osm7120	CTTCTTTGATTCTCATAGACTCTGAACCTGAACAG	R	INFUSION
osm7121	TTCAGGTTCAGAGTCTATGAGAATCAAAGAAGTTAT	F	INFUSION
osm7122	TTCACCCTTGGAGTTAATTAATCTCTTAAGTTCATTGTTAT	R	INFUSION
osm7123	TTCTAAAATAGAAAATTCCGACACCGTAGAAGAGC	R	INFUSION
osm7124	CTTCTACGGTGTCGGAATTTTCTATTTTAGAAAAC	F	INFUSION
osm7125	TGCTTTTAACAGATGCGGATGTCTTTTGGCGACCAC	R	INFUSION
osm7126	TCGCCAAAAGACATCCGCATCTGTTAAAAGCAATAA	F	INFUSION
osm7127	ATGTACCAGGCGAAGCGCTTCTATGTCCGGATGAC	F	INFUSION
osm7128	TAATTTTACTATTGTTATTTTCTATTTTAGAAAAC	R	INFUSION
osm7129	TTCTAAAATAGAAAATAACAATAGTAAAATTACGAA	F	INFUSION
osm7130	TGCTTTTAACAGATGCGTTGACAAGATTCAAACGTC	R	INFUSION
osm7131	TTTGAATCTTGTCAACGCATCTGTTAAAAGCAATAA	F	INFUSION
osm7132	TAGCAACGATGTTCACATTTTCTATTTTAGAAAAC	R	INFUSION
osm7133	TTCTAAAATAGAAAATGTGAACATCGTTGCTAATG	F	INFUSION
osm7140	CTTCTTTGATTCTCATATCAGCTTGTAAAGTAAGC	R	INFUSION
osm7141	TACTTTACAAGCTGATATGAGAATCAAAGAAGTTAT	F	INFUSION
osm7204	CTTTGTTAAATCAGCGGCCGCATGTTTACCGATTCATATGTA	F	INFUSION
osm7205	CTTGGAGTTAATTAACCCGGGGATCCTCATATTTTC	R	INFUSION
osm7254	GCTTTGTTAAATCAGCGGCCGCATGATGAC	F	INFUSION

NAME	SEQUENCE	ORIENTATION	PURPOSE
osm7255	CTTGGAGTTAATTAACCCGGGGATCCTATCATTATTTGAATTACCA	R	INFUSION
osm7256	CTTTGTTAAATCAGCGGCCGCATGAAGCACACTCCAAATTCT	F	INFUSION
osm7257	CTTGGAGTTAATTAACCCGGGGATCCTAAAAACCTTGTGTTTTGA	R	INFUSION
osm7487	CTTCTTTGATTCTCATATCATTATTTGAATTACCAT	R	INFUSION
osm7488	TAATTCAAATAATGATATGAGAATCAAAGAAGTTAT	F	INFUSION
osm7491	TAATTTTACTATTGTTTGATATATTATTTGAAACAG	R	INFUSION
osm7492	TTCAAATAATATATCAAACAATAGTAAAATTACGAA	F	INFUSION
osm7493	GATTGCATAGCTCACCTGATATATTATTTGAAACAG	R	INFUSION
osm7494	TTCAAATAATATATCAGGTGAGCTATGCAATCCTTC	F	INFUSION
osm7495	TATGCAAATCATCTTTAGGAATTTTGCTTGCATACA	R	INFUSION
osm7496	TGCAAGCAAAATTCCTAAAGATGATTTGCATAAGAC	F	INFUSION
osm7497	GATTGCATAGCTCACCTGATATATTATTTGAAACAG	R	INFUSION
osm7498	TTCAAATAATATATCAGGTGAGCTATGCAATCCTTC	F	INFUSION
osm7499	GCTTTGTTAAATCAGCGGCCGCATGCTCAAGTACGTGGAATCTTT	F	INFUSION
osm7500	CTTTGTTAAATCAGCGGCCGCATGTTTCTTTGTTACTCAGAAAA	F	INFUSION
osm7638	CTTTGTTAAATCAGCGGCCGCATGGTTACACTCTCTCAAGAAAA	F	INFUSION
osm7653	GTTGCGGCCGCTGTGTAGAGAAGAGTAAATATAAA	R	CLONING
osm7654	GTTGCGGCCGCTTTGAAAACGATGCAATAGTT	R	CLONING
osm7677	GGAGTATTAAAACAACTCGAGAAATGCGTGAAACTC	F	INFUSION
osm7678	CCTCTGAATCCGCAACTGATATATTATTTGAAACAG	R	INFUSION
osm7679	TTCAAATAATATATCAGTTGCGGATTCAGAGGAGAA	F	INFUSION
osm7680	TGCTTTTAACAGATGCCTCTTTGTGGGATTCCATCA	R	INFUSION
osm7681	GGAATCCCACAAAGAGGCATCTGTTAAAAGCAATAATG	F	INFUSION
osm7682	CCTCTGAATCCGCAACAGGAATTTTGCTTGCATACAC	R	INFUSION
osm7683	TGCAAGCAAAATTCCTGTTGCGGATTCAGAGGAG	F	INFUSION
osm7684	GGGAGTAATACAGCTTTGATATATTATTTGAAACAGC	R	INFUSION
osm7685	TTCAAATAATATATCAAAGCTGTATTACTCCCCTTC	F	INFUSION
osm7686	TGCTTTTAACAGATGCTTCTAAAGCCTTTAATCGTACA	R	INFUSION
osm7687	ATTAAAGGCTTTAGAAGCATCTGTTAAAAGCAATAATG	F	INFUSION
osm7688	GGGAGTAATACAGCTTAGGAATTTTGCTTGCATACAC	R	INFUSION
osm7689	TGCAAGCAAAATTCCTAAGCTGTATTACTCCCCTTC	F	INFUSION
osm7690	AAATCAAGGATATGAGAATTCCGAAAGAAAGTATGT	F	INFUSION
osm7691	AATCGGTACGTGCACAAACTTTTTTATTGGAAACTGTT	R	INFUSION
osm7692	TTGTGCACGTACCGATTTTATGCCAGTTGATTTACAG	F	INFUSION

NAME	SEQUENCE	ORIENTATION	PURPOSE
osm7693	TTTCAATTGGTGTCTTGGAATTGAATCTATGCAAACG	R	INFUSION
osm7694	TAGATTCAATTCCAAGACACCAATTGAAATTGCCAAA	F	INFUSION
osm7695	TGAGTTCACTAGATCTCCCCCATTGTTTCGAGATGACAT ATAAGGC	R	INFUSION
osm7696	AATGGGGGAGATCTAGTGAACTCAAGTGAAAAGCTTTT AGAATTGTC	F	INFUSION
osm7697	GTCTTCTAAAATCCTCAAAGTTGTTGGCCAGAAACG	R	INFUSION
osm7698	GGCCAACAACTTTGAGGATTTTAGAAGACAAATAAGGA AAC	F	INFUSION
osm7699	GAAGAGCTGTAGGATCCGAAAAAATGCCTTCATTGC	R	INFUSION
osm7700	TTTTTCGGATCCTACAGCTCTTCATCCTGATGACCA	F	INFUSION
osm7740	GCTTATTTAGAAGTGGCGCGCCTCTCTTAAGTTCATTGT TATTC	R	INFUSION
osm7830	GACGAACAAGGTTCCTATAATTGGTTTCGATTATGTTTT T	R	INFUSION
osm7831	TCGAAACCAATTATAGGAACCTTGTTCGTCAAACAAAA C	F	INFUSION
osm7878	TTTTGTCCATCTTCATCGTCATCATTAACAAGCAATAG	R	INFUSION
osm7879	CTTGTTAATGATGACGATGAAGATGGACAAAAAGACTA T	F	INFUSION
osm7880	AACTAGCCGTCATCATTGCTGCTCCGATCATGATCT	R	INFUSION
osm7881	CATGATCGGAGCAGCAATGATGACGGCTAGTTTTAAAG	F	INFUSION
osm7882	GAGTTTCACGCATTTCTCGAGTTGTTTTAATACTCCTTC	R	INFUSION

6.1.3 Plasmid table

NAME	DESCRIPTION	OBTAINED FROM	USAGE
pAV133	pUra4^{AfeI}	(Vještica et al., 2020)	Single integration at ura4
pAV530	pUra4^{AfeI}-p^{pak2}-mCherry-SynZip3-term^{ScADH}	Lab Stock, Derived from pAV133	Single integration at ura4
pSM200	pREP41-HA	(Craven et al., 1998)	Pombe expression
pSM206	pFA6a-GFP-kanMX	(Bähler et al., 1998)	pombe WACH
pSM237	pRIP82	Lab Stock, Derived from pSM200	Multiple integration at ura4
pSM617	pREP3x	Lab Stock, Derived from pSM200	Pombe expression
pSM619	pREP41	Lab Stock, Derived from pSM200	Pombe expression
pSM676	pFA6a-3GFP-kanMX	Lab Stock, Derived from pSM206	pombe WACH
pSM677	pFA6a-mCherry-kanMX	Lab Stock, Derived from pSM206	pombe WACH

NAME	DESCRIPTION	OBTAINED FROM	USAGE
pSM684	pFA6a-mCherry-natMX	Lab Stock, Derived from pSM206	pombe WACH
pSM685	pFA6a-tdTomato-natMX	Lab Stock, Derived from pSM206	pombe WACH
pSM693	pFA6a-hphMX	Lab Stock, Derived from pSM206	pombe WACH
pSM694	pFA6a-bleMX	Lab Stock, Derived from pSM206	pombe WACH
pSM893	pREP41-GFP-ypt3	Lab Stock, Derived from pSM200	Pombe expression
pSM1538	pFA6a-sfGFP-kanMX	Lab Stock, Derived from pSM206	pombe WACH
pSM1542	pRIP82-p^{ste11}-dVenus	Lab Stock, Derived from pSM237	Multiple integration at ura4
pSM1768	pFA6a-GBP-mCherry-bleMX	Lab Stock, Derived from pSM206	pombe WACH
pSM1638	pRIP-p^{fus1}-sfGFP	Lab Stock, Derived from pSM237	Multiple integration at ura4
pSM1650	pRIP-p^{fus1}-fus1N-sfGFP	Regular cloning : $pSM1638^{NotI/BamHI}$ + $(WT^{osm3005\text{-}osm3026})^{NotI/BamHI}$	Multiple integration at ura4
pSM1656	pRIP-p^{fus1}-fus1-sfGFP	Regular cloning : $pSM1638^{NotI/XmaI}$ + $(WT^{osm3005\text{-}osm3006})^{NotI/XmaI}$	Multiple integration at ura4
pSM1657	pRIP-p^{fus1}-for3-sfGFP	Regular cloning : $pSM1568^{NotI/XmaI}$ + $(WT^{osm3007\text{-}osm3008})^{NotI/XmaI}$	Multiple integration at ura4
pSM1658	pRIP-p^{fus1}-cdc12-sfGFP	Regular cloning : $pSM1638^{NotI/XmaI}$ + $(WT^{osm3009\text{-}osm3010})^{NotI/XmaI}$	Multiple integration at ura4
pSM1659	pRIP-p^{fus1}-fus1N-fus1C-sfGFP	3-point ligation cloning : $pSM1638^{NotI/XmaI}$ + $(WT^{osm3005\text{-}osm3026})^{NotI/BamHI}$ +$(WT^{osm3027\text{-}osm3006})^{BamHI/XmaI}$	Multiple integration at ura4
pSM1660	pRIP-p^{fus1}-fus1N-for3C-sfGFP	3-point ligation cloning : $pSM1638^{NotI/XmaI}$ + $(WT^{osm3005\text{-}osm3026})^{NotI/BamHI}$ +$(WT^{osm3029\text{-}osm3008})^{BamHI/XmaI}$	Multiple integration at ura4
pSM1661	pRIP-p^{fus1}-fus1N-cdc12C-sfGFP	3-point ligation cloning : $pSM1638^{NotI/XmaI}$ + $(WT^{osm3005\text{-}osm3026})^{NotI/BamHI}$ +$(WT^{osm3031\text{-}osm3010})^{BamHI/XmaI}$	Multiple integration at ura4
pSM1662	pRIP-p^{fus1}-for3N-fus1C-sfGFP	3-point ligation cloning : $pSM1638^{NotI/XmaI}$ + $(WT^{osm3007\text{-}osm3028})^{NotI/BamHI}$ +$(WT^{osm3027\text{-}osm3006})^{BamHI/XmaI}$	Multiple integration at ura4

NAME	DESCRIPTION	OBTAINED FROM	USAGE
pSM1663	pRIP-p^{fus1}-cdc12N-fus1C-sfGFP	3-point ligation cloning : $pSM1638^{NotI/XmaI}$ + $(WT^{osm3009\text{-}osm3030})^{NotI/BamHI}$ +$(WT^{osm3027\text{-}osm3006})^{BamHI/XmaI}$	Multiple integration at ura4
pSM1823	pRIP-p^{nmt41}-sfGFP	Lab Stock, Derived from pSM619	Multiple integration at ura4
pSM1825	pRIP-p^{fus1}-fus1N-cdc12CΔolig-sfGFP	3-point ligation cloning : $pSM1638^{NotI/XmaI}$ + $(WT^{osm3005\text{-}osm3026})^{NotI/BamHI}$ +$(WT^{osm3031\text{-}osm3521})^{BamHI/XmaI}$	Multiple integration at ura4
pSM1826	pRIP-p^{nmt41}-fus1N-sfGFP	Subcloning : $pSM1650^{KpnI/NotI}$ + $pSM1823^{KpnI/NotI}$	Multiple integration at ura4
pSM1884	pRIP-p^{fus1}-fus1N-for3C-cdc12olig-sfGFP	Regular cloning : $pSM1660^{XmaI}$ + $(WT^{osm3773\text{-}osm3010})^{XmaI}$	Multiple integration at ura4
pSM2081	pFA6a-bsdMX	Lab Stock, Derived from pSM206	pombe WACH
pSM2194	pFA6a-$fus1^{5'UTR}$-acp2-sfGFP-kanMX-$fus1^{3'UTR}$	Regular cloning : $pSM1538^{NotI}$ + $(YSM3355^{osm5330\text{-}osm5331})^{NotI}$	Endogenous integration
pSM2203	pFA6a-$acp2^{5'UTR}$-$acp2^{R12A,Y77A}$-sfGFP-kanMX-$acp2^{3'UTR}$	SDM : $(pSM2194^{osm5432/5433})^{osm5434/5435}$	Endogenous integration
pSM2229	$pUra4^{AfeI}$-p^{nmt41}-fus1-sfGFP	Lab Stock, Derived from pAV133	Single integration at ura4
pSM2250	$pUra4^{AfeI}$-p^{nmt41}-GFP-ypt3	Subcloning : $pAV133^{PstI/XmaI}$+ $pSM893^{PstI/XmaI}$	Single integration at ura4
pSM2251	pFA6a-$fus1^{5'UTR}$-fus1_K879A-sfGFP-kanMX-$fus1^{3'UTR}$	SDM : $pSM2827^{osm5453/54354}$	Endogenous integration
pSM2252	pFA6a-$fus1^{5'UTR}$-fus1_I951A-sfGFP-kanMX-$fus1^{3'UTR}$	SDM : $pSM2827^{osm5455/54356}$	Endogenous integration
pSM2253	pFA6a-$fus1^{5'UTR}$-fus1_GN1087,1088RP-sfGFP-kanMX-$fus1^{3'UTR}$	SDM : $pSM2827^{osm5457/54358}$	Endogenous integration
pSM2254	pFA6a-$fus1^{5'UTR}$-fus1_K1112A-sfGFP-kanMX-$fus1^{3'UTR}$	SDM : $pSM2827^{osm5459/54360}$	Endogenous integration
pSM2390	pRIP-p^{fus1}-CRY2olig-For3N-fus1C-sfGFP	Lab Stock, Derived from pAV133	Multiple integration at ura4
pSM2475	$pUra4^{AfeI}$-p^{fus1}-CRY2PHR-fus1C-sfGFP	Lab Stock, Derived from pSM1662	Single integration at ura4
pSM2478	$pUra4^{PmeI}$-p^{nmt41}-fus1-sfGFP	3-point ligation cloning : $pSM2229^{AatII/StuI}$ + $(pSM2229^{osm4577\text{-}osm6582})^{AatII/PmeI}$ +$(pSM2229^{osm6583\text{-}osm6183})^{PmeI/StuI}$	Single integration at ura4

NAME	DESCRIPTION	OBTAINED FROM	USAGE
pSM2507	pFA6a-fus1$^{5'UTR}$ - fus1$^{\Delta 501-749}$-sfGFP-kanMX-fus1$^{3'UTR}$	3-point ligation cloning : pSM2251$^{SalI/PacI}$ + (pSM2251$^{osm1772-osm6576}$)$^{SalI/BamHI}$ +(pSM2229$^{osm3031-osm3521}$)$^{BamHI/PacI}$	Endogenous integration
pSM2594	pUra4^{AfeI}-p^{fus1}-fus1N-fus1C-sfGFP	Subcloning : pSM2478$^{KpnI/SacI}$+ pSM1659$^{KpnI/SacI}$	Single integration at ura4
pSM2595	pUra4^{AfeI}-p^{fus1}-fus1N-cdc12C-sfGFP	Subcloning : pSM2478$^{KpnI/SacI}$+ pSM1661$^{KpnI/SacI}$	Single integration at ura4
pSM2596	pUra4^{AfeI}-p^{fus1}-fus1N-cdc12CΔolig-sfGFP	Subcloning : pSM2478$^{KpnI/SacI}$+ pSM1825$^{KpnI/SacI}$	Single integration at ura4
pSM2600	pUra4^{PmeI}-p^{nmt1}-fus1N-sfGFP	3-point ligation cloning : pSM2478$^{KpnI/SacI}$+ (pSM617$^{osm3091-osm3516}$)$^{KpnI/NotI}$ +pSM1826$^{NotI/SacI}$	Single integration at ura4
pSM2601	pUra4^{PmeI}-p^{nmt1}-fus1N$^{1-730}$-sfGFP	3-point ligation cloning: pSM2600$^{NotI/MscI}$+ (pSM2600$^{osm3005-osm4021}$)$^{NotI/BamHI}$ + (pSM2600$^{osm2217-osm6064}$)$^{BamHI/MscI}$	Single integration at ura4
pSM2602	pUra4^{PmeI}-p^{nmt1}-fus1-sfGFP	Subcloning : pSM2600$^{NotI/XmaI}$ + pSM1656$^{NotI/XmaI}$	Single integration at ura4
pSM2604	pUra4^{AfeI}-p^{fus1}-fus1N-for3C-sfGFP	Subcloning : pSM2595$^{ClaI/MscI}$+ pSM1660$^{ClaI/MscI}$	Single integration at ura4
pSM2605	pUra4^{AfeI}-p^{fus1}-fus1N-for3C-cdc12olig-sfGFP	Subcloning : pSM2595$^{ClaI/MscI}$+ pSM1884$^{ClaI/MscI}$	Single integration at ura4
pSM2621	pFA6a-fus1$^{5'UTR}$-fus1$^{1-868}$-fus1$^{792-1377}$-sfGFP-kanMX-fus1$^{3'UTR}$	Infusion cloning : pSM2507$^{SalI/PacI}$ + WT$^{osm7119-osm7120}$ + WT$^{osm7121-osm7122}$	Endogenous integration
pSM2622	pFA6a-fus1$^{5'UTR}$-fus1$^{1-791}$-cdc12$^{882-1390}$-fus1$^{1278-1372}$-sfGFP-kanMX-fus1$^{3'UTR}$	Infusion cloning : pSM2507$^{AfeI/PacI}$+WT$^{osm7127-osm7128}$+ WT$^{osm7129-osm7130}$+WT$^{osm7131-osm7122}$	Endogenous integration
pSM2625	pFA6a-fus1$^{5'UTR}$-fus1$^{\Delta 492-791}$-sfGFP-kanMX-fus1$^{3'UTR}$	Infusion cloning : pSM2507$^{SalI/PacI}$+WT$^{osm7119-osm7140}$ +WT$^{osm7141-osm7122}$	Endogenous integration
pSM2630	pUra4^{PmeI}-p^{nmt1}-fus1N$^{93-792}$-sfGFP	Infusion cloning : pSM2600$^{NotI/XmaI}$ + pSM2600$^{osm7204-osm7205}$	Single integration at ura4
pSM2631	pFA6a-fus1$^{5'UTR}$-fus1$^{1-791}$-for3$^{718-1265}$-fus1$^{1278-1372}$-sfGFP-kanMX-fus1$^{3'UTR}$	Infusion cloning : pSM2507$^{SalI/PacI}$+WT$^{osm6396-osm7123}$+ WT$^{osm7124-osm7125}$+WT$^{osm7126-osm7122}$	Endogenous integration

NAME	DESCRIPTION	OBTAINED FROM	USAGE
pSM2632	pFA6a-fus1$^{5'UTR}$-fus1$^{1-791}$-cdc12$^{928-1390}$-fus1$^{1278-1372}$-sfGFP-kanMX-fus1$^{3'UTR}$	Infusion cloning : pSM2507$^{AfeI/PacI}$+WT$^{osm7127-osm7132}$+ WT$^{osm7133-osm7130}$+WT$^{osm7131-osm7122}$	Endogenous integration
pSM2644	pUra4^{PmeI}-p^{nmt1}-fus1N$^{1-500}$-sfGFP	Infusion cloning : pSM2600$^{NotI/XmaI}$ + pSM2600$^{osm7254-osm7255}$	Single integration at ura4
pSM2645	pUra4^{PmeI}-p^{nmt1}-fus1N$^{431-755}$-sfGFP	Infusion cloning : pSM2600$^{NotI/XmaI}$+ pSM2600$^{osm7256-osm7257}$	Single integration at ura4
pSM2691	pFA6a-fus1$^{5'UTR}$-fus1N-fus1C-sfGFP-kanMX-fus1$^{3'UTR}$	Subcloning : pSM2251$^{XhoI/XmaI}$+ pSM2594$^{XhoI/XmaI}$	Endogenous integration
pSM2692	pFA6a-fus1$^{5'UTR}$-fus1N-cdc12C-sfGFP-kanMX-fus1$^{3'UTR}$	Subcloning : pSM2251$^{XhoI/XmaI}$+ pSM2595$^{XhoI/XmaI}$	Endogenous integration
pSM2693	pFA6a-fus1$^{5'UTR}$-fus1N-for3C-sfGFP-kanMX-fus1$^{3'UTR}$	Subcloning : pSM2251$^{XhoI/XmaI}$+ pSM2604$^{XhoI/XmaI}$	Endogenous integration
pSM2694	pFA6a-fus1$^{5'UTR}$-fus1N-cdc12CΔolig-sfGFP-kanMX-fus1$^{3'UTR}$	Subcloning : pSM2251$^{XhoI/XmaI}$+ pSM2596$^{XhoI/XmaI}$	Endogenous integration
pSM2695	pFA6a-fus1$^{5'UTR}$-fus1N-for3C-cdc12olig-sfGFP-kanMX-fus1$^{3'UTR}$	Subcloning : pSM2692$^{XhoI/MscI}$+ pSM2605$^{XhoI/MscI}$	Endogenous integration
pSM2697	pFA6a-fus1$^{5'UTR}$-fus1$^{\Delta 501-791}$-sfGFP-kanMX-fus1$^{3'UTR}$	Infusion cloning : pSM2507$^{SalI/PacI}$+WT$^{osm7119-osm7487}$ +WT$^{osm7488-osm7122}$	Endogenous integration
pSM2699	pFA6a-fus1$^{5'UTR}$-fus1$^{1-791}$-cdc12$^{882-972}$-cdc12$^{882-1390}$-fus1$^{1278-1372}$-sfGFP-kanMX-fus1$^{3'UTR}$	Infusion cloning : pSM2507$^{AfeI/PacI}$ + WT$^{osm7127-osm7128}$ + WT$^{osm7129-osm7491}$ + WT$^{osm7492-osm7130}$ + WT$^{osm7131-osm7122}$	Endogenous integration
pSM2700	pFA6a-fus1$^{5'UTR}$-fus1$^{1-791}$-cdc12$^{882-972}$-cdc12$^{882-972}$-fus1$^{869-1372}$-sfGFP-kanMX-fus1$^{3'UTR}$	Infusion cloning : pSM2507$^{AfeI/PacI}$ + WT$^{osm7127-osm7128}$+ WT$^{osm7129-osm7491}$ + WT$^{osm7492-osm7493}$ + WT$^{osm7494-osm7122}$	Endogenous integration
pSM2701	pFA6a-fus1$^{5'UTR}$-fus1$^{1-868}$-cdc12$^{973-1390}$-fus1$^{1278-1372}$-sfGFP-kanMX-fus1$^{3'UTR}$	Infusion cloning : pSM2507$^{AfeI/PacI}$+WT$^{osm7127-osm7495}$+ WT$^{osm7496-osm7130}$+WT$^{osm7131-osm7122}$	Endogenous integration
pSM2702	pFA6a-fus1$^{5'UTR}$-fus1$^{1-791}$-cdc12$^{928-972}$-fus1$^{869-1372}$-sfGFP-kanMX-fus1$^{3'UTR}$	Infusion cloning : pSM2507$^{AfeI/PacI}$+WT$^{osm7127-osm7132}$+ WT$^{osm7133-osm7497}$+WT$^{osm7498-osm7122}$	Endogenous integration
pSM2703	pUra4^{PmeI}-p^{nmt1}-fus1N$^{191-792}$-sfGFP	Infusion cloning : pSM2600$^{NotI/XmaI}$+ pSM2600$^{osm7499-osm7205}$	Single integration at ura4
pSM2704	pUra4^{PmeI}-p^{nmt1}-fus1N$^{293-792}$-sfGFP	Infusion cloning : pSM2600$^{NotI/XmaI}$+ pSM2600$^{osm7500-osm7205}$	Single integration at ura4

NAME	DESCRIPTION	OBTAINED FROM	USAGE
pSM2825	pUra4^{PmeI}-p^{nmt1}-fus1N$^{140-792}$-sfGFP	Infusion cloning : pSM2600$^{NotI/XmaI}$+ pSM2600$^{osm7638-osm7205}$	Single integration at ura4
pSM2828	pUra4^{PmeI}-p^{ste11}-fus1-sfGFP	Regular cloning : pSM2602$^{KpnI/NotI}$ + (pSM1542$^{osm2646-osm7653}$)$^{KpnI/NotI}$	Single integration at ura4
pSM2829	pUra4^{PmeI}-p^{pak2}-fus1-sfGFP	Regular cloning : pSM2602$^{KpnI/NotI}$ + (pAV530$^{osm4819-osm7654}$)$^{KpnI/NotI}$	Single integration at ura4
pSM2844	pFA6a-fus1$^{5'UTR}$-fus1$^{1-791}$-cdc12$^{882-972}$-cdc12$^{882-972}$-fus1$^{869-1372}$(KEYTG935-939CARTD-sfGFP-kanMX-fus1$^{3'UTR}$	Infusion cloning : pSM2700$^{EcoRI/PacI}$ + pSM2700$^{osm7690-osm7691}$ + pSM2700$^{osm7692-osm7122}$	Endogenous integration
pSM2845	pFA6a-fus1$^{5'UTR}$-fus1$^{1-791}$-cdc12$^{882-972}$-cdc12$^{882-972}$-fus1$^{869-1372}$(L959K-sfGFP-kanMX-fus1$^{3'UTR}$	Infusion cloning : pSM2700$^{EcoRI/PacI}$ + pSM2700$^{osm7690-osm7693}$ + pSM2700$^{osm7694-osm7122}$	Endogenous integration
pSM2846	pFA6a-fus1$^{5'UTR}$-fus1$^{1-791}$-cdc12$^{882-972}$-cdc12$^{882-972}$-fus1$^{869-1372}$(EEVMEV1006-1011NGGDLVNS-sfGFP-kanMX-fus1$^{3'UTR}$	Infusion cloning : pSM2700$^{EcoRI/PacI}$ + pSM2700$^{osm7690-osm7695}$ + pSM2700$^{osm7696-osm7122}$	Endogenous integration
pSM2847	pFA6a-fus1$^{5'UTR}$-fus1$^{1-791}$-cdc12$^{882-972}$-cdc12$^{882-972}$-fus1$^{869-1372}$(R1054E-sfGFP-kanMX-fus1$^{3'UTR}$	Infusion cloning : pSM2700$^{EcoRI/PacI}$+ pSM2700$^{osm7690-osm7697}$+ pSM2700$^{osm7698-osm7122}$	Endogenous integration
pSM2848	pFA6a-fus1$^{5'UTR}$-fus1$^{1-791}$-cdc12$^{882-972}$-cdc12$^{882-972}$-fus1$^{869-1372}$(NHK1182-1184DPT-sfGFP-kanMX-fus1$^{3'UTR}$	Infusion cloning : pSM2700$^{EcoRI/PacI}$+ pSM2700$^{osm7690-osm7699}$+ pSM2700$^{osm7700-osm7122}$	Endogenous integration
pSM2849	pFA6a-fus1$^{5'UTR}$-fus1KEYTG935-939CARTD-sfGFP-kanMX-fus1$^{3'UTR}$	Infusion cloning : pSM2700$^{EcoRI/PacI}$+ pSM2827$^{osm7690-osm7691}$+ pSM2700$^{osm7692-osm7122}$	Endogenous integration
pSM2850	pFA6a-fus1$^{5'UTR}$-fus1L959K-sfGFP-kanMX-fus1$^{3'UTR}$	Infusion cloning : pSM2700$^{EcoRI/PacI}$+ pSM2827$^{osm7690-osm7693}$+ pSM2700$^{osm7694-osm7122}$	Endogenous integration

NAME	DESCRIPTION	OBTAINED FROM	USAGE
pSM2851	pFA6a-fus1$^{5'UTR}$-fus1EEVMEV1006-1011NGGDLVNS-sfGFP-kanMX-fus1$^{3'UTR}$	Infusion cloning : pSM2700$^{EcoRI/PacI}$+ pSM2827$^{osm7690\text{-}osm7695}$+ pSM2700$^{osm7696\text{-}osm7122}$	Endogenous integration
pSM2852	pFA6a-fus1$^{5'UTR}$-fus1R1054E-sfGFP-kanMX-fus1$^{3'UTR}$	Infusion cloning : pSM2700$^{EcoRI/PacI}$+ pSM2827$^{osm7690\text{-}osm7697}$+ pSM2700$^{osm7698\text{-}osm7122}$	Endogenous integration
pSM2853	pFA6a-fus1$^{5'UTR}$-fus1NHK1182-1184DPT-sfGFP-kanMX-fus1$^{3'UTR}$	Infusion cloning : pSM2700$^{EcoRI/PacI}$+ pSM2827$^{osm7690\text{-}osm7699}$+ pSM2700$^{osm7700\text{-}osm7122}$	Endogenous integration
pSM2854	pFA6a-fus1$^{5'UTR}$-fus1$^{1\text{-}791}$-cdc12$^{882\text{-}972}$-cdc12$^{882\text{-}972}$-Sjfus1$^{908\text{-}1317}$-fus1$^{1278\text{-}1372}$-sfGFP-kanMX-fus1$^{3'UTR}$	Infusion cloning : pSM2700$^{XhoI/PacI}$+ pSM2700$^{osm7677\text{-}osm7678}$+ SjWT$^{osm7679\text{-}osm7680}$+ pSM2700$^{osm7681\text{-}osm7122}$	Endogenous integration
pSM2855	pFA6a-fus1$^{5'UTR}$-fus1$^{1\text{-}868}$-Sjfus1$^{908\text{-}1317}$-fus1$^{1278\text{-}1372}$-sfGFP-kanMX-fus1$^{3'UTR}$	Infusion cloning : pSM2700$^{XhoI/PacI}$+ pSM2701$^{osm7677\text{-}osm7682}$+ SjWT$^{osm7683\text{-}osm7680}$+ pSM2700$^{osm7681\text{-}osm7122}$	Endogenous integration
pSM2856	pFA6a-fus1$^{5'UTR}$-fus1$^{1\text{-}791}$-cdc12$^{882\text{-}972}$-cdc12$^{882\text{-}972}$-Sofus$^{857\text{-}1265}$-fus1$^{1278\text{-}1372}$-sfGFP-kanMX-fus1$^{3'UTR}$	Infusion cloning : pSM2700$^{XhoI/PacI}$+ pSM2700$^{osm7677\text{-}osm7684}$+ SjWT$^{osm7685\text{-}osm7686}$+ pSM2700$^{osm7687\text{-}osm7122}$	Endogenous integration
pSM2857	pFA6a-fus1$^{5'UTR}$-fus1$^{1\text{-}868}$-Sofus1$^{857\text{-}1265}$-fus1$^{1278\text{-}1372}$-sfGFP-kanMX-fus1$^{3'UTR}$	Infusion cloning : pSM2700$^{XhoI/PacI}$+ pSM2701$^{osm7677\text{-}osm7688}$+ SjWT$^{osm7689\text{-}osm7686}$+ pSM2700$^{osm7687\text{-}osm7122}$	Endogenous integration
pSM2913	pFA6a-fus1$^{5'UTR}$-fus1-kanMX-fus1$^{3'UTR}$	Infusion cloning : pSM2827$^{EcoRI/AscI}$+ pSM2827$^{osm7690\text{-}osm7740}$	Endogenous integration
pSM2914	pFA6a-fus1$^{5'UTR}$-fus1$^{1\text{-}791}$-cdc12$^{882\text{-}972}$-cdc12$^{882\text{-}972}$-fus1$^{869\text{-}1372}$-kanMX-fus1$^{3'UTR}$	Infusion cloning : pSM2827$^{EcoRI/AscI}$+ pSM2700$^{osm7690\text{-}osm7740}$	Endogenous integration
pSM2915	pFA6a-fus1$^{5'UTR}$-fus1$^{1\text{-}868}$-cdc12$^{973\text{-}1390}$-fus1$^{1278\text{-}1372}$-kanMX-fus1$^{3'UTR}$	Infusion cloning : pSM2827$^{EcoRI/AscI}$+ pSM2701$^{osm7690\text{-}osm7740}$	Endogenous integration

NAME	DESCRIPTION	OBTAINED FROM	USAGE
pSM2916	pFA6a-fus1$^{5'UTR}$-fus1$^{1-791}$-cdc12$^{928-1390}$-fus1$^{1278-1372}$-kanMX-fus1$^{3'UTR}$	Infusion cloning : pSM2827$^{EcoRI/AscI}$+ pSM2632$^{osm7690-osm7740}$	Endogenous integration
pSM2917	pFA6a-fus1$^{5'UTR}$-fus1$^{1-791}$-cdc12$^{882-972}$-cdc12$^{882-1390}$-fus1$^{1278-1372}$-kanMX-fus1$^{3'UTR}$	Infusion cloning : pSM2827$^{EcoRI/AscI}$+ pSM2699$^{osm7690-osm7740}$	Endogenous integration
pSM2918	pFA6a-fus1$^{5'UTR}$-fus1$^{1-791}$-for3$^{718-1265}$-fus1$^{1278-1372}$-kanMX-fus1$^{3'UTR}$	Infusion cloning : pSM2827$^{EcoRI/AscI}$+ pSM2631$^{osm7690-osm7740}$	Endogenous integration
pSM2924	pFA6a-fus1$^{5'UTR}$-fus1$^{1-791}$-cdc12$^{882-972}$-cdc12$^{882-1390}$(E1168R-fus1$^{1278-1372}$-sfGFP-kanMX-fus1$^{3'UTR}$	Infusion cloning : pSM2700$^{EcoRI/PacI}$+ pSM2699$^{osm7690-osm7830}$+ pSM2699$^{osm7831-osm7122}$	Endogenous integration
pSM2937	pFA6a-fus1$^{5'UTR}$-fus1$^{1-491}$-CRY2PHR-fus1$^{792-1372}$-sfGFP-kanMX-fus1$^{3'UTR}$	Infusion cloning : pSM2625$^{SalI/XhoI}$+ pSM2625$^{osm7119-osm7878}$ +pSM2475$^{osm7879-osm7880}$+ pSM2625$^{osm7881-osm7882}$	Endogenous integration
pSM2938	pFA6a-fus1$^{5'UTR}$-fus1$^{1-491}$-CRY2olig-fus1$^{792-1372}$-sfGFP-kanMX-fus1$^{3'UTR}$	Infusion cloning : pSM2625$^{SalI/XhoI}$+ pSM2625$^{osm7119-osm7878}$ +pSM2390$^{osm7879-osm7880}$+ pSM2625$^{osm7881-osm7882}$	Endogenous integration
pSM2940	pFA6a-fus1$^{5'UTR}$-fus1$^{1-491}$-FUS-fus1$^{792-1372}$-sfGFP-kanMX-fus1$^{3'UTR}$	Infusion cloning : pSM2625$^{XhoI/SwaI}$+fus1$^{XhoIsite-491}$-FUS-fus1$^{792-SwaIsite}$ ordered as a gBlock	Endogenous integration
pSM2941	pFA6a-fus1$^{5'UTR}$-fus1$^{1-491}$-FUS^{12E}-fus1$^{792-1372}$-sfGFP-kanMX-fus1$^{3'UTR}$	Infusion cloning : pSM2625$^{XhoI/SwaI}$+fus1$^{XhoIsite-491}$-FUS^{12E}-fus1$^{792-SwaIsite}$ ordered as a gBlock	Endogenous integration
pSM2961	pFA6a-fus1$^{5'UTR}$-fus1R1054E-kanMX-fus1$^{3'UTR}$	Infusion cloning : pSM2827$^{EcoRI/AscI}$+ pSM2852$^{osm7690-osm7740}$	Endogenous integration
pSM2962	pFA6a-fus1$^{5'UTR}$-fus1$^{1-791}$-cdc12$^{882-972}$-cdc12$^{882-972}$-fus1$^{869-1372}$(R1054E-kanMX-fus1$^{3'UTR}$	Infusion cloning : pSM2827$^{EcoRI/AscI}$+ pSM2847$^{osm7690-osm7740}$	Endogenous integration
pSM2963	pFA6a-fus1$^{5'UTR}$-fus1$^{1-791}$-cdc12$^{882-972}$-cdc12$^{882-1390}$(E1168R-fus1$^{1278-1372}$-kanMX-fus1$^{3'UTR}$	Infusion cloning : pSM2827$^{EcoRI/AscI}$+ pSM2924$^{osm7690-osm7740}$	Endogenous integration

6.2 Strains construction

Strains were constructed using standard genetic manipulation of *S. pombe* either by tetrad dissection or transformation and can be found in the strain table. Oligonucleotides and plasmids used can be found in respective dedicated tables, with details on how the plasmids were constructed.

myo52-tdTomato:natMX, fus1-sfGFP:kanMX, acp2-sfGFP:kanMX, exo84-GFP:kanMX, exo70-GFP:kanMX, agn2-sfGFP:kanMX, eng2-sfGFP:kanMX, myo51-sfGFP:kanMX, fim1-mCherry:natMX, acp1-sfGFP:kanMX, myo52-GFP:kanMX, fim1-GBP-mCherry:bleMX, fim1-sfGFP:kanMX, cdc12-3GFP:kanMX and tea1-mCherry:kanMX tags were constructed by PCR-based gene targeting of a fragment from a template pFA6a plasmid containing the appropriate tag and resistance cassette, amplified with primers carrying 5' extensions corresponding to the last 78 coding nucleotides of the ORF and the first 78 nucleotides of the 3'UTR, which was transformed and integrated in the genome by homologous recombination, as previously described (Bähler et al., 1998). Similarly, acp1Δ::hphMX, acp2Δ::bleMX, fus1Δ::hphMX and for3Δ::bsdMX were constructed by PCR-based gene targeting of a fragment from a template pFA6a plasmid containing the appropriate resistance cassette, amplified with primers carrying 5' extensions corresponding to the last 78 nucleotides of the 5'UTR and the first 78 nucleotides of the 3'UTR, which was transformed and integrated in the genome by homologous recombination, and acp1$^{\Delta 233\text{-}256}$-sfGFP:kanMX, acp2$^{\Delta 244\text{-}268}$-sfGFP:kanMX and fus1$^{\Delta 1278\text{-}1372}$-sfGFP:kanMX were constructed by PCR-based gene targeting of a fragment from a template pFA6a plasmid with primers carrying 5' extensions corresponding to the 78 nucelotides upstream the deleted region and the first 78 nucleotides of the 3'UTR, which was transformed and integrated in the genome by homologous recombination.

The functionality of the tagged proteins was verified by comparing the phenotype of the tagged strain with that of the deletion strain. For tagged Acp1 and Acp2 alleles, the number of ectopic foci was quantified and found to be as in wildtype cells. Reduced functionality was only observed for tagged Agn2 and Eng2 alleles, which in combination (but not individually) showed reduced fusion efficiency.

For point mutations of Acp2 (R12A,Y77A) and Fus1 (K879A, I951A, GN1087,1088RP, K1112A), site directed mutagenesis was conducted on plasmids constructed as followed 5'UTR-ORF-sfGFP-kanMX-3'UTR by PCR amplification of the full fragment from strains YSM3355 or YSM3312 with primers carrying unique restriction sites, which was then cloned into a pFA6a based plasmid (pSM2194 and pSM2827, respectively). After site-directed mutagenesis, the resulting plasmid (pSM2203, pSM2251, pSM2252, pSM2253 and pSM2254, respectively) was sequenced, NotI or SalI-SacII digested, gel purified, and transformed.

Construction of the strains expressing formin constructs from the *fus1* promotor at the *ura4* locus as a multicopy integration (ura4-294:p^{fus1}:fus1-sfGFP:ura4+, ura4-294:p^{fus1}:cdc12-sfGFP:ura4+, ura4-294:p^{fus1}:for3-sfGFP:ura4+, ura4-294:p^{fus1}-fus1N$^{1\text{-}792}$-fus1C$^{793\text{-}1372}$-sfGFP:ura4+, ura4-294:p^{fus1}-cdc12N$^{1\text{-}887}$-fus1C$^{793\text{-}1372}$-sfGFP:ura4+, ura4-294:p^{fus1}-for3N$^{1\text{-}714}$-fus1C$^{793\text{-}1372}$-sfGFP:ura4+, ura4-294:p^{fus1}:fus1N$^{1\text{-}792}$-sfGFP:ura4+) were done by homologous recombination of a transformed ura4^{EndORF}-ura4$^{3'UTR}$-p^{fus1}-ForminConstruct-sfGFP-ura4^{StartORF}-ura4$^{5'UTR}$ fragment, obtained from StuI digestion of a pRIP based plasmid (pSM1656, pSM1658, pSM1657, pSM1659, pSM1663, pSM1662 and pSM1650, respectively). Such recombination recreates a new integration site, which has been shown to be unstable and to lead to

multiple insertion (Vještica et al., 2020), which is why we switched to single integration vectors for the rest of the study.

Construction of the strains expressing fus1N, fus1N-Fus1C, Fus1N-Cdc12C, Fus1N-For3C, Fus1N-Cdc12CΔolig and Fus1N-For3C-Cdc12olig chimeras from the *fus1* promotor at the *ura4* locus as a single integration (ura4+:p^{fus1}:$fus1N^{1-792}$-sfGFP, ura4+:p^{fus1}:$fus1N^{1-792}$-$fus1C^{793-1372}$-sfGFP, ura4+:p^{fus1}:$fus1N^{1-792}$-$cdc12C^{888-1841}$-sfGFP, ura4+:p^{fus1}:$fus1N^{1-792}$-$for3C^{715-1461}$-sfGFP, ura4+:p^{fus1}:$fus1N^{1-792}$-$cdc12CΔolig^{888-1451}$-sfGFP, ura4+:pfus1:$fus1N^{1-792}$-$for3C^{715-1461}$-$cdc12olig^{1446-1841}$-sfGFP) were done by homologous recombination of a transformed $ura4^{5'UTR}$-$ura4^{ORF}$-$ura4^{3'UTR}$-p^{fus1}-ForminConstruct-sfGFP-$ura4^{3''}$ fragment, obtained from PmeI digestion of a $pUra4^{PmeI}$ based plasmid (pSM2812, pSM2594, pSM2595, pSM2604, pSM2596 and pSM2605, respectively). This leads to a stable single integration at the *ura4* locus (Vještica et al., 2020).

Construction of the strains expressing fus1 constructs under *nmt1* promotor at the *ura4* locus as a single integration (ura4+:p^{nmt1}:$fus1N^{1-792}$-sfGFP:termnmt, ura4+:p^{nmt1}:$fus1N^{1-730}$-sfGFP:$term^{nmt}$ ura4+:p^{nmt1}:$fus1N^{1-500}$-sfGFP:$term^{nmt}$, ura4+:p^{nmt1}:$fus1N^{93-792}$-sfGFP:$term^{nmt}$, ura4+:p^{nmt1}:$fus1N^{140-792}$-sfGFP:$term^{nmt}$, ura4+:p^{nmt1}:$fus1N^{191-792}$-sfGFP:$term^{nmt}$, ura4+:p^{nmt1}:$fus1N^{293-792}$-sfGFP:$term^{nmt}$, ura4+:p^{nmt1}:$fus1N^{431-755}$-sfGFP:$term^{nmt}$, ura4+:p^{nmt1}:fus1-sfGFP:$term^{nmt}$) were done by homologous recombination of a transformed $ura4^{5'UTR}$-$ura4^{ORF}$-$ura4^{3'UTR}$-p^{nmt1}-Fus1Construct-sfGFP-$ura4^{3''}$ fragment, obtained from PmeI digestion of a $pUra4^{PmeI}$ based plasmid (pSM2812, pSM2594, pSM2595, pSM2604, pSM2596 and pSM2605, respectively).

Construction of the strains expressing Fus1 under either *ste11* or *pak2* promotor at the *ura4* locus as a single integration (ura4+:pste11:fus1-sfGFP and ura4+:ppak2:fus1-sfGFP) were done by homologous recombination of a transformed $ura4^{5'UTR}$-$ura4^{ORF}$-$ura4^{3'UTR}$-$p^{ste11\ or\ pak2}$-Fus1-sfGFP-$ura4^{3''}$ fragment, obtained from PmeI digestion of a $pUra4^{PmeI}$ based plasmid (pSM2828 and pSM2829, respectively).

Construction of the strain expressing ypt3 under the *nmt41* promotor at the *ura4* locus (ura4+:pnmt41:GFP-ypt3) was done by integration of a $ura4^{5'UTR}$-$ura4^{ORF}$-$ura4^{3'UTR}$-p^{nmt1}-GFP-ypt3-$ura4^{3''}$ fragment, which was linearized with AfeI from a $pUra4^{AfeI}$ based plasmid (pSM2250). This construct is in principle similar to that published by (Cheng et al., 2002), which was shown to rescue the ypt3-i5 mutant phenotype. However, we note that we were unable to construct a GFP-ypt3 expressed as single copy from the native genomic locus, suggesting that GFP tagging impairs Ypt3 function.

Construction of the strains expressing tagged formin constructs from the endogenous locus ($fus1N^{1-792}$-$fus1C^{793-1372}$-sfGFP:kanMX, $fus1N^{1-792}$-$cdc12C^{888-1841}$-sfGFP:kanMX, $fus1N^{1-792}$-$for3C^{715-1461}$-sfGFP:kanMX, $fus1N^{1-792}$-$cdc12CΔolig^{888-1451}$-sfGFP:kanMX, $fus1N^{1-792}$-$for3C^{715-1461}$-$cdc12olig^{1446-1841}$-sfGFP:kanMX, $fus1^{1-868}$-$fus1^{792-1372}$-sfGFP:kanMX, $fus1^{1-791}$-$cdc12^{928-972}$-$fus1^{869-1372}$-sfGFP:kanMX, $fus1^{1-791}$-$cdc12^{882-972}$-$cdc12^{882-972}$-$fus1^{869-1372}$-sfGFP:kanMX, $fus1^{1-791}$-$for3^{718-1265}$-$fus1^{1278-1372}$-sfGFP:kanMX, $fus1^{1-868}$-$cdc12^{973-1390}$-$fus1^{1278-1372}$-sfGFP:kanMX, $fus1^{1-791}$-$cdc12^{928-1390}$-$fus1^{1278-1372}$-sfGFP:kanMX, $fus1^{1-791}$-$cdc12^{882-1390}$-$fus1^{1278-1372}$-sfGFP:kanMX, $fus1^{1-791}$-$cdc12^{882-972}$-$cdc12^{882-1390}$-$fus1^{1278-1372}$-sfGFP:kanMX, $fus1^{1-868}$-$Sjfus1^{908-1317}$-$fus1^{1278-1372}$-sfGFP:kanMX, $fus1^{1-868}$-$Sofus1^{857-1265}$-$fus1^{1278-1372}$-sfGFP:kanMX, $fus1^{1-792}$-$cdc12^{882-972}$-$cdc12^{882-972}$-$Sjfus1^{908-1317}$-$fus1^{1278-1372}$-sfGFP:kanMX, $fus1^{1-792}$-$cdc12^{882-972}$-$cdc12^{882-972}$-$Sofus1^{857-1265}$-$fus1^{1278-1372}$-sfGFP:kanMX, $fus1^{Δ501-749}$-sfGFP:kanMX, $fus1^{Δ501-791}$-sfGFP:kanMX, $fus1^{Δ492-791}$-sfGFP:kanMX, $fus1^{1-491}$-FUS^{12E}-$fus1^{792-1372}$-sfGFP:kanMX, $fus1^{1-491}$-FUS-$fus1^{792-1372}$-sfGFP:kanMX, $fus1^{1-491}$-$CRY2_{PHR}$-$fus1^{792-1372}$-sfGFP:kanMX, $fus1^{1-491}$-CRY2olig-$fus1^{792-1372}$-sfGFP:kanMX, fus1(KEYTG935-

939CARTD)-sfGFP:kanMX, fus1(L959K)-sfGFP:kanMX, fus1(EEVMEV1006-1011NGGDLVNS)-sfGFP:kanMX, fus1(R1054E)-sfGFP:kanMX, fus1(NHK1182-1184DPT)-sfGFP:kanMX, fus1$^{1\text{-}792}$-cdc12$^{882\text{-}972}$-cdc12$^{882\text{-}972}$-fus1$^{869\text{-}1372}$(KEYTG935-939CARTD)-sfGFP:kanMX, fus1$^{1\text{-}792}$-cdc12$^{882\text{-}972}$-cdc12$^{882\text{-}972}$-fus1$^{869\text{-}1372}$(L959K)-sfGFP:kanMX, fus1$^{1\text{-}792}$-cdc12$^{882\text{-}972}$-cdc12$^{882\text{-}972}$-fus1$^{869\text{-}1372}$(EEVMEV1006-1011NGGDLVNS)-sfGFP:kanMX, fus1$^{1\text{-}792}$-cdc12$^{882\text{-}972}$-cdc12$^{882\text{-}972}$-fus1$^{869\text{-}1372}$(R1054E)-sfGFP:kanMX, fus1$^{1\text{-}792}$-cdc12$^{882\text{-}972}$-cdc12$^{882\text{-}972}$-fus1$^{869\text{-}1372}$(NHK1182-1184DPT)-sfGFP:kanMX, fus1$^{1\text{-}792}$-cdc12$^{882\text{-}972}$-cdc12$^{882\text{-}1390}$(E1168R)-fus1$^{1278\text{-}1372}$-sfGFP:kanMX) were done by homologous recombination of a transformed fus1$^{5'\text{UTR}}$-ForminConstruct-sfGFP-kanMX-fus1$^{3'\text{UTR}}$ fragment, obtained from a gel purified, SalI and SacII or AatII and SacII (Cdc12 FH2 contains an endogenous SalI site) digested pFA6a based plasmid (pSM2690, pSM2691, pSM2692, pSM2693, pSM2694, pSM2621, pSM2702, pSM2700, pSM2631, pSM2701, pSM2632, pSM2622, pSM2699, pSM2855, pSM2857, pSM2854, pSM2856, pSM2507, pSM2697, pSM2625, pSM2941, pSM2940, pSM2937, pSM2938, pSM2849, pSM2850, pSM2851, pSM2852, pSM2853, pSM2844, pSM2845, pSM2846, pSM2847, pSM2848 and pSM2924, respectively).

Similarly, construction of the strains expressing untagged formin constructs from the endogenous locus (fus1:kanMX, fus1$^{1\text{-}791}$-cdc12$^{882\text{-}972}$-cdc12$^{882\text{-}972}$-fus1$^{869\text{-}1372}$:kanMX, fus1$^{1\text{-}791}$-for3$^{718\text{-}1265}$-fus1$^{1278\text{-}1372}$:kanMX, fus1$^{1\text{-}868}$-cdc12$^{973\text{-}1390}$-fus1$^{1278\text{-}1372}$:kanMX, fus1$^{1\text{-}791}$-cdc12$^{928\text{-}1390}$-fus1$^{1278\text{-}1372}$:kanMX, fus1$^{1\text{-}792}$-cdc12$^{882\text{-}972}$-cdc12$^{882\text{-}1390}$-fus1$^{1278\text{-}1372}$:kanMX, fus1(R1054E):kanMX, fus1$^{1\text{-}792}$-cdc12$^{882\text{-}972}$-cdc12$^{882\text{-}972}$-fus1$^{869\text{-}1372}$(R1054E):kanMX, fus1$^{1\text{-}792}$-cdc12$^{882\text{-}972}$-cdc12$^{882\text{-}1390}$(E1168R-fus1$^{1278\text{-}1372}$):kanMX) were done by homologous recombination of a transformed fus1$^{5'\text{UTR}}$-ForminConstruct-sfGFP-kanMX-fus1$^{3'\text{UTR}}$ fragment, obtained from a gel purified, SalI and SacII or AatII and SacII digested pFA6a based plasmid (pSM2913, pSM2914, pSM2918, pSM2915, pSM2916, pSM2917, pSM2961, pSM2962 and pSM2963, respectively).

acp1Δ::kanMX and acp2Δ::kanMX are derived from the Bioneer collection (Kim et al., 2010). ura4-D18:p^{map3}:GFP:ura4+ (Dudin et al., 2015), for3-3GFP:ura4+ (Martin & Chang, 2006), leu1-32:p^{nmt41}:GFP-cdc8:ura4+ (Skoumpla et al., 2007), leu1-32:p^{nmt41}:GFP-CHD:leu1+ (Gift from M.K. Balasubramanian), leu1-32:p^{act1}:LifeAct-mCherry:leu1+ (Huang et al., 2012), cdc12-112 (Chang et al., 1996), fus1Δ::LEU2+ (Petersen et al., 1998b), leu1-32:p^{cdc8}:mNeonGreen-cdc8:term^{cdc8}:term^{ScADH1}:leu1+ (Gift from M.K. Balasubramanian), ade6+:p^{act1}:LifeAct-sfGFP:term^{ScADH1}:bsdMX and his5+:p^{act1}:CRIB-3mCherry:bsdMX (Vještica et al., 2020) trace back to the aforementioned papers or are kind gifts from the afore mentioned labs.

6.3 Growth conditions

For mating experiments, homothallic (*h90*) strains able to switch mating types were used, where cells were grown in liquid or agar Minimum Sporulation Media (MSL), with or without nitrogen (+/- N) (Egel et al., 1994; Vjestica et al., 2016). For interphase experiments, cells were grown in liquid or agar Edinburgh minimal medium (EMM) supplemented with amino acids as required.

Live imaging of *S. pombe* mating cells protocol was adapted from (Vjestica et al., 2016). Briefly, cells were first pre-cultured overnight in MSL+N at 25°C, then diluted to OD_{600} = 0.05 into MSL+N at 25°C for 20 hours. Exponentially growing cells were then pelleted, washed in MSL-N by 3 rounds of centrifugation, and resuspended in MSL-N to an OD_{600} of 1.5. Cells were then grown 3 hours at 30°C to allow mating in

liquid, added on 2% agarose MSL-N pads, and sealed with VALAP. We allowed the pads to rest for 30 min at 30°C before overnight imaging, for 3 h before live imaging, or for 6h, 9h, 21h or 33h at 25°C for 9h, 12h, 24h, and 36h post-starvation fusion efficiencies snapshot imaging, respectively.

For Correlative Light Electron Microscopy (CLEM) imaging, as described in (Muriel et al., 2021), cells were grown for mating as described above. After washes to remove nitrogen, cells were added into MSL-N plates. We allowed cells to mate for 5 h. A few microliters of MSL-N were pipetted onto the cells to form a thick slurry, which was pipetted onto a 3 mm-wide, 0.1 mm-deep specimen carrier (Wohlwend type A) closed with a flat lid (Wohlwend type B) for high-pressure freezing with a HPM100 (Leica Microsystems). The carrier sandwich was disassembled in liquid nitrogen before freeze substitution. High-pressure frozen samples were processed by freeze substitution and embedding in Lowicryl HM20 using the Leica AFS 2 robot as described in (Kukulski et al., 2012). 300 nm sections were cut with a diamond knife using a Leica Ultracut E or Ultracut UC7 ultramicrotome, collected in H2O, and picked up on carbon-coated 200-mesh copper grids (AGS160; Agar Scientific). For Light Microscopy, the grid was inverted onto a 1× PBS drop on a microscope coverslip, which was mounted onto a microscope slide and imaged using the DeltaVision platform described below. The grid was then recovered, rinsed in H2O, and dried before post-staining with Reynolds lead citrate for 10 min. 15 nm protein A–coupled gold beads were adsorbed to the top of the section as fiducials for tomography.

For interphase imaging, cells were grown to exponential phase at 30°C in EMM+ALU media, pelleted and added to 2% agarose EMM+ALU pads. For CK-666 (Sigma), LatA (Enzo Life Sciences) and 1,6-hexanediol treatments in figures 2.9 and 4.3, the drugs were added directly before imaging to the final resuspension, to a final concentration of 500 µM, 200 µM, and 20% respectively. In this case, cells were simply imaged without pad between slide and coverslip. The slide was allowed to rest for 5 minutes before imaging for the first 2 drugs, while it was imaged right away for 1,6-hexanediol treatment. For the 37°C treatment in Figure 4.3, cells were grown to exponential phase at 30°C in EMM+ALU media, then shifted to 37°C for 6h, concentrated by quick centrifugation, transported to the microscope on a 40°C carrier, and imaged between slide and coverslip at 40°C. All strains containing a repressible *nmt* promotor were grown at least 24h without thiamine before imaging, as to have a fully uninhibited promotor.

6.4 Microscopy

Images presented in Figures 2.1, 2.2, 2.3A, 2.4, 2.7A-G, 2.8, 3.1, 3.2, 3.3, 3.4, 3.5, 3.6, 3.7, 4.1D, 4.2C, 4.4 and 4.5A were obtained using a DeltaVision platform (Applied Precision) composed of a customized inverted microscope (IX-71; Olympus), a UPlan Apochromat 100×/1.4 NA oil objective, a camera (CoolSNAP HQ2; Photometrics or 4.2Mpx PrimeBSI sCMOS camera; Photometrics), and a color combined unit illuminator (Insight SSI 7; Social Science Insights). Images were acquired using softWoRx v4.1.2 software (Applied Precision). Images were acquired every 5 minutes during 9 to 15 hours. To limit photobleaching, overnight videos were captured by optical axis integration (OAI) imaging of a 4.6 µm z-section, which is essentially a real-time z-sweep.

Images presented in Figures 2.3F, 2.6, 2.7K, 2.9, 4.1A, 4.2B and 4.3A were obtained using a spinning-disk microscope composed of an inverted microscope (DMI4000B; Leica) equipped with an HCX Plan

Apochromat 100×/1.46 NA oil objective and an UltraVIEW system (PerkinElmer; including a real-time confocal scanning head [CSU22; Yokagawa Electric Corporation], solid-state laser lines, and an electron-multiplying charge coupled device camera [C9100; Hamamatsu Photonics]). Time-lapse images were acquired at 1s interval using the Volocity software (PerkinElmer).

Images used to obtain Figures 4.3B and 4.5E were acquired using a ZEISS LSM 980 scanning confocal microscope with 4 confocal Detectors (2x GaAsP, 2x PMT), an Airyscan2 detector optimized for a 60x/1.518 NA oil objective, and 6 Laser Lines (405nm, 445nm, 488nm, 514nm, 561nm, 640nm) on inverted Microscope Axio Observer 7. For Figure 4.3B we used images acquired using the Airyscan2 detector and processed with the Zen3.3 (blue edition) software for super resolution. For Figure 4.5E we switched to the confocal mode as the lower fluorescence intensity required. We acquired images every second, and we bleached the cells by 1 iteration of a 25% (4.3B) or 10% (4.5E) 488nm laser power pulse after 5 time points and kept recording the fluorescence recovery for 5 (4.3B) or 2 minutes (4.5E). Temperature was controlled by an incubation chamber around the microscope.

Images used to obtain Figure 2.5 were acquired following CLEM, as described in (Muriel et al., 2021). TEMs were acquired on a FEI Tecnai 12 at 120 kV using a bottom mount FEI Eagle camera (4kx4k). Low-magnification images were acquired at 17.816 nm pixel size and high magnification at 1.205 nm pixel size. For tomographic reconstruction of regions of interest, tilt series were acquired at 1.205 nm pixel size (Tecnai) or 1.1 nm pixel size (TF20) over a tilt range as large as possible up to ±60° at 1° increments using the Serial EM software (Mastronarde, 2005). The IMOD software package with gold fiducial alignment (Kremer et al., 1996; Mastronarde & Held, 2017) was used for tomogram reconstruction.

6.5 Quantification and statistical analysis

Fusion efficiencies as in Figures 2.1A, 2.3G, 3.1C, 3.2C, 3.2E, 3.2J, 3.3B-D, 3.3F, 3.4C, 3.5C, 3.6C, 3.7C, 3.7F, 4.1E, 4.4B and 4.5B-C were calculated as in (Dudin et al., 2015). Briefly, at the specified time post-starvation, mating pairs and fused pairs were quantified using the ImageJ Plugin ObjectJ, and the subsequent fusion efficiency was calculated using the following equation:

$$Fusion\ Efficiency = \frac{\text{Fused Pairs}}{\text{Mating Pairs}} \times 100$$

Fusion Times as in Figures 2.1C, 2.3E, 2.7J, 2.8C, 3.2I, 3.3H and 3.4D were calculated using the 5-minutes time lapse overnight movies using the 2-dots Myo52-tdTomato stage (Dudin et al., 2015) as a marker for the beginning of the fusion process and either the entry of GFP expressed under control of the P-cell-specific p^{map3} promoter into the *h-* partner, or the maximum intensity of the Myo52-tdTomato dot, the two of which perfectly correlate (Dudin et al., 2015), as a marker for the end of the process. Persistence times as in Figures 2.1D, 2.3E and 2.8C were calculated using the 5-minutes time lapse overnight movies using fusion time as beginning and last appearance of the Myo52-tdTomato dot as end of the post-fusion focus lifetime. Fusion times and persistence times vary between experiments because, for all experiments but panels 2.1A and 2.1C, only early timepoints were considered to avoid Myo52 bleaching, which most certainly induces a

bias toward quickly fusing cells. The WT control was imaged and quantified for each experiment to allow comparison within an experiment.

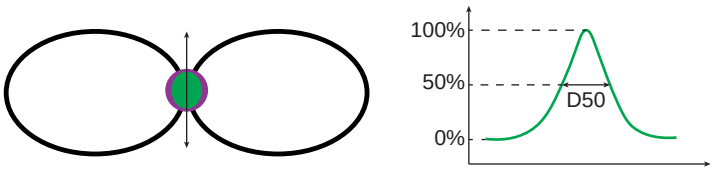

Figure 6.1 Fusion Profiles and Width at half maximum
Explicative Sketches of the proceedings in recording fusion fluorescence profiles and their associated width at half maximum (D50).

Fusion Focus intensities at fusion time were obtained using the 5-minutes time lapse overnight movies using either the entry of GFP into the *h-* partner, or the maximum intensity of the Myo52-tdTomato dot to determine the moment of fusion. On that frame, a fluorescence profile across the fusion focus perpendicular to the long axis of the mating pair (Figure 6.1, left) was recorded and either used directly as in Figures 2.2D-F, 2.4F-K, 3.2G and 4.1B or only the central points of the profiles were used to obtain boxplots as in Figure 2.3D, 4.5D and 4.5F. Profiles were background-subtracted and corrected for bleaching as follows: First, the cell fluorescence intensity was recorded over time in a square of about 7x7 pixels in 12 control (non-mating) cell. These fluorescence profiles were averaged, and the mean was fitted to a double exponential as it was describing our data better (Vicente et al., 2007):

$$\text{Signal}_{photobleaching-correction}(t) = \text{Ae}^{-Bt} + \text{Ce}^{-Dt}$$

We then used this fit to correct the fluorescence profiles across the fusion focus for photobleaching. After subtracting background signal, the value at each timepoint was divided by the photo-bleaching correction signal:

$$\text{Signal}_{\text{BleachingCorrected}} = \frac{\text{Signal}_t - \text{Signal}_{\text{Background}}}{\text{Signal}_{photobleaching-correction}(t)}$$

Corrected profiles were then either directly averaged and plotted, or further normalized to the mean of the WT maximum. Widths at Half maximum (D50) as in Figures 3.2H, 4.1C and 4.4C were then calculated using those fluorescence profiles as explained in Figure 6.1. This was done for each cell and then plotted as a boxplot.

Patch to cytosol ratios as in Figure 2.7H were calculated from the ratio of the mean fluorescence intensity of 5 circular ROIs centered on patches (which gives the patch intensity) to the mean fluorescence signal of 5 circular ROIs centered on cytosolic signal per cell. The same operation was repeated on 36 cells and plotted.

Total fluorescence intensities as in Figures 2.2G, 2.3B and 2.3D in mating pairs were obtained using single OAI scan snapshots on regular slides, 7h post-starvation, by outlining the mating pairs and recoding the mean fluorescence intensity for each of them. Background fluorescence was assessed by a small square

ROI in an area devoid of cells on each image, averaged over all images, and subtracted from fluorescence intensity measurements. Similarly, total fluorescence intensities as in Figures 3.3G in mating pairs at fusion time were obtained using 5-minutes time lapse overnight movies where fusion time was assessed for each mating cell and the signal bleaching-corrected as described above.

The number of ectopic foci as in Figures 2.3E, 2.4M, 2.6A and 2.7I-J was assessed using the 5-minutes time lapse overnight movies during the fusion process between the 2-dot stage and the fusion time by simply counting the number of time-frames showing an ectopic Myo52-tdTomato or any other marker. The numbers vary between experiments because the DeltaVision camera was upgraded in the middle of the project, allowing us to detect more delocalization events. To assess colocalization at ectopic foci as in Figures 2.4M-P, single and double-color ectopic foci were identified as above and the colocalization was calculated with the following formula :

$$Percentage\ of\ Colocalization\ = \frac{2 \times \mathrm{EctopicFoci}_{\mathrm{BothMarkers}}}{\mathrm{EctopicFoci}_{Marker1} + \mathrm{EctopicFoci}_{Marker2}} \times 100$$

The proportion of ectopic foci containing a given marker as in Figure 2.6B-G, 2.9A-E and 2.9G was derived from the ratio of ectopic foci containing the given marker to the total number, which gave a ratio for each cell. That ratio was then averaged over all the recorded cells. For all experiments shown in Figure 2.9, only ectopic foci present at the cell sides were considered.

For3-3GFP retrograde flow was identified by visual inspection of spinning disk time-lapse imaging acquired at 1s interval. Only linear For3 dot movements present over at least 5 consecutive time frames were considered. Dots were manually tracked using the ImageJ multi-point tool and instantaneous speeds calculated and averaged per track. Kymographs were constructed using the ImageJ reslice tool along a 5-pixel-wide line along the For3 dot track.

Fus1 and Cdc12 homology modelling as in Figure 3.6E was done in collaboration with Justyna Iwaszkiewicz from the Swiss Institute of Bioinformatics in Lausanne. The suitable templates for Fus1 and Cdc12 structure modelling were found using HHpred tool (Zimmermann et al., 2018). The models of Fus1 protein were calculated based on the template of diaphanous protein from mice, stored under 3OBV code in the Protein Data Bank (Otomo et al., 2010). The sequence identity in case of these protein sequences is 20%. The yeast S. cerevisiae BNI protein structure, stored under 5UX1 code in Protein Data Bank, served as a template for Cdc12 protein (Xu et al., 2004). Both sequences share 34% of sequence identity. For modeling of Fus1 and Cdc12 proteins' dimer we used the dimeric structure of FMNL3 protein bound to actin, stored in PDB under the 4EAH code (Thompson et al., 2013). Fus1 protein shared around 23% and Cdc12 around 25% of sequence identity with this template. The models' structures were calculated with the use of Modeller 9v18 program (Sali & Blundell, 1993). The models of Fus1 and Cdc12 proteins were aligned with UCSF Chimera visualization program (Pettersen et al., 2004). The alignments points, where the opposite charge residues were present in both sequences or where a group of charged amino acid appeared in only one of the sequences, were identified. We took into account the fragments that were exposed on the surface of the models, thus accessible for interactions with other proteins and not interfering with dimerization of the domain or with actin elongation.

The monopolar percentage was assessed by using single fluorescence snapshot images and visually assessing the distribution of CRIB as monopolar (decorating only one pole) or bipolar (decorating the two poles at similar intensities). The ratio of the first category divided by the sum of the two gave the monopolar percentage as shown in Figure 4.2D. Note that even WT bipolar cells can appear monopolar using this assay, as we can capture them in a time in CRIB oscillations where only one cell tip is decorated, or before NETO.

FRAP data analysis was performed by recording the fluorescence intensity of the bleached area using a manually fitted ROI. This ROI was moved over the time course of the time lapse as the cells sometimes shift or the foci sometimes move. As the conditions we used for bleaching only partially bleach the observed structure, we could follow the structure through the whole time-lapse. Cells where the Fus1 foci couldn't be followed over the entire time course of the time lapse were excluded from the analysis as well as movies where the focus was lost during the acquisition. All the remaining traces were bleaching corrected by dividing them by an average of fluorescence traces from at least 10 control cells for each experiment. They were then scaled as follow :

$$\text{Traces}_{\text{scaled}} = \frac{\text{Traces}_t - \text{Traces}_{t=1\ post\ bleaching}}{\text{Mean}\left(\text{Traces}_{\text{pre bleaching}}\right) - \text{Traces}_{t=1\ post\ bleaching}}$$

The resulting scaled traces were then averaged for each strain and plotted from the first post-beaching point along with their standard error. The average trace for each strain was then used to fit the following conventional FRAP equation :

$$f(t) = A(1 - e^{-\tau t})$$

We obtained the following R^2 : 0.9915 for Fus1N-Tips, 0.8966 for Fus1N-Clusters, 0.9113 for WT, 0.9409 for FUS^{12E}, 0.9268 for FUS, 0.9322 for $CRY2_{PHR}$ and 0.9244 for CRY2olig. We used the fittings values of τ to calculate the half-times recovery $\tau_{½}$ as follow :

$$\tau_{1/2} = \frac{ln(0.5)}{\tau}$$

We then obtained only one value per strain, which was indicated directly on the figure.

All plots, fittings, corrections and normalisations were made using MATLAB home-made scripts. For boxplots, the central line indicates the median, the circle, if present, indicates the mean, and the bottom and top edges of the box indicate the 25th and 75th percentiles, respectively. The whiskers extend to the most extreme data points not considered outliers. For bar plots and fluorescent profiles, errorbars represent the standard deviation. For the two FRAP plots, shaded areas represent the standard error. Statistical p-values were obtained using a two-sided t-test, after normal distribution had been visually checked using a simple histogram. No further verification was made to ascertain that the data met assumptions of the statistical approach. All values below 0.05 are mentioned in the figures, including sample size.

7. References

A, M., Fung, T. S., Francomacaro, L. M., Huynh, T., Kotila, T., Svindrych, Z., & Higgs, H. N. (2020). Regulation of INF2-mediated actin polymerization through site-specific lysine acetylation of actin itself. *Proc Natl Acad Sci U S A*, *117*(1), 439-447. https://doi.org/10.1073/pnas.1914072117

A, M., Fung, T. S., Kettenbach, A. N., Chakrabarti, R., & Higgs, H. N. (2019). A complex containing lysine-acetylated actin inhibits the formin INF2. *Nat Cell Biol*, *21*(5), 592-602. https://doi.org/10.1038/s41556-019-0307-4

Ács-Szabó, L., Papp, L. A., Antunovics, Z., Sipiczki, M., & Miklós, I. (2018). Assembly of Schizosaccharomyces cryophilus chromosomes and their comparative genomic analyses revealed principles of genome evolution of the haploid fission yeasts. *Sci Rep*, *8*(1), 14629. https://doi.org/10.1038/s41598-018-32525-9

Aghamohammadzadeh, S., & Ayscough, K. R. (2009). Differential requirements for actin during yeast and mammalian endocytosis. *Nat Cell Biol*, *11*(8), 1039-1042. https://doi.org/10.1038/ncb1918

Aguilar, P. S., Heiman, M. G., Walther, T. C., Engel, A., Schwudke, D., Gushwa, N., Kurzchalia, T., & Walter, P. (2010). Structure of sterol aliphatic chains affects yeast cell shape and cell fusion during mating. *Proc Natl Acad Sci U S A*, *107*(9), 4170-4175. https://doi.org/10.1073/pnas.0914094107

Ahmed, S., Bu, W., Lee, R. T., Maurer-Stroh, S., & Goh, W. I. (2010). F-BAR domain proteins: Families and function. *Commun Integr Biol*, *3*(2), 116-121. https://doi.org/10.4161/cib.3.2.10808

Ahuja, R., Pinyol, R., Reichenbach, N., Custer, L., Klingensmith, J., Kessels, M. M., & Qualmann, B. (2007). Cordon-bleu is an actin nucleation factor and controls neuronal morphology. *Cell*, *131*(2), 337-350. https://doi.org/10.1016/j.cell.2007.08.030

Akin, O., & Mullins, R. D. (2008). Capping protein increases the rate of actin-based motility by promoting filament nucleation by the Arp2/3 complex. *Cell*, *133*(5), 841-851. https://doi.org/10.1016/j.cell.2008.04.011

Alberti, S., Gladfelter, A., & Mittag, T. (2019). Considerations and Challenges in Studying Liquid-Liquid Phase Separation and Biomolecular Condensates. *Cell*, *176*(3), 419-434. https://doi.org/10.1016/j.cell.2018.12.035

Alberts, A. S. (2001). Identification of a carboxyl-terminal diaphanous-related formin homology protein autoregulatory domain. *J Biol Chem*, *276*(4), 2824-2830. https://doi.org/10.1074/jbc.M006205200

Alberts, B., Johnson, A., Lewis, J., Morgan, D., Raff, M., Roberts, K., & Walter, P. (2014). *Molecular Biology of the Cell*. Garland Science. https://books.google.ch/books?id=_NkpygAACAAJ

Alfredsson-Timmins, J., Kristell, C., Henningson, F., Lyckman, S., & Bjerling, P. (2009). Reorganization of chromatin is an early response to nitrogen starvation in Schizosaccharomyces pombe. *Chromosoma*, *118*(1), 99-112. https://doi.org/10.1007/s00412-008-0180-6

Amatruda, J. F., Cannon, J. F., Tatchell, K., Hug, C., & Cooper, J. A. (1990). Disruption of the actin cytoskeleton in yeast capping protein mutants. *Nature*, *344*(6264), 352-354. https://doi.org/10.1038/344352a0

Amatruda, J. F., & Cooper, J. A. (1992). Purification, characterization, and immunofluorescence localization of Saccharomyces cerevisiae capping protein. *J Cell Biol*, *117*(5), 1067-1076. https://doi.org/10.1083/jcb.117.5.1067

Andrianantoandro, E., & Pollard, T. D. (2006). Mechanism of actin filament turnover by severing and nucleation at different concentrations of ADF/cofilin. *Mol Cell*, *24*(1), 13-23. https://doi.org/10.1016/j.molcel.2006.08.006

Arai, R., Nakano, K., & Mabuchi, I. (1998). Subcellular localization and possible function of actin, tropomyosin and actin-related protein 3 (Arp3) in the fission yeast Schizosaccharomyces pombe. *Eur J Cell Biol*, *76*(4), 288-295. https://doi.org/10.1016/s0171-9335(98)80007-1

Archer, S. J., Vinson, V. K., Pollard, T. D., & Torchia, D. A. (1994). Elucidation of the poly-L-proline binding site in Acanthamoeba profilin I by NMR spectroscopy. *FEBS Lett*, *337*(2), 145-151. https://doi.org/10.1016/0014-5793(94)80262-9

Arellano, M., Durán, A., & Pérez, P. (1996). Rho 1 GTPase activates the (1-3)beta-D-glucan synthase and is involved in Schizosaccharomyces pombe morphogenesis. *Embo j*, *15*(17), 4584-4591.

Babu, M. M. (2016). The contribution of intrinsically disordered regions to protein function, cellular complexity, and human disease. *Biochem Soc Trans*, *44*(5), 1185-1200. https://doi.org/10.1042/bst20160172

Bähler, J., Wu, J. Q., Longtine, M. S., Shah, N. G., McKenzie, A., 3rd, Steever, A. B., Wach, A., Philippsen, P., & Pringle, J. R. (1998). Heterologous modules for efficient and versatile PCR-based gene targeting in Schizosaccharomyces pombe. *Yeast*, *14*(10), 943-951. https://doi.org/10.1002/(sici)1097-0061(199807)14:10<943::Aid-yea292>3.0.Co;2-y

Baker, J. L., Courtemanche, N., Parton, D. L., McCullagh, M., Pollard, T. D., & Voth, G. A. (2015). Electrostatic interactions between the Bni1p Formin FH2 domain and actin influence actin filament nucleation. *Structure*, *23*(1), 68-79. https://doi.org/10.1016/j.str.2014.10.014

Balasubramanian, M. K., Helfman, D. M., & Hemmingsen, S. M. (1992). A new tropomyosin essential for cytokinesis in the fission yeast S. pombe. *Nature*, *360*(6399), 84-87. https://doi.org/10.1038/360084a0

Balasubramanian, M. K., Hirani, B. R., Burke, J. D., & Gould, K. L. (1994). The Schizosaccharomyces pombe cdc3+ gene encodes a profilin essential for cytokinesis. *J Cell Biol*, *125*(6), 1289-1301. https://doi.org/10.1083/jcb.125.6.1289

Barr, M. M., Tu, H., Van Aelst, L., & Wigler, M. (1996). Identification of Ste4 as a potential regulator of Byr2 in the sexual response pathway of Schizosaccharomyces pombe. *Mol Cell Biol*, *16*(10), 5597-5603. https://doi.org/10.1128/mcb.16.10.5597

Baum, B., & Kunda, P. (2005). Actin nucleation: spire - actin nucleator in a class of its own. *Curr Biol*, *15*(8), R305-308. https://doi.org/10.1016/j.cub.2005.04.004

Bear, J. E., & Gertler, F. B. (2009). Ena/VASP: towards resolving a pointed controversy at the barbed end. *J Cell Sci*, *122*(Pt 12), 1947-1953. https://doi.org/10.1242/jcs.038125

Behrens, R., & Nurse, P. (2002). Roles of fission yeast tea1p in the localization of polarity factors and in organizing the microtubular cytoskeleton. *J Cell Biol*, *157*(5), 783-793. https://doi.org/10.1083/jcb.200112027

Bendezú, F. O., & Martin, S. G. (2011). Actin cables and the exocyst form two independent morphogenesis pathways in the fission yeast. *Mol Biol Cell*, *22*(1), 44-53. https://doi.org/10.1091/mbc.E10-08-0720

Bendezú, F. O., & Martin, S. G. (2013). Cdc42 explores the cell periphery for mate selection in fission yeast. *Curr Biol*, *23*(1), 42-47. https://doi.org/10.1016/j.cub.2012.10.042

Bennett, V., & Baines, A. J. (2001). Spectrin and ankyrin-based pathways: metazoan inventions for integrating cells into tissues. *Physiol Rev*, *81*(3), 1353-1392. https://doi.org/10.1152/physrev.2001.81.3.1353

Berro, J., & Pollard, T. D. (2014). Synergies between Aip1p and capping protein subunits (Acp1p and Acp2p) in clathrin-mediated endocytosis and cell polarization in fission yeast. *Mol Biol Cell*, *25*(22), 3515-3527. https://doi.org/10.1091/mbc.E13-01-0005

Bhattacharya, N., Ghosh, S., Sept, D., & Cooper, J. A. (2006). Binding of myotrophin/V-1 to actin-capping protein: implications for how capping protein binds to the filament barbed end. *J Biol Chem*, *281*(41), 31021-31030. https://doi.org/10.1074/jbc.M606278200

Billault-Chaumartin, I., & Martin, S. G. (2019). Capping Protein Insulates Arp2/3-Assembled Actin Patches from Formins. *Curr Biol*, *29*(19), 3165-3176.e3166. https://doi.org/10.1016/j.cub.2019.07.088

Biro, M., Romeo, Y., Kroschwald, S., Bovellan, M., Boden, A., Tcherkezian, J., Roux, P. P., Charras, G., & Paluch, E. K. (2013). Cell cortex composition and homeostasis resolved by integrating proteomics and quantitative imaging. *Cytoskeleton (Hoboken)*, *70*(11), 741-754. https://doi.org/10.1002/cm.21142

Blanchoin, L., & Pollard, T. D. (1999). Mechanism of interaction of Acanthamoeba actophorin (ADF/ Cofilin) with actin filaments. *J Biol Chem*, *274*(22), 15538-15546. https://doi.org/10.1074/jbc.274.22.15538

Blanchoin, L., & Pollard, T. D. (2002). Hydrolysis of ATP by polymerized actin depends on the bound divalent cation but not profilin. *Biochemistry*, *41*(2), 597-602. https://doi.org/10.1021/bi011214b

Blanchoin, L., Pollard, T. D., & Hitchcock-DeGregori, S. E. (2001). Inhibition of the Arp2/3 complex-nucleated actin polymerization and branch formation by tropomyosin. *Curr Biol*, *11*(16), 1300-1304. https://doi.org/10.1016/s0960-9822(01)00395-5

Blanchoin, L., & Staiger, C. J. (2010). Plant formins: diverse isoforms and unique molecular mechanism. *Biochim Biophys Acta*, *1803*(2), 201-206. https://doi.org/10.1016/j.bbamcr.2008.09.015

Boettner, D. R., D'Agostino, J. L., Torres, O. T., Daugherty-Clarke, K., Uygur, A., Reider, A., Wendland, B., Lemmon, S. K., & Goode, B. L. (2009). The F-BAR protein Syp1 negatively regulates WASp-Arp2/3 complex activity during endocytic patch formation. *Curr Biol*, *19*(23), 1979-1987. https://doi.org/10.1016/j.cub.2009.10.062

Bohnert, K. A., Grzegorzewska, A. P., Willet, A. H., Vander Kooi, C. W., Kovar, D. R., & Gould, K. L. (2013). SIN-dependent phosphoinhibition of formin multimerization controls fission yeast cytokinesis. *Genes Dev*, *27*(19), 2164-2177. https://doi.org/10.1101/gad.224154.113

Bohnert, K. A., Willet, A. H., Kovar, D. R., & Gould, K. L. (2013). Formin-based control of the actin cytoskeleton during cytokinesis. *Biochem Soc Trans*, *41*(6), 1750-1754. https://doi.org/10.1042/bst20130208

Boiero Sanders, M., Antkowiak, A., & Michelot, A. (2020). Diversity from similarity: cellular strategies for assigning particular identities to actin filaments and networks. *Open Biol*, *10*(9), 200157. https://doi.org/10.1098/rsob.200157

Bombardier, J. P., Eskin, J. A., Jaiswal, R., Corrêa, I. R., Jr., Xu, M. Q., Goode, B. L., & Gelles, J. (2015). Single-molecule visualization of a formin-capping protein 'decision complex' at the actin filament barbed end. *Nat Commun*, *6*, 8707. https://doi.org/10.1038/ncomms9707

Brawley, C. M., & Rock, R. S. (2009). Unconventional myosin traffic in cells reveals a selective actin cytoskeleton. *Proc Natl Acad Sci U S A*, *106*(24), 9685-9690. https://doi.org/10.1073/pnas.0810451106

Breitsprecher, D., & Goode, B. L. (2013). Formins at a glance. *J Cell Sci*, *126*(Pt 1), 1-7. https://doi.org/10.1242/jcs.107250

Breitsprecher, D., Kiesewetter, A. K., Linkner, J., Vinzenz, M., Stradal, T. E., Small, J. V., Curth, U., Dickinson, R. B., & Faix, J. (2011). Molecular mechanism of Ena/VASP-mediated actin-filament elongation. *Embo j*, *30*(3), 456-467. https://doi.org/10.1038/emboj.2010.348

Breitsprecher, D., Koestler, S. A., Chizhov, I., Nemethova, M., Mueller, J., Goode, B. L., Small, J. V., Rottner, K., & Faix, J. (2011). Cofilin cooperates with fascin to disassemble filopodial actin filaments. *J Cell Sci*, *124*(Pt 19), 3305-3318. https://doi.org/10.1242/jcs.086934

Bretscher, A. (1981). Fimbrin is a cytoskeletal protein that crosslinks F-actin in vitro. *Proc Natl Acad Sci U S A*, *78*(11), 6849-6853. https://doi.org/10.1073/pnas.78.11.6849

Brown, J. W., & McKnight, C. J. (2010). Molecular model of the microvillar cytoskeleton and organization of the brush border. *PLoS One*, *5*(2), e9406. https://doi.org/10.1371/journal.pone.0009406

Burke, T. A., Christensen, J. R., Barone, E., Suarez, C., Sirotkin, V., & Kovar, D. R. (2014). Homeostatic actin cytoskeleton networks are regulated by assembly factor competition for monomers. *Curr Biol*, *24*(5), 579-585. https://doi.org/10.1016/j.cub.2014.01.072

Cam, H. P., & Whitehall, S. (2016). Analysis of Heterochromatin in Schizosaccharomyces pombe. *Cold Spring Harb Protoc*, *2016*(11). https://doi.org/10.1101/pdb.top079889

Campellone, K. G., & Welch, M. D. (2010). A nucleator arms race: cellular control of actin assembly. *Nat Rev Mol Cell Biol*, *11*(4), 237-251. https://doi.org/10.1038/nrm2867

Cao, W., Goodarzi, J. P., & De La Cruz, E. M. (2006). Energetics and kinetics of cooperative cofilin-actin filament interactions. *J Mol Biol*, *361*(2), 257-267. https://doi.org/10.1016/j.jmb.2006.06.019

Carnahan, R. H., & Gould, K. L. (2003). The PCH family protein, Cdc15p, recruits two F-actin nucleation pathways to coordinate cytokinetic actin ring formation in Schizosaccharomyces pombe. *J Cell Biol*, *162*(5), 851-862. https://doi.org/10.1083/jcb.200305012

Casella, J. F., & Torres, M. A. (1994). Interaction of Cap Z with actin. The NH2-terminal domains of the alpha 1 and beta subunits are not required for actin capping, and alpha 1 beta and alpha 2 beta heterodimers bind differentially to actin. *J Biol Chem*, *269*(9), 6992-6998.

Castagnetti, S., Behrens, R., & Nurse, P. (2005). End4/Sla2 is involved in establishment of a new growth zone in Schizosaccharomyces pombe. *J Cell Sci*, *118*(Pt 9), 1843-1850. https://doi.org/10.1242/jcs.02311

Chang, F. (1999). Movement of a cytokinesis factor cdc12p to the site of cell division. *Curr Biol*, *9*(15), 849-852. https://doi.org/10.1016/s0960-9822(99)80372-8

Chang, F., Drubin, D., & Nurse, P. (1997). cdc12p, a protein required for cytokinesis in fission yeast, is a component of the cell division ring and interacts with profilin. *J Cell Biol*, *137*(1), 169-182. https://doi.org/10.1083/jcb.137.1.169

Chang, F., Woollard, A., & Nurse, P. (1996). Isolation and characterization of fission yeast mutants defective in the assembly and placement of the contractile actin ring. *J Cell Sci*, *109 (Pt 1)*, 131-142.

Che, D. L., Duan, L., Zhang, K., & Cui, B. (2015). The Dual Characteristics of Light-Induced Cryptochrome 2, Homo-oligomerization and Heterodimerization, for Optogenetic Manipulation in Mammalian Cells. *ACS Synth Biol*, *4*(10), 1124-1135. https://doi.org/10.1021/acssynbio.5b00048

Chen, A., Arora, P. D., McCulloch, C. A., & Wilde, A. (2017). Cytokinesis requires localized β-actin filament production by an actin isoform specific nucleator. *Nat Commun*, *8*(1), 1530. https://doi.org/10.1038/s41467-017-01231-x

Chen, C., Ding, X., Akram, N., Xue, S., & Luo, S. Z. (2019). Fused in Sarcoma: Properties, Self-Assembly and Correlation with Neurodegenerative Diseases. *Molecules*, *24*(8). https://doi.org/10.3390/molecules24081622

Chen, M. J., Shih, C. L., & Wang, K. (1993). Nebulin as an actin zipper. A two-module nebulin fragment promotes actin nucleation and stabilizes actin filaments. *J Biol Chem*, *268*(27), 20327-20334.

Cheng, H., Sugiura, R., Wu, W., Fujita, M., Lu, Y., Sio, S. O., Kawai, R., Takegawa, K., Shuntoh, H., & Kuno, T. (2002). Role of the Rab GTP-binding protein Ypt3 in the fission yeast exocytic pathway and its connection to calcineurin function. *Mol Biol Cell*, *13*(8), 2963-2976. https://doi.org/10.1091/mbc.01-09-0463

Cheng, L., Zhang, J., Ahmad, S., Rozier, L., Yu, H., Deng, H., & Mao, Y. (2011). Aurora B regulates formin mDia3 in achieving metaphase chromosome alignment. *Dev Cell*, *20*(3), 342-352. https://doi.org/10.1016/j.devcel.2011.01.008

Chereau, D., Kerff, F., Graceffa, P., Grabarek, Z., Langsetmo, K., & Dominguez, R. (2005). Actin-bound structures of Wiskott-Aldrich syndrome protein (WASP)-homology domain 2 and the implications for filament assembly. *Proc Natl Acad Sci U S A*, *102*(46), 16644-16649. https://doi.org/10.1073/pnas.0507021102

Chhabra, E. S., & Higgs, H. N. (2006). INF2 Is a WASP homology 2 motif-containing formin that severs actin filaments and accelerates both polymerization and depolymerization. *J Biol Chem*, *281*(36), 26754-26767. https://doi.org/10.1074/jbc.M604666200

Chhabra, E. S., Ramabhadran, V., Gerber, S. A., & Higgs, H. N. (2009). INF2 is an endoplasmic reticulum-associated formin protein. *J Cell Sci*, *122*(Pt 9), 1430-1440. https://doi.org/10.1242/jcs.040691

Christensen, J. R., Hocky, G. M., Homa, K. E., Morganthaler, A. N., Hitchcock-DeGregori, S. E., Voth, G. A., & Kovar, D. R. (2017). Competition between Tropomyosin, Fimbrin, and ADF/Cofilin drives their sorting to distinct actin filament networks. *Elife*, *6*. https://doi.org/10.7554/eLife.23152

Chugh, P., & Paluch, E. K. (2018). The actin cortex at a glance. *J Cell Sci*, *131*(14). https://doi.org/10.1242/jcs.186254

Clayton, J. E., Pollard, L. W., Sckolnick, M., Bookwalter, C. S., Hodges, A. R., Trybus, K. M., & Lord, M. (2014). Fission yeast tropomyosin specifies directed transport of myosin-V along actin cables. *Mol Biol Cell*, *25*(1), 66-75. https://doi.org/10.1091/mbc.E13-04-0200

Clayton, J. E., Sammons, M. R., Stark, B. C., Hodges, A. R., & Lord, M. (2010). Differential regulation of unconventional fission yeast myosins via the actin track. *Curr Biol*, *20*(16), 1423-1431. https://doi.org/10.1016/j.cub.2010.07.026

Collins, A., Warrington, A., Taylor, K. A., & Svitkina, T. (2011). Structural organization of the actin cytoskeleton at sites of clathrin-mediated endocytosis. *Curr Biol*, *21*(14), 1167-1175. https://doi.org/10.1016/j.cub.2011.05.048

Colpan, M., Moroz, N. A., & Kostyukova, A. S. (2013). Tropomodulins and tropomyosins: working as a team. *J Muscle Res Cell Motil*, *34*(3-4), 247-260. https://doi.org/10.1007/s10974-013-9349-6

Coluccio, A. E., Rodriguez, R. K., Kernan, M. J., & Neiman, A. M. (2008). The yeast spore wall enables spores to survive passage through the digestive tract of Drosophila. *PLoS One*, *3*(8), e2873. https://doi.org/10.1371/journal.pone.0002873

Conibear, E. (2010). Converging views of endocytosis in yeast and mammals. *Curr Opin Cell Biol*, *22*(4), 513-518. https://doi.org/10.1016/j.ceb.2010.05.009

Cooper, J. A. (1987). Effects of cytochalasin and phalloidin on actin. *J Cell Biol*, *105*(4), 1473-1478. https://doi.org/10.1083/jcb.105.4.1473

Cooper, J. A., Buhle, E. L., Jr., Walker, S. B., Tsong, T. Y., & Pollard, T. D. (1983). Kinetic evidence for a monomer activation step in actin polymerization. *Biochemistry*, *22*(9), 2193-2202. https://doi.org/10.1021/bi00278a021

Cortés, J. C., Carnero, E., Ishiguro, J., Sánchez, Y., Durán, A., & Ribas, J. C. (2005). The novel fission yeast (1,3)beta-D-glucan synthase catalytic subunit Bgs4p is essential during both cytokinesis and polarized growth. *J Cell Sci*, *118*(Pt 1), 157-174. https://doi.org/10.1242/jcs.01585

Cortés, J. C., Ishiguro, J., Durán, A., & Ribas, J. C. (2002). Localization of the (1,3)beta-D-glucan synthase catalytic subunit homologue Bgs1p/Cps1p from fission yeast suggests that it is involved in septation, polarized growth, mating, spore wall formation and spore germination. *J Cell Sci*, *115*(Pt 21), 4081-4096. https://doi.org/10.1242/jcs.00085

Cortés, J. C., Konomi, M., Martins, I. M., Muñoz, J., Moreno, M. B., Osumi, M., Durán, A., & Ribas, J. C. (2007). The (1,3)beta-D-glucan synthase subunit Bgs1p is responsible for the fission yeast primary septum formation. *Mol Microbiol*, *65*(1), 201-217. https://doi.org/10.1111/j.1365-2958.2007.05784.x

Coulton, A. T., East, D. A., Galinska-Rakoczy, A., Lehman, W., & Mulvihill, D. P. (2010). The recruitment of acetylated and unacetylated tropomyosin to distinct actin polymers permits the discrete regulation of specific myosins in fission yeast. *J Cell Sci*, *123*(Pt 19), 3235-3243. https://doi.org/10.1242/jcs.069971

Courtemanche, N. (2018). Mechanisms of formin-mediated actin assembly and dynamics. *Biophys Rev*, *10*(6), 1553-1569. https://doi.org/10.1007/s12551-018-0468-6

Courtemanche, N., Lee, J. Y., Pollard, T. D., & Greene, E. C. (2013). Tension modulates actin filament polymerization mediated by formin and profilin. *Proc Natl Acad Sci U S A*, *110*(24), 9752-9757. https://doi.org/10.1073/pnas.1308257110

Courtemanche, N., & Pollard, T. D. (2012). Determinants of Formin Homology 1 (FH1) domain function in actin filament elongation by formins. *J Biol Chem*, *287*(10), 7812-7820. https://doi.org/10.1074/jbc.M111.322958

Courtemanche, N., & Pollard, T. D. (2013). Interaction of profilin with the barbed end of actin filaments. *Biochemistry*, *52*(37), 6456-6466. https://doi.org/10.1021/bi400682n

Craven, R. A., Griffiths, D. J., Sheldrick, K. S., Randall, R. E., Hagan, I. M., & Carr, A. M. (1998). Vectors for the expression of tagged proteins in Schizosaccharomyces pombe. *Gene*, *221*(1), 59-68. https://doi.org/10.1016/s0378-1119(98)00434-x

Crockford, D., Turjman, N., Allan, C., & Angel, J. (2010). Thymosin beta4: structure, function, and biological properties supporting current and future clinical applications. *Ann N Y Acad Sci*, *1194*, 179-189. https://doi.org/10.1111/j.1749-6632.2010.05492.x

Croft, W., Hill, C., McCann, E., Bond, M., Esparza-Franco, M., Bennett, J., Rand, D., Davey, J., & Ladds, G. (2013). A physiologically required G protein-coupled receptor (GPCR)-regulator of G protein signaling (RGS) interaction that compartmentalizes RGS activity. *J Biol Chem*, *288*(38), 27327-27342. https://doi.org/10.1074/jbc.M113.497826

Curto, M., Sharifmoghadam, M. R., Calpena, E., De León, N., Hoya, M., Doncel, C., Leatherwood, J., & Valdivieso, M. H. (2014). Membrane organization and cell fusion during mating in fission yeast requires multipass membrane protein Prm1. *Genetics*, *196*(4), 1059-1076. https://doi.org/10.1534/genetics.113.159558

Dass, R., Mulder, F. A. A., & Nielsen, J. T. (2020). ODiNPred: comprehensive prediction of protein order and disorder. *Sci Rep*, *10*(1), 14780. https://doi.org/10.1038/s41598-020-71716-1

DeNofrio, D., Hoock, T. C., & Herman, I. M. (1989). Functional sorting of actin isoforms in microvascular pericytes. *J Cell Biol*, *109*(1), 191-202. https://doi.org/10.1083/jcb.109.1.191

Di Nardo, A., Gareus, R., Kwiatkowski, D., & Witke, W. (2000). Alternative splicing of the mouse profilin II gene generates functionally different profilin isoforms. *J Cell Sci*, *113 Pt 21*, 3795-3803.

Dohrmann, M., & Wörheide, G. (2017). Dating early animal evolution using phylogenomic data. *Sci Rep*, *7*(1), 3599. https://doi.org/10.1038/s41598-017-03791-w

Dominguez, R. (2016). The WH2 Domain and Actin Nucleation: Necessary but Insufficient. *Trends Biochem Sci*, *41*(6), 478-490. https://doi.org/10.1016/j.tibs.2016.03.004

Dong, Y., Pruyne, D., & Bretscher, A. (2003). Formin-dependent actin assembly is regulated by distinct modes of Rho signaling in yeast. *J Cell Biol*, *161*(6), 1081-1092. https://doi.org/10.1083/jcb.200212040

Drazic, A., Aksnes, H., Marie, M., Boczkowska, M., Varland, S., Timmerman, E., Foyn, H., Glomnes, N., Rebowski, G., Impens, F., Gevaert, K., Dominguez, R., & Arnesen, T. (2018). NAA80 is actin's N-terminal acetyltransferase and regulates cytoskeleton assembly and cell motility. *Proc Natl Acad Sci U S A*, *115*(17), 4399-4404. https://doi.org/10.1073/pnas.1718336115

Drees, B., Brown, C., Barrell, B. G., & Bretscher, A. (1995). Tropomyosin is essential in yeast, yet the TPM1 and TPM2 products perform distinct functions. *J Cell Biol*, *128*(3), 383-392. https://doi.org/10.1083/jcb.128.3.383

Dudin, O., Bendezú, F. O., Groux, R., Laroche, T., Seitz, A., & Martin, S. G. (2015). A formin-nucleated actin aster concentrates cell wall hydrolases for cell fusion in fission yeast. *J Cell Biol*, *208*(7), 897-911. https://doi.org/10.1083/jcb.201411124

Dudin, O., Merlini, L., Bendezú, F. O., Groux, R., Vincenzetti, V., & Martin, S. G. (2017). A systematic screen for morphological abnormalities during fission yeast sexual reproduction identifies a mechanism of actin aster formation for cell fusion. *PLoS Genet*, *13*(4), e1006721. https://doi.org/10.1371/journal.pgen.1006721

Dudin, O., Merlini, L., & Martin, S. G. (2016). Spatial focalization of pheromone/MAPK signaling triggers commitment to cell-cell fusion. *Genes Dev*, *30*(19), 2226-2239. https://doi.org/10.1101/gad.286922.116

Duncan, M. C., Cope, M. J., Goode, B. L., Wendland, B., & Drubin, D. G. (2001). Yeast Eps15-like endocytic protein, Pan1p, activates the Arp2/3 complex. *Nat Cell Biol*, *3*(7), 687-690. https://doi.org/10.1038/35083087

Düster, R., Kaltheuner, I. H., Schmitz, M., & Geyer, M. (2021). 1,6-Hexanediol, commonly used to dissolve liquid-liquid phase separated condensates, directly impairs kinase and phosphatase activities. *J Biol Chem*, *296*, 100260. https://doi.org/10.1016/j.jbc.2021.100260

East, D. A., & Mulvihill, D. P. (2011). Regulation and function of the fission yeast myosins. *J Cell Sci*, *124*(Pt 9), 1383-1390. https://doi.org/10.1242/jcs.078527

Edwards, M., McConnell, P., Schafer, D. A., & Cooper, J. A. (2015). CPI motif interaction is necessary for capping protein function in cells. *Nat Commun*, *6*, 8415. https://doi.org/10.1038/ncomms9415

Edwards, M., Zwolak, A., Schafer, D. A., Sept, D., Dominguez, R., & Cooper, J. A. (2014). Capping protein regulators fine-tune actin assembly dynamics. *Nat Rev Mol Cell Biol*, *15*(10), 677-689. https://doi.org/10.1038/nrm3869

Egel, R. (1977). Selective spore survival during replica-plating of fission yeast. *Arch Microbiol*, *112*(1), 109-110. https://doi.org/10.1007/bf00446662

Egel, R., Willer, M., Kjaerulff, S., Davey, J., & Nielsen, O. (1994). Assessment of pheromone production and response in fission yeast by a halo test of induced sporulation. *Yeast*, *10*(10), 1347-1354. https://doi.org/10.1002/yea.320101012

Eitzen, G. (2003). Actin remodeling to facilitate membrane fusion. *Biochim Biophys Acta*, *1641*(2-3), 175-181. https://doi.org/10.1016/s0167-4889(03)00087-9

Elam, W. A., Kang, H., & De la Cruz, E. M. (2013). Biophysics of actin filament severing by cofilin. *FEBS Lett*, *587*(8), 1215-1219. https://doi.org/10.1016/j.febslet.2013.01.062

Ennomani, H., Letort, G., Guérin, C., Martiel, J. L., Cao, W., Nédélec, F., De La Cruz, E. M., Théry, M., & Blanchoin, L. (2016). Architecture and Connectivity Govern Actin Network Contractility. *Curr Biol*, *26*(5), 616-626. https://doi.org/10.1016/j.cub.2015.12.069

Erdős, G., Pajkos, M., & Dosztányi, Z. (2021). IUPred3: prediction of protein disorder enhanced with unambiguous experimental annotation and visualization of evolutionary conservation. *Nucleic Acids Res*, *49*(W1), W297-w303. https://doi.org/10.1093/nar/gkab408

Estes, J. E., Selden, L. A., Kinosian, H. J., & Gershman, L. C. (1992). Tightly-bound divalent cation of actin. *J Muscle Res Cell Motil*, *13*(3), 272-284. https://doi.org/10.1007/bf01766455

Estravís, M., Rincón, S. A., Santos, B., & Pérez, P. (2011). Cdc42 regulates multiple membrane traffic events in fission yeast. *Traffic*, *12*(12), 1744-1758. https://doi.org/10.1111/j.1600-0854.2011.01275.x

Evangelista, M., Blundell, K., Longtine, M. S., Chow, C. J., Adames, N., Pringle, J. R., Peter, M., & Boone, C. (1997). Bni1p, a yeast formin linking cdc42p and the actin cytoskeleton during polarized morphogenesis. *Science*, *276*(5309), 118-122. https://doi.org/10.1126/science.276.5309.118

Fair, B. J., & Pleiss, J. A. (2017). The power of fission: yeast as a tool for understanding complex splicing. *Curr Genet*, *63*(3), 375-380. https://doi.org/10.1007/s00294-016-0647-6

Farrell, K. B., McDonald, S., Lamb, A. K., Worcester, C., Peersen, O. B., & Di Pietro, S. M. (2017). Novel function of a dynein light chain in actin assembly during clathrin-mediated endocytosis. *J Cell Biol*, *216*(8), 2565-2580. https://doi.org/10.1083/jcb.201604123

Feeser, E. A., Ignacio, C. M., Krendel, M., & Ostap, E. M. (2010). Myo1e binds anionic phospholipids with high affinity. *Biochemistry*, *49*(43), 9353-9360. https://doi.org/10.1021/bi1012657

Fehon, R. G., McClatchey, A. I., & Bretscher, A. (2010). Organizing the cell cortex: the role of ERM proteins. *Nat Rev Mol Cell Biol*, *11*(4), 276-287. https://doi.org/10.1038/nrm2866

Feierbach, B., & Chang, F. (2001). Roles of the fission yeast formin for3p in cell polarity, actin cable formation and symmetric cell division. *Curr Biol*, *11*(21), 1656-1665. https://doi.org/10.1016/s0960-9822(01)00525-5

Ferron, F., Rebowski, G., Lee, S. H., & Dominguez, R. (2007). Structural basis for the recruitment of profilin-actin complexes during filament elongation by Ena/VASP. *Embo j*, *26*(21), 4597-4606. https://doi.org/10.1038/sj.emboj.7601874

Foth, B. J., Goedecke, M. C., & Soldati, D. (2006). New insights into myosin evolution and classification. *Proc Natl Acad Sci U S A*, *103*(10), 3681-3686. https://doi.org/10.1073/pnas.0506307103

Franzmann, T. M., & Alberti, S. (2019). Prion-like low-complexity sequences: Key regulators of protein solubility and phase behavior. *J Biol Chem*, *294*(18), 7128-7136. https://doi.org/10.1074/jbc.TM118.001190

Freedman, S. L., Suarez, C., Winkelman, J. D., Kovar, D. R., Voth, G. A., Dinner, A. R., & Hocky, G. M. (2019). Mechanical and kinetic factors drive sorting of F-actin cross-linkers on bundles. *Proc Natl Acad Sci U S A*, *116*(33), 16192-16197. https://doi.org/10.1073/pnas.1820814116

Fyrberg, E. A., Fyrberg, C. C., Biggs, J. R., Saville, D., Beall, C. J., & Ketchum, A. (1998). Functional nonequivalence of Drosophila actin isoforms. *Biochem Genet*, *36*(7-8), 271-287. https://doi.org/10.1023/a:1018785127079

Gachet, Y., & Hyams, J. S. (2005). Endocytosis in fission yeast is spatially associated with the actin cytoskeleton during polarised cell growth and cytokinesis. *J Cell Sci*, *118*(Pt 18), 4231-4242. https://doi.org/10.1242/jcs.02530

Gaillard, J., Ramabhadran, V., Neumanne, E., Gurel, P., Blanchoin, L., Vantard, M., & Higgs, H. N. (2011). Differential interactions of the formins INF2, mDia1, and mDia2 with microtubules. *Mol Biol Cell*, *22*(23), 4575-4587. https://doi.org/10.1091/mbc.E11-07-0616

Galletta, B. J., Chuang, D. Y., & Cooper, J. A. (2008). Distinct roles for Arp2/3 regulators in actin assembly and endocytosis. *PLoS Biol*, *6*(1), e1. https://doi.org/10.1371/journal.pbio.0060001

Galletta, B. J., Mooren, O. L., & Cooper, J. A. (2010). Actin dynamics and endocytosis in yeast and mammals. *Curr Opin Biotechnol*, *21*(5), 604-610. https://doi.org/10.1016/j.copbio.2010.06.006

Gallo Castro, D., & Martin, S. G. (2018). Differential GAP requirement for Cdc42-GTP polarization during proliferation and sexual reproduction. *J Cell Biol*, *217*(12), 4215-4229. https://doi.org/10.1083/jcb.201806016

Gandhi, M., Achard, V., Blanchoin, L., & Goode, B. L. (2009). Coronin switches roles in actin disassembly depending on the nucleotide state of actin. *Mol Cell*, *34*(3), 364-374. https://doi.org/10.1016/j.molcel.2009.02.029

Gao, L., & Bretscher, A. (2008). Analysis of unregulated formin activity reveals how yeast can balance F-actin assembly between different microfilament-based organizations. *Mol Biol Cell*, *19*(4), 1474-1484. https://doi.org/10.1091/mbc.e07-05-0520

Gao, L., Liu, W., & Bretscher, A. (2010). The yeast formin Bnr1p has two localization regions that show spatially and temporally distinct association with septin structures. *Mol Biol Cell*, *21*(7), 1253-1262. https://doi.org/10.1091/mbc.e09-10-0861

Gateva, G., Kremneva, E., Reindl, T., Kotila, T., Kogan, K., Gressin, L., Gunning, P. W., Manstein, D. J., Michelot, A., & Lappalainen, P. (2017). Tropomyosin Isoforms Specify Functionally Distinct Actin Filament Populations In Vitro. *Curr Biol*, *27*(5), 705-713. https://doi.org/10.1016/j.cub.2017.01.018

Girao, H., Geli, M. I., & Idrissi, F. Z. (2008). Actin in the endocytic pathway: from yeast to mammals. *FEBS Lett*, *582*(14), 2112-2119. https://doi.org/10.1016/j.febslet.2008.04.011

Glotzer, M. (2017). Cytokinesis in Metazoa and Fungi. *Cold Spring Harb Perspect Biol*, *9*(10). https://doi.org/10.1101/cshperspect.a022343

Goddard, A., Ladds, G., Forfar, R., & Davey, J. (2006). Identification of Gnr1p, a negative regulator of G alpha signalling in Schizosaccharomyces pombe, and its complementation by human G beta subunits. *Fungal Genet Biol*, *43*(12), 840-851. https://doi.org/10.1016/j.fgb.2006.06.005

Gokhin, D. S., & Fowler, V. M. (2011). Tropomodulin capping of actin filaments in striated muscle development and physiology. *J Biomed Biotechnol*, *2011*, 103069. https://doi.org/10.1155/2011/103069

Goley, E. D., Rodenbusch, S. E., Martin, A. C., & Welch, M. D. (2004). Critical conformational changes in the Arp2/3 complex are induced by nucleotide and nucleation promoting factor. *Mol Cell*, *16*(2), 269-279. https://doi.org/10.1016/j.molcel.2004.09.018

Goley, E. D., & Welch, M. D. (2006). The ARP2/3 complex: an actin nucleator comes of age. *Nat Rev Mol Cell Biol*, *7*(10), 713-726. https://doi.org/10.1038/nrm2026

Goode, B. L., & Eck, M. J. (2007). Mechanism and function of formins in the control of actin assembly. *Annu Rev Biochem*, *76*, 593-627. https://doi.org/10.1146/annurev.biochem.75.103004.142647

Gorelik, R., Yang, C., Kameswaran, V., Dominguez, R., & Svitkina, T. (2011). Mechanisms of plasma membrane targeting of formin mDia2 through its amino terminal domains. *Mol Biol Cell*, *22*(2), 189-201. https://doi.org/10.1091/mbc.E10-03-0256

Graziano, B. R., DuPage, A. G., Michelot, A., Breitsprecher, D., Moseley, J. B., Sagot, I., Blanchoin, L., & Goode, B. L. (2011). Mechanism and cellular function of Bud6 as an actin nucleation-promoting factor. *Mol Biol Cell*, *22*(21), 4016-4028. https://doi.org/10.1091/mbc.E11-05-0404

Gressin, L., Guillotin, A., Guérin, C., Blanchoin, L., & Michelot, A. (2015). Architecture dependence of actin filament network disassembly. *Curr Biol*, *25*(11), 1437-1447. https://doi.org/10.1016/j.cub.2015.04.011

Guillen-Chable, F., Bayona, A., Rodríguez-Zapata, L. C., & Castano, E. (2021). Phase Separation of Intrinsically Disordered Nucleolar Proteins Relate to Localization and Function. *Int J Mol Sci*, *22*(23). https://doi.org/10.3390/ijms222313095

Gunning, P., O'Neill, G., & Hardeman, E. (2008). Tropomyosin-based regulation of the actin cytoskeleton in time and space. *Physiol Rev*, *88*(1), 1-35. https://doi.org/10.1152/physrev.00001.2007

Gunning, P. W., Ghoshdastider, U., Whitaker, S., Popp, D., & Robinson, R. C. (2015). The evolution of compositionally and functionally distinct actin filaments. *J Cell Sci*, *128*(11), 2009-2019. https://doi.org/10.1242/jcs.165563

Hall, A. E., & Rose, M. D. (2019). Cell fusion in yeast is negatively regulated by components of the cell wall integrity pathway. *Mol Biol Cell*, *30*(4), 441-452. https://doi.org/10.1091/mbc.E18-04-0236

Hammer, J. A., 3rd, & Sellers, J. R. (2011). Walking to work: roles for class V myosins as cargo transporters. *Nat Rev Mol Cell Biol*, *13*(1), 13-26. https://doi.org/10.1038/nrm3248

Hansen, S. D., & Mullins, R. D. (2010). VASP is a processive actin polymerase that requires monomeric actin for barbed end association. *J Cell Biol*, *191*(3), 571-584. https://doi.org/10.1083/jcb.201003014

Harris, E. S., Li, F., & Higgs, H. N. (2004). The mouse formin, FRLalpha, slows actin filament barbed end elongation, competes with capping protein, accelerates polymerization from monomers, and severs filaments. *J Biol Chem*, *279*(19), 20076-20087. https://doi.org/10.1074/jbc.M312718200

Hatanaka, M., & Shimoda, C. (2001). The cyclic AMP/PKA signal pathway is required for initiation of spore germination in Schizosaccharomyces pombe. *Yeast*, *18*(3), 207-217. https://doi.org/10.1002/1097-0061(200102)18:3<207::Aid-yea661>3.0.Co;2-i

Hayles, J., & Nurse, P. (2018). Introduction to Fission Yeast as a Model System. *Cold Spring Harb Protoc*, *2018*(5). https://doi.org/10.1101/pdb.top079749

Heiman, M. G., & Walter, P. (2000). Prm1p, a pheromone-regulated multispanning membrane protein, facilitates plasma membrane fusion during yeast mating. *J Cell Biol*, *151*(3), 719-730. https://doi.org/10.1083/jcb.151.3.719

Helston, R. M., Box, J. A., Tang, W., & Baumann, P. (2010). Schizosaccharomyces cryophilus sp. nov., a new species of fission yeast. *FEMS Yeast Res*, *10*(6), 779-786. https://doi.org/10.1111/j.1567-1364.2010.00657.x

Herman, I. M. (1993). Actin isoforms. *Curr Opin Cell Biol*, *5*(1), 48-55. https://doi.org/10.1016/s0955-0674(05)80007-9

Hernandez-Valladares, M., Kim, T., Kannan, B., Tung, A., Aguda, A. H., Larsson, M., Cooper, J. A., & Robinson, R. C. (2010). Structural characterization of a capping protein interaction motif defines a family of actin filament regulators. *Nat Struct Mol Biol*, *17*(4), 497-503. https://doi.org/10.1038/nsmb.1792

Hernández, J. M., & Podbilewicz, B. (2017). The hallmarks of cell-cell fusion. *Development*, *144*(24), 4481-4495. https://doi.org/10.1242/dev.155523

Hetrick, B., Han, M. S., Helgeson, L. A., & Nolen, B. J. (2013). Small molecules CK-666 and CK-869 inhibit actin-related protein 2/3 complex by blocking an activating conformational change. *Chem Biol*, *20*(5), 701-712. https://doi.org/10.1016/j.chembiol.2013.03.019

Higgs, H. N. (2005). Formin proteins: a domain-based approach. *Trends Biochem Sci*, *30*(6), 342-353. https://doi.org/10.1016/j.tibs.2005.04.014

Higgs, H. N., & Peterson, K. J. (2005). Phylogenetic analysis of the formin homology 2 domain. *Mol Biol Cell*, *16*(1), 1-13. https://doi.org/10.1091/mbc.e04-07-0565

Hirota, K., Tanaka, K., Watanabe, Y., & Yamamoto, M. (2001). Functional analysis of the C-terminal cytoplasmic region of the M-factor receptor in fission yeast. *Genes Cells*, *6*(3), 201-214. https://doi.org/10.1046/j.1365-2443.2001.00415.x

Hitchcock-DeGregori, S. E., Sampath, P., & Pollard, T. D. (1988). Tropomyosin inhibits the rate of actin polymerization by stabilizing actin filaments. *Biochemistry*, *27*(26), 9182-9185. https://doi.org/10.1021/bi00426a016

Hodges, A. R., Krementsova, E. B., Bookwalter, C. S., Fagnant, P. M., Sladewski, T. E., & Trybus, K. M. (2012). Tropomyosin is essential for processive movement of a class V myosin from budding yeast. *Curr Biol*, *22*(15), 1410-1416. https://doi.org/10.1016/j.cub.2012.05.035

Hoffman, C. S., Wood, V., & Fantes, P. A. (2015). An Ancient Yeast for Young Geneticists: A Primer on the Schizosaccharomyces pombe Model System. *Genetics*, *201*(2), 403-423. https://doi.org/10.1534/genetics.115.181503

Hofweber, M., Hutten, S., Bourgeois, B., Spreitzer, E., Niedner-Boblenz, A., Schifferer, M., Ruepp, M. D., Simons, M., Niessing, D., Madl, T., & Dormann, D. (2018). Phase Separation of FUS Is Suppressed by Its Nuclear Import Receptor and Arginine Methylation. *Cell*, *173*(3), 706-719.e713. https://doi.org/10.1016/j.cell.2018.03.004

Holmes, K. C., Popp, D., Gebhard, W., & Kabsch, W. (1990). Atomic model of the actin filament. *Nature*, *347*(6288), 44-49. https://doi.org/10.1038/347044a0

Homa, K. E., Zsolnay, V., Anderson, C. A., O'Connell, M. E., Neidt, E. M., Voth, G. A., Bidone, T. C., & Kovar, D. R. (2021). Formin Cdc12's specific actin assembly properties are tailored for cytokinesis in fission yeast. *Biophys J*, *120*(15), 2984-2997. https://doi.org/10.1016/j.bpj.2021.06.023

Honoré, B., Madsen, P., Andersen, A. H., & Leffers, H. (1993). Cloning and expression of a novel human profilin variant, profilin II. *FEBS Lett*, *330*(2), 151-155. https://doi.org/10.1016/0014-5793(93)80262-s

Huang, J., Huang, Y., Yu, H., Subramanian, D., Padmanabhan, A., Thadani, R., Tao, Y., Tang, X., Wedlich-Soldner, R., & Balasubramanian, M. K. (2012). Nonmedially assembled F-actin cables incorporate into the actomyosin ring in fission yeast. *J Cell Biol*, *199*(5), 831-847. https://doi.org/10.1083/jcb.201209044

Huang, S., Robinson, R. C., Gao, L. Y., Matsumoto, T., Brunet, A., Blanchoin, L., & Staiger, C. J. (2005). Arabidopsis VILLIN1 generates actin filament cables that are resistant to depolymerization. *Plant Cell*, *17*(2), 486-501. https://doi.org/10.1105/tpc.104.028555

Husson, C., Renault, L., Didry, D., Pantaloni, D., & Carlier, M. F. (2011). Cordon-Bleu uses WH2 domains as multifunctional dynamizers of actin filament assembly. *Mol Cell*, *43*(3), 464-477. https://doi.org/10.1016/j.molcel.2011.07.010

Huxley, H. E. (1969). The mechanism of muscular contraction. *Science*, *164*(3886), 1356-1365. https://doi.org/10.1126/science.164.3886.1356

Hyman, A. A., Weber, C. A., & Jülicher, F. (2014). Liquid-liquid phase separation in biology. *Annu Rev Cell Dev Biol*, *30*, 39-58. https://doi.org/10.1146/annurev-cellbio-100913-013325

Imai, Y., & Yamamoto, M. (1992). Schizosaccharomyces pombe sxa1+ and sxa2+ encode putative proteases involved in the mating response. *Mol Cell Biol*, *12*(4), 1827-1834. https://doi.org/10.1128/mcb.12.4.1827-1834.1992

Inoue, A., Saito, J., Ikebe, R., & Ikebe, M. (2002). Myosin IXb is a single-headed minus-end-directed processive motor. *Nat Cell Biol*, *4*(4), 302-306. https://doi.org/10.1038/ncb774

Iskratsch, T., Reijntjes, S., Dwyer, J., Toselli, P., Dégano, I. R., Dominguez, I., & Ehler, E. (2013). Two distinct phosphorylation events govern the function of muscle FHOD3. *Cell Mol Life Sci*, *70*(5), 893-908. https://doi.org/10.1007/s00018-012-1154-7

Iwasa, J. H., & Mullins, R. D. (2007). Spatial and temporal relationships between actin-filament nucleation, capping, and disassembly. *Curr Biol*, *17*(5), 395-406. https://doi.org/10.1016/j.cub.2007.02.012

Jansen, S., & Goode, B. L. (2019). Tropomyosin isoforms differentially tune actin filament length and disassembly. *Mol Biol Cell*, *30*(5), 671-679. https://doi.org/10.1091/mbc.E18-12-0815

Jégou, A., Carlier, M. F., & Romet-Lemonne, G. (2013). Formin mDia1 senses and generates mechanical forces on actin filaments. *Nat Commun*, *4*, 1883. https://doi.org/10.1038/ncomms2888

Jenuwein, T., & Allis, C. D. (2001). Translating the histone code. *Science*, *293*(5532), 1074-1080. https://doi.org/10.1126/science.1063127

Jin, H., McCaffery, J. M., & Grote, E. (2008). Ergosterol promotes pheromone signaling and plasma membrane fusion in mating yeast. *J Cell Biol*, *180*(4), 813-826. https://doi.org/10.1083/jcb.200705076

Johnson, M., East, D. A., & Mulvihill, D. P. (2014). Formins determine the functional properties of actin filaments in yeast. *Curr Biol*, *24*(13), 1525-1530. https://doi.org/10.1016/j.cub.2014.05.034

Johnston, A. B., Hilton, D. M., McConnell, P., Johnson, B., Harris, M. T., Simone, A., Amarasinghe, G. K., Cooper, J. A., & Goode, B. L. (2018). A novel mode of capping protein-regulation by twinfilin. *Elife*, *7*. https://doi.org/10.7554/eLife.41313

Kadzik, R. S., Homa, K. E., & Kovar, D. R. (2020). F-Actin Cytoskeleton Network Self-Organization Through Competition and Cooperation. *Annu Rev Cell Dev Biol*, *36*, 35-60. https://doi.org/10.1146/annurev-cellbio-032320-094706

Kaksonen, M., Sun, Y., & Drubin, D. G. (2003). A pathway for association of receptors, adaptors, and actin during endocytic internalization. *Cell*, *115*(4), 475-487. https://doi.org/10.1016/s0092-8674(03)00883-3

Kaksonen, M., Toret, C. P., & Drubin, D. G. (2005). A modular design for the clathrin- and actin-mediated endocytosis machinery. *Cell*, *123*(2), 305-320. https://doi.org/10.1016/j.cell.2005.09.024

Kamasaki, T., Arai, R., Osumi, M., & Mabuchi, I. (2005). Directionality of F-actin cables changes during the fission yeast cell cycle. *Nat Cell Biol*, *7*(9), 916-917. https://doi.org/10.1038/ncb1295

Kandasamy, M. K., Burgos-Rivera, B., McKinney, E. C., Ruzicka, D. R., & Meagher, R. B. (2007). Class-specific interaction of profilin and ADF isovariants with actin in the regulation of plant development. *Plant Cell*, *19*(10), 3111-3126. https://doi.org/10.1105/tpc.107.052621

Kandasamy, M. K., McKinney, E. C., & Meagher, R. B. (2002). Functional nonequivalency of actin isovariants in Arabidopsis. *Mol Biol Cell*, *13*(1), 251-261. https://doi.org/10.1091/mbc.01-07-0342

Karagiannis, J., Bimbó, A., Rajagopalan, S., Liu, J., & Balasubramanian, M. K. (2005). The nuclear kinase Lsk1p positively regulates the septation initiation network and promotes the successful completion of cytokinesis in response to perturbation of the actomyosin ring in Schizosaccharomyces pombe. *Mol Biol Cell*, *16*(1), 358-371. https://doi.org/10.1091/mbc.e04-06-0502

Kennedy, M. J., Hughes, R. M., Peteya, L. A., Schwartz, J. W., Ehlers, M. D., & Tucker, C. L. (2010). Rapid blue-light-mediated induction of protein interactions in living cells. *Nat Methods*, *7*(12), 973-975. https://doi.org/10.1038/nmeth.1524

Kerber, M. L., & Cheney, R. E. (2011). Myosin-X: a MyTH-FERM myosin at the tips of filopodia. *J Cell Sci*, *124*(Pt 22), 3733-3741. https://doi.org/10.1242/jcs.023549

Kijima, S. T., Hirose, K., Kong, S. G., Wada, M., & Uyeda, T. Q. (2016). Distinct Biochemical Properties of Arabidopsis thaliana Actin Isoforms. *Plant Cell Physiol*, *57*(1), 46-56. https://doi.org/10.1093/pcp/pcv176

Kijima, S. T., Staiger, C. J., Katoh, K., Nagasaki, A., Ito, K., & Uyeda, T. Q. P. (2018). Arabidopsis vegetative actin isoforms, AtACT2 and AtACT7, generate distinct filament arrays in living plant cells. *Sci Rep*, *8*(1), 4381. https://doi.org/10.1038/s41598-018-22707-w

Kim, D. U., Hayles, J., Kim, D., Wood, V., Park, H. O., Won, M., Yoo, H. S., Duhig, T., Nam, M., Palmer, G., Han, S., Jeffery, L., Baek, S. T., Lee, H., Shim, Y. S., Lee, M., Kim, L., Heo, K. S., Noh, E. J., . . . Hoe, K. L. (2010). Analysis of a genome-wide set of gene deletions in the fission yeast Schizosaccharomyces pombe. *Nat Biotechnol*, *28*(6), 617-623. https://doi.org/10.1038/nbt.1628

Kim, K., Galletta, B. J., Schmidt, K. O., Chang, F. S., Blumer, K. J., & Cooper, J. A. (2006). Actin-based motility during endocytosis in budding yeast. *Mol Biol Cell*, *17*(3), 1354-1363. https://doi.org/10.1091/mbc.e05-10-0925

Kim, K., McCully, M. E., Bhattacharya, N., Butler, B., Sept, D., & Cooper, J. A. (2007). Structure/function analysis of the interaction of phosphatidylinositol 4,5-bisphosphate with actin-capping protein: implications for how capping protein binds the actin filament. *J Biol Chem*, *282*(8), 5871-5879. https://doi.org/10.1074/jbc.M609850200

Kim, K., Yamashita, A., Wear, M. A., Maéda, Y., & Cooper, J. A. (2004). Capping protein binding to actin in yeast: biochemical mechanism and physiological relevance. *J Cell Biol*, *164*(4), 567-580. https://doi.org/10.1083/jcb.200308061

Kislauskis, E. H., Li, Z., Singer, R. H., & Taneja, K. L. (1993). Isoform-specific 3'-untranslated sequences sort alpha-cardiac and beta-cytoplasmic actin messenger RNAs to different cytoplasmic compartments. *J Cell Biol*, *123*(1), 165-172. https://doi.org/10.1083/jcb.123.1.165

Kjaerulff, S., Lautrup-Larsen, I., Truelsen, S., Pedersen, M., & Nielsen, O. (2005). Constitutive activation of the fission yeast pheromone-responsive pathway induces ectopic meiosis and reveals ste11 as a mitogen-activated protein kinase target. *Mol Cell Biol*, *25*(5), 2045-2059. https://doi.org/10.1128/mcb.25.5.2045-2059.2005

Klemm, S. L., Shipony, Z., & Greenleaf, W. J. (2019). Chromatin accessibility and the regulatory epigenome. *Nat Rev Genet*, *20*(4), 207-220. https://doi.org/10.1038/s41576-018-0089-8

Koestler, S. A., Rottner, K., Lai, F., Block, J., Vinzenz, M., & Small, J. V. (2009). F- and G-actin concentrations in lamellipodia of moving cells. *PLoS One*, *4*(3), e4810. https://doi.org/10.1371/journal.pone.0004810

Kojima, H., Ishijima, A., & Yanagida, T. (1994). Direct measurement of stiffness of single actin filaments with and without tropomyosin by in vitro nanomanipulation. *Proc Natl Acad Sci U S A*, *91*(26), 12962-12966. https://doi.org/10.1073/pnas.91.26.12962

Kovar, D. R., Drøbak, B. K., & Staiger, C. J. (2000). Maize profilin isoforms are functionally distinct. *Plant Cell*, *12*(4), 583-598. https://doi.org/10.1105/tpc.12.4.583

Kovar, D. R., Harris, E. S., Mahaffy, R., Higgs, H. N., & Pollard, T. D. (2006). Control of the assembly of ATP- and ADP-actin by formins and profilin. *Cell*, *124*(2), 423-435. https://doi.org/10.1016/j.cell.2005.11.038

Kovar, D. R., Kuhn, J. R., Tichy, A. L., & Pollard, T. D. (2003). The fission yeast cytokinesis formin Cdc12p is a barbed end actin filament capping protein gated by profilin. *J Cell Biol*, *161*(5), 875-887. https://doi.org/10.1083/jcb.200211078

Kovar, D. R., & Pollard, T. D. (2004). Insertional assembly of actin filament barbed ends in association with formins produces piconewton forces. *Proc Natl Acad Sci U S A*, *101*(41), 14725-14730. https://doi.org/10.1073/pnas.0405902101

Kovar, D. R., Sirotkin, V., & Lord, M. (2011). Three's company: the fission yeast actin cytoskeleton. *Trends Cell Biol*, *21*(3), 177-187. https://doi.org/10.1016/j.tcb.2010.11.001

Kovar, D. R., Wu, J. Q., & Pollard, T. D. (2005). Profilin-mediated competition between capping protein and formin Cdc12p during cytokinesis in fission yeast. *Mol Biol Cell*, *16*(5), 2313-2324. https://doi.org/10.1091/mbc.e04-09-0781

Kremer, J. R., Mastronarde, D. N., & McIntosh, J. R. (1996). Computer visualization of three-dimensional image data using IMOD. *J Struct Biol*, *116*(1), 71-76. https://doi.org/10.1006/jsbi.1996.0013

Krendel, M., & Mooseker, M. S. (2005). Myosins: tails (and heads) of functional diversity. *Physiology (Bethesda)*, *20*, 239-251. https://doi.org/10.1152/physiol.00014.2005

Kuhn, J. R., & Pollard, T. D. (2007). Single molecule kinetic analysis of actin filament capping. Polyphosphoinositides do not dissociate capping proteins. *J Biol Chem*, *282*(38), 28014-28024. https://doi.org/10.1074/jbc.M705287200

Kukulski, W., Schorb, M., Welsch, S., Picco, A., Kaksonen, M., & Briggs, J. A. (2012). Precise, correlated fluorescence microscopy and electron tomography of lowicryl sections using fluorescent fiducial markers. *Methods Cell Biol*, *111*, 235-257. https://doi.org/10.1016/b978-0-12-416026-2.00013-3

Kumari, N., & Yadav, S. (2019). Modulation of protein oligomerization: An overview. *Prog Biophys Mol Biol*, *149*, 99-113. https://doi.org/10.1016/j.pbiomolbio.2019.03.003

Kurahashi, H., Imai, Y., & Yamamoto, M. (2002). Tropomyosin is required for the cell fusion process during conjugation in fission yeast. *Genes Cells*, *7*(4), 375-384. https://doi.org/10.1046/j.1365-2443.2002.00526.x

Ladds, G., Rasmussen, E. M., Young, T., Nielsen, O., & Davey, J. (1996). The sxa2-dependent inactivation of the P-factor mating pheromone in the fission yeast Schizosaccharomyces pombe. *Mol Microbiol*, *20*(1), 35-42. https://doi.org/10.1111/j.1365-2958.1996.tb02486.x

Lanzetti, L. (2007). Actin in membrane trafficking. *Curr Opin Cell Biol*, *19*(4), 453-458. https://doi.org/10.1016/j.ceb.2007.04.017

Laplante, C., Huang, F., Tebbs, I. R., Bewersdorf, J., & Pollard, T. D. (2016). Molecular organization of cytokinesis nodes and contractile rings by super-resolution fluorescence microscopy of live fission yeast. *Proc Natl Acad Sci U S A*, *113*(40), E5876-e5885. https://doi.org/10.1073/pnas.1608252113

Lebrand, C., Dent, E. W., Strasser, G. A., Lanier, L. M., Krause, M., Svitkina, T. M., Borisy, G. G., & Gertler, F. B. (2004). Critical role of Ena/VASP proteins for filopodia formation in neurons and in function downstream of netrin-1. *Neuron*, *42*(1), 37-49. https://doi.org/10.1016/s0896-6273(04)00108-4

Lecointre, G., Guyader, H. L., Visset, D., Bosquet, G., Charrier, D., Dejouannet, J. F., Haessig, T., & Norwood, J. (2017). *Classification phylogénétique du vivant*. Belin. https://books.google.ch/books?id=Gl6ytAEACAAJ

Lee, I. J., Coffman, V. C., & Wu, J. Q. (2012). Contractile-ring assembly in fission yeast cytokinesis: Recent advances and new perspectives. *Cytoskeleton (Hoboken)*, *69*(10), 751-763. https://doi.org/10.1002/cm.21052

Lee, W. L., Bezanilla, M., & Pollard, T. D. (2000). Fission yeast myosin-I, Myo1p, stimulates actin assembly by Arp2/3 complex and shares functions with WASp. *J Cell Biol*, *151*(4), 789-800. https://doi.org/10.1083/jcb.151.4.789

Levone, B. R., Lenzken, S. C., Antonaci, M., Maiser, A., Rapp, A., Conte, F., Reber, S., Mechtersheimer, J., Ronchi, A. E., Mühlemann, O., Leonhardt, H., Cardoso, M. C., Ruepp, M. D., & Barabino, S. M. L. (2021). FUS-dependent liquid-liquid phase separation is important for DNA repair initiation. *J Cell Biol*, *220*(5). https://doi.org/10.1083/jcb.202008030

Levskaya, A., Weiner, O. D., Lim, W. A., & Voigt, C. A. (2009). Spatiotemporal control of cell signalling using a light-switchable protein interaction. *Nature*, *461*(7266), 997-1001. https://doi.org/10.1038/nature08446

Li, S., Yoshizawa, T., Yamazaki, R., Fujiwara, A., Kameda, T., & Kitahara, R. (2021). Pressure and Temperature Phase Diagram for Liquid-Liquid Phase Separation of the RNA-Binding Protein Fused in Sarcoma. *J Phys Chem B*, *125*(25), 6821-6829. https://doi.org/10.1021/acs.jpcb.1c01451

Lin, J. J., Hegmann, T. E., & Lin, J. L. (1988). Differential localization of tropomyosin isoforms in cultured nonmuscle cells. *J Cell Biol*, *107*(2), 563-572. https://doi.org/10.1083/jcb.107.2.563

Lin, M. C., Galletta, B. J., Sept, D., & Cooper, J. A. (2010). Overlapping and distinct functions for cofilin, coronin and Aip1 in actin dynamics in vivo. *J Cell Sci*, *123*(Pt 8), 1329-1342. https://doi.org/10.1242/jcs.065698

Lo Presti, L., Chang, F., & Martin, S. G. (2012). Myosin Vs organize actin cables in fission yeast. *Mol Biol Cell*, *23*(23), 4579-4591. https://doi.org/10.1091/mbc.E12-07-0499

Machesky, L. M., Atkinson, S. J., Ampe, C., Vandekerckhove, J., & Pollard, T. D. (1994). Purification of a cortical complex containing two unconventional actins from Acanthamoeba by affinity chromatography on profilin-agarose. *J Cell Biol*, *127*(1), 107-115. https://doi.org/10.1083/jcb.127.1.107

Machnicka, B., Czogalla, A., Hryniewicz-Jankowska, A., Bogusławska, D. M., Grochowalska, R., Heger, E., & Sikorski, A. F. (2014). Spectrins: a structural platform for stabilization and activation of membrane channels, receptors and transporters. *Biochim Biophys Acta*, *1838*(2), 620-634. https://doi.org/10.1016/j.bbamem.2013.05.002

MacLean-Fletcher, S., & Pollard, T. D. (1980). Mechanism of action of cytochalasin B on actin. *Cell*, *20*(2), 329-341. https://doi.org/10.1016/0092-8674(80)90619-4

Mallavarapu, A., & Mitchison, T. (1999). Regulated actin cytoskeleton assembly at filopodium tips controls their extension and retraction. *J Cell Biol*, *146*(5), 1097-1106. https://doi.org/10.1083/jcb.146.5.1097

Martin, S. G. (2009). Microtubule-dependent cell morphogenesis in the fission yeast. *Trends Cell Biol*, *19*(9), 447-454. https://doi.org/10.1016/j.tcb.2009.06.003

Martin, S. G. (2016). Role and organization of the actin cytoskeleton during cell-cell fusion. *Semin Cell Dev Biol*, *60*, 121-126. https://doi.org/10.1016/j.semcdb.2016.07.025

Martin, S. G., & Chang, F. (2006). Dynamics of the formin for3p in actin cable assembly. *Curr Biol*, *16*(12), 1161-1170. https://doi.org/10.1016/j.cub.2006.04.040

Martin, S. G., Rincón, S. A., Basu, R., Pérez, P., & Chang, F. (2007). Regulation of the formin for3p by cdc42p and bud6p. *Mol Biol Cell*, *18*(10), 4155-4167. https://doi.org/10.1091/mbc.e07-02-0094

Masters, T. A., Kendrick-Jones, J., & Buss, F. (2017). Myosins: Domain Organisation, Motor Properties, Physiological Roles and Cellular Functions. *Handb Exp Pharmacol*, *235*, 77-122. https://doi.org/10.1007/164_2016_29

Mastronarde, D. N. (2005). Automated electron microscope tomography using robust prediction of specimen movements. *J Struct Biol*, *152*(1), 36-51. https://doi.org/10.1016/j.jsb.2005.07.007

Mastronarde, D. N., & Held, S. R. (2017). Automated tilt series alignment and tomographic reconstruction in IMOD. *J Struct Biol*, *197*(2), 102-113. https://doi.org/10.1016/j.jsb.2016.07.011

Mata, J., & Bähler, J. (2006). Global roles of Ste11p, cell type, and pheromone in the control of gene expression during early sexual differentiation in fission yeast. *Proc Natl Acad Sci U S A*, *103*(42), 15517-15522. https://doi.org/10.1073/pnas.0603403103

Matheos, D., Metodiev, M., Muller, E., Stone, D., & Rose, M. D. (2004). Pheromone-induced polarization is dependent on the Fus3p MAPK acting through the formin Bni1p. *J Cell Biol*, *165*(1), 99-109. https://doi.org/10.1083/jcb.200309089

Matsudaira, P. (1994). Actin crosslinking proteins at the leading edge. *Semin Cell Biol*, *5*(3), 165-174. https://doi.org/10.1006/scel.1994.1021

McCullough, B. R., Grintsevich, E. E., Chen, C. K., Kang, H., Hutchison, A. L., Henn, A., Cao, W., Suarez, C., Martiel, J. L., Blanchoin, L., Reisler, E., & De La Cruz, E. M. (2011). Cofilin-linked changes in actin filament flexibility promote severing. *Biophys J*, *101*(1), 151-159. https://doi.org/10.1016/j.bpj.2011.05.049

McElhinny, A. S., Kazmierski, S. T., Labeit, S., & Gregorio, C. C. (2003). Nebulin: the nebulous, multifunctional giant of striated muscle. *Trends Cardiovasc Med*, *13*(5), 195-201. https://doi.org/10.1016/s1050-1738(03)00076-8

McGough, A., Pope, B., Chiu, W., & Weeds, A. (1997). Cofilin changes the twist of F-actin: implications for actin filament dynamics and cellular function. *J Cell Biol*, *138*(4), 771-781. https://doi.org/10.1083/jcb.138.4.771

Mejillano, M. R., Kojima, S., Applewhite, D. A., Gertler, F. B., Svitkina, T. M., & Borisy, G. G. (2004). Lamellipodial versus filopodial mode of the actin nanomachinery: pivotal role of the filament barbed end. *Cell*, *118*(3), 363-373. https://doi.org/10.1016/j.cell.2004.07.019

Merino, F., Pospich, S., & Raunser, S. (2020). Towards a structural understanding of the remodeling of the actin cytoskeleton. *Seminars in Cell & Developmental Biology* (Vol. 102, pp. 51-64). Academic Press. https://doi.org/10.1016/j.semcdb.2019.11.018

Merlini, L., Dudin, O., & Martin, S. G. (2013). Mate and fuse: how yeast cells do it. *Open Biol*, *3*(3), 130008. https://doi.org/10.1098/rsob.130008

Merlini, L., Khalili, B., Bendezú, F. O., Hurwitz, D., Vincenzetti, V., Vavylonis, D., & Martin, S. G. (2016). Local Pheromone Release from Dynamic Polarity Sites Underlies Cell-Cell Pairing during Yeast Mating. *Curr Biol*, *26*(8), 1117-1125. https://doi.org/10.1016/j.cub.2016.02.064

Merlini, L., Khalili, B., Dudin, O., Michon, L., Vincenzetti, V., & Martin, S. G. (2018). Inhibition of Ras activity coordinates cell fusion with cell-cell contact during yeast mating. *J Cell Biol*, *217*(4), 1467-1483. https://doi.org/10.1083/jcb.201708195

Miao, Y., Wong, C. C., Mennella, V., Michelot, A., Agard, D. A., Holt, L. J., Yates, J. R., 3rd, & Drubin, D. G. (2013). Cell-cycle regulation of formin-mediated actin cable assembly. *Proc Natl Acad Sci U S A*, *110*(47), E4446-4455. https://doi.org/10.1073/pnas.1314000110

Michelot, A., Berro, J., Guérin, C., Boujemaa-Paterski, R., Staiger, C. J., Martiel, J. L., & Blanchoin, L. (2007). Actin-filament stochastic dynamics mediated by ADF/cofilin. *Curr Biol*, *17*(10), 825-833. https://doi.org/10.1016/j.cub.2007.04.037

Michelot, A., Costanzo, M., Sarkeshik, A., Boone, C., Yates, J. R., 3rd, & Drubin, D. G. (2010). Reconstitution and protein composition analysis of endocytic actin patches. *Curr Biol*, *20*(21), 1890-1899. https://doi.org/10.1016/j.cub.2010.10.016

Michelot, A., Derivery, E., Paterski-Boujemaa, R., Guérin, C., Huang, S., Parcy, F., Staiger, C. J., & Blanchoin, L. (2006). A novel mechanism for the formation of actin-filament bundles by a nonprocessive formin. *Curr Biol*, *16*(19), 1924-1930. https://doi.org/10.1016/j.cub.2006.07.054

Michelot, A., & Drubin, D. G. (2011). Building distinct actin filament networks in a common cytoplasm. *Curr Biol*, *21*(14), R560-569. https://doi.org/10.1016/j.cub.2011.06.019

Michelot, A., Guérin, C., Huang, S., Ingouff, M., Richard, S., Rodiuc, N., Staiger, C. J., & Blanchoin, L. (2005). The formin homology 1 domain modulates the actin nucleation and bundling activity of Arabidopsis FORMIN1. *Plant Cell*, *17*(8), 2296-2313. https://doi.org/10.1105/tpc.105.030908

Mishra, M., Huang, J., & Balasubramanian, M. K. (2014). The yeast actin cytoskeleton. *FEMS Microbiol Rev*, *38*(2), 213-227. https://doi.org/10.1111/1574-6976.12064

Mogilner, A., & Oster, G. (2003). Force generation by actin polymerization II: the elastic ratchet and tethered filaments. *Biophys J*, *84*(3), 1591-1605. https://doi.org/10.1016/s0006-3495(03)74969-8

Mogilner, A., & Rubinstein, B. (2005). The physics of filopodial protrusion. *Biophys J*, *89*(2), 782-795. https://doi.org/10.1529/biophysj.104.056515

Mohandas, N., & Gallagher, P. G. (2008). Red cell membrane: past, present, and future. *Blood*, *112*(10), 3939-3948. https://doi.org/10.1182/blood-2008-07-161166

Monahan, Z., Ryan, V. H., Janke, A. M., Burke, K. A., Rhoads, S. N., Zerze, G. H., O'Meally, R., Dignon, G. L., Conicella, A. E., Zheng, W., Best, R. B., Cole, R. N., Mittal, J., Shewmaker, F., & Fawzi, N. L. (2017). Phosphorylation of the FUS low-complexity domain disrupts phase separation, aggregation, and toxicity. *Embo j*, *36*(20), 2951-2967. https://doi.org/10.15252/embj.201696394

Moseley, J. B., & Goode, B. L. (2005). Differential activities and regulation of Saccharomyces cerevisiae formin proteins Bni1 and Bnr1 by Bud6. *J Biol Chem*, *280*(30), 28023-28033. https://doi.org/10.1074/jbc.M503094200

Moseley, J. B., & Goode, B. L. (2006). The yeast actin cytoskeleton: from cellular function to biochemical mechanism. *Microbiol Mol Biol Rev*, *70*(3), 605-645. https://doi.org/10.1128/mmbr.00013-06

Moseley, J. B., Sagot, I., Manning, A. L., Xu, Y., Eck, M. J., Pellman, D., & Goode, B. L. (2004). A conserved mechanism for Bni1- and mDia1-induced actin assembly and dual regulation of Bni1 by Bud6 and profilin. *Mol Biol Cell*, *15*(2), 896-907. https://doi.org/10.1091/mbc.e03-08-0621

Muriel, O., Michon, L., Kukulski, W., & Martin, S. G. (2021). Ultrastructural plasma membrane asymmetries in tension and curvature promote yeast cell fusion. *J Cell Biol*, *220*(10). https://doi.org/10.1083/jcb.202103142

Murk, K., Wittenmayer, N., Michaelsen-Preusse, K., Dresbach, T., Schoenenberger, C. A., Korte, M., Jockusch, B. M., & Rothkegel, M. (2012). Neuronal profilin isoforms are addressed by different signalling pathways. *PLoS One*, *7*(3), e34167. https://doi.org/10.1371/journal.pone.0034167

Murray, D. T., Kato, M., Lin, Y., Thurber, K. R., Hung, I., McKnight, S. L., & Tycko, R. (2017). Structure of FUS Protein Fibrils and Its Relevance to Self-Assembly and Phase Separation of Low-Complexity Domains. *Cell*, *171*(3), 615-627.e616. https://doi.org/10.1016/j.cell.2017.08.048

Nag, S., Larsson, M., Robinson, R. C., & Burtnick, L. D. (2013). Gelsolin: the tail of a molecular gymnast. *Cytoskeleton (Hoboken)*, *70*(7), 360-384. https://doi.org/10.1002/cm.21117

Nagai, R., & Rebhun, L. I. (1966). Cytoplasmic microfilaments in streaming Nitella cells. *J Ultrastruct Res*, *14*(5), 571-589. https://doi.org/10.1016/s0022-5320(66)80083-7

Nagy, S., Ricca, B. L., Norstrom, M. F., Courson, D. S., Brawley, C. M., Smithback, P. A., & Rock, R. S. (2008). A myosin motor that selects bundled actin for motility. *Proc Natl Acad Sci U S A*, *105*(28), 9616-9620. https://doi.org/10.1073/pnas.0802592105

Nakano, K., & Mabuchi, I. (2006). Actin-capping protein is involved in controlling organization of actin cytoskeleton together with ADF/cofilin, profilin and F-actin crosslinking proteins in fission yeast. *Genes Cells*, *11*(8), 893-905. https://doi.org/10.1111/j.1365-2443.2006.00987.x

Nambiar, R., McConnell, R. E., & Tyska, M. J. (2010). Myosin motor function: the ins and outs of actin-based membrane protrusions. *Cell Mol Life Sci*, *67*(8), 1239-1254. https://doi.org/10.1007/s00018-009-0254-5

Naranjo-Ortiz, M. A., & Gabaldón, T. (2019). Fungal evolution: diversity, taxonomy and phylogeny of the Fungi. *Biol Rev Camb Philos Soc*, *94*(6), 2101-2137. https://doi.org/10.1111/brv.12550

Narita, A., Takeda, S., Yamashita, A., & Maéda, Y. (2006). Structural basis of actin filament capping at the barbed-end: a cryo-electron microscopy study. *Embo j*, *25*(23), 5626-5633. https://doi.org/10.1038/sj.emboj.7601395

Neidt, E. M., Scott, B. J., & Kovar, D. R. (2009). Formin differentially utilizes profilin isoforms to rapidly assemble actin filaments. *J Biol Chem*, *284*(1), 673-684. https://doi.org/10.1074/jbc.M804201200

Neidt, E. M., Skau, C. T., & Kovar, D. R. (2008). The cytokinesis formins from the nematode worm and fission yeast differentially mediate actin filament assembly. *J Biol Chem*, *283*(35), 23872-23883. https://doi.org/10.1074/jbc.M803734200

Niggli, V., & Rossy, J. (2008). Ezrin/radixin/moesin: versatile controllers of signaling molecules and of the cortical cytoskeleton. *Int J Biochem Cell Biol*, *40*(3), 344-349. https://doi.org/10.1016/j.biocel.2007.02.012

Nolen, B. J., Tomasevic, N., Russell, A., Pierce, D. W., Jia, Z., McCormick, C. D., Hartman, J., Sakowicz, R., & Pollard, T. D. (2009). Characterization of two classes of small molecule inhibitors of Arp2/3 complex. *Nature*, *460*(7258), 1031-1034. https://doi.org/10.1038/nature08231

Nurse, P., & Thuriaux, P. (1980). Regulatory genes controlling mitosis in the fission yeast Schizosaccharomyces pombe. *Genetics*, *96*(3), 627-637. https://doi.org/10.1093/genetics/96.3.627

Oda, T., Iwasa, M., Aihara, T., Maéda, Y., & Narita, A. (2009). The nature of the globular- to fibrous-actin transition. *Nature*, *457*(7228), 441-445. https://doi.org/10.1038/nature07685

Odronitz, F., & Kollmar, M. (2007). Drawing the tree of eukaryotic life based on the analysis of 2,269 manually annotated myosins from 328 species. *Genome Biol*, *8*(9), R196. https://doi.org/10.1186/gb-2007-8-9-r196

Ohshima, S., Abe, H., & Obinata, T. (1989). Isolation of profilin from embryonic chicken skeletal muscle and evaluation of its interaction with different actin isoforms. *J Biochem*, *105*(6), 855-857. https://doi.org/10.1093/oxfordjournals.jbchem.a122765

Otomo, T., Tomchick, D. R., Otomo, C., Machius, M., & Rosen, M. K. (2010). Crystal structure of the Formin mDia1 in autoinhibited conformation. *PLoS One*, *5*(9). https://doi.org/10.1371/journal.pone.0012896

Otomo, T., Tomchick, D. R., Otomo, C., Panchal, S. C., Machius, M., & Rosen, M. K. (2005). Structural basis of actin filament nucleation and processive capping by a formin homology 2 domain. *Nature*, *433*(7025), 488-494. https://doi.org/10.1038/nature03251

Otsubo, Y., & Yamamoto, M. (2012). Signaling pathways for fission yeast sexual differentiation at a glance. *J Cell Sci*, *125*(Pt 12), 2789-2793. https://doi.org/10.1242/jcs.094771

Pak, C. W., Kosno, M., Holehouse, A. S., Padrick, S. B., Mittal, A., Ali, R., Yunus, A. A., Liu, D. R., Pappu, R. V., & Rosen, M. K. (2016). Sequence Determinants of Intracellular Phase Separation by Complex Coacervation of a Disordered Protein. *Mol Cell*, *63*(1), 72-85. https://doi.org/10.1016/j.molcel.2016.05.042

Papp, G., Bugyi, B., Ujfalusi, Z., Barkó, S., Hild, G., Somogyi, B., & Nyitrai, M. (2006). Conformational changes in actin filaments induced by formin binding to the barbed end. *Biophys J*, *91*(7), 2564-2572. https://doi.org/10.1529/biophysj.106.087775

Pappas, C. T., Krieg, P. A., & Gregorio, C. C. (2010). Nebulin regulates actin filament lengths by a stabilization mechanism. *J Cell Biol*, *189*(5), 859-870. https://doi.org/10.1083/jcb.201001043

Patel, A., Lee, H. O., Jawerth, L., Maharana, S., Jahnel, M., Hein, M. Y., Stoynov, S., Mahamid, J., Saha, S., Franzmann, T. M., Pozniakovski, A., Poser, I., Maghelli, N., Royer, L. A., Weigert, M., Myers, E. W., Grill, S., Drechsel, D., Hyman, A. A., & Alberti, S. (2015). A Liquid-to-Solid Phase Transition of the ALS Protein FUS Accelerated by Disease Mutation. *Cell*, *162*(5), 1066-1077. https://doi.org/10.1016/j.cell.2015.07.047

Paul, A. S., & Pollard, T. D. (2008). The role of the FH1 domain and profilin in formin-mediated actin-filament elongation and nucleation. *Curr Biol*, *18*(1), 9-19. https://doi.org/10.1016/j.cub.2007.11.062

Paul, A. S., & Pollard, T. D. (2009). Review of the mechanism of processive actin filament elongation by formins. *Cell Motil Cytoskeleton*, *66*(8), 606-617. https://doi.org/10.1002/cm.20379

Pelham, R. J., Jr., & Chang, F. (2001). Role of actin polymerization and actin cables in actin-patch movement in Schizosaccharomyces pombe. *Nat Cell Biol*, *3*(3), 235-244. https://doi.org/10.1038/35060020

Perrin, B. J., & Ervasti, J. M. (2010). The actin gene family: function follows isoform. *Cytoskeleton (Hoboken)*, *67*(10), 630-634. https://doi.org/10.1002/cm.20475

Petersen, J., Nielsen, O., Egel, R., & Hagan, I. M. (1998a). F-actin distribution and function during sexual differentiation in Schizosaccharomyces pombe. *J Cell Sci*, *111 (Pt 7)*, 867-876.

Petersen, J., Nielsen, O., Egel, R., & Hagan, I. M. (1998b). FH3, a domain found in formins, targets the fission yeast formin Fus1 to the projection tip during conjugation. *J Cell Biol*, *141*(5), 1217-1228. https://doi.org/10.1083/jcb.141.5.1217

Petersen, J., Weilguny, D., Egel, R., & Nielsen, O. (1995). Characterization of fus1 of Schizosaccharomyces pombe: a developmentally controlled function needed for conjugation. *Mol Cell Biol*, *15*(7), 3697-3707. https://doi.org/10.1128/mcb.15.7.3697

Pettersen, E. F., Goddard, T. D., Huang, C. C., Couch, G. S., Greenblatt, D. M., Meng, E. C., & Ferrin, T. E. (2004). UCSF Chimera–a visualization system for exploratory research and analysis. *J Comput Chem, 25*(13), 1605-1612. https://doi.org/10.1002/jcc.20084

Polakova, S., Benko, Z., Zhang, L., & Gregan, J. (2014). Mal3, the Schizosaccharomyces pombe homolog of EB1, is required for karyogamy and for promoting oscillatory nuclear movement during meiosis. *Cell Cycle*, *13*(1), 72-77. https://doi.org/10.4161/cc.26815

Pollard, L. W., & Lord, M. (2014). Getting myosin-V on the right track: tropomyosin sorts transport in yeast. *Bioarchitecture*, *4*(1), 35-38. https://doi.org/10.4161/bioa.28204

Pollard, T. D. (2016). Actin and Actin-Binding Proteins. *Cold Spring Harb Perspect Biol*, *8*(8). https://doi.org/10.1101/cshperspect.a018226

Pollard, T. D. (2017). What We Know and Do Not Know About Actin. *Handb Exp Pharmacol*, *235*, 331-347. https://doi.org/10.1007/164_2016_44

Pollard, T. D., & Korn, E. D. (1973). Acanthamoeba myosin. I. Isolation from Acanthamoeba castellanii of an enzyme similar to muscle myosin. *J Biol Chem*, *248*(13), 4682-4690.

Pollard, T. D., & O'Shaughnessy, B. (2019). Molecular Mechanism of Cytokinesis. *Annu Rev Biochem*, *88*, 661-689. https://doi.org/10.1146/annurev-biochem-062917-012530

Pollard, T. D., & Wu, J. Q. (2010). Understanding cytokinesis: lessons from fission yeast. *Nat Rev Mol Cell Biol*, *11*(2), 149-155. https://doi.org/10.1038/nrm2834

Popowicz, G. M., Schleicher, M., Noegel, A. A., & Holak, T. A. (2006). Filamins: promiscuous organizers of the cytoskeleton. *Trends Biochem Sci*, *31*(7), 411-419. https://doi.org/10.1016/j.tibs.2006.05.006

Porta, J. C., & Borgstahl, G. E. (2012). Structural basis for profilin-mediated actin nucleotide exchange. *J Mol Biol*, *418*(1-2), 103-116. https://doi.org/10.1016/j.jmb.2012.02.012

Poukkula, M., Kremneva, E., Serlachius, M., & Lappalainen, P. (2011). Actin-depolymerizing factor homology domain: a conserved fold performing diverse roles in cytoskeletal dynamics. *Cytoskeleton (Hoboken)*, *68*(9), 471-490. https://doi.org/10.1002/cm.20530

Pring, M., Evangelista, M., Boone, C., Yang, C., & Zigmond, S. H. (2003). Mechanism of formin-induced nucleation of actin filaments. *Biochemistry*, *42*(2), 486-496. https://doi.org/10.1021/bi026520j

Proctor, S. A., Minc, N., Boudaoud, A., & Chang, F. (2012). Contributions of turgor pressure, the contractile ring, and septum assembly to forces in cytokinesis in fission yeast. *Curr Biol*, *22*(17), 1601-1608. https://doi.org/10.1016/j.cub.2012.06.042

Proszynski, T. J., Klemm, R., Bagnat, M., Gaus, K., & Simons, K. (2006). Plasma membrane polarization during mating in yeast cells. *J Cell Biol*, *173*(6), 861-866. https://doi.org/10.1083/jcb.200602007

Pruyne, D., Evangelista, M., Yang, C., Bi, E., Zigmond, S., Bretscher, A., & Boone, C. (2002). Role of formins in actin assembly: nucleation and barbed-end association. *Science*, *297*(5581), 612-615. https://doi.org/10.1126/science.1072309

Quinlan, M. E., Heuser, J. E., Kerkhoff, E., & Mullins, R. D. (2005). Drosophila Spire is an actin nucleation factor. *Nature*, *433*(7024), 382-388. https://doi.org/10.1038/nature03241

Ramachander, R., Kim, C. A., Phillips, M. L., Mackereth, C. D., Thanos, C. D., McIntosh, L. P., & Bowie, J. U. (2002). Oligomerization-dependent association of the SAM domains from Schizosaccharomyces pombe Byr2 and Ste4. *J Biol Chem*, *277*(42), 39585-39593. https://doi.org/10.1074/jbc.M207273200

Ramalingam, N., Zhao, H., Breitsprecher, D., Lappalainen, P., Faix, J., & Schleicher, M. (2010). Phospholipids regulate localization and activity of mDia1 formin. *Eur J Cell Biol*, *89*(10), 723-732. https://doi.org/10.1016/j.ejcb.2010.06.001

Rana, U., Brangwynne, C. P., & Panagiotopoulos, A. Z. (2021). Phase separation vs aggregation behavior for model disordered proteins. *J Chem Phys*, *155*(12), 125101. https://doi.org/10.1063/5.0060046

Rao, J. N., Madasu, Y., & Dominguez, R. (2014). Mechanism of actin filament pointed-end capping by tropomodulin. *Science*, *345*(6195), 463-467. https://doi.org/10.1126/science.1256159

Reber, S., Jutzi, D., Lindsay, H., Devoy, A., Mechtersheimer, J., Levone, B. R., Domanski, M., Bentmann, E., Dormann, D., Mühlemann, O., Barabino, S. M. L., & Ruepp, M. D. (2021). The phase separation-dependent FUS interactome reveals nuclear and cytoplasmic function of liquid-liquid phase separation. *Nucleic Acids Res*, *49*(13), 7713-7731. https://doi.org/10.1093/nar/gkab582

Reymann, A. C., Boujemaa-Paterski, R., Martiel, J. L., Guérin, C., Cao, W., Chin, H. F., De La Cruz, E. M., Théry, M., & Blanchoin, L. (2012). Actin network architecture can determine myosin motor activity. *Science*, *336*(6086), 1310-1314. https://doi.org/10.1126/science.1221708

Reymann, A. C., Martiel, J. L., Cambier, T., Blanchoin, L., Boujemaa-Paterski, R., & Théry, M. (2010). Nucleation geometry governs ordered actin networks structures. *Nat Mater*, *9*(10), 827-832. https://doi.org/10.1038/nmat2855

Rincón, S. A., Estravís, M., & Pérez, P. (2014). Cdc42 regulates polarized growth and cell integrity in fission yeast. *Biochem Soc Trans*, *42*(1), 201-205. https://doi.org/10.1042/bst20130155

Rincón, S. A., Ye, Y., Villar-Tajadura, M. A., Santos, B., Martin, S. G., & Pérez, P. (2009). Pob1 participates in the Cdc42 regulation of fission yeast actin cytoskeleton. *Mol Biol Cell*, *20*(20), 4390-4399. https://doi.org/10.1091/mbc.e09-03-0207

Rivero, F., Muramoto, T., Meyer, A. K., Urushihara, H., Uyeda, T. Q., & Kitayama, C. (2005). A comparative sequence analysis reveals a common GBD/FH3-FH1-FH2-DAD architecture in formins from Dictyostelium, fungi and metazoa. *BMC Genomics*, *6*, 28. https://doi.org/10.1186/1471-2164-6-28

Roberts-Galbraith, R. H., Chen, J. S., Wang, J., & Gould, K. L. (2009). The SH3 domains of two PCH family members cooperate in assembly of the Schizosaccharomyces pombe contractile ring. *J Cell Biol*, *184*(1), 113-127. https://doi.org/10.1083/jcb.200806044

Roberts-Galbraith, R. H., Ohi, M. D., Ballif, B. A., Chen, J. S., McLeod, I., McDonald, W. H., Gygi, S. P., Yates, J. R., 3rd, & Gould, K. L. (2010). Dephosphorylation of F-BAR protein Cdc15 modulates its conformation and stimulates its scaffolding activity at the cell division site. *Mol Cell*, *39*(1), 86-99. https://doi.org/10.1016/j.molcel.2010.06.012

Robinson, R. C., Turbedsky, K., Kaiser, D. A., Marchand, J. B., Higgs, H. N., Choe, S., & Pollard, T. D. (2001). Crystal structure of Arp2/3 complex. *Science*, *294*(5547), 1679-1684. https://doi.org/10.1126/science.1066333

Rollason, R., Wherlock, M., Heath, J. A., Heesom, K. J., Saleem, M. A., & Welsh, G. I. (2016). Disease causing mutations in inverted formin 2 regulate its binding to G-actin, F-actin capping protein (CapZ α-1) and profilin 2. *Biosci Rep*, *36*(1), e00302. https://doi.org/10.1042/bsr20150252

Romero, P., Obradovic, Z., Li, X., Garner, E. C., Brown, C. J., & Dunker, A. K. (2001). Sequence complexity of disordered protein. *Proteins*, *42*(1), 38-48. https://doi.org/10.1002/1097-0134(20010101)42:1<38::aid-prot50>3.0.co;2-3

Romero, S., Le Clainche, C., Didry, D., Egile, C., Pantaloni, D., & Carlier, M. F. (2004). Formin is a processive motor that requires profilin to accelerate actin assembly and associated ATP hydrolysis. *Cell*, *119*(3), 419-429. https://doi.org/10.1016/j.cell.2004.09.039

Rottner, K., Faix, J., Bogdan, S., Linder, S., & Kerkhoff, E. (2017). Actin assembly mechanisms at a glance. *J Cell Sci*, *130*(20), 3427-3435. https://doi.org/10.1242/jcs.206433

Rottner, K., Hänisch, J., & Campellone, K. G. (2010). WASH, WHAMM and JMY: regulation of Arp2/3 complex and beyond. *Trends Cell Biol*, *20*(11), 650-661. https://doi.org/10.1016/j.tcb.2010.08.014

Rotty, J. D., Wu, C., Haynes, E. M., Suarez, C., Winkelman, J. D., Johnson, H. E., Haugh, J. M., Kovar, D. R., & Bear, J. E. (2015). Profilin-1 serves as a gatekeeper for actin assembly by Arp2/3-dependent and -independent pathways. *Dev Cell*, *32*(1), 54-67. https://doi.org/10.1016/j.devcel.2014.10.026

Rouiller, I., Xu, X. P., Amann, K. J., Egile, C., Nickell, S., Nicastro, D., Li, R., Pollard, T. D., Volkmann, N., & Hanein, D. (2008). The structural basis of actin filament branching by the Arp2/3 complex. *J Cell Biol*, *180*(5), 887-895. https://doi.org/10.1083/jcb.200709092

Rould, M. A., Wan, Q., Joel, P. B., Lowey, S., & Trybus, K. M. (2006). Crystal structures of expressed non-polymerizable monomeric actin in the ADP and ATP states. *J Biol Chem*, *281*(42), 31909-31919. https://doi.org/10.1074/jbc.M601973200

Royle, S. J. (2006). The cellular functions of clathrin. *Cell Mol Life Sci*, *63*(16), 1823-1832. https://doi.org/10.1007/s00018-005-5587-0

Safer, D., Elzinga, M., & Nachmias, V. T. (1991). Thymosin beta 4 and Fx, an actin-sequestering peptide, are indistinguishable. *J Biol Chem*, *266*(7), 4029-4032.

Saha, S., Mundia, M. M., Zhang, F., Demers, R. W., Korobova, F., Svitkina, T., Perieteanu, A. A., Dawson, J. F., & Kashina, A. (2010). Arginylation regulates intracellular actin polymer level by modulating actin properties and binding of capping and severing proteins. *Mol Biol Cell*, *21*(8), 1350-1361. https://doi.org/10.1091/mbc.e09-09-0829

Sakamoto, C., Kawamoto, C., Takeuchi, K., Miyamoto, I., & Shuntoh, H. (2004). Fission yeast epsin, Ent1p is required for endocytosis and involved in actin organization. *Kobe J Med Sci*, *50*(1-2), 47-57.

Sali, A., & Blundell, T. L. (1993). Comparative protein modelling by satisfaction of spatial restraints. *J Mol Biol, 234*(3), 779-815. https://doi.org/10.1006/jmbi.1993.1626

Samarin, S., Romero, S., Kocks, C., Didry, D., Pantaloni, D., & Carlier, M. F. (2003). How VASP enhances actin-based motility. *J Cell Biol*, *163*(1), 131-142. https://doi.org/10.1083/jcb.200303191

Sánchez-Paredes, E., Kawasaki, L., Ongay-Larios, L., & Coria, R. (2011). The Gα subunit signals through the Ste50 protein during the mating pheromone response in the yeast Kluyveromyces lactis. *Eukaryot Cell*, *10*(4), 540-546. https://doi.org/10.1128/ec.00285-10

Schiffhauer, E. S., Luo, T., Mohan, K., Srivastava, V., Qian, X., Griffis, E. R., Iglesias, P. A., & Robinson, D. N. (2016). Mechanoaccumulative Elements of the Mammalian Actin Cytoskeleton. *Curr Biol*, *26*(11), 1473-1479. https://doi.org/10.1016/j.cub.2016.04.007

Schönichen, A., & Geyer, M. (2010). Fifteen formins for an actin filament: a molecular view on the regulation of human formins. *Biochim Biophys Acta*, *1803*(2), 152-163. https://doi.org/10.1016/j.bbamcr.2010.01.014

Schulte, A., Stolp, B., Schönichen, A., Pylypenko, O., Rak, A., Fackler, O. T., & Geyer, M. (2008). The human formin FHOD1 contains a bipartite structure of FH3 and GTPase-binding domains required for activation. *Structure*, *16*(9), 1313-1323. https://doi.org/10.1016/j.str.2008.06.008

Scott, B. J., Neidt, E. M., & Kovar, D. R. (2011). The functionally distinct fission yeast formins have specific actin-assembly properties. *Mol Biol Cell*, *22*(20), 3826-3839. https://doi.org/10.1091/mbc.E11-06-0492

Segev, N., Avinoam, O., & Podbilewicz, B. (2018). Fusogens. *Curr Biol*, *28*(8), R378-r380. https://doi.org/10.1016/j.cub.2018.01.024

Seike, T., Maekawa, H., Nakamura, T., & Shimoda, C. (2019). The asymmetric chemical structures of two mating pheromones reflect their differential roles in mating of fission yeast. *J Cell Sci*, *132*(12). https://doi.org/10.1242/jcs.230722

Shekhar, S., Kerleau, M., Kühn, S., Pernier, J., Romet-Lemonne, G., Jégou, A., & Carlier, M. F. (2015). Formin and capping protein together embrace the actin filament in a ménage à trois. *Nat Commun*, *6*, 8730. https://doi.org/10.1038/ncomms9730

Shekhar, S., Pernier, J., & Carlier, M. F. (2016). Regulators of actin filament barbed ends at a glance. *J Cell Sci*, *129*(6), 1085-1091. https://doi.org/10.1242/jcs.179994

Shen, X. X., Steenwyk, J. L., LaBella, A. L., Opulente, D. A., Zhou, X., Kominek, J., Li, Y., Groenewald, M., Hittinger, C. T., & Rokas, A. (2020). Genome-scale phylogeny and contrasting modes of genome evolution in the fungal phylum Ascomycota. *Sci Adv*, *6*(45). https://doi.org/10.1126/sciadv.abd0079

Shi, C., Kaminskyj, S., Caldwell, S., & Loewen, M. C. (2007). A role for a complex between activated G protein-coupled receptors in yeast cellular mating. *Proc Natl Acad Sci U S A*, *104*(13), 5395-5400. https://doi.org/10.1073/pnas.0608219104

Shi, M., You, K., Chen, T., Hou, C., Liang, Z., Liu, M., Wang, J., Wei, T., Qin, J., Chen, Y., Zhang, M. Q., & Li, T. (2021). Quantifying the phase separation property of chromatin-associated proteins under physiological conditions using an anti-1,6-hexanediol index. *Genome Biol*, *22*(1), 229. https://doi.org/10.1186/s13059-021-02456-2

Shimoda, C. (2004). Forespore membrane assembly in yeast: coordinating SPBs and membrane trafficking. *J Cell Sci*, *117*(Pt 3), 389-396. https://doi.org/10.1242/jcs.00980

Shin, M., van Leeuwen, J., Boone, C., & Bretscher, A. (2018). Yeast Aim21/Tda2 both regulates free actin by reducing barbed end assembly and forms a complex with Cap1/Cap2 to balance actin assembly between patches and cables. *Mol Biol Cell*, *29*(8), 923-936. https://doi.org/10.1091/mbc.E17-10-0592

Shin, Y., Berry, J., Pannucci, N., Haataja, M. P., Toettcher, J. E., & Brangwynne, C. P. (2017). Spatiotemporal Control of Intracellular Phase Transitions Using Light-Activated optoDroplets. *Cell*, *168*(1-2), 159-171.e114. https://doi.org/10.1016/j.cell.2016.11.054

Sinnar, S. A., Antoku, S., Saffin, J. M., Cooper, J. A., & Halpain, S. (2014). Capping protein is essential for cell migration in vivo and for filopodial morphology and dynamics. *Mol Biol Cell*, *25*(14), 2152-2160. https://doi.org/10.1091/mbc.E13-12-0749

Sipiczki, M. (2000). Where does fission yeast sit on the tree of life? *Genome Biol*, *1*(2), Reviews1011. https://doi.org/10.1186/gb-2000-1-2-reviews1011

Sipiczki, M., & Bozsik, A. (2000). The use of morphomutants to investigate septum formation and cell separation in Schizosaccharomyces pombe. *Arch Microbiol*, *174*(6), 386-392. https://doi.org/10.1007/s002030000214

Sirotkin, V., Beltzner, C. C., Marchand, J. B., & Pollard, T. D. (2005). Interactions of WASp, myosin-I, and verprolin with Arp2/3 complex during actin patch assembly in fission yeast. *J Cell Biol*, *170*(4), 637-648. https://doi.org/10.1083/jcb.200502053

Sirotkin, V., Berro, J., Macmillan, K., Zhao, L., & Pollard, T. D. (2010). Quantitative analysis of the mechanism of endocytic actin patch assembly and disassembly in fission yeast. *Mol Biol Cell*, *21*(16), 2894-2904. https://doi.org/10.1091/mbc.E10-02-0157

Sizonenko, G. I., Karpova, T. S., Gattermeir, D. J., & Cooper, J. A. (1996). Mutational analysis of capping protein function in Saccharomyces cerevisiae. *Mol Biol Cell*, *7*(1), 1-15. https://doi.org/10.1091/mbc.7.1.1

Skau, C. T., Courson, D. S., Bestul, A. J., Winkelman, J. D., Rock, R. S., Sirotkin, V., & Kovar, D. R. (2011). Actin filament bundling by fimbrin is important for endocytosis, cytokinesis, and polarization in fission yeast. *J Biol Chem*, *286*(30), 26964-26977. https://doi.org/10.1074/jbc.M111.239004

Skau, C. T., & Kovar, D. R. (2010). Fimbrin and tropomyosin competition regulates endocytosis and cytokinesis kinetics in fission yeast. *Curr Biol*, *20*(16), 1415-1422. https://doi.org/10.1016/j.cub.2010.06.020

Skau, C. T., Neidt, E. M., & Kovar, D. R. (2009). Role of tropomyosin in formin-mediated contractile ring assembly in fission yeast. *Mol Biol Cell*, *20*(8), 2160-2173. https://doi.org/10.1091/mbc.e08-12-1201

Skau, C. T., & Waterman, C. M. (2015). Specification of Architecture and Function of Actin Structures by Actin Nucleation Factors. *Annu Rev Biophys*, *44*, 285-310. https://doi.org/10.1146/annurev-biophys-060414-034308

Skoumpla, K., Coulton, A. T., Lehman, W., Geeves, M. A., & Mulvihill, D. P. (2007). Acetylation regulates tropomyosin function in the fission yeast Schizosaccharomyces pombe. *J Cell Sci*, *120*(Pt 9), 1635-1645. https://doi.org/10.1242/jcs.001115

Slajcherová, K., Fišerová, J., Fischer, L., & Schwarzerová, K. (2012). Multiple actin isotypes in plants: diverse genes for diverse roles? *Front Plant Sci*, *3*, 226. https://doi.org/10.3389/fpls.2012.00226

Small, J. V., Isenberg, G., & Celis, J. E. (1978). Polarity of actin at the leading edge of cultured cells. *Nature*, *272*(5654), 638-639. https://doi.org/10.1038/272638a0

Smith, M. A., Blankman, E., Gardel, M. L., Luettjohann, L., Waterman, C. M., & Beckerle, M. C. (2010). A zyxin-mediated mechanism for actin stress fiber maintenance and repair. *Dev Cell*, *19*(3), 365-376. https://doi.org/10.1016/j.devcel.2010.08.008

Sodek, J., Hodges, R. S., Smillie, L. B., & Jurasek, L. (1972). Amino-acid sequence of rabbit skeletal tropomyosin and its coiled-coil structure. *Proc Natl Acad Sci U S A*, *69*(12), 3800-3804. https://doi.org/10.1073/pnas.69.12.3800

Sohrmann, M., Fankhauser, C., Brodbeck, C., & Simanis, V. (1996). The dmf1/mid1 gene is essential for correct positioning of the division septum in fission yeast. *Genes Dev*, *10*(21), 2707-2719. https://doi.org/10.1101/gad.10.21.2707

Song, B. D., & Schmid, S. L. (2003). A molecular motor or a regulator? Dynamin's in a class of its own. *Biochemistry*, *42*(6), 1369-1376. https://doi.org/10.1021/bi027062h

Soulard, A., Friant, S., Fitterer, C., Orange, C., Kaneva, G., Mirey, G., & Winsor, B. (2005). The WASP/Las17p-interacting protein Bzz1p functions with Myo5p in an early stage of endocytosis. *Protoplasma*, *226*(1-2), 89-101. https://doi.org/10.1007/s00709-005-0108-4

Spector, I., Shochet, N. R., Blasberger, D., & Kashman, Y. (1989). Latrunculins--novel marine macrolides that disrupt microfilament organization and affect cell growth: I. Comparison with cytochalasin D. *Cell Motil Cytoskeleton*, *13*(3), 127-144. https://doi.org/10.1002/cm.970130302

Staiger, C. J., Goodbody, K. C., Hussey, P. J., Valenta, R., Drøbak, B. K., & Lloyd, C. W. (1993). The profilin multigene family of maize: differential expression of three isoforms. *Plant J*, *4*(4), 631-641. https://doi.org/10.1046/j.1365-313x.1993.04040631.x

Staus, D. P., Taylor, J. M., & Mack, C. P. (2011). Enhancement of mDia2 activity by Rho-kinase-dependent phosphorylation of the diaphanous autoregulatory domain. *Biochem J*, *439*(1), 57-65. https://doi.org/10.1042/bj20101700

Suarez, C., Carroll, R. T., Burke, T. A., Christensen, J. R., Bestul, A. J., Sees, J. A., James, M. L., Sirotkin, V., & Kovar, D. R. (2015). Profilin regulates F-actin network homeostasis by favoring formin over Arp2/3 complex. *Dev Cell*, *32*(1), 43-53. https://doi.org/10.1016/j.devcel.2014.10.027

Sun, Y., Martin, A. C., & Drubin, D. G. (2006). Endocytic internalization in budding yeast requires coordinated actin nucleation and myosin motor activity. *Dev Cell*, *11*(1), 33-46. https://doi.org/10.1016/j.devcel.2006.05.008

Svitkina, T. (2018). The Actin Cytoskeleton and Actin-Based Motility. *Cold Spring Harb Perspect Biol*, *10*(1). https://doi.org/10.1101/cshperspect.a018267

Svitkina, T. M., Bulanova, E. A., Chaga, O. Y., Vignjevic, D. M., Kojima, S., Vasiliev, J. M., & Borisy, G. G. (2003). Mechanism of filopodia initiation by reorganization of a dendritic network. *J Cell Biol*, *160*(3), 409-421. https://doi.org/10.1083/jcb.200210174

Takano, K., Toyooka, K., & Suetsugu, S. (2008). EFC/F-BAR proteins and the N-WASP-WIP complex induce membrane curvature-dependent actin polymerization. *Embo j*, *27*(21), 2817-2828. https://doi.org/10.1038/emboj.2008.216

Takeya, R., Taniguchi, K., Narumiya, S., & Sumimoto, H. (2008). The mammalian formin FHOD1 is activated through phosphorylation by ROCK and mediates thrombin-induced stress fibre formation in endothelial cells. *Embo j*, *27*(4), 618-628. https://doi.org/10.1038/emboj.2008.7

Tanaka, K., Takeda, S., Mitsuoka, K., Oda, T., Kimura-Sakiyama, C., Maéda, Y., & Narita, A. (2018). Structural basis for cofilin binding and actin filament disassembly. *Nat Commun*, *9*(1), 1860. https://doi.org/10.1038/s41467-018-04290-w

Taoka, M., Ichimura, T., Wakamiya-Tsuruta, A., Kubota, Y., Araki, T., Obinata, T., & Isobe, T. (2003). V-1, a protein expressed transiently during murine cerebellar development, regulates actin polymerization via interaction with capping protein. *J Biol Chem*, *278*(8), 5864-5870. https://doi.org/10.1074/jbc.M211509200

Taslimi, A., Vrana, J. D., Chen, D., Borinskaya, S., Mayer, B. J., Kennedy, M. J., & Tucker, C. L. (2014). An optimized optogenetic clustering tool for probing protein interaction and function. *Nat Commun*, *5*, 4925. https://doi.org/10.1038/ncomms5925

Tatebe, H., Nakano, K., Maximo, R., & Shiozaki, K. (2008). Pom1 DYRK regulates localization of the Rga4 GAP to ensure bipolar activation of Cdc42 in fission yeast. *Curr Biol*, *18*(5), 322-330. https://doi.org/10.1016/j.cub.2008.02.005

Terman, J. R., & Kashina, A. (2013). Post-translational modification and regulation of actin. *Curr Opin Cell Biol*, *25*(1), 30-38. https://doi.org/10.1016/j.ceb.2012.10.009

Thompson, M. E., Heimsath, E. G., Gauvin, T. J., Higgs, H. N., & Kull, F. J. (2013). FMNL3 FH2-actin structure gives insight into formin-mediated actin nucleation and elongation. *Nat Struct Mol Biol, 20*(1), 111-118. https://doi.org/10.1038/nsmb.2462

Ti, S. C., & Pollard, T. D. (2011). Purification of actin from fission yeast Schizosaccharomyces pombe and characterization of functional differences from muscle actin. *J Biol Chem*, *286*(7), 5784-5792. https://doi.org/10.1074/jbc.M110.199794

Tilney, L. G., Connelly, P. S., Vranich, K. A., Shaw, M. K., & Guild, G. M. (1998). Why are two different cross-linkers necessary for actin bundle formation in vivo and what does each cross-link contribute? *J Cell Biol*, *143*(1), 121-133. https://doi.org/10.1083/jcb.143.1.121

Tojkander, S., Gateva, G., & Lappalainen, P. (2012). Actin stress fibers--assembly, dynamics and biological roles. *J Cell Sci*, *125*(Pt 8), 1855-1864. https://doi.org/10.1242/jcs.098087

Tolliday, N., VerPlank, L., & Li, R. (2002). Rho1 directs formin-mediated actin ring assembly during budding yeast cytokinesis. *Curr Biol*, *12*(21), 1864-1870. https://doi.org/10.1016/s0960-9822(02)01238-1

Tsompana, M., & Buck, M. J. (2014). Chromatin accessibility: a window into the genome. *Epigenetics Chromatin*, *7*(1), 33. https://doi.org/10.1186/1756-8935-7-33

Tu, H., Barr, M., Dong, D. L., & Wigler, M. (1997). Multiple regulatory domains on the Byr2 protein kinase. *Mol Cell Biol*, *17*(10), 5876-5887. https://doi.org/10.1128/mcb.17.10.5876

Vaillant, D. C., Copeland, S. J., Davis, C., Thurston, S. F., Abdennur, N., & Copeland, J. W. (2008). Interaction of the N- and C-terminal autoregulatory domains of FRL2 does not inhibit FRL2 activity. *J Biol Chem*, *283*(48), 33750-33762. https://doi.org/10.1074/jbc.M803156200

Vavylonis, D., Kovar, D. R., O'Shaughnessy, B., & Pollard, T. D. (2006). Model of formin-associated actin filament elongation. *Mol Cell*, *21*(4), 455-466. https://doi.org/10.1016/j.molcel.2006.01.016

Vavylonis, D., Wu, J. Q., Hao, S., O'Shaughnessy, B., & Pollard, T. D. (2008). Assembly mechanism of the contractile ring for cytokinesis by fission yeast. *Science*, *319*(5859), 97-100. https://doi.org/10.1126/science.1151086

Vedula, P., & Kashina, A. (2018). The makings of the 'actin code': regulation of actin's biological function at the amino acid and nucleotide level. *J Cell Sci*, *131*(9). https://doi.org/10.1242/jcs.215509

Vicente, N. B., Zamboni, J. E. D., Adur, J. F., Paravani, E. V., & Casco, V. H. (2007). Photobleaching correction in fluorescence microscopy images. *Journal of Physics: Conference Series*, *90*, 012068. https://doi.org/10.1088/1742-6596/90/1/012068

Vidali, L., van Gisbergen, P. A., Guérin, C., Franco, P., Li, M., Burkart, G. M., Augustine, R. C., Blanchoin, L., & Bezanilla, M. (2009). Rapid formin-mediated actin-filament elongation is essential for polarized plant cell growth. *Proc Natl Acad Sci U S A*, *106*(32), 13341-13346. https://doi.org/10.1073/pnas.0901170106

Vignjevic, D., Kojima, S., Aratyn, Y., Danciu, O., Svitkina, T., & Borisy, G. G. (2006). Role of fascin in filopodial protrusion. *J Cell Biol*, *174*(6), 863-875. https://doi.org/10.1083/jcb.200603013

Vizcarra, C. L., Kreutz, B., Rodal, A. A., Toms, A. V., Lu, J., Zheng, W., Quinlan, M. E., & Eck, M. J. (2011). Structure and function of the interacting domains of Spire and Fmn-family formins. *Proc Natl Acad Sci U S A*, *108*(29), 11884-11889. https://doi.org/10.1073/pnas.1105703108

Vještica, A., Marek, M., Nkosi, P. J., Merlini, L., Liu, G., Bérard, M., Billault-Chaumartin, I., & Martin, S. G. (2020). A toolbox of stable integration vectors in the fission yeast Schizosaccharomyces pombe. *J Cell Sci*, *133*(1). https://doi.org/10.1242/jcs.240754

Vjestica, A., Merlini, L., Dudin, O., Bendezu, F. O., & Martin, S. G. (2016). Microscopy of Fission Yeast Sexual Lifecycle. *J Vis Exp*(109). https://doi.org/10.3791/53801

von der Ecken, J., Müller, M., Lehman, W., Manstein, D. J., Penczek, P. A., & Raunser, S. (2015). Structure of the F-actin-tropomyosin complex. *Nature*, *519*(7541), 114-117. https://doi.org/10.1038/nature14033

Vyas, A., Freitas, A. V., Ralston, Z. A., & Tang, Z. (2021). Fission Yeast Schizosaccharomyces pombe: A Unicellular "Micromammal" Model Organism. *Curr Protoc*, *1*(6), e151. https://doi.org/10.1002/cpz1.151

Wagner, E., & Glotzer, M. (2016). Local RhoA activation induces cytokinetic furrows independent of spindle position and cell cycle stage. *J Cell Biol*, *213*(6), 641-649. https://doi.org/10.1083/jcb.201603025

Wang, J., Neo, S. P., & Cai, M. (2009). Regulation of the yeast formin Bni1p by the actin-regulating kinase Prk1p. *Traffic*, *10*(5), 528-535. https://doi.org/10.1111/j.1600-0854.2009.00893.x

Wang, N., Lo Presti, L., Zhu, Y. H., Kang, M., Wu, Z., Martin, S. G., & Wu, J. Q. (2014). The novel proteins Rng8 and Rng9 regulate the myosin-V Myo51 during fission yeast cytokinesis. *J Cell Biol*, *205*(3), 357-375. https://doi.org/10.1083/jcb.201308146

Wawro, B., Greenfield, N. J., Wear, M. A., Cooper, J. A., Higgs, H. N., & Hitchcock-DeGregori, S. E. (2007). Tropomyosin regulates elongation by formin at the fast-growing end of the actin filament. *Biochemistry*, *46*(27), 8146-8155. https://doi.org/10.1021/bi700686p

Waxman, D., & Peck, J. R. (1999). Sex and adaptation in a changing environment. *Genetics*, *153*(2), 1041-1053. https://doi.org/10.1093/genetics/153.2.1041

Wear, M. A., Yamashita, A., Kim, K., Maéda, Y., & Cooper, J. A. (2003). How capping protein binds the barbed end of the actin filament. *Curr Biol*, *13*(17), 1531-1537. https://doi.org/10.1016/s0960-9822(03)00559-1

Weber, A., Pennise, C. R., Babcock, G. G., & Fowler, V. M. (1994). Tropomodulin caps the pointed ends of actin filaments. *J Cell Biol*, *127*(6 Pt 1), 1627-1635. https://doi.org/10.1083/jcb.127.6.1627

Weber, A., Pennise, C. R., & Fowler, V. M. (1999). Tropomodulin increases the critical concentration of barbed end-capped actin filaments by converting ADP.P(i)-actin to ADP-actin at all pointed filament ends. *J Biol Chem*, *274*(49), 34637-34645. https://doi.org/10.1074/jbc.274.49.34637

Weichert, M., Herzog, S., Robson, S. A., Brandt, R., Priegnitz, B. E., Brandt, U., Schulz, S., & Fleißner, A. (2020). Plasma Membrane Fusion Is Specifically Impacted by the Molecular Structure of Membrane Sterols During Vegetative Development of Neurospora crassa. *Genetics*, *216*(4), 1103-1116. https://doi.org/10.1534/genetics.120.303623

Weis, W. I., & Kobilka, B. K. (2018). The Molecular Basis of G Protein-Coupled Receptor Activation. *Annu Rev Biochem*, *87*, 897-919. https://doi.org/10.1146/annurev-biochem-060614-033910

Welch, M. D., Iwamatsu, A., & Mitchison, T. J. (1997). Actin polymerization is induced by Arp2/3 protein complex at the surface of Listeria monocytogenes. *Nature*, *385*(6613), 265-269. https://doi.org/10.1038/385265a0

Wells, A. L., Lin, A. W., Chen, L. Q., Safer, D., Cain, S. M., Hasson, T., Carragher, B. O., Milligan, R. A., & Sweeney, H. L. (1999). Myosin VI is an actin-based motor that moves backwards. *Nature*, *401*(6752), 505-508. https://doi.org/10.1038/46835

Wiggan, O., Shaw, A. E., DeLuca, J. G., & Bamburg, J. R. (2012). ADF/cofilin regulates actomyosin assembly through competitive inhibition of myosin II binding to F-actin. *Dev Cell*, *22*(3), 530-543. https://doi.org/10.1016/j.devcel.2011.12.026

Winkelman, J. D., Suarez, C., Hocky, G. M., Harker, A. J., Morganthaler, A. N., Christensen, J. R., Voth, G. A., Bartles, J. R., & Kovar, D. R. (2016). Fascin- and α-Actinin-Bundled Networks Contain Intrinsic Structural Features that Drive Protein Sorting. *Curr Biol*, *26*(20), 2697-2706. https://doi.org/10.1016/j.cub.2016.07.080

Wioland, H., Jegou, A., & Romet-Lemonne, G. (2019). Torsional stress generated by ADF/cofilin on cross-linked actin filaments boosts their severing. *Proc Natl Acad Sci U S A*, *116*(7), 2595-2602. https://doi.org/10.1073/pnas.1812053116

Wood, V., Gwilliam, R., Rajandream, M. A., Lyne, M., Lyne, R., Stewart, A., Sgouros, J., Peat, N., Hayles, J., Baker, S., Basham, D., Bowman, S., Brooks, K., Brown, D., Brown, S., Chillingworth, T., Churcher, C., Collins, M., Connor, R., . . . Nurse, P. (2002). The genome sequence of Schizosaccharomyces pombe. *Nature*, *415*(6874), 871-880. https://doi.org/10.1038/nature724

Wright, P. E., & Dyson, H. J. (2015). Intrinsically disordered proteins in cellular signalling and regulation. *Nat Rev Mol Cell Biol*, *16*(1), 18-29. https://doi.org/10.1038/nrm3920

Wu, B., & Guo, W. (2015). The Exocyst at a Glance. *J Cell Sci*, *128*(16), 2957-2964. https://doi.org/10.1242/jcs.156398

Wu, C., Asokan, S. B., Berginski, M. E., Haynes, E. M., Sharpless, N. E., Griffith, J. D., Gomez, S. M., & Bear, J. E. (2012). Arp2/3 is critical for lamellipodia and response to extracellular matrix cues but is dispensable for chemotaxis. *Cell*, *148*(5), 973-987. https://doi.org/10.1016/j.cell.2011.12.034

Wu, D. (2005). Signaling mechanisms for regulation of chemotaxis. *Cell Res*, *15*(1), 52-56. https://doi.org/10.1038/sj.cr.7290265

Wu, J. Q., Bähler, J., & Pringle, J. R. (2001). Roles of a fimbrin and an alpha-actinin-like protein in fission yeast cell polarization and cytokinesis. *Mol Biol Cell*, *12*(4), 1061-1077. https://doi.org/10.1091/mbc.12.4.1061

Wu, J. Q., Sirotkin, V., Kovar, D. R., Lord, M., Beltzner, C. C., Kuhn, J. R., & Pollard, T. D. (2006). Assembly of the cytokinetic contractile ring from a broad band of nodes in fission yeast. *J Cell Biol*, *174*(3), 391-402. https://doi.org/10.1083/jcb.200602032

Xie, H., Vucetic, S., Iakoucheva, L. M., Oldfield, C. J., Dunker, A. K., Uversky, V. N., & Obradovic, Z. (2007). Functional anthology of intrinsic disorder. 1. Biological processes and functions of proteins with long disordered regions. *J Proteome Res*, *6*(5), 1882-1898. https://doi.org/10.1021/pr060392u

Xu, Y., Moseley, J. B., Sagot, I., Poy, F., Pellman, D., Goode, B. L., & Eck, M. J. (2004). Crystal structures of a Formin Homology-2 domain reveal a tethered dimer architecture. *Cell*, *116*(5), 711-723. https://doi.org/10.1016/s0092-8674(04)00210-7

Xue-Franzén, Y., Kjaerulff, S., Holmberg, C., Wright, A., & Nielsen, O. (2006). Genomewide identification of pheromone-targeted transcription in fission yeast. *BMC Genomics*, *7*, 303. https://doi.org/10.1186/1471-2164-7-303

Xue, B., Leyrat, C., Grimes, J. M., & Robinson, R. C. (2014). Structural basis of thymosin-β4/profilin exchange leading to actin filament polymerization. *Proc Natl Acad Sci U S A*, *111*(43), E4596-4605. https://doi.org/10.1073/pnas.1412271111

Yamamoto, M. (1996). The molecular control mechanisms of meiosis in fission yeast. *Trends Biochem Sci*, *21*(1), 18-22.

Yamashiro, S., Gokhin, D. S., Kimura, S., Nowak, R. B., & Fowler, V. M. (2012). Tropomodulins: pointed-end capping proteins that regulate actin filament architecture in diverse cell types. *Cytoskeleton (Hoboken)*, *69*(6), 337-370. https://doi.org/10.1002/cm.21031

Yamashita, A., Maeda, K., & Maéda, Y. (2003). Crystal structure of CapZ: structural basis for actin filament barbed end capping. *Embo j*, *22*(7), 1529-1538. https://doi.org/10.1093/emboj/cdg167

Yang, C., Czech, L., Gerboth, S., Kojima, S., Scita, G., & Svitkina, T. (2007). Novel roles of formin mDia2 in lamellipodia and filopodia formation in motile cells. *PLoS Biol*, *5*(11), e317. https://doi.org/10.1371/journal.pbio.0050317

Ye, J., Zheng, Y., Yan, A., Chen, N., Wang, Z., Huang, S., & Yang, Z. (2009). Arabidopsis formin3 directs the formation of actin cables and polarized growth in pollen tubes. *Plant Cell*, *21*(12), 3868-3884. https://doi.org/10.1105/tpc.109.068700

Yin, H. L., Janmey, P. A., & Schleicher, M. (1990). Severin is a gelsolin prototype. *FEBS Lett*, *264*(1), 78-80. https://doi.org/10.1016/0014-5793(90)80769-f

Yonetani, A., Lustig, R. J., Moseley, J. B., Takeda, T., Goode, B. L., & Chang, F. (2008). Regulation and targeting of the fission yeast formin cdc12p in cytokinesis. *Mol Biol Cell*, *19*(5), 2208-2219. https://doi.org/10.1091/mbc.e07-07-0731

Yu, J., Fischman, D. A., & Steck, T. L. (1973). Selective solubilization of proteins and phospholipids from red blood cell membranes by nonionic detergents. *J Supramol Struct*, *1*(3), 233-248. https://doi.org/10.1002/jss.400010308

Zhang, L., & Maddox, A. S. (2010). Anillin. *Curr Biol*, *20*(4), R135-136. https://doi.org/10.1016/j.cub.2009.12.017

Zhang, R., Zhang, C., Zhao, Q., & Li, D. (2013). Spectrin: structure, function and disease. *Sci China Life Sci*, *56*(12), 1076-1085. https://doi.org/10.1007/s11427-013-4575-0

Zhang, X., Bi, E., Novick, P., Du, L., Kozminski, K. G., Lipschutz, J. H., & Guo, W. (2001). Cdc42 interacts with the exocyst and regulates polarized secretion. *J Biol Chem*, *276*(50), 46745-46750. https://doi.org/10.1074/jbc.M107464200

Zigmond, S. H., Evangelista, M., Boone, C., Yang, C., Dar, A. C., Sicheri, F., Forkey, J., & Pring, M. (2003). Formin leaky cap allows elongation in the presence of tight capping proteins. *Curr Biol*, *13*(20), 1820-1823. https://doi.org/10.1016/j.cub.2003.09.057

Zimmermann, D., Homa, K. E., Hocky, G. M., Pollard, L. W., De La Cruz, E. M., Voth, G. A., Trybus, K. M., & Kovar, D. R. (2017). Mechanoregulated inhibition of formin facilitates contractile actomyosin ring assembly. *Nat Commun*, *8*(1), 703. https://doi.org/10.1038/s41467-017-00445-3

Zimmermann, D., & Kovar, D. R. (2019). Feeling the force: formin's role in mechanotransduction. *Curr Opin Cell Biol*, *56*, 130-140. https://doi.org/10.1016/j.ceb.2018.12.008

Zimmermann, L., Stephens, A., Nam, S. Z., Rau, D., Kübler, J., Lozajic, M., Gabler, F., Söding, J., Lupas, A. N., & Alva, V. (2018). A Completely Reimplemented MPI Bioinformatics Toolkit with a New HHpred Server at its Core. *J Mol Biol, 430*(15), 2237-2243. https://doi.org/10.1016/j.jmb.2017.12.007